Palacký University Olomouc

Faculty of Science

Laboratory of Growth Regulators

Mgr. Gabriel Gonzalez

Doctoral Thesis

Heterocyclic compounds targeting the neurodegenerative diseases

P1527 Biology

1501V019 Experimental biology

Supervisor

Prof. Ing. Miroslav Strnad, CSc. DSc

Olomouc

2021

Bibliografická identifikace

Jméno a příjmení autora	Gabriel Gonzalez
Název práce	Heterocyklické sloučeniny cílené proti neurodegenerativním onemocněním
Typ práce	Disertační
Pracoviště	Laboratoř růstových regulátorů
Vedoucí práce	Prof. Ing. Miroslav Strnad, CSc. DSc.
Rok obhajoby práce	2021

Abstrakt — Předložená disertační práce se zabývá *in vitro* modelováním Parkinsonovy choroby na neuronálních SH-SY5Y buňkách a identifikací sloučenin schopných indukovat neuroprotektivní aktivitu. V rámci práce byly testovány kandidátní skupiny sloučenin, jako jsou přírodní cytokininy a jejich metability, nové syntetické pentacyklické triterpeny, purinové bioisostery cytokininu kinetinu a steroidů izolovaných z korálu Sinularia polydactyla. Použity byly modely neurodegenerace indukované salsolinolem-, glutamátem- a 3-nitropropionovou kyselinou na neuronálních SH-SY5Y buňkách. U přírodních cytokininů a bioisosterů kinetinu byla prokázána neuroprotektivní aktivita pomocí redukce oxidativního stresu, zatímco triterpenické deriváty dramaticky redukovaly apoptózu, oxidativní stres a mitochondriální dysfunkci na salsolinolovém a glutamátovém modelu degenerace. Dva deriváty izolovaných steroidů vykazovaly neuroprotektivní aktivitu vůči modelu mitochondriální dysfunkce či Huntingtonově chorobě indukované3-nitropropionovou kyselinou. Tyto deriváty vykazovaly další související biologickou aktivitu jako je antagonismus androgenového receptoru.

Klíčová slova	Parkinsonova choroba, *in vitro* modely, salsolinol, glutamát, neuroprotekce, SH-SY5Y
Počet stran	86
Počet příloh	5
Jazyk	Anglický

Bibliographical identification

Author's first name and surname	Gabriel Gonzalez
Title of thesis	Heterocyclic compounds targeting the neurodegenerative diseases
Type of thesis	Ph.D. Thesis
Department	Laboratory of Growth Regulators
Supervisor	Prof. Ing. Miroslav Strnad, CSc. DSc.
The year of presentation	2021

Abstract — The present dissertation is focused on *in vitro* modelling of Parkinson's disease on neuronal SH-SY5Y cells and identification of compounds capable of inducing neuroprotective activity. Candidate groups of compounds such as natural cytokinins and their metabolites, novel synthetic pentacyclic triterpenes, purine bioisosteres of cytokinin kinetin, and steroids isolated from *Sinularia polydactyla* coral were tested. Models of salsolinol-, glutamate- and 3-nitropropionic acid-induced neurodegeneration on neuronal SH-SY5Y cells were used. While natural cytokinins and kinetin bioisosters showed the neuroprotective activity by reducing oxidative stress, triterpene derivatives dramatically reduced apoptosis, oxidative stress, and mitochondrial dysfunction in both salsolinol and glutamate degeneration model. Two derivatives of isolated steroids showed neuroprotective activity against a model of mitochondrial dysfunction or Huntington's disease induced by 3-nitropropionic acid. These derivatives also demonstrated other related biological activity such as antagonism on androgen receptor.

Keywords	Parkinson's disease, *in vitro* models, salsolinol, glutamate, neuroprotection, SH-SY5Y
Number of pages	86
Number of appendices	5
Language	English

Declaration of Authorship

Hereby I declare that the Ph.D. thesis and the work presented in it is my original work except where otherwise indicated.

In Olomouc, _____

Gabriel Gonzalez

Acknowledgements

Content

List of abbreviations

3-NPA – 3-nitropropionic acid

5-HT – 5-hydroxytryptamine

5-HT$_{1A}$ – 5-hydroxytryptamine 1A receptor

6-OHDA – 6-hydroxydopamine

A30P – change of 30th alanine to proline

A53T – change of 53rd alanine to proline

Ac-DEVD-AMC – Ac-Asp-Glu-Val-Asp -7-amino-4-methylcoumarin

Ac-DEVD-CHO – N-Acetyl-Asp-Glu-Val- -Asp-al

AD – Alzheimer's disease

ADME - absorption, distribution, metabolism, and excretion

ACh - acetylcholine

AChE - acetylcholinesterase

ALP - autophagy lysosomal pathway

AMPA - α-amino-3-hydroxy-5-methyl-4-isoxazolepropionic acid

ANOVA – Analysis of variance

AO – acridine orange

ARE – antioxidant response element

ATCC – American tissue culture collection

ATP – adenosine triphosphate

ATRA – all-trans retinoic acid

BAX – Bcl-2-associated protein X

BChE – butyrylcholinesterase

CMA – chaperone-mediated autophagy

CNS – central nervous system

COMT – catechol-*O*-methyl transferase

COX-2 – cyclooxygenase-2

CsA – cyclosporin A

CSF – cerebrospinal fluid

D$_{1/2}$RS – dopamine D$_1$ and D$_2$ receptors

DA - dopamine

DAergic - dopaminergic

DAT – dopamine transporter

DBS – deep brain stimulation

DFO - deferoxamine

DHE - dihydroethidium

DMDHIQ+ - 1,2-dimethyl-6,7-dihydroxyisoquinolinium ion

DMEM/F12 – Dulbecco's Modified Eagle Medium/Nutrient Mixture F-12

DMSO – dimethyl sulfoxide

DNA – deoxyribonucleic acid

E46K - change of 46th glutamate to lysin

ECACC – European collection of authenticated cell cultures

EDTA - Ethylenediaminetetraacetic acid

ER – endoplasmic reticulum

ETC – electron transport chain

FA – Friedreich's ataxia

FAF1 - FAS-associated factor 1

FDA – U.S. Food and Drug Administration

FMN – flavin mononucleotide

G2019S - change of 2019th glycine to serine

GABA – gamma aminobutyric acid

GBA – glucocerebrosidase gene

GDNF - glial cell-derived neurotrophic factor

GLP1 - glucagon-like peptide 1

Glu - glutamate

GPe - globus pallidus externa

GPi - globus pallidus interna

Grp75 - The chaperone glucose-regulated protein 75

GSH - glutathione

GSK – glycogen synthase kinase

H50Q - change of 50th histidine to glutamine

HBSS – Hank's ballanced salt solution

HPLC-MS – high performance liquid chromatography with mass spectrometry

HSC70 – heat shock cognate 71kDA protein

HSP70 – heat shock protein 70

CHIP - carboxy-terminus of HSP70--interacting protein

iNOS – inducible nitric oxide synthase

Ireb-2 – iron-responsive element--binding protein 2

JNK – c-Jun N-terminal kinase

KEAP-1 - Kelch-like ECH-associated protein 1

KFERQ – lysine-phenylalanine--glutamate-arginine-glutamine

LAMP2A - Lysosome-associated membrane protein 2

LB – Lewy bodies

LBD – Lewy body dementia

LDH – lactate dehydrogenase

L-DOPA - L-3,4-dihydroxyphenylalanine

LRRK2 – leucin-rich repeat kinase 2

MAO – monoamine oxidase

MAO-B – monoamine oxidase-B

MHC - major histocompatibility complex

MMP – mitochondrial membrane potential

MPO - myeloperoxidase

mPTP – mitochondrial permeability transition pores

MPTP – 1-methyl-4-phenyl-1,2,3,6-tetra hydropyridine

MSN – medium spiny-sized neuron(s)

mTOR - mammalian target of rapamycin

mTORC1 - mammalian target of rapamycin complex 1

mt-OS – mitochondrial oxidative stress

NAC – *N*-acetylcysteine

NADH/NAD$^+$- nicotinamide adenine dinucleotide reduced and oxidized forms

NADPH - nicotinamide adenine dinucleotide phosphate

NAT – noradrenaline transporter

nBM – nucleus basalis of Meynert

NEC-1 – necrostatin-1

NLR - nucleotide-binding oligomerization domain-like receptor

NMDA - *N*-methyl-D-aspartate receptor

NMR – nuclear magnetic resonance

NO – nitric oxide

NQO1 - NAD(P)H quinone oxidoreductase 1

Nrf-2 - Nuclear factor erythroid 2-related factor 2

OS – oxidative stress

PARK - 18 specific chromosomal regions called locus PARK

PBS – phosphate buffer saline

PD – Parkinson's disease

PDD – Parkinson's disease with dementia

PI – propidium iodide

PI3K/Akt – phosphoinositol-3-kinase/protein kinase B

PINK1 – PTEN-induced kinase 1

PPAR-γ - peroxisome proliferation-activated receptor

PSF - protein-associated splicing factor

SAL - salsolinol

SER - serotonin

SERT – serotonin transporter

SNpc – substantia nigra pars compacta

SNpr – substantia nigra pars reticulata

SOD1/2 – superoxide dismutase 1/2

STN – subthalamic nuclei

TH – tyrosine hydroxylase

TIQs - tetraisoquinolines

TRPC1 - transient receptor potential channel 1

UCH-L1 - Ubiquitin carboxy-terminal hydrolase L1

UPS – ubiquitin-proteasome system

VGCC – voltage-gated calcium channel

α-SYN – α-synuclein

Introduction

Nowadays, the neurodegenerative diseases have experienced a dramatic rise in the number of newly diagnosed patients. Additionally, the well-known motor-related neurodegeneration such as Parkinson's disease is limited to symptomatic treatment, and thus the call for disease-modifying agents is even more urgent now. Currently the field of drug discovery of new disease-modifying drug candidates expanded from FDA-drug repurposing over natural compounds towards novel designed synthetic compounds. Within the doctoral thesis, the main focus was dedicated towards the establishing and usage of *in vitro* models associated with the disorder related to dopaminergic neurons such as Parkinson's disease by the cell death inducers such as salsolinol, glutamate and 3-nitropropionic acid on human SH-SY5Y cells differentiated by *all-trans* retinoic acid into neuronal dopaminergic and cholinergic phenotype.

In vitro models served as a tool for measurement of neuroprotective activity of several drug candidates. During the evaluation of neuroprotection *in vitro,* the main part of my work was to screen the drug candidates of natural origin: the plant hormones cytokinins and their metabolites and steroids isolated from the Red Sea Soft Coral; and to those synthetically prepared such as novel synthetic pentacyclic triterpenes and kinetin bioisosteric derivatives.

The neuroprotective effect of the most active derivatives was subsequently validated by orthogonal cytotoxicity tests (lactate dehydrogenase (LDH) release assay and propidium iodide (PI) test), followed by measurement of superoxide radical formation as a marker of oxidative stress (dihydroethidium (DHE) assay), and finalised by a caspase-3,7 activation assay. In the case of active triterpenes, their neuroprotective effect was evaluated using mitochondria by either mitochondrial membrane potential (MMP) measurement (JC10 assay) or by mitochondrial permeability transition pore (mPTP) opening assay (Calcein AM/CoCl$_2$ assay).

Aims and scope

Various natural and synthetic compounds display promising activities in Parkinson's disease-modifying therapy based on neuroprotection. Human *in vitro* models of PD, especially those induced by natural metabolites of dopamine known to possess some neurotoxicity, serve as a suitable tool for identification of new neuroprotective agents. Up to now natural plant hormones cytokinins have demonstrated promising protective activities in several stress-induced models and some Parkinson's disease-related models. However, no systematic study of cytokinins on idiopathic PD model has been published. Similarly, in the case of triterpenes, especially betulines, only few publications demonstrated neuroprotective effect in *in vitro* PD models. The new natural compounds and their synthetic analogues bring a new possibility to find suitable neuroprotective drug candidates as disease-modifying medications for PD.

The main aims of this doctoral thesis are:

- Testing and searching new neuroprotective agents in *in vitro* salsolinol-, glutamate- and 3-nitropropionic acid-induced models of PD, oxidative damage and Huntington's disease/mitochondrial damage on human dopaminergic neuron-like SH-SY5Y cells.

- The systematic evaluation of potential neuroprotective effects of natural cytokinins and their metabolites.

- Screening of neuroprotective effects of novel synthetic pentacyclic triterpenes with a deeper study of processes involved in the neuroprotection.

- Testing of novel kinetin bioisosteres in a glutamate-induced model of oxidative damage focusing on oxidative stress and the caspase-3/7 activity.

- Identification of new protective agents in a series of steroids isolated from soft coral *Sinularia polydactyla* using 3-nitropropionic acid-induced model of Huntington's disease/mitochondrial damage.

Literature review

1. Parkinson's disease

1.1. Basal ganglia: Normal function and Parkinson's disease

Parkinson's disease (PD) is the most common motor-related disorder which has experienced a dramatical rise in the number of newly diagnosed patients. The current incidence of PD is in the patients at the age of sixty and older which is 1% of the world's population [1-4]. More importantly as the increase in new PD cases rose in the last years, and the estimated number of patients in 2040 can reach up to 12 - 13 million patients globally [5, 6]. PD patients suffer from motor- and non-motor-related symptoms. Among the PD characteristic motor-related symptoms belong tremor, slowness of movements (bradykinesia), muscle rigidity, impaired gait and posture [7-9], while non-motor symptoms consist of olfactory loss, sleep disruption, problems linked with the gastrointestinal tract, psychiatric (depression, anxiety, apathy and psychosis) and cognitive impairments such as dementia [10]. From the clinical point of view, the most affected part of brain is *substantia nigra pars compacta* (SNpc) as a key structure of basal ganglia within the midbrain area. Within SNpc a dramatic loss of doparminergic (DAergic) neurons resulted in consequent dopamine (DA) depletion for entire *basal ganglia* projections. Interestingly, other regions containing non-dopaminergic neurons such as *vagus dorsal motor nucleus*, *locus coeruleus* and *raphe nuclei*) were proposed to be degenerated even before by SNpc pathology [11]. In order to understand the mechanism of motor-problems associated with PD caused by the loss of neurons in SNpc within basal ganglia, it is necessary to describe signalling pathways of the basal ganglia nuclei. Basal ganglia consist of several nuclei such as striatum containing medium-spiny-sized neurons (MSNs), SNpc, globus pallidus externa and interna (GPe and GPi), substantia nigra pars reticulate (SNpr), subthalamic nuclei (STN) and thalamus. All nuclei interactions result in the direct, indirect and hyperdirect pathways, which are responsible for the movement or its inhibition. As can be seen in Figure 1, the direct pathway begins with activated cortex which excites striato-nigral MSNs in striatum. Striatal MSNs continues with signalling by an inhibitory release of gamma-amino butyric acid (GABA) towards GPi and SNpr, so that these nuclei become inhibited. The absence of inhibitory action of GPi and SNpr via GABA, causes disinhibition of Thalamus which activates the cortex by glutamate release and it results in the movement. On the other hand, indirect pathway begins by activation of striato-pallidal MSNs which release GABA towards GPe.

Since GPe is inhibited, STN provides an excitatory signal to SNpr which becomes activated and inhibits thalamus. As a result, thalamus is not able to excite the cortex and the signalling ends up in reduction of movement [12, 13].
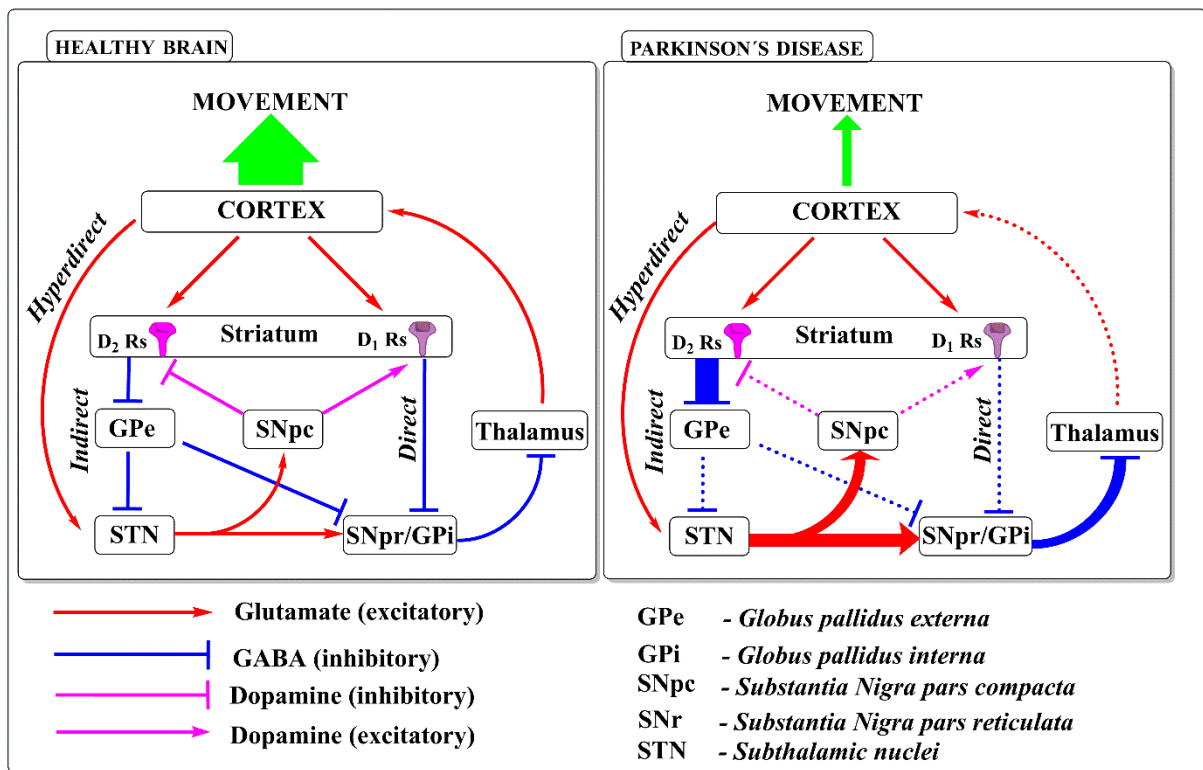
Figure 1 – **Normal and pathological projection of basal ganglia with direct and indirect pathways.** D_1 and D_2Rs – dopamine receptors D_1 and D_2. (Modified and taken from http://www.prextontherapeutics.com/r_and_d/science_and_technology.html)

Finally, the hyperdirect pathway starts with the excitatory glutamate signal from cortex directly to STN which becomes activated and activates GPi/SNpr by glutamate as well. As a result, GPi/SNpr inhibit Thalamus and its activity which ends up in similar outcome as indirect pathway. Furthermore, MSNs of the direct and indirect pathway are known to differ in expression of dopamine receptors. D_1 receptor expression is linked with MSNs of the direct pathway, while expression of D_2 receptors with MSNs of the indirect pathway [14, 15]. Additionally, besides the differential expression of D_1 receptors of striato-nigral neurons, they also express substance P and dynorphin, while the striato-pallidal neurons are characterized by expression of encephalin along with the mentioned D_2 receptors. The other difference between the MSNs expressing DA receptors is related to their ability to excite. More specifically, D_2 MSNs were identified as more excitable neurons than D_1 MSNs, and under PD pathology this

difference even increases [16]. As mentioned above SNpc nuclei are significant players within basal ganglia. These nuclei produce dopamine and project to striatum which facilitates a direct pathway by activation of D_1 receptors and subsequent striatal GABA release. On the other hand the activation of D_2 receptors results in the blockade of striatal GABA release [17]. During PD pathology 50-80% of SNpc neurons are lost when the first symptoms appear and as a result the imbalance rises in favour of indirect pathway [18-22].

1.2. Forms of Parkinson's disease, aspects of disease and molecular hallmarks

PD is a heterogeneous disease, which includes many forms. Idiopathic PD predominates with approx. 80 % and more of incidence of all diagnosed PD. This form is characterized by an unknown cause of the disorder. On the other hand, familial PD with hereditary causes of the disease has the incidence only of 10% in all PD cases [23]. Other forms may include drug-induced parkinsonism, vascular parkinsonism, multiple system atrophy, progressive supranuclear palsy, corticobasal syndrome, dementia with Lewy bodies, normal pressure hydrocephalus, various tremors involving essential tremor and rare causes of parkinsonism (conditions as Wilson's disease) [24]. As mentioned above, in most patients, the specific cause of the disease is unknown. On the other hand, some genetic and pathophysiological aspects were also identified.

1.3. Pathological aspects of PD

1.3.1. Genetic factors in PD

The first PD-related gene *SNCA* encoding α-synuclein was discovered in 1997 [25]. Mutations in *SNCA* gene (PARK1 locus) were found to be a rare cause of PD while the significant contributory role of α-synuclein (α-SYN) with PD is currently more clarified [11, 26-29]. Generally, α-SYN plays an important regulatory role in vesicle trafficking, docking, and priming later fusion and neurotransmitter release. It was found that α-SYN regulates axonal transport, but there is still a gap in understanding of its physiological function in normal human brain [30]. On the other hand its pathological role in PD was described as a major component of Lewy bodies (LB) and Lewy neurites. LBs are intracellular proteinaceous inclusions mainly constituted from α-SYN and other proteins such as phosphorylated tau and amyloid beta [31, 32]. It was found that LB pathological spreading starts from peripheral nervous system, more

precisely from olfactory bulb which continues from caudal (frontal) towards rostral (rear) brainstem [30]. Patients suffering from LBs are frequently diagnosed as PD with dementia (PDD) or Lewy body dementia (LBD) [33]. Interestingly, the study of Gomperts et al. 2013 revealed that amyloid beta protein contributory role in LBs lies in progressive cognitive decline, not affecting motor impairment, in both PDD and LBB [34]. The mechanism of α-SYN toxicity towards DAergic neurons can be attributed to the formation of oligomers, proto-fibrils and fibrils. These proteinaceous structures along with other misfolded proteins such as amyloids are able to induce impairments of mitochondria, oxidative stress, excitotoxicity and neuroinflammation which consequently lead to neuronal death [32, 35]. As mentioned above PD is also associated with *SNCA* gene mutations. Interestingly mutations in *SNCA* e.g. A53T, A30P, E46K and H50Q are the direct cause of rare early onset familial PD [36]. Despite the rare-associations between *SNCA* gene mutations and PD, the *SNCA* gene multiplications (duplication, triplications and more copies) are tightly linked with an increasing risk of idiopathic PD with progressive cognitive impairment [30].

The next discovered *PRKN* gene encoding protein Parkin was found to be associated with autosomal recessive early onset PD [37, 38]. The Parkin protein has a function as E3 ligase contributing to misfolding protein clearance by covalent binding to ubiquitin on a substrate protein, which as a result aids its degradation [39]. In connection to previous *SNCA*, the presence of Parkin along with α-SYN was identified in LBs [40]. Additionally, it was shown that mutation in Parkin induced amyloid protein aggregation in SNpc [40]. Unlike *SNCA*, the role of Parkin seems to be more direct towards the PD pathology and progression as indicated above. More importantly, the direct effect of Parkin towards PD pathology was shown in the study using Parkin-deficient mice or on idiopathic PD patients. Within the study, the lack of or deficient Parkin was tightly linked with the loss of neurons in *locus coeruleus* [40]. Other study pointed out correlation between juvenile parkinsonism and associated Parkin mutations, and the decline of ubiquitin-ligase activity in the SNpc [41, 42]. The last evidence of an important role of Parkin was found in SNpc, in which Parkin regulates the release of DA [43].

DJ-1 as a product of *PARK7* gene is a dimer protein found in cytoplasm, nucleus and mitochondria playing an important protective role for neurons [44]. The neuroprotective effect of DJ-1 is linked with regulation of PI3K/Akt pathway, antioxidant activity, chaperone and protease activity [45]. Moreover DJ-1 promotes tyrosine hydroxylase (TH) expression by negative regulation of the transcriptional repressor (protein-associated splicing factor - PSF), which in turn provides sufficient levels of TH in DAergic neurons within SNpc [44]. As mentioned above, DJ-1 can act as a regulator for protein degradation system (e.g. degradation

of misfolded α-SYN) by binding of chaperones such as HSP70, carboxy-terminus of HSP70-interacting protein (CHIP) and mitochondrial HSP70/mortalin/Grp75 [46]. In connection to PD, DJ-1 is associated with early-onset PD. Many studies showed that the absence or mutations of DJ-1 led to locomotor deficits, D_2 receptor decreased expression [47] and could result in autosomal recessive PD [48].

Leucin-rich repeat kinase 2 (*LRRK2*; PARK8) gene encodes protein Dardarin which is involved in processes such as trafficking, autophagy, protein synthesis, cytoskeletal function and also has implication to mitochondrial homeostasis (fusion/fission) [49]. Interestingly, the highest expression of *LRRK2* is located in striatal MSNs, macrophages and microglial cells suggesting its regulatory role in inflammation [37, 50]. In contrast to previous PD-related genes, mutated *LRRK2* is the most common cause of the autosomal dominant PD. The mutation G2019S with the highest occurrence is linked both to familial and idiopathic form of PD with late-onset [37, 51]. Interestingly, several point mutations of PARK8 were found to be responsible for significant DAergic neuron degeneration with or without LB aggregation. Additionally the study also found the connection between p-tau pathology and *LRRK2* mutations [52].

One of the most common genetic risk factors of PD was found in the *GBA* gene. *GBA* gene encoding the lysosomal protein glucocerebrosidase, despite its main function (degradation of glucocerebroside into glucose and ceramide), plays a significant role in decomposition of sphingolipids [53, 54]. Taking its natural activity into account, *GBA* mutations were found to end up in an impairment of lysosomal enzyme function driving aggregation of α-SYN and LB pathology [30]. Additionally, *GBA* mutations have also implications in alteration of lipid levels, triggering of lysosomal storage disease or synucleinopathy, and dysfunction of autophagy machinery [55].

Finally, the last gene associated with PD is *PINK1* encodes protein PTEN-induced putative kinase 1. PTEN-induced putative kinase 1 is another protein with a protective function especially towards the stress-induced mitochondria dysfunction [56]. Additionally, *PINK1* was proven as a cell-survival factor, mutations of which dramatically increase cell vulnerability, mitochondrial dysfunction and degeneration of SNpc neurons. Overall, *PINK1* mutations are linked with the familial form of PD [56, 57].

1.3.2. The role of neurotransmitters in PD

The roles of neurotransmitters within PD have been discussed for many years. Despite the essential DAergic system which in the course of time decay by SNpc degeneration, other neurotransmitters such as serotonin (SER), acetylcholine (ACh), gamma-aminobutyric acid (GABA) and glutamate (Glu) appear to be negatively influenced by PD pathology. The effect of DA and its metabolism is included in the next chapter in subsection "Oxidative stress".

First, the serotonin system impairments are linked with motor and non-motor symptoms, specifically tremor, cognitive dysfunction, depression and psychosis. Additional symptom such as L-3,4-dihydroxyphenylalanine (L-DOPA)-associated dyskinesia was also tightly linked with the SER system [58]. Mechanistic insight within SER system was brought by *in vivo* and human studies. Specifically, 1-methyl-4-phenyl-1,2,3,6-tetrahydropyridine (MPTP)-induced model of PD on mice caused significant reduction of 5-hydroxytryptamine (5-HT also known as serotonin) levels in *prefrontal cortex* [59]. This observation was also described by the other group [60]. As expected a decreased 5-HT levels and depression were found to be in a strong correlation [61]. Next *in vivo* study using macaque monkeys identified a drop in 5-HT transporters (SERT) in *cortex* and *anterior cingulate* [62]. PD patient study revealed that approx. 25% of serotonergic receptor ($5-HT_{1A}$) decline in raphe nuclei correlated with solemnity of resting tremor symptoms [63]. Additionally, the reduction of 5-HT and SERT was also observed in *raphe nuclei* and *prefrontal cortex* of PD patient brains [64, 65].

Second, the ACh was found to be potentially involved within PD pathology. Especially, cell clusters – nucleus basalis of Meynert (nBM; cholinergic phenotype) located in the subventricular zone of forebrain were found to be lost in Alzheimer's disease, Lewy body dementia and in PD [66, 67]. Interestingly, post-mortem study revealed LB inclusions and loss of neurons in nBM in PD patients with cognitive dysfunction [68].

GABA inhibitory system was proposed to be involved in PD based on abnormalities in olfaction in approx. 80% diagnosed PD patients [33]. The olfactory bulb and midbrain neuronal functions are regulated by glial cell-derived neurotrophic factor (GDNF) which is controlled by GABA/Ca^{2+} system. Interestingly, the roles of GDNF and GABA were shown in the study Ibanez et al. 2017. Within the study administration of GDNF induced the neuroprotective effect towards GABAergic neurons of striatum but not to SNpc neurons [47]. In connection to calcium, Ca^{2+} fluxes are controlled by GABA receptors directly or via astrocytes [69]. Within PD, Ca^{2+} buffering system is impaired due to mitochondria dysfunction which leads to excitotoxicity and subsequently to neuronal death in SNpc [70]. These observations indicated

the involvement of GABA system collapse in the loss of DAergic neurons in PD by loss of GDNF and excitotoxicity [71].

Finally, glutamate as the last neurotransmitter is known as the main contributor to excitotoxicity. The glutamate neurotransmission is linked with STN activity[72], which is known to bind ionotrophic receptors *N*-methyl-D-aspartate (NMDA) or α-amino-3-hydroxy-5-methyl-4-isoxazolepropionic acid (AMPA). Alternatively, it is responsible for opening of voltage-gated calcium (Ca^{2+}) channels (VGCC). Both receptors and channels cause excessive Ca^{2+} flux into neurons which impairs mitochondria and increases oxidative stress [73, 74]. Excitotoxicity as a consequent event was described in several environmental toxin exposures [73, 75-77] or as a direct action of glial cells [78].

1.3.3. The molecular hallmarks in PD and role of toxins

As mentioned in the previous chapter, idiopathic PD is the major form in the diagnosis rate of all PD cases with an unknown cause. On the other hand, several key molecular hallmarks such as oxidative stress, mitochondrial dysfunction, α-SYN misfolding and aggregation, impairment of ubiquitin-proteasome and autophagy-lysosomal systems, neuroinflammation and excitotoxicity were identified in PD patients' brains, in *in vitro* and *in vivo* experiments. These molecular hallmarks were also attributed to other forms of PD. Aside from these hallmarks, the endogenous (DA and its metabolites) and environmental (pesticides) toxic agents also play an important role in PD pathology.

1.3.3.1. The involvement of oxidative stress in PD

Oxidative stress (OS) is involved in many metabolic processes and its dysregulation leads to dramatic toxic effects to human body [79, 80]. PD is in general associated with high levels of OS as demonstrated by detection of highly oxidized DNA, proteins and lipids and reduced levels of glutathione (GSH) [81] in SNpc of PD patients. Studies also pointed out several sources of OS such as cellular and organelle dysfunction associated glial cells [82] and mitochondria dysfunction[83]. Furthermore enzymes and proteins e.g. nicotinamide adenine dinucleotide phosphate oxidase (NADPH oxidase), inducible nitric oxide synthase (iNOS), astrocytic myeloperoxidase (MPO) [84-90], monoamine oxidase (MAO), NAD(P)H quinone oxidoreductase 1 (NQO1) [91], DJ-1[92], *LRRK2*[93], tyrosine hydroxylase [94] have been shown to be strongly involved in PD pathology. Another source of OS is tightly connected to

metals and is related for example to iron imbalances causing Fenton's and Haber-Weiss' reactions [95]. Additionally, a hormonal pathway of androgens was found to facilitate oxidative stress in PD [96]. More importantly, DA metabolism was found to be a relatively huge source of OS and its imbalance can lead to neuronal cell death directly by DA or by its toxic metabolites [97, 98]. Finally, there is no doubt that significant contribution to overall OS can be addressed to the impairment of antioxidant defence system (represented, for example, by superoxide dismutase, catalase, reduced GSH and down-regulation of Nuclear factor erythroid 2-related factor 2 (Nrf-2)/ antioxidant responsive element (ARE) pathway) [99, 100], neuroinflammation (cyclooxygenase-2 and tumour necrosis factor-α) and mitochondrial dysfunction (impairment of complexes of electron-transport chain). Neuroinflammation and mitochondrial dysfunction in PD are discussed separately in the following chapters.

NADPH-oxidase

NADPH oxidase activation leads to generation of superoxide radicals. From the clinical point of view the elevated activity of microglial NADPH oxidase was observed in PD patient brains [101]. The pathological role of this enzyme was described in many PD models [85, 101, 102]. Chung et al. 2011 demonstrated microglial activation of NADPH oxidase associated with elevated OS in MPTP-induced model PD *in vivo*. Administration of MPTP was associated with elevation of superoxide radicals together with oxidation of DNA and proteins in brain of mice [103].

Inducible nitric oxide synthase (iNOS)

Inducible nitric oxide synthase is involved in many neurological disorders including PD. Despite its physiological function such in maturation, developmental processes, response to injury, and inflammatory trauma to induced cell repair or cell death [104], it was shown that nitric oxide (NO) production is a key toxic process in mitochondrial impairment within several neurological diseases [105]. In connection to PD pathology, it was shown that microglia-mediated elevation of iNOS (NO production) in combination with increase of NADPH oxidase activity (O_2.⁻ radicals formation) resulted in formation of ONOO.⁻ peroxynitrate radicals. These peroxynitrites were found to be harmful to DAergic neurons since the presence of nitrated tyrosine residues was found in PD patients [106, 107]. Interestingly, early PD patients with cognitive impairment had low levels of NO metabolites in serum. It was suggested that NO metabolites can be used as early biomarkers of PD [108]. Additionally, many *in vivo* studies using PD models brought evidence about upregulation of iNOS and its toxic role towards

DAergic neurons with resulting aldose reductase downregulation (a key enzyme involved in DA synthesis) [109]. Furthermore, the *in vivo* studies also showed that inhibition of iNOS by 7-nitroindazole [87] or its knockout [110] made mice resistant or less sensitive to MPTP toxicity. Indeed, MPTP intoxication was tightly linked with iNOS up-regulation in *substantia nigra* and the formation of peroxynitrite radicals [111, 112]. Moreover, based on these findings it appears the inhibition of iNOS can be used as a promising target for PD [113].

Myeloperoxidase – (MPO)

Another key enzyme involved in oxidative stress is MPO, which was found in high levels in mesencephalon PD patients. MPO contributes to immune response by the generation of highly toxic hypochlorous or hypobromous acids from hydrogen peroxide and chlorine or bromine anions. Interestingly, animal studies utilizing MPTP toxin showed several markers of MPO-driven pathology e.g., the presence of the marker of MPO protein damage – 3-chlorotyrosine, MPTP resistance in MPO-deficient mice and MPO-induced oxidative modification of α-SYN. Furthermore, MPO was shown to contribute to OS production by the catalytic conversion of NO_2^- to $NO_2 \cdot^-$ which subsequently led to additional protein damage [114].

Monoamine oxidase (MAO)

MAO especially MAO-B as a key hydrolase enzyme of DA metabolism (but also other amines in general) also contributes to pathology of PD. Especially MAO-B was found to be upregulated in PD patients. Interestingly, increased MAO-B expression was associated with a progressive loss of DAergic neurons in SNpc [115]. It was shown that MAO-B contributes to PD pathology by increased metabolism of DA which leads to DA depletion (the loss of signalling) and production of hydrogen peroxide. Taking into account the high concentration of iron in SNpc and the production of hydrogen peroxide induced by MAO-B, the level of highly reactive hydroxyl radical may even increase. These factors contribute directly and indirectly to the loss of SNpc neurons. Additionally, the existence of MAO-B inhibitors e.g. rasagiline as PD therapeutics, indicates the importance of MAO-B contribution to PD pathology.

Iron dysregulation and dopamine metabolism

Iron imbalances along with dopamine metabolism became one of the most important factors in PD pathology. It was shown that iron accumulation phenomenon is also a part of the brain

ageing [116]. Magnetic resonance imaging study revealed that nuclei with high concentrations of iron are mainly *putamen*, *globus pallidus*, *red nucleus* and *substantia nigra*. On the other hand age-related iron accumulation was identified in thalamus and dentate nuclei [117]. In PD, iron and neuromelanine (a metabolite of DA) are key mediators contributing to progressive neurodegeneration in OS in SNpc [118, 119]. As mentioned above, DAergic neurons are vulnerable to OS especially generated by iron by Fentom's and Haber-Weiss' reactions. First Fenton's reaction is mediated by ferrous (Fe^{2+}) ions and hydrogen peroxide which produces hydroxyl radicals, while Haber-Weiss's reaction is driven by superoxide radicals and hydrogen peroxide. As a result, an additional amount of hydroxyl radicals is generated [120]. Fe^{2+} in large amounts was also found to induce high OS, DNA damage and cell death by autophagy within SNpc [95]. Iron was also described as an inducer of the Lewy body formation [121-125]. In the search for a mechanism of iron accumulation, studies have shown impairments such as i) high iron influx through transferrin receptor-2/divalent metal transporter1 endocytosis and diffusion of ferric citrate [126]; disruption of iron metabolism through the loss of intracellular homeostasis; and impairment of iron efflux system or combination of these events [127]. One of the central control proteins is iron regulatory protein 1 and 2 (IRP1/2) which sensor cytoplasmic iron levels and regulates other proteins of iron homeostasis [127]. The study on parkinsonian mice showed that disruption of *Ireb2* gene regulating IRP1/2 led in an iron accumulation [128]. On the other hand, the IRP1/2 activity was also detected unaltered in SNpc and thus other proteins of the iron regulatory pathway are involved in PD [129]. Proteins associated with a high risk of PD also include transferrin and transferrin-2 receptor [130, 131]. The transferin/transferrin receptor complex could potentially contribute to a mitochondrial impairment by iron influx to mitochondria of SNpc neurons [131]. Interestingly, analysis of PD tissue has found to have an increased ferritin (iron storage regulatory protein) in microglia, astrocytes, non-pigmented neurons and damaged DAergic neurons[132]. Other studies confirmed these findings in SNpc of PD samples [133]. On the other hand, study using SNpc homogenates revealed lower levels of ferritin indicating the loss of storage capacity [134]; it was also confirmed by other authors[135]. The combination of unbound ferrous ions along with the other iron-binding element such as neuromelanin was indicated as another source of toxic iron within PD pathology [136, 137]. Furthermore, some studies also showed that ferroportin-ceruloplasmin (iron-efflux system) is altered in PD. Especially, a decreased ceruloplamin activity was identified in SNpc while in other non-degenerated areas its activity remained normal. Another factor - the amyloid precursor protein – also known for stabilization of ferroportin was found to be decreased in SNpc in PD [118, 138].

As mentioned above, PD is characterized by the loss of DA producing neurons. In addition, the iron-rich neurons are known for their relatively high metabolic activity and high content of DA metabolites, which, however, were suspected of being neurotoxic when their imbalance occurred [139]. Besides the role of iron on toxicity of DA or its metabolites, it has to be noted that DA is normally stably stored in synaptic vesicles at relatively lower pH. On the other hand, while the vesicles are impaired by e.g. synucleinopathic state, DA is prone to be oxidized into DA-quinone and becomes more reactive and toxic[140]. In addition, non-enzymatic catalytic degradation of DA with the contribution of iron appears to cause dramatic damage to DAergic neurons [97, 141, 142]. The mechanism of DA-iron mediated toxicity starts with formation of iron-DA complexes followed by subsequent oxidation to DA-quinone and highly neurotoxic 6-hydroxydopamine (6-OHDA) [143]. DA-quinones are known to form highly cytotoxic and genotoxic adducts with nucleophiles (such as SH-groups), guanine base of DNA[144], and polyunsaturated fatty acids [145]. Interestingly, some evidences showed a negative involvement of DA-quinones on glutathione peroxidases, the antioxidant enzymes. In context to glutathione peroxidases, especially glutathione peroxidase 4 function has an inhibitory effect toward ferroptosis (non-apoptotic iron-mediated cell death) and its genetical ablation led to dramatic degeneration of motor neurons indicating the strong involvement of ferroptosis [146]. Moreover, the covalent modification of the mitochondrial glutathione peroxidase 4 by DA-quinone inhibits its physiological activity against oxidative stress and ferroptosis [147]. As the second option, DA-quinones form a cyclic product leuco-dopaminechrome which progressively oxidises to dopaminechrome (DAchrome) also known as aminochrome (monomeric form of neuromelanine). Interestingly, DAchrome was found to be neurotoxic via various pathological processes such as α-SYN aggregation, mitochondrial dysfunction, OS, autophagy and ubiquitin-proteasome system (UPS) impairment, endoplasmic reticulum stress, and neuroinflammation [148-150]. Since the DAchrome levels are enzymatically regulated by both neurons and astrocytes, it appears that its toxicity is more likely linked with chronic progression of PD. Non-enzymatic reaction of DA can also result in neurotoxic tetrahydroisoquinolines [141]. Both 6-OHDA and TIQs are described in detail in the chapter on *in vitro* PD models. In the case of 6-OHDA, its production was shown not to be altered in the presence of antioxidant enzymes or radical scavengers. However, the situation changed when the iron chelator EDTA was used, which confirmed the important role of iron in the formation of these DA toxic substances. Additionally, 6-OHDA also disrupted iron regulatory proteins such as ferritin, leading to an increase in labile iron pool [151, 152] and consequently resulted in overwhelming the antioxidant system [143]. Taken together, it was shown that some DA-metabolites possess

more toxic effects than hydroxyl radicals [153] and in combination with iron accumulation in SNpc of PD patients could explain the selective loss of DAergic neurons [97].

Antioxidant response system (superoxide dismutase, catalase and Nrf-2/ARE pathway)

In the case of antioxidant response enzymes, superoxide dismutase is the first that is essential for maintaining the level of superoxide radicals by conversion of O_2. to H_2O_2 and O_2. Superoxidase dismutase exists in two forms, SOD1 (Cu/Zn as a cofactor) located in cytosol, peroxisomes and intermembrane space of mitochondria and mitochondrial SOD2 (Mn as a cofactor). SOD1 and SOD2 were found to be important protective enzymes in numerous *in vivo* and *in vitro* models. In particular, in an MPTP-induced model of PD in mice, an association between SOD1 and SOD2 activity as factors causing resistance toward toxin was found [154, 155]. Interestingly, study using the paraquat-induced model of PD on SH-SY5Y cell line and *Drosophila melanogaster* revealed that both SODs can reduce damage from toxin-induced superoxide radical formation. More importantly, the authors found different pattern in SOD-mediated protective effects. In acute (high concentration) of paraquat, SOD2 activity played a more important role, while chronic exposure to lower paraquat concentrations was associated with the involvement of SOD1, not SOD2. In addition, DAergic neurons were characterised by a specific expression of SOD1 [156]. Based on these observations of SOD-induced protective activity, a group of small molecules (SOD mimetics) was developed as a potential PD treatment [157]. Another enzyme is catalase, which, in addition, is known to decompose hydrogen peroxide in cells as the most common ROS besides superoxide radical. It was found that mutated α-SYN negatively regulates the catalase expression as well as its activity. The catalase expression is induced by the interaction of the catalase expression regulator, the peroxisome proliferation-activated receptor (PPAR-γ) and the mutated α-SYN [158]. In addition, α-SYN can also cause permeabilization of vesicles for DA which is then oxidized and produces hydrogen peroxide together with superoxide radicals [159]. Taken together, these findings indicate that the catalase activity and expression can be dramatically affected by PD pathology.

Finally, the last and one of the most important regulators of OS is the Nrf-2 – ARE pathway as a key modulator of antioxidant GSH. This signalling pathway is responsible for maintenance of OS homeostasis and has a protective effect towards noxious chemicals. Nrf-2 is a transcription factor that is continuously regulated by UPS through ubiquitin ligases such as Kelch-like ECH-associated protein 1 (Keap1), glycogen synthase kinase 3β) and E3 ubiquitin ligase Hrd1 [160] . Activation of Nrf-2 pathway, by disruption of Nrf-2 – ubiquitin-proteasome system (UPS), was found after application of agents able to oxidize, alkylate and reduce SH-

groups of Keap1 protein and also in the case of electrophilic agents [161]. Activated Nrf-2 is then transported and interacts with ARE region in DNA where it triggers expression of antioxidant genes such as heme oxygenase-1 [162], NAD(P)H:quinone oxidoreductase-1 (NQO1) [163], superoxide dismutase 2 (SOD2) [164], and GSH biosynthetic enzymes: glutathione S-transferases [165], glutathione-synthesizing enzymes glutamate-cysteine ligase catalytic subunit and glutamate-cysteine ligase modifier subunit [166]. Interestingly DJ-1 was identified to be involved in Nrf-2 activity along with thioredoxin-1 reductase [167]. In addition, other PD-related genes such as Parkin and PINK1 also interacts with the Nrf-2/ARE pathway [168-172]. Furthermore, the gene analysis revealed a strong relation between increased Nrf-2 expression and downregulation of 31 genes of ARE regions in PD patients suggesting a key role of the pathway in PD [173].

1.3.4. Neuroinflammation

The evidence of neuroinflammation as a part of pathological processes in PD was supported by many clinical and preclinical studies [174-176]. Especially, the cells with an immune response such as microglia and astrocytes were found to be activated [177] along with altered monocytes and its precursors in PD [178]. In the brain, microglia are key cells in the clearance of α-SYN [179]. On the contrary, PD-induced over-activated microglia and also astrocytes were responsible for a harmful neuroinflammtory action via Toll-like receptor 4 or 2 pathway, which resulted in the neurotoxic activity toward DAergic neurons and other cells [180-182]. In relation to this, *in vivo* study showed that oligomeric α-SYN can induce elevation of iNOS and the tumour necrosis factor as well as interferon secretion [183]. From the mechanistic point of view, several mechanisms have been proposed including the activation of inflammasome and cytokine production [184, 185], and the phenotypic switch of astrocytes from their normal to the neurotoxic phenotype [186-188]. In particular, increased levels of transforming growth factor-β1, interleukin-6 and 1β were detected in PD patients' brain and cerebrospinal fluid (CSF) [189-191]. These cytokines were suggested to be the products of already active inflammatosome – complex of Toll-like receptors and nucleotide-binding oligomerization domain-like receptors (NLRs) [192]. The secretion of interleukin-1β is preceded by caspase-1 activation and cleavage of pro- interleukin-β to a proinflammatory form. The existence of inflammasome was described in several autoimmune diseases and neurodegenerations including PD [193, 194]. In the context to PD, evidence from *in vitro* experiments indicated that the exposure to extracellular α-SYN promotes interleukin-1β elevation via NLR3

inflammasome [184, 185, 195], or inflammasome even exacerbated α-SYN aggregation in neurons [194]. However, it has to be noted that molecular mechanisms are still unclear[196]. In addition to these and the previously-mentioned markers (iNOS a MPO) of neuroinflammation, dramatically increased levels of cyclo-oxygenase-2 were identified in DAergic neurons of the brains of PD patients and in mouse PD models *post mortem [197]*. In addition, it seems very likely that the direct immune action of microglia is not only an important player in PD neuroinflammation. Recently, the existence of meningeal lymphatic vasculature was discovered, and thus CNS antigens can be in a contact with lymphocytes and antigen-presenting cells [198, 199]. Logically, the further involvement of neuroinflammation in PD comes from the activated adaptive immune system through the major histocompatibility complex I and II (MHC). Indeed, infiltration and proliferation of CD4+ T-cells was found in PD contributing to neurodegeneration by an increase of proinflammatory cytokines interferon gamma, tumor necrosis factor and interleukin-1β. It was also found that microglia can act via MHC I and II system towards T-cells by binding and presenting α-SYN as an autoantigen [200-203]. Infiltration of cells of peripheral immunity could be also increased by blood-brain barrier penetration since the brain resident mast cells were found to release histamine and cytokines (the degranulation), which affect integrity and vasodilatation of blood-brain barrier and neurons [204, 205]. As the above-mentioned increase in proinflammatory cytokines usually continues, astrocytes become prone to change to a neurotoxic phenotype. This phenomenon was observed *in vivo* after application of MPTP toxin, in which subsequent administration of cytokines led to the loss of astrocyte-mediated neuroprotection [206]. Similarly, α-SYN oligomers affected astrocytes in a similar way, but the application of glucagon-like peptide 1 receptor agonist resulted in prevention of phenotypic changes. This evidence indicates that astrocytes may be one of the key targets in the treatment of PD [186, 187].

1.3.5. Mitochondrial dysfunction in PD

Mitochondria dysfunction is one the most common characteristics of degenerated DAergic neurons in PD. In fact, mitochondria and oxidative stress are in a close relation since the abnormal activity of complex I of mitochondrial electron transport chain (ETC) was identified in PD [207-210]. In general, the experimental toxin-induced models show a fundamental involvement of complex I in PD pathology and neuronal cells both *in vivo* and *in vitro* (discussed in detail in the following chapter). In addition to the possible effects of environmental toxins, DA metabolites and several already discussed proteins, such as Parkin,

PINK1 and DJ-1, are associated with mitochondrial dysfunction [211]. In the context of complex I, its dysfunction is very strongly associated with the elevation of OS, especially with increase of superoxide radicals. In general, ETC begins with complex I activity, in which two electrons from nicotine amide adenine dinucleotide (NADH) is accepted to flavin mononucleotide (FMN) and continuing to iron-sulphur centers with the ultimate target of coenzyme Q. Superoxide radicals are formed by the reaction of oxygen and reduced FMN in presence of high ratio of $NADH/NAD^+$. Interestingly, the complex I-induced OS was also described for reversal ETC under low ADP concentrations. Here, the electron source comes from succinate in complex II, which reduces FMN and then increases superoxide radical formation by complex I [212]. According to Tretter et al. 2004, it appears that the moderate inhibition of complex I may lead to higher production of reactive oxygen species (ROS), in particular, superoxide radicals and hydrogen peroxide, which even increases the blockade of complex I. The result is the loss of the ability of ETC to produce ATP, leading to mitochondrial damage and DAergic neuronal death [213].

Interestingly, the study of Burbulla [214] on DAergic neurons derived from idiopathic and familial PD patients revealed a time-dependent cascade of pathological events, starting with mitochondrial dysfunction, manifested in oxidative stress leading to dopamine oxidation, leading to impairment of the glucocerebrosidase and lysosomal activity and ending by accumulation of α-SYN. The authors further highlighted the maintenance of mitochondrial oxidative stress (mt-OS) and contribution of DA metabolism to mitochondrial dysfunction. First, the effect of mt-OS was proved by the treatment with *N*-acetylcystein and TEMPO (mitochondrial antioxidants), which prevented accumulation of oxidized DA and increased glucocerebrosidase activity. In addition, the mitochondrial oxidative stress was linked with voltage gated calcium channels where its blockade by isradipine or calcineurin inhibitor FK506 led to similar reduction of DA oxidation. Finally, the treatment by the inhibitor of TH - α-methyl-β-tyrosine resulted in the drop of mt-OS, DA oxidation and α-SYN levels [214]. This evidence has shown the importance of mitochondrial health in relation to PD.

1.3.6. Impairment of ubiquitin-proteasome (UPS) and autophagy-lysosomal systems

As mentioned above, one of the most common characteristics of PD are misfolded and aggregated forms of α-SYN – LBs [215, 216]. UPS is a regulatory system providing regulation of misfolded or damaged proteins by their degradation in cytosol, nucleus and endoplasmic reticulum (ER) [217]. Involvement of UPS in α-SYN protein misfolding and its degradation

together with the protein Parkin and Ubiquitin carboxy-terminal hydrolase L1 (UCH-L1) has been described in PD [218]. In particular, experimental models using UPS inhibition have shown LB accumulation with subsequent degeneration of DAergic neurons *in vivo* and *in vitro* [219, 220]. *In vitro* studies further highlighted the toxic effect of ubiquitin hydrolase inactivation on neuronal cultures [219, 221] or chronic inhibition of UPS and protein oxidation by aggregation, oxidative stress, and mitochondrial dysfunction [222, 223]. UCH-L1 protein is known for its contribution to ubiquitin production. Despite its co-localization with LB [218], UCH-L1 inactivation did not lead to DAergic neuron degeneration, and yet axonal dystrophy or motor ataxia manifested itself [224]. Similarly, Parkin-mutated mice did not show any signs of parkinsonism [225]. On the other hand, Drosophila model with Parkin mutations exhibited selective degeneration of DAergic neurons accompanied with motor symptoms [226, 227]. The second regulatory system affected by PD are molecular chaperones, which are mainly involved in the regulation of protein misfolding [228, 229]. Specifically, heat-shock proteins (HSP 26, 40, 60, 70, 90, and 100) were found to be associated with PD [229, 230]. It was shown that HSPs can decrease toxicity of α-SYN aggregates or tau fibrils by formation of low molecular weight (MW) oligomers or bigger insoluble structures exhibiting lower toxicity [231, 232]. Additionally, HSPs also regulate UPS and autophagy-lysosomal systems [232, 233]. Interestingly, HSP70-mediated overexpression or co-expression was found to be potent against α-SYN aggregates, [234] MPTP-induced and rotenone-induced toxicity in multiple *in vitro* and *in vivo* models of PD [235]. On the other hand, increased toxicity was linked with mutation in ATP-ase domain of HSP70 [236]. Finally, the autophagy lysosomal pathway (ALP) is the last key mediator in PD. When the UPS is no longer efficient in degradation of the large proteinaceous plagues, the ALP is required [237, 238]. In general, ALP is divided into three pathways: minor-, major- and autophagy-mediated by chaperones. Especially, chaperones-mediated autophagy (CMA) was widely discussed for its association with PD. The detailed mechanism was described in Crotzer et al. 2005. Briefly, CMA requires the binding of heat-shock cognate 71 kDa protein (HSC70) to a substrate protein by recognizing specific sequence KFERQ. Then HSC70 docks the substrate protein into the lysosomal membrane receptor – lysosome-associated membrane protein 2 (LAMP2A). Subsequent transport to the lysosome results in the substrate protein being degraded [239]. Interestingly, α-SYN aggregates were shown to be degraded specifically by CMA [237]. Several pieces of evidence have pointed to a close correlation between vulnerability of the PD brain and dysfunction of LAMP2A, HSC70 and overall ALP [240, 241]. In addition, ALP disorder has also been detected in PD patients *post mortem*. More specifically, SNpc area was characterized by elevation of the ALP markers

together with microtubule-associated protein 1 light chain 3 (LC3) [242-244] and with decreased levels LAMP1, LAM2A and HSC70, which strongly suggest involvement of CMA dysregulation in PD [245, 246]. Besides these markers, the autophagy downstream signalling (mTOR, PI3K/AKT) was identified to be affected in PD [247].

1.4. PD treatment and disease-modifying therapy

L-3,4-dihydroxyphenylalanine (L-DOPA)

Similarly as other neurodegenerative diseases, PD treatment is currently driven via symptomatic therapy. The first class of drugs are motor symptomatic therapeutics as illustrated in figure 2.

The first and the most effective symptomatic drug is the DA precursor L-3,4-dihydroxyphenylalanine known as levodopa or L-DOPA usually administered in combination with an aromatic amino acid decarboxylase inhibitor N-amino-alpha-methyl-3-hydroxy-L-tyrosine known as carbidopa or benserazide to prevent L-DOPA degradation before blood brain barrier penetration. L-DOPA treatment is associated with phenomenon called "on" and "off" times determining when the drug works and the symptoms disappear (on time) and does not work or effect vanishes (off time). In case of L-DOPA the off-time is predictable however it could be also sudden [248]. On the other hand, L-DOPA suffers from adverse effects such as nausea, vomiting, orthostatic hypotension, sedation, confusion, sleep disturbance, hallucinations and dyskinesias (involuntary movements). In particular, dyskinesia is a characteristic effect of L-DOPA. Another problematic return of increased symptoms of PD called - wearing off – is strongly associated with L-DOPA [249]. Unfortunately, it was shown that 50% of patients treated with L-DOPA suffer from wearing off and one out of three patients develop dyskinesia within 2 years after the start of L-DOPA treatment. Particularly in patients with early onset PD, there is a significant risk of development of these side effects, so L-DOPA treatment is often delayed, despite the motor complications of PD patients [249].
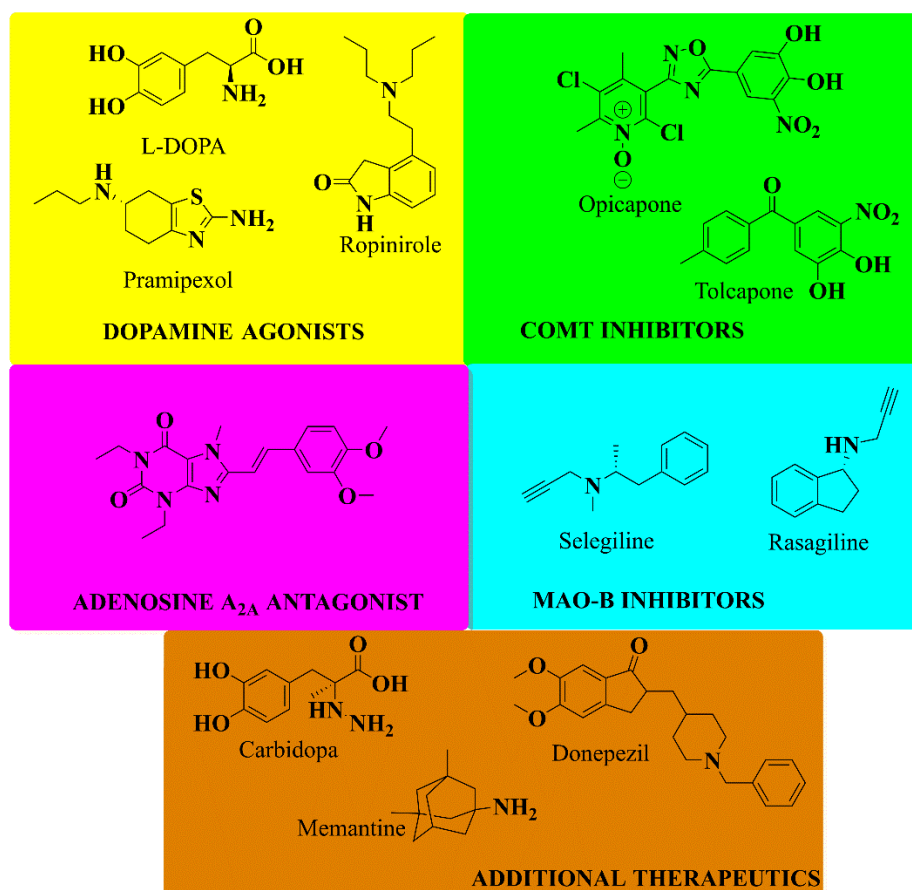
Figure 2 – FDA approved drugs used as symptomatic treatment for Parkinson's disease

Dopamine receptor agonists

As mentioned above, dopaminergic therapy is the most promising in relieving symptoms. For this reason, another class of "dopamine receptor agonists" has emerged as an alternative to L-DOPA. Clinically used DA (D_1- and D_2 type receptors) agonists are pramipexol, ropinirole, rotigotine and apomorphine. These drugs are also used as monotherapy or as an adjuvant to L-DOPA [250]. In a randomized study, the effect of DA agonists was compared with L-DOPA and MAO-B inhibitors. Within the study, patients reported better improvement in symptoms with L-DOPA than with DA agonists or MAO-B [251]. However, another study showed that ropinirole was associated with a reduction in the development of dyskinesia compared to the L-DOPA cohort [252]. DA agonists generally have adverse effects such as orthostatic hypotension, sleepiness, hallucinations and leg oedema, or certain behavioural problems, such as pathological gambling, compulsive shopping, eating, hypersexuality and other impulse-control disorders associated with psychiatric problems [253].

Catechol-O-methyltransferase inhibitors

Alternatively, additional therapy has been developed in order to improve the pharmacological profile of L-DOPA. The first type of compounds in this series are inhibitors of catechol-*O*-methyltransferase (COMT) – entacapone, opicapone and tolcapone, which block the methylation of the hydroxyl groups of L-DOPA or DA. These drugs have been found to increase L-DOPA and DA levels. In addition, the concomitant treatment with opicapone has been shown to reduce off time. Often the combination for the treatment of PD consists of L-DOPA, carbidopa and entacapone. Contrary to its advantages, the use of COMT inhibitors appears to be limited due to tolcapone-mediated hepatotoxicity. Other side effects include nausea, postural hypotension, diarrhoea and orange discoloration of urine. COMT inhibitors have shown to have no effect on L-DOPA-induced dyskinesia [254, 255].

Monoamine oxidase-B (MAO-B) inhibitors

The next class of additive drugs are the MAO-B inhibitors selegiline, rasagiline and safinamide, which affect the DA deamination reaction. MAO-B inhibitors are regularly used for early and mild PD, but also for late PD in combination with L-DOPA. Interestingly, application of safinamide, a multifactorial drug (MAO-B, DA-reuptake, VGCC inhibitor and intercellular calcium blocker) showed an increase of on time without dyskinesia and reduction of off time [256].

Adenosine A_{2A} receptor antagonists

Istradefylline is an adenosine A_{2A} receptor antagonist and is one of the latest FDA-approved drugs (2019) to treat predominantly PD patients with off episodes. It is used in combination with L-DOPA/carbidopa. Reports in the literature have shown a mild positive effect on PD patients suffering from an L-DOPA-induced side effect, but it is still accompanied by side effects such as dyskinesia, dizziness, constipation, nausea, hallucinations and insomnia [257].

Surgical therapy

In addition to drug-controlled medications, surgical treatment based on pulse generators called deep brain stimulation (DBS) is used. DBS targets nuclei with PD abnormal functions of thalamus and STN/GPi, in which thalamic DBS is the most commonly used. In a cohort study of 255 patients, the improvement in PD symptoms with DBS was found to be significantly better compared to pharmacotherapy. On the other hand, the risk of developing adverse effects with the use of DBS exceeded conventional drugs with a 3.8-fold higher risk [258]. In the

context to STN and GPi –DBS, the interesting therapeutical differences of DBS targets were described in another cohort study. In the first group of DBS-STN patients, dopaminergic treatment was required less and the visuomotor processing speed dropped, compared to DBS-GPi patients. On the other hand, DBS-STN was associated with an increase in depression, while DBS-GPi patients improved. Overall ,DBS-STN was considered a better target than GPi [259]. The use of DBS-STN was also applied in early PD patients who reported a significant improvement in quality of life score in favour to DBS-STN with medication vs medication alone [260].

Non-motor symptom treatments

As mentioned in the introduction part, PD shows not only motor but also non-motor symptoms mentioned in the introduction part. Therefore, the medications for non-motor complications are used. The first class of drugs for treatment of non-motor symptoms are the well-known acetylcholinesterase inhibitors, such as donepezil, rivastigmine or galanthamine. These drugs are usually used to improve cognitive functions. Decreased hallucinations have also been reported, along with improved postural stability or fall frequency in patients [261, 262]. Memantine (an NMDA antagonist) as a second example of another non-motor medication is also used in PD patients who have a moderate effect on cognitive impairment. However, its clinical use is still under investigation [263]. As long as PD is associated with dementia or anti-PD motor therapy-induced hallucinations, antipsychotics such as quentiapine and clozapine have been found to be effective in ameliorating these conditions [263, 264]. Another PD hallucination-linked treatment is managed by pimavanserin. The 5-hydroxytryptamin 2A receptor agonist has recently been approved by the FDA [265]. In addition, there are also other drug treatments that improve other symptoms, such as dysautonomia [266], orthostatic hypotension[267], urological problems, and constipation [268].

Disease-modifying therapies

As mentioned earlier, the proper treatment that could alter the course of PD still has not been found and symptomatic treatment has only limited effects. The disease-modifying therapy is defined as intervention, that influences the underlying processes of degeneration, which results in slowing or regenerating effects of the disease [269]. This area of new class of drug development has experienced an interesting and very challenging progress over the years. It currently includes several types of therapeutic strategies, such as α-synuclein modulators, neurotrophic and neuroprotective agents and neuroinflammation modulators, targeted therapy,

and kinase inhibitors. Based on the topic of this work, the main attention is paid to the last three classes of compounds. All therapies are reviewed in Colombo et al. 2020 [270]. Because this area is relatively young, no drugs have been approved and their activities are under investigation in preclinical development or clinical trials I-III.

Neuroprotective agents

The first promising molecular targets of neuroprotective agents in this region came from the Nrf2 pathway. For example, the recently developed Nrf-2 modulator KKPA4026 elicited a protective effect in Drosophila PD model and improved the motor functions of MPTP - intoxicated mice [271, 272]. Interestingly, other Nrf-2 activators with a potentially promising activity are being developed by Keapstone Therapeutics [273]. Finally, DA-9805, a mixture of three herbal extracts, demonstrated neuroprotective activities in MPP$^+$-induced PD on human SH-SY5Y cells and in a mouse model of PD by maintaining TH expression, OS reducing effect, increasing DA levels in striatum, and improving motor functions [274].

Another target was the FAS-associated factor 1 (FAF1), which is involved in the oxidative stress/PARP1 pathway leading to caspase-3-mediated apoptosis of DAergic neurons. It is also involved in the MPTP-induced model of PD [275]. FAF1 inhibitors include the neuroprotective compound KM-819 [276], which is currently undergoing the phase I clinical trials, from which the data suggest that KM-819 is well tolerated in patients [275].

Thiazolidinediones, and in particular MDSC-0160, are modulators of peroxisome proliferator-activated receptor gamma (PPAR-γ). This class of compounds is currently also being investigated for the treatment of PD. MDSC-0160 showed a protective effect against neurotoxin injury and had a positive effect on mitochondrial metabolism in DAergic neurons of the human midbrain. Moreover, the neuroprotective effect was confirmed in the MPP$^+$ model on *Caenorhabditis elegans,* which showed that MDSC-0160 is able to block the loss of DAergic neurons. The genetic mouse PD model revealed that MDSC-0160 reduced motor impairment by downregulating the mTOR pathway and autophagy. These *in vivo* models also revealed that MDSC-0160 reached sufficient concentrations in the brain and was able to eliminate the loss of nigral neurons, depletion of striatal DA, and TH expression. MDSC-0160 is currently used in diabetic patients and is undergoing the phase 2 clinical trials in patients with PD [277].

Neuroinflammation modulators

The second class of substances focuses on neuroinflammatory processes. The first example of these compounds is Exanatide, a glucagon-like peptid 1 (GLP1) agonist and an approved drug for type 2 diabetes [278]. Interestingly, GLP1 has been identified as a neuroinflammatory modulator in various PD and Alzheimer's diseases models affecting mitochondria [279]. From the mechanistic point of view, Exanatide-mediated agonism against GLP1 leads to activation of the insulin pathway, mTOR and Akt with consequent neurotrophic effects [278]. In PD patients, Exanatide demonstrated mild but statistically significant effects for 48 weeks. On the other hand, subsequent drug applications did not show any beneficial effects [278], which indicated poor availability to the brain. This hypothesis has been confirmed and a new subcutaneous formulation of PT-302 has recently been developed. Overall, this drug reached the furthest clinical evaluation (phase III clinical trials). The new PT-302 formulation has demonstrated sustainable drug levels in cerebrospinal fluid and plasma for more than 20 days. Phase II clinical trials are currently underway with PT-302 in early PD patients [280].

AAD-2004, an anti-inflammatory agent with antioxidant properties, is another example of an anti-inflammatory drug candidate. This compound is known to mediate anti-inflammatory effects *via* inhibition of prostaglandin E synthase-1, which has been observed upregulated in DAergic neurons of PD patients and in mice intoxicated by 6-OHDA [281]. AAD-2004 is currently undergoing phase I clinical trials [282, 283].

Other compounds such as LBT-3627 [284-286], MRx0029 and MRx0004/5[287, 288] have been shown to be effective in inducing anti-inflammatory activities and OS-reducing effects associated with neuroprotective effects *in vivo* and *in vitro*.

Targeted therapy

Compounds in this group target proteins associated with the familial form of PD, such as DJ-1, Parkin, PINK1, glucocerebrosidase and Heme oxygenase-1 (HO-1). There is evidence to suggest that their role also contributes to idiopathic PD, and therefore these substances may be potentially useful for much wider applications [270]. Almost all compounds, with the exception of glucocerebrosidase modulators, are in preclinical evaluation.

The first example, the DJ-1 modulator CB101 acts as a molecular chaperone with affinity for DJ-1 and has been shown to be protective against DAergic neurons *in vivo* in MPTP-induced model of PD [289]. Another interesting compound that inspired this dissertation is kinetin. This derivative of natural plant hormones cytokinins showed a neuroprotective effect through *PINK1*, as its metabolite kinetin ribosyl triphosphate (KTP) acted as a "neo-substrate" with

higher potency than ATP for the kinase. Moreover, KTP increased the amount and recruitment of Parkin protein, which had a beneficial effect on mitochondria and apoptosis. In addition, kinetin showed a protective effect against oxidative stress and ubiquitin-proteasome system inhibition in human SH-SY5Y cells. Currently, based on the kinetin results, Mitokinin Inc. is developing a new class of N^6-substituted ATP analogues [290].

An interesting approach based on the recombinant Parkin CV-06 protein was developed by Cellivery Therapeutics. *In vivo* studies using MPTP-induced PD mice revealed a potent effect of CV-06 in this model on increasing DA levels, preventing motor dysfunction, and losing TH^+ neurons in SNpc [291].

Another group of drug candidates are glucocerebrosidase modulators, of which Venglustat is the first example. This compound is glucosylceramide synthase inhibitor that has been shown to decrease the toxicity of elevated glucosylceramides. In a study using an *in vivo* model of PD with a glucocerebrosidase genetic mouse, Venglustat was shown to slow the accumulation of α-SYN and Tau protein and interestingly slowed cognitive decline [292]. Venglustat did not show any signs of adverse effects in patients with PD with mutations in the *GBA* gene. Decreased levels of glucosylceramides have been detected in both cerebrospinal fluid and plasma due to mechanism of action of this drug. The efficacy of Venglustat against PD is currently being investigated in phase 2 clinical trials [293, 294]. The second glucocerebrosidase modulator is LTI-291, which acts as a its stimulator with a beneficial effect on sphingolipid metabolism in lysosomes. An *in vitro* study demonstrated LTI-291-induced glucocerebrosidase restoration in a human H4 neuroglioma cell model overexpressing α-SYN. LTI-291-mediated reduction in α-SYN accumulation by restoring lysosomal activity has also been observed in another study [295]. As a result, LTI-291 underwent phase I clinical trials in which good drug tolerability and brain penetration was found.

Finally, the HO-1 inhibitor AZ-001 has recently been discovered, but is still under development. The current results indicate that AZ-001 can almost completely reduce HO-1 mRNA and halve HO-1 proteins compared to controls, thus significantly affecting ROS levels in mitochondria [296].

Kinase inhibitors

As with cancer, kinases play an important role in neurodegeneration. These days, the therapeutic use of inhibitors for the kinases *LRRK2*, c-ABL, and c-JUN *N*-terminal kinase (JNK) and mammalian target of rapamycin complex 1 (mTORC1) have been identified as promising candidates for the treatment of PD. *LRRK2* also belongs to kinases strongly

associated in PD, as mentioned above. The most developed drug candidates for this kinase are DNL-201 and ION-859. Despite the importance of the target in PD, the use of *LRRK2* inhibitors has raised concerns about their adverse effects due to abnormal accumulation of secretory lysosome-related organelles called lamellar bodies [297].

LRRK2 kinase

DNL-201 as the first *LRRK2* inhibitor with brain penetration [298] has been evaluated in phase Ia clinical trials in which DNL-201 provided good tolerability and mainly almost 90% *LRRK2* inhibition in the brain. Moreover, DNL-201 provided good tolerability at low dose and its use was associated with no or mild adverse effects in phase Ib clinical trials in the double-blind study in PD patients [299]. To avoid adverse effects associated with *LRRK2* inhibition, ION-859 has been proposed as a 2′-O-methoxyethyl-phospohorothioate-modified oligonucleotide with intrathecal application (injection into the spinal canal or subarachnoid space). ION-859 has been shown to have a beneficial effect in a mouse PD model induced by preformed α-SYN fibrils [300]. This drug candidate is currently undergoing phase I clinical trials with tolerability, safety and pharmacokinetics [301].

c-ABL kinase

c-Abl kinase activity is crucial in many physiological processes, such as formation of synapses, neurite outgrowth, neurogenesis, etc., and increased levels of phosphorylated c-Abl have been found in PD patients. In addition, c-ABL kinase contributes to the α-SYN pathology by inhibiting Parkin E3-ligase [302] and phosphorylating α-SYN on tyrosine 39 [303]. Both events strongly correlate with the progression of PD. The evidence is that negative genetic modulation of c-ABL reduces pathology of α-synuclein [303]. Currently, two examples of c-ABL drug candidates for the treatment of PD, Nilotinib and SCC-138, have shown a neuroprotective effect in preclinical studies [304, 305]. In particular, an *in vivo* study revealed Nilotinib-mediated neuroprotection in Parkin-independent manner with improved behaviour improvement [304]. Furthermore, Nilotinib has been shown to be well tolerated clinically [306] with a positive effect on total or oligomer/total α-SYN levels in cerebrospinal fluid [307]. Phase 2 clinical trials confirmed the effect of Nilotinib on α-SYN oligomer formation in PD patients [308]. On the other hand, in patients with moderate to advanced PD, the clinical study of Nitonib did not show any improvement due to poor cerebrospinal fluid penetration [309]. Second, SSC-138 is an interesting c-Abl inhibitor targeting the T315I mutation, which has been identified as poorly druggable. Its protective activity was demonstrated in the mouse MPTP-

model of PD. Subsequent clinical study indicated SSC-138 as a good cerebral penetrant achieving effective concentrations in patients' CSF comparable to *in vivo* studies [310]. Phase 2 clinical trials are currently underway in early PD patients with non-dopaminergic treatment [311].

c-JUN N-terminal kinase (JNK)

The regulator of T-cell differentiation and apoptosis JNK is also involved in PD. In particular, JNK activated by COX-2 has been found in DAergic neurons in both *in vivo* models and in patients with PD [312]. On the other hand, the characteristic progression of apoptotic cell death of DAergic neurons was reduced by inhibition of JNK *in vitro* and *in vivo* [313]. Currently, the development of JNK inhibitors for PD treatment is limited to an *in vitro* study performed by Imago Therapeutics, in which a highly selective inhibitor prevented the toxic effect of amyloid beta in human cortical neurons [314].

mTORC1

Finally, the last kinase is mTORC1, which is known to be an indicator of nutrient status and cell redox. In the context of PD, an *in vivo* study in a 6-OHDA-induced model of PD treated with L-DOPA showed that blockade of mTORC1 (CCI-779) leads to decline in L-DOPA-induced dyskinesia [315]. These days, the combined administration of RTB-101 (Dactolisib – mTORC1 inhibitor) and Sirolimus (rapamycin) in the phase I clinical study on 45 patients with PD is undergoing [316].

2. Human dopaminergic SH-SY5Y cell line *and in vitro* models of PD

The evidence presented above suggests that proper understanding of the disease and effective treatment of PD is still a burning issue. *In vitro* and in vivo models of PD and related pathologies are used to understand the pathology of PD and to develop effective disease-modifying therapeutics. PD models are divided into two classes, genetic and toxin-induced models.

First, genetic models focus on gene alterations that can subsequently lead to progressive degeneration of DAergic neurons. Unfortunately, only a few models capable of achieving such an effect have been developed [317]. Furthermore, it was also shown that even significant genetic modifications did not provide degeneration of DAergic neurons over time [318, 319] or the effect of the gene modifications within the models did not cover PD pathology [320] or

response to treatment as in humans [321]. Overall, α-SYN overexpression model, as the most common PD model exhibits various pathological features of PD [322]. In the future, the question of the use of these models for the study of PD and the development of neuroprotective agents still remains.

Currently, toxin-induced PD models are the most commonly used. These are known to mimic several PD features, such as increased oxidative stress, dysregulation of apoptosis, organelle damage (mitochondria, endoplasmic reticulum, etc.) and cell death of DAergic neurons. On the other hand, several reports suggest that toxins do not cover the full spectrum of PD pathology, e.g. α-SYN pathology [323] as they focus more on DAergic neuronal degeneration [77]. In particular, Lewy body pathology has been shown to precede degeneration of DAergic neurons, making this pathology very important for incorporation into any PD model [324]. As discussed below, several toxins are able to cause changes in PD proteins, yet most toxins have not shown such effect on the cell level. It is generally suggested that instead of using synthetic PD toxins (MPTP or MPP+) or 6-OHDA, which cause acute and dramatic cell death, PD mimetics may provide more chronical neuronal damage with a broader spectrum of pathology, as exemplified by the use of aminochrome [325]. Despite these disadvantages, toxin-induced models are accepted by the general scientific community and provide significant and reproducible results *in vitro* and *in vivo*.

2.1. Human dopaminergic neuroblastoma cell line SH-SY5Y

This work is based mainly on toxin-induced *in vitro* models of PD using the human dopaminergic neuronal cell line SH-SY5Y. The SH-SY5Y cell line is third subclone from the parental neuroblastoma cell line SK-N-SH. The original SK-N-SH cells were isolated from the bone marrow of a 4-year-old female patient in 1970 [326]. This cell line consist of a heterogenous N-neuronal, S-schwann and I-mixed cell population [327]. The SH-SY5Y cell line is widely used in PD research due to its neuronal and dopaminergic properties, such as the expression of dopamine-β-hydroxylase [326], the dopamine transporter (DAT) and the dopamine receptors D2 and D3 [328], tyrosine hydroxylase (TH) [329] and dopamine production [330]. In addition, SH-SY5Y cell line has also adrenergic (production of noradrenalin [331]) and cholinergic properties (expression of acetylcholinesterase and butyrylcholinesterase) [326]. Despite its cancer nature, most genes associated with PD pathology have been shown to remain intact [332]. SH-SY5Y cells are often used in PD research, but also in other disorders such as Alzheimer's disease, amyotrophic lateral sclerosis,

neurotoxicity, etc. [332, 333]. One of the biggest advantages of this cell line is its ability to differentiate into a mature neuron-like phenotype. In contrast to the fluctuating cell cycle of undifferentiated SH-SY5Y, differentiation synchronizes the cell cycle in G0 phase to gain a homogenous neuronal population with reduced proliferation [334, 335]. From a morphological point of view, it is known that differentiated cells have a higher number of elongated neurites, higher electrical excitability, synaptophysin-positive functional synapses and expression of mature neuronal markers [331, 336, 337]. These markers are β-III-tubulin, microtubule-associated protein-2, synapthophysis, NeuN, synaptic associated protein-97 and neuron specific enolase [337, 338]. In addition, dopaminergic markers such as TH, DAT, D_2 and D_3 receptors are even elevated due to differentiation [337]. Differentiation protocols include many types of agents that regulate the phenotype of differentiated cells, e.g. *all-trans* retinoic acid (ATRA), phorbol esters, brain-derived nerve factor, and staurosporine [339]. Within this thesis ATRA-mediated differentiation has been used, which is except of above mentioned evidence characterized by elevation of cholinergic phenotype (high expression of AChE, BChE, choline acetyl transferase, vesicular monoamine transporter [339, 340]. Interestingly, ATRA-differentiated SH-SY5Y has been shown to be sensitive to carbachol (cholinergic agonist) stimulation, resulting in increased noradrenaline release and calcium influx [334]. Surprisingly, SH-SY5Y has also been shown to be able to spontaneously form α-SYN aggregates without transfection [341]. Unlike primary cultures, the SH-SY5Y cell line provides easier and cheaper cultivation [342]. In addition, unlike rodent cell lines, SH-SY5Y cells are of human origin, so the results obtained from the cell line could potentially have greater transferability to clinical practice [343, 344].

2.2. 6-Hydroxydopamine (6-OHDA)

6-Hydroxydopamine (6-OHDA) as dopamine (DA) metabolite is one of the oldest toxins used in *in vitro* and *in vivo* experiment to induce PD. In addition to its nature role in the pathology of PD described in the chapter "Iron Dysregulation and Dopamine Metabolism", 6-OHDA is used as an agent capable of inducing oxidative stress, mitochondrial dysfunction, endoplasmi reticulum stress with subsequent neuronal cell death by apoptosis [345, 346]. In general, 6-OHDA is not a stable molecule because it autooxidises to semiquinone and hydrogen peroxide. In addition, the toxic effect of 6-OHDA is similar to H_2O_2 [347], but several signs of 6-OHDA-mediated toxicity differ dramatically. First, unlike hydrogen peroxide-induced cell death, 6-OHDA-induced toxicity and mitochondrial dysfunction are not prevented by the

antioxidant enzyme catalase [346] and antioxidant applications [348]. There is only an exception and this was superoxide dismutase (SOD)-induced protection against 6-OHDA toxicity on SH-SY5Y cells [346]. Second, 6-OHDA utilizes the dopamine (DAT) and noradrenaline transporters (NAT) to transport into nerve cells. Interestingly, 6-OHDA in the form of quinone has been shown to covalently bind to DAT or NAT, which blocks the reuptake of these transporters, especially DA [349, 350]. This toxin can also cause protein damage, mainly by covalent binding of nucleophilic amino acid side chains and its quinone forms [351]. Third, as already mentioned in previous sections, 6-OHDA can contribute to toxicity by increasing the iron content from iron-storing proteins [151, 152]. This leads to increase in oxidative stress through Fenton reactions. More importantly, this toxin also mediates toxicity through inhibitory effects on complexes I and IV [352]. More specifically, the effect of 6-OHDA to complex I has been found to be reversible and facilitated by calcium, but not iron [345]. However, studies using deferoxamine (DFO, iron chelator) and 6-OHDA have shown interesting but different bindings on complex I. DFO has been identified as an activator of complex I, which acts independently of the chelating properties of this molecule. When 6-OHDA was co-administered with DFO, 6-OHDA the complex I inhibitory constant is dramatically increase 10-fold. This effect was explained by allosteric modulation of the protector (DFO) together with the inhibitor (6-OHDA) [348]. Endoplasmic reticulum stress as another mode of action of 6-OHDA was discussed in a study by Tao et al. 2016, in which 6-OHDA intoxication led to an elevation in the endoplasmic reticulum chaperone Bip and other ER-related proteins such as phosphorus-PERK and p-IRE1. ER stress was also accompanied by a dramatic increase in calcium and the levels of activated of caspase 12 [353]. Overall, 6-OHDA is an effective agent that mimics PD features such as oxidative stress, damage of mitochondria, ER stress and increased apoptosis. On the other hand, 6-OHDA does not affect α-synuclein pathology [354].

2.3. MPTP/MPP[+], Rotenone, Paraquat

Synthetic agents will be discussed within this group of PD toxins. MPTP is the first and the classic PD inductor. In contrast to 6-OHDA, MPTP-induced toxicity in DAergic neurons is driven by inhibition of mitochondrial complex I. This toxin is oxidized to the active metabolite 1-methyl-4-phenyl-1,2,3,6-tetrahydropyridinium (MPP[+]) [355]. MPP[+] has high specificity for DAT, but also NAT and SERT, by which it is transported to neurons when administered to extracellular space. MPP[+] subsequently accumulates in the mitochondria, where it blocks

complex I, leading to the loss of ATP production and an increase of oxidative stress (OS) [356]. In case of MPP^+-induced OS, one report showed that MPP^+ contributes to the overall toxicity by redistribution of DA in the cytosol, which in oxidized form is highly toxic to DAergic neurons [355]. Furthermore, $MPTP/MPP^+$ has been identified to increases in OS due to iNOS and NADPH-oxidase activity [110, 113, 357]. Interestingly, ER stress was also associated with this toxin, specifically through the down-regulation of transient receptor potential channel 1 (TRPC1). This channel is essential for maintaining Ca^{2+} levels in the endoplasmic reticulum. In addition, silencing TRPC1 has been shown to increase the unfolded protein response activity and decrease of the PI3K/Akt survival pathway [358]. Overall, MPTP is a suitable toxin for both *in vivo* and *in vitro* applications recapitulating degeneration of DAergic neurons by patobiochemical processes similar to those found in PD DAergic neurons, as well as manifestations of behavioural motor impairment in animals. On the other hand, this toxin is not an endotoxin and therefore lacks the ability to induce protein aggregation [359].

Rotenone as the second synthetic PD toxin is a pesticide sharing that has similar chemical features to MPTP. In fact, due to its lipophilicity, the toxin is able to cross the blood–brain barrier. Once rotenone enters the cells, it starts to accumulate in mitochondria and subsequently causes inhibition of complex I [360, 361]. Interestingly, rotenone has been shown to mediate toxicity via microglial NADPH-oxidase, but not neuronal [362]. In addition, rotenone exerts its toxic effect by inducing several processes such as lowering glutathione levels, increasing membrane lipid peroxidation [363], and inhibiting ubiquitin-proteasome system [364].

Finally, it is the insecticide paraquat, which is considered a potential environmental factor contributing to the development of PD. From a mechanistic point of view, paraquat induces toxicity through redox cycling depleting NADPH and causing oxidative stress, in particular through the formation of superoxide radicals and subsequently hydrogen peroxide. As a result, the high lipid peroxidation was detected in paraquat model [364]. In addition, paraquat has been identified as a reversible acotinase inhibitor [365]. The second mode of paraquat action is the inhibitory effect on complex I of mitochondrial respiratory chain [366]. However, unlike other toxins, paraquat is able to induced intracellular protein aggregation of α-SYN and amyloid fibrils [367]. Furthermore, paraquat triggers apoptotic cell death by multiple mode of actions. Especially, several proteins are involved in paraquat-induced apoptosis, such as Bcl-2 proteins, tumor necrosis factor (TNF-α), cell death-inducing DFF45-like effector (CIDE), Bak-assisted mitochondrial permeabilization with cytochrome c release and JNK activation [368].

2.4. Salsolinol

Salsolinol (Sal) is an example of tetrahydroisoquinolines (TIQs), an interesting group of compounds produced in the human body by the mechanisms described in the section "Oxidative stress – Iron Dysregulation and Dopamine Metabolism". Sal has already been reported to be associated with PD through its occurrence in the urine of PD patients treated with L-DOPA [369], but also in the health subjects [370] or in the rat brains after ethanol treatment [371]. The origin of Sal was explained by Pictet-Spengler reaction of DA and acetaldehyde to give racemic R/S-Sal. On the other hand, a stereoselective enzymatic reaction of (R)-salsolinol synthase leading to R-Sal has been found [372, 373]. In general, both isomers have been identified in the brain, however R-form predominates, as suggested by a number of studies [374-377]. Interestingly, the occurrence of Sal is not limited to the human brain, but has also been identified in food products such as cocoa, cheese, bananas, flour, eggs, beer, milk, and fish [378-381]. This evidence shows that Sal is both an endogenous and an environmental agent. It is structurally similar to MPTP and is also metabolized to *N*-methyl-R-salsolinol and further to 1,2-dimethyl-6,7-dihydroxyisoquinolinium ion (DMDHIQ+) [382-385]. Salsolinol as well as both metabolites provide a neurotoxic effect similar to MPTP and MPP$^+$. In the context of PD pathology, Sal has been shown to have toxic effects against multiple brain cells. In particular, its higher doses are used to induce PD pathology in the SH-SY5Y, PC12 and MSC5 cell lines. The mechanism of action of the toxin is based on the inhibition of complex I [386, 387] and II [388], accompanied with ATP depletion, increased levels of Bcl-2-associated X protein (BAX) and cytochrome c release [387, 388] and endoplasmic reticulum stress-associated with TRPC1 down-regulation [389]. In addition, some studies have shown that its metabolite *N*-methyl-R-Sal is also able disrupt mitochondria by mPTP production followed by the loss of MMP [390]. Interestingly, other authors have also revealed a toxic potentiation of *N*-methyl-R-Sal in α-SYN overexpression-induced damage of PC12 cells, suggesting the involvement of tetrahydroisoquinolines in the pathology of protein aggregation [391]. However, more studies should be performed to clearly show some correlations. Sal, like its metabolites, affects mitochondria and is also known to be a potent inducer of oxidative stress by inhibitory effect towards Cu/Zn-SOD [392], catalase and the expression of glutathione peroxidases [393]. In contrast to the induction of apoptosis by *N*-methyl-R-Sal, Sal has been found to be an inducer of both apoptosis and necrosis. Interestingly, the concomitant treatment of Sal with Cu^{2+} leads to higher levels of oxidative stress and a predominance of necrotic cell death than the treatment with SAL alone [394, 395]. Overall, Sal is a suitable toxin to mimic PD pathology because

exhibits classic PD features such as oxidative stress, mitochondrial dysfunction, elevated cell death (apoptosis/necrosis), endoplasmic reticulum stress [98], and even oxidative modifications of Neurofilament-L with subsequent aggregation [396].

2.5. 3-Nitropropionic acid (3-NPA)

3-Nitropropionic acid (3-NPA) is a typical toxin used in selective damage of mitochondria and also as a mimic of Huntington's disease [77]. In cells, 3-NPA acts as a suicide substrate for complex II (succinate dehydrogenase) of the mitochondrial respiratory chain [397]. The mechanism of action of this toxin is still under investigation, and several aspects have been identified. 3-NPA-mediated inhibition of complex II leads to the loss of MPP and disruption of energy supply to neuronal cells, opening of mPTP, triggering of the intrinsic apoptotic pathway by activation of BAX and release of cytochrome c. Interestingly, BAX-deficient cells did not prevent mPTP production in mitochondria. In addition to 3-NPA-induced mitochondrial damage and oxidative stress, 3-NPA has also been shown to adversely affect glutathione biosynthesis by blocking the key enzyme glutamate-cysteine ligase, leading to a dramatic increase in oxidative stress. Interestingly, 3-NPA is a time- and dose-dependent toxin that induces biochemical changes before signs of toxicity, as evidenced by other authors [398]. In addition, autophagy as a key mediator of cell survival is strongly triggered by 3-NPA. Autophagy, together with the Nrf-2 pathway or mPTP inhibition, is thought to play an important role in inducing neuroprotective effects in this model [399, 400].

2.6. Glutamate

As mentioned in the previous section, glutamate (Glu) plays important roles in the physiology and pathology of the brain. In the case of imitation of PD or other neurodegenerative diseases, Glu can be used as an excitotoxin or a substance causing oxidative damage. Since the results of this thesis are obtained from the glutamate model on the neuron-like SH-SY5Y cell line, the mechanism of glutamate-mediated toxicity is more dedicated to the neuroblastoma cell line. The first proposed mechanism of Glu toxicity is the well-known activation of ionotrophic NMDA and AMPA receptors and metabotrophic mGlu receptor. Activated NMDA receptors, which are ion channels that allow Ca^{2+} to move inside cells. Excessive calcium influx causes an increase in neuronal nitric oxide synthase activity (nNOS), which affects mitochondria, ER stress, general cell depolarization, and organelle damage [401]. In the case of mGlu receptors,

their contribution to excitotoxity is indirectly controlled. More specially, activation of glutamate receptors mGlu 1 and 5 leads to induction of phospholipase C signalling, which increases Ca^{2+} flux from intracellular stores. Elevated intracellular calcium levels lead to activation of protein kinase C, Pyk2 and Src. Src in particular is then responsible for the phosphorylation of NMDA on tyrosine moiety. This action leads to NMDA up-regulation and increased channel permeability [402, 403]. As mentioned above, mitochondria and endoplasmic reticulum are damaged by Glu. More specifically, with pathological calcium influx, mitochondrial membrane potential (MMP) is lost, leading to the opening of mitochondrial permeability transition pores (mPTP), the up-regulation of phospholipase A2 and xanthine oxidase. Because MMP is lost, respiratory chain enzymes are inhibited. Furthermore, Glu-mediated toxicity continues to disrupt the antioxidant system by inhibiting catalase and superoxide dismutase activity and glutathione production [404, 405] resulting in increased oxidative stress and ATP loss [406]. In the latter case, the effect of Glu on the endoplasmic reticulum is modulated via over-activated AMPA receptors, leading to an increase in Ca^{2+}, followed by activation of endoplasmic ryanodine receptors (RyRs). These receptors contribute to Ca^{2+} overload, which leads to ER Ca^{2+} depletion [407]. NMDA expression is still debated in connection with the use of SH-SY5Y [401], despite the detected increase in Ca^{2+} levels after Glu administration. Some authors have suggested that calcium elevation is independent of NMDA receptors. Currently, the expression of NR1 subunit was proved [408]. On the other hand, SH-SY5Y cells express AMPA receptors[409], so that a potential effect of Glu on induction of ER stress is possible. In particular, the Glu-induced model of cell death in SH-SY5Y is driven by blockade of the cystine/glutamate antiporter, a key transporter for glutathione production from cystine. Therefore, glutathione depletion along with superoxide dismutase down-regulation, increased NADPH-oxidase, lipoxidation, and increased calcium levels has been found as key mode of action in a model using SH-SY5Y cells [102, 410, 411]. The end result is that the cells die by apoptosis [401], but also by necroptosis [411].

Materials and Methods

Materials and Instrumentation

Materials purchased from Sigma Aldrich: Dulbecco's Modified Eagle Medium/Nutrient Mixture F-12 (DMEM/F-12, D8437), penicillin, streptomycin, fetal bovine serum, trypsin, propidium iodide, dihydroethidium, *all-trans* retinoic acid, *N*-acetylcysteine, deferoxamine, cyclosporine-A, R-lipoic acid, galantamine, galactose, glucose, salsolinol hydrobromide, glutamate monosodium salt, buffer components for One-step caspase 3,7 assay, acridine orange, the mitochondrial membrane JC10 kit and cobalt (II) chloride, 3-nitropropionic acid and Ac-DEVD-CHO. Materials obtained from ThermoFisher: the neurite outgrowth kit (Invitrogen™), Calcein AM and LDH-release kit ((Pierce LDH Cytotoxicity Assay Kit) were obtained from ThermoFisher. The caspase-3,7 substrate (Ac-DEVD-AMC) was provided by Enzo Life Sciences Inc. Infinite M200 Pro reader (Tecan, Austria), DM IL LED fluorescence microscope (Leica Microsystems, Germany) with a DP73 high-performance digital camera (Olympus, Tokyo, Japan).

SH-SY5Y Cell Culture

The human neuroblastoma cell line SH-SY5Y was obtained from ATCC (American Type Culture Collection, Manassas, VA, USA) and ECACC (European Collection of Authenticated Cell Culture, Salisbury, UK). In general, cells were grown in the tissue culture treated plastic Petri dish at maximum density 80%, at 37 °C in a humidified 5% CO_2 atmosphere. For the cultivation and seeding of cells the complete medium: Dulbecco's modified Eagle's Medium and Ham's F12 Nutrient Mixture (DMEM:F-12, 1:1; Sigma Aldrich D8437), supplemented with 10% filtrated fetal bovine serum (FBS) and 1% penicillin and streptomycin was used. Only cells up to passage 20 were used for experiments. During the cultivation the media were changed twice or thrice a week.

Before the performance of experiments, the cells underwent two-phase procedure: i) seeding and ii) differentiation. First, the cells were seeded into 96-multiwell plate at densities according to type of assay (5000, 7000, 10000 and 20000 cells per well) in 100 µl total volumes of the complete culture medium in each well. The following day, 100µL of *all-trans* retinoic acid-containing 1% FBS DMEM/F12 medium was added to the cells to the final concentration of 10 µM and incubation was continued for further 48 h to induce differentiation. Such procedure results in extension of neurites, elongation of cell bodies and signs of neurite network. This phenotype was called "neuron-like SH-SY5Y cells".

Microscopy

Microscopy was used to provide the visual demonstrations or qualitative analysis as support to the oxidative stress, mPTP opening and acridine orange/propidium iodide assays, while the quantification was performed by the 96-multiwell plate reader. In general micrographs of neuron-like SH-SY5Y cells were observed under the DM IL LED fluorescence microscope (Leica Microsystems, Germany) with a DP73 high-performance digital camera (Olympus, Tokyo, Japan). The cells were recorded under brightfield setup or using appropriate excitation filters. Figures were further uniformly processed (slight adjustment of contrast) in ImageJ software (Fiji) due to moderated signal-to-noise ratio. The adjustments did not affect the resulting observations. In case of the mPTP assay, for detailed observation the region of interested (ROI) was taken.

Cell Membrane Staining (Neurite Outgrowth kit, Invitrogen™)

In order to observe full phenotypic changes of SH-SY5Y cells, the density of 5000 cells per well was used for differentiation procedure. Neuron-like SH-SY5Y cells were stained by Neurite outgrowth kit (Invitrogen™) as stated in the manufacturer's protocol at 533 and 585 nm excitation and emission wavelengths. The protocol had slight modification as described in detail here [412, 413].

Cell Treatment

Before the compounds were used for *in vitro* experiments, the stock solution (10 – 100 mM or 1M N-acetylcysteine and toxin Salsolinol - SAL) in DMSO were prepared. All stock solutions were kept at -20°C, expect 1M SAL, which was stored at -78°C. In case of glutamate, the monosodium glutamate was dissolved in 1% DMEM/F12 medium to gain 160 mM concentration and resulted solution was filtered using 0.2 μm filter. Finally, 3-NPA was properly dissolved in distilled water and neutralized by fresh NaOH solution to obtain 1M solution, which was subsequently filtered using 0.2 μm syringe filter.

Generally, the old media after differentiation were replaced by a new fresh 1% DMEM/F12 medium supplemented with test compounds (stock solution of compounds 10mM – 100mM) at concentrations of 0.1, 1 and 10 μM (with 7 000 cells per well for cytotoxicity tests), or together with the toxin SAL at 500 μM (with 7000-10000 cells per well) or 3-NPA at 20 mM (with 7000 cells per well), 160 mM Glu or 20 mM 3-NPA (with 20 000 cells per well) for an

appropriate duration for the assay type (viability, cell death etc.). The levels of DMSO in media was kept ≤0.1 %.

Cell Viability and Cell Death

Calcein AM was used for measurement of the viability of neuron-like SH-SY5Y cells seed at density 7000 cells per well after treatments. Briefly, the protocol referenced here [414] was used with adjustment of Calcein AM concentration to 0.75 μM and time 50 minutes of incubation as shown in publication I-II and IV [412, 413, 415]. The number of living cells was measured by an Infinite M200 Pro microplate reader (Tecan, Austria) with 495 and 517 nm excitation and emission wavelengths, respectively.

Complementary, the cytotoxicity assays such as PI and LDH were used. Briefly, overall cell death of neuron-like cells (SAL model: 10 000 cells per well; Glu-model: 20 000 cells per well) was quantified according to Stone et al. 2003 [416] with modifications. Briefly, with Sal-model, the treated media was aspirated and changed to a 1 μg/ml solution of PI in PBS. On the other hand cells exposed to Glu-induction or 3-NPA had weaker adherence, and thus PI solution in PBS was added directly to media to reach same concentration- 1 μg/ml solution. Cells were incubated for further 15-25 minutes at room temperature, with subsequent quantification by an Infinite M200 Pro reader (Tecan, Austria) with 535 and 617 excitation and emission wavelengths. For cytotoxicity using the LDH-release assay the commercial kit (Pierce LDH Cytotoxicity Assay Kit, ThermoFisher) was used according to manufacturer protocol. Resulting PI fluorescence or LDH absorbance of toxins was set as 100% of cell death.

Measurement of Oxidative Stress by the Dihydroethidium (DHE) Assay

The superoxide radical formation as a marker of oxidative stress was evaluated using DHE assay as used in [417]. In our case, SAL- and Glu-exposed neuron-like SH-SY5Y cells for 24 and 4 hours in 96-multiwell plates were centrifuged at 500 g for 330 s. Then the culture media were replaced (following aspiration) with 10 μM DHE solution in PBS and kept in dark for 30 minutes. Subsequently, DHE fluorescence was quantified by plate reader at 500 and 580 nm excitation and emission wavelength, respectively. Similarly, as the PI and LDH assay, DHE-stained cells of toxin groups were counted as 100% of superoxide radical formation. Additionally, micrographs of DHE-stained cells were taken for visual demonstrations.

Measurement of Caspase-3/7 Activity

For quantification of caspase 3/7, the one step caspase-3/7 assays were performed according to [418] with minor modification in Ac-DEVD-AMC concentration (75µM. Briefly, SAL-exposed cells were subjected to reaction mixture (caspase-3,7 buffer and components with cells in 96-multiwell plates) for 24 hours, while Glu-exposed cells for 1 hour of treatment. The cells were incubated for 2 h (Sal model) and 3 h (Glu model) at 37°C, respectively. Caspase-3/7 activity was quantified by a microplate reader at 346 and 438 nm excitation and emission wavelengths, respectively. Similarly to previous assays, toxin groups were set to 100% of caspase 3/7 activity.

Measurement of Mitochondrial Membrane (MMP) Potential by JC10 Assay

The effect of compounds on MMP in both models was measured by the mitochondrial membrane potential kit containing JC10 dye by manufacturer's procedure (mitochondrial membrane potential kit MAK-159, Sigma Aldrich, Merck). In experimental setup, 20 000 neuron-like cells per well were exposed to toxins (SAL model, 24 hours) and (Glu-model, 1 hour) and measured by the kit. MMP of healthy controls (DMSO vehicle) was set as 100%.

Measurement of Mitochondrial Permeability Transition Pore Opening by Calcein AM/CoCl$_2$ Assay

Mitochondrial permeability transition pore opening was quantified by the Calcein AM/CoCl$_2$ assay according to [419] with modifications. Briefly, neuron-like SH-SY5Y cells (20 000 cells/well) exposed to SAL or co-treated with the tested compounds for 24 h were centrifuged at 500 g for 330 s. Further, after the aspiration of media, a solution of 1 µM Calcein AM and 2 mM CoCl$_2$ in Hank's balanced salt solution (HBSS) was added to cells in the plate and were incubated at 37 °C for 20 min. After incubation, Calcein fluorescence intensity was measured by an Infinite M200 Pro (Tecan, Austria) by microplate reader at 488 and 517 nm excitation and emission wavelengths. The fluorescence intensity of healthy controls (DMSO control) was set as 1 (fold-increase). Additionally, fluorescence micrographs were taken as visual demonstrations of the effect of compounds.

In vitro Models of Cell Death – Acridine Orange (AO)/Propidium Iodide (PI) Double Staining

Neuron-like SH-SY5Y cells (10 000 cells/well) were treated by compounds in Sal-model as shown above for 24 hours and underwent centrifugation as described in previous sections.

Then the medium was replaced by AO (0.5 µM)/PI (1 µg/mL) PBS solution and cells were kept at r.t. for 25 min. Finally, fluorescence images were taken for visual assessment.

Statistical Analysis

All experiments were performed in triplicates and repeated in three to five (n = 3 – 5) independent days. Data are expressed as mean ± SEM. GraphPad Prism 8.4.3 was used to calculate all means ± SEM and also for graphical expression of data. Additionally, for the publication V [420] the GraphPad Prism was also used to calculate the statistical analysis – ANOVA with Tukey *post hoc* test.

The statistical analysis for publications I-IV [412, 413, 415, 421] was performed by the PAST (ver. 1.97) software package [422]. The experiments were evaluated by the Student´s t-test (differentiation of SH-SY5Y) shown in publication I [412], non-parametric Kruskal-Wallis test with Mann-Whitney *post hoc* test with sequential Bonferroni correction used here [412, 413, 415, 421]. A value of P < 0.05 was considered significant.

Survey of Published Results

In this part of the thesis, the main goal was to establish *in vitro* models of neurodegeneration and used them to identify new neuroprotective agents from various classes of compounds, such as natural cytokinins, synthetic pentacyclic triterpenes prepared by Dr. Milan Urban´s group, kinetin bioisosteres prepared in the Laboratory of Growth Regulators and also Dr. Miroslav Soural´s group and finally steroids isolated from red sea soft coral. For selected compounds, their effect was evaluated at the level of oxidative stress, caspase-3/7 activation and mitochondrial parameters (MMP and mPTP). A detailed description of the results and a discussion is included in the attached publications I-V [412, 413, 415, 420, 421].

Publication I

Gonzalez, G.; Grúz, J.; D'Acunto, C.W.; Kaňovský, P.; Strnad, M. Cytokinin Plant Hormones Have Neuroprotective Activity in In Vitro Models of Parkinson's Disease. *Molecules* 2021, *26*, 361.

Cytokinins are adenine-based phytohormones that regulate key processes in plants, such as cell division and differentiation, root and shoot growth, apical dominance, branching and seed germination. In the preliminary studies they have also shown protective activities against human neurodegenerative diseases. To extend the knowledge of the protection (protective activity) they offer, we investigated activities of natural cytokinins against salsolinol (SAL)-induced toxicity (a Parkinson's disease model) and glutamate (Glu)-induced death of neuron-like dopaminergic SH-SY5Y cells. Therefore, this study was undertaken to examine neuroprotective (anti-parkinsonian) activities of almost all known naturally occurring CKs in the selected SAL- and Glu-induced models of neurodegeneration. First, we evaluated each of the CKs' oxygen radical absorbance capacity (ORAC) and (in safety tests) cytotoxicity towards neuron-like SH-SY5Y cells. Then we evaluated the compounds' neuroprotective effects and influence on oxidative stress levels by measuring superoxide radicals production (dihydroethidium, DHE assay) and apoptotic caspase-3,7 activities. The results provide the first reported systematic indications of the relationships between natural CKs' structures and neuroprotective activities. We found that kinetin-3-glucoside, *cis*-zeatin riboside and N^6-isopentenyladenosine were active in the SAL-induced PD model. In addition, *trans*-, *cis*-zeatin and kinetin along with the iron chelator deferoxamine (DFO) and the necroptosis inhibitor

necrostatin 1 (NEC-1) significantly reduced cell death rates in the Glu-induced model. Lactate dehydrogenase assays revealed that the cytokinins provided lower neuroprotective activity than DFO and NEC-1. Moreover, they reduced apoptotic caspase-3/7 activities less strongly than DFO. However, the cytokinins had very similar effects to DFO and NEC-1 on superoxide radical production. Overall, they showed protective activity in the SAL-induced model of parkinsonian neuronal cell death and the Glu-induced model of oxidative damage mainly by reduction of oxidative stress [412].

<u>Publication II</u>

Gonzalez, G.; Hodoň, J.; Kazakova, A.; D'Acunto, C. W.; Kaňovský, P.; Urban, M.; Strnad, M., Novel pentacyclic triterpenes exhibiting strong neuroprotective activity in SH-SY5Y cells in salsolinol- and glutamate-induced neurodegeneration models. *European Journal of Medicinal Chemistry* **2021,** *213***, 113168**

Another class of compounds which was selected for evaluation of neuroprotective activity in two models of neurodegeneration on human neuron-like SH-SY5Y cells were the pentacyclic triterpenes synthetized by Dr. Milan Urban and his group from the Department of Organic Chemistry and the Institute of Molecular and Translational Medicine of Palacký University in Olomouc. Ten derivatives were first tested in the cytotoxicity assay in which compounds 5b, 8, 10 and 12 at 10µM together with cyclosporine A (CsA) at 5µM (positive control for *in vitro* models and inhibitor of mPTP formation) significantly decreased viability. Screening of all derivatives on SAL-induced model of PD resulted in identification of derivatives 3 and 4 as the most active representatives, which were even slightly better than 1000 µM *N*-acetylcysteine (NAC). Interestingly, the compounds 3 and 4 consist of a betuline scaffold bearing triazolyl-tetraacetyl-β-d-galactose substituent or triazolyl-tetraacetyl-β-D-glucose substituent. To further investigate this scaffold, the compound 10 (a betuline derivative bearing a triazole substituent), 12 (free betulinic acid) and 13 (triazolylmethanol bearing tetraacetyl-β-D-galactose) were synthetized. These substructures were tested along with free D-galactose and D-glucose. The results showed that only the derivative 10 completely protected neuronal cells from salsolinol intoxication, yet it should be noted that higher concentration was accompanied with toxicity. The identified derivatives 3, 4 and 10 also decreased levels of cell death in the Sal-model. Further study showed that both 4 and 10 reduced oxidative stress. However, more interesting results came from the measurement of the caspase-3/7 activity, in which 4 demonstrated a dose-

dependent reduction comparable to NAC, while **10** induced a dramatic inhibition equal to the nanomolar caspase-3/7 inhibitor Ac-DEVD-CHO. No inhibition was detected for CsA, indicating that CsA-mediated protection is afforded by reducing necrosis. In order to reveal the key factor of compound **4**-mediated protection, we also measured the MMP and opening of mPTP in our Sal-model, as there is some evidence of betuline-mediated blockade of mPTPs as a mechanism of hepatoprotection [423]. Interestingly, only the compound 4 together with NAC positive control were able to induce a significant dose-dependent reversion of MPP. Moreover, all derivatives blocked mPTP opening better than NAC and the mPTP inhibitor CsA. In fact, NAC showed a better blocking effect than CsA, suggesting that the primary cause of mPTP is the oxidative stress generated by salsolinol. Importantly, the effect of the compound **10** on mPTP was suggested to be responsible for its strong inhibition of caspase-3/7 activity. The derivatives **4** and **10** also showed neuroprotection in the Glu-model, with **10** exhibiting the most significant oxidative stress reducing effect among the test compounds, while the neuroprotective activity of **4** was probably due MMP recovery [413].

Publication III

Maková, B.; Mik, V.; Lišková, B.; Gonzalez, G.; Vítek, D.; Medvedíková, M.; Monfort, B.; Ručilová, V.; Kadlecová, A.; Khirsariya, P.; Gándara Barreiro, Z.; Havlíček, L.; Zatloukal, M.; Soural, M.; Paruch, K.; D'Autréaux, B.; Hajdúch, M.; Strnad, M.; Voller, J., Cytoprotective activities of kinetin purine isosteres. *Biorganic Medicinal Chemistry* **2021,** *33***, 115993.**

A panel of kinetin bioisosteres was purchased or synthetized and accurately characterised by analytical methods such as ^{1}H NMR, ^{13}C NMR, purity was determined by HPLC, by high resolution mass (HRMS) and C, H, N analysis. Their biological activity was evaluated on the *in vitro* model of GSH depletion induced by buthionine sulphoximine (BSO) on the Friedrieich's ataxia (FA) patient-derived fibroblasts and glutamate-induced (Glu-) model of oxidative damage on human neuron-like SH-SY5Y cells. From the panel of compounds, selected derivative 6 was identified as highly active against BSO-induced toxicity to FA fibroblasts. In addition, kinetin bioisosteres have been proved to be effective in correcting aberrant splicing of the *ELP1* gene in FA patient fibroblasts. In the Glu-model, the most promising scaffolds 6, 10 and 22 were identified as active, decreasing Glu toxicity to neuron-like SH-SY5Y from both cellular banks (ATCC and ECACC). These derivatives also showed

the protective effect against oxidative stress, and the selected derivative 6 reduced caspase-3/7 activity in the Glu-model. Finally, kinetin bioisosteres also displayed suitable parameters of absorption, distribution, metabolism and excretion (ADME) [421].

Publication IV

Tammam, M. A.; Rárová, L.; Kvasnicová, M.; Gonzalez, G.; Emam, A. M.; Mahdy, A.; Strnad, M.; Ioannou, E.; Roussis, V., Bioactive Steroids from the Red Sea Soft Coral Sinularia polydactyla. *Marine Drugs* **2020,** *18* **(12), 632.**

Six new and twenty already isolated steroids from soft coral *Sinularia polydactyla* collected from the Hurghada reef in the Red Sea were characterized by NMR and HPLC-MS. Furthermore, biological activities such as cytotoxicity, anti-inflammatory, anti-angiogenic, androgen receptor-regulated transcription and neuroprotective activity on 3-nitriopropionic acid-induced (3-NPA) model of Huntington's disease or mitochondrial damage of compounds 3-7, 9-12, 14-20 and 22-26 were studied. The steroids demonstrated the cytotoxic effect on HeLa and MCF7 cancer cell lines (22 and 23), inhibition of migration of endothelial cells (11, 12, 22 and 23), and inhibition of androgen receptor (11, 10, 16, 20). Steroids 11 and 23 at 10 µM did not show cytotoxic activity for neuron-like SH-SY5Y cells, while likely to increase viability and reduce cell death comparable to 100 µM *N*-acetylcysteine in the 3-NPA model on neuron-like SH-SY5Y cells [415].

Publication V

Kiełczewska, U.; Jorda, R.; Gonzalez, G.; Morzycki, J. W.; Ajani, H.; Svrčková, K.; Štěpánková, Š.; Wojtkielewicz, A., The synthesis and cholinesterase inhibitory activities of solasodine analogues with seven-membered F ring. *The Journal of Steroid Biochemistry and Molecular Biology* **2021,** *205* **, 105776.**

Thirteen derivatives with solasodine scaffold bearing seven-membered F ring with nitrogen placed at position 22a were synthetized. These compounds were evaluated for their ability to inhibit acetylcholiesterase (AChE) and butyrylcholinesterase (BChE). The inhibitory activity was found in micromolar concentrations, especially derivative 8 showed non-competitive inhibition with IC50$_{eeAChE}$ = 8.51 µM and IC50$_{eqBChE}$= 7.05 µM. Further molecular docking

study of derivative 8 with AChE revealed following interactions: hydrogen bonds with S293, stabilization of rings by hydrophobic interaction of the ring A (compound 8) or the side chain amino acids Y341 and W286 in case of the ring B and C. Finally, the biological tests demonstrated no toxic effects of compounds on differentiated SH-SY5Y cells. Moreover, the derivatives 13, 14 and 17 showed a strong neuroprotective effect against glutamate-induced oxidative damage outperforming positive controls galantamine and lipoic acid [420].

Conclusions and Perspectives

All three *in vitro* models were successfully used as tools for identification of several lead structures within all candidate groups. In addition, the protective activities of the positive controls observed in the models used are consistent with previously published results. In several cases, such as cytokinins and betuline derivatives, not much known in the literature in the field of PD research, the newly identified neuroprotective activity of these compounds opened the way to study their mechanism of actions but also design and develop new more potent analogues.

- All neuroprotective cell models have been successfully used according to published literature data.

- A large panel of cytokinins was evaluated in the salsolinol-induced (SAL-) model of PD and the glutamate-induced (Glu-) model of oxidative damage on neuron-like SH-SY5Y cells. The identified compounds with neuroprotective activities were kinetin-3-glucoside, *cis*-zeatin riboside and N^6-isopentenyladenosine (SAL-model), and *cis*-/*trans*-zeatin and kinetin (Glu-model).

- The new pentacyclic triterpenes were evaluated in the salsolinol and glutamate model, from which the two most promising compounds were selected for a further study. This research revealed that the effects caused by compound 4 was due to the protection of mitochondria, while derivative 10 showed a strong effect on caspase-3/7 activity and on the reduction of oxidative stress. Both compounds have undergone the structure-activity relationship study (SAR) and can serve as a tool for the development of the next generation of compounds.

- Among the prepared bioisosteres of kinetin, three derivatives (6, 10 and 22) showed a promising neuroprotective activity in Glu-model by reducing oxidative stress. In addition, substance 6 contributed to its significant neuroprotection by reducing the caspase-3/7 activity in the Glu-model.

- Interestingly, two steroids isolated from Red Sea soft coral *Sinularia polydactyla* increased viability and reduced cell death of neuron-like SH-SY5Y cells after 3-nitropropionic acid intoxication.

Together, the primary goal of this thesis, the identification of several neuroprotective agents within our PD models, was achieved. In addition, the selection of active compounds gave us the opportunity to study their mechanism of action in subsequent molecular biological studies. In the case of active cytokinins in particular, mechanistic studies have focused on their effects

on oxidative stress in both models. As astrocytes are the primary defence against oxidative stress for neurons, our goal in the future is to study the effects of cytokinins on astrocytes and to evaluate their mechanism of action. In the case of triterpenes, the published study gave us two leading structures, which will be studied in detail in the following works. More specifically, the following can be selected as future aims: i) reduction of undesired cytotoxicity at higher concentration (more suitable heterocycles and removal of Michael acceptor moiety), ii) modification of betulines by various sugar substitutions to make compounds more soluble and iii) the study of their mechanism of action in oxidative stress (Glu-model) and on mitochondria (Sal- and Glu-model to identify the molecular target). Finally, our *in vitro* models and several new toxin-induced models are in development: for example, the 3-nitropropinoic-induced model of death of glial A172 cells or the scopolamine-induced cognitive impairment model on U87MG-derived cholinergic neurons and on neuron-like SH-SY5Y cells, and oligomers-induced models (synuclein/amyloid-beta fragment 25-35) of PD (or Alzheimer disease) on neuron-like SH-SY5Y or U87MG-derived cholinergic neurons, respectively. We also hope that the newly discovered active substances will also be tested on more complex 3D *in vitro* models, for example on cerebral organoids also known as "minibrains".

List of Publications

I. **Gonzalez, G.**; Grúz, J.; D'Acunto, C.W.; Kaňovský, P.; Strnad, M. Cytokinin Plant Hormones Have Neuroprotective Activity in In Vitro Models of Parkinson's Disease. *Molecules* 2021, *26*, 361.

II. **Gonzalez, G.**; Hodoň, J.; Kazakova, A.; D'Acunto, C. W.; Kaňovský, P.; Urban, M.; Strnad, M., Novel pentacyclic triterpenes exhibiting strong neuroprotective activity in SH-SY5Y cells in salsolinol- and glutamate-induced neurodegeneration models. *European Journal of Medicinal Chemistry* 2021, *213*, 113168

III. Maková, B.; Mik, V.; Lišková, B.; **Gonzalez, G.**; Vítek, D.; Medvedíková, M.; Monfort, B.; Ručilová, V.; Kadlecová, A.; Khirsariya, P.; Gándara Barreiro, Z.; Havlíček, L.; Zatloukal, M.; Soural, M.; Paruch, K.; D'Autréaux, B.; Hajdúch, M.; Strnad, M.; Voller, J., Cytoprotective activities of kinetin purine isosteres. *Biorganic Medicinal Chemistry* 2021, *33*, 115993.

IV. Tammam, M. A.; Rárová, L.; Kvasnicová, M.; **Gonzalez, G.**; Emam, A. M.; Mahdy, A.; Strnad, M.; Ioannou, E.; Roussis, V., Bioactive Steroids from the Red Sea Soft Coral Sinularia polydactyla. *Marine Drugs* 2020, *18* (12), 632.

V. Kiełczewska, U.; Jorda, R.; **Gonzalez, G.**; Morzycki, J. W.; Ajani, H.; Svrčková, K.; Štěpánková, Š.; Wojtkielewicz, A., The synthesis and cholinesterase inhibitory activities of solasodine analogues with seven-membered F ring. *The Journal of Steroid Biochemistry and Molecular Biology* 2021, *205*, 105776.

Book chapter

I. Voller, J.; Maková, B.; Kadlecová, A.; **Gonzalez, G.**; Strnad, M., Plant Hormone Cytokinins for Modulating Human Aging and Age-Related Diseases. In *Hormones in Ageing and Longevity*, Rattan, S.; Sharma, R., Eds. Springer International Publishing: Cham, 2017; pp 311-335.

Contribution Report

I.   The first author – performing *in vitro* culture and neuroprotection experiments, methodology, interpretation of results, creation of graphics (graphs, figures and tables), statistical analysis and manuscript writing.

II.   The first author – performing *in vitro* culture and neuroprotection experiments, deeper cellular biology study, methodology, interpretation of results, creation of graphics (graphs, figures and tables), statistical analysis and manuscript writing.

III.   Co-author – cooperation in writing results, materials and methods (glutamate model), performing *in vitro* culture and neuroprotection experiments, methodology (glutamate model for neuron-like SH-SY5Y) and statistical analysis.

IV.   Co-author – writing results, materials and methods (3-nitropropionic acid-model), creation of figure 6A, B, C, performing *in vitro* culture and neuroprotection experiments, methodology (3-nitropropionic acid-induced model for neuron-like SH-SY5Y cell culture) and statistical analysis.

V.   Co-author – co-operation in writing results and materials, providing cell line SH-SY5Y (ECACC) with culture and treatment protocols for glutamate model, statistical analysis and creation of graphics (Figure 6).

Book chapter

I.   Co-author – co-operation in writing section "14.5. Neuroprotective Activity of Cytokinins"

References

[1]   Van Den Eeden, S. K.; Tanner, C. M.; Bernstein, A. L.; Fross, R. D.; Leimpeter, A.; Bloch, D. A.; Nelson, L. M., Incidence of Parkinson's disease: variation by age, gender, and race/ethnicity. *Am. J. Epidemiol.* **2003,** 157, (11), 1015-22.

[2]   Tysnes, O. B.; Storstein, A., Epidemiology of Parkinson's disease. *J. Neural Transm.* **2017,** 124, (8), 901-905.

[3]   de Lau, L. M. L.; Breteler, M. M. B., Epidemiology of Parkinson's disease. *The Lancet Neurology* **2006,** 5, (6), 525-535.

[4]   Wood-Kaczmar, A.; Gandhi, S.; Wood, N. W., Understanding the molecular causes of Parkinson's disease. *Trends Mol. Med.* **2006,** 12, (11), 521-8.

[5]   Dorsey, E. R.; Sherer, T.; Okun, M. S.; Bloem, B. R., The Emerging Evidence of the Parkinson Pandemic. *J. Parkinsons Dis.* **2018,** 8, (s1), S3-S8.

[6]   Dorsey, E. R.; Elbaz, A.; Nichols, E.; Abd-Allah, F.; Abdelalim, A.; Adsuar, J. C.; Ansha, M. G.; Brayne, C.; Choi, J.-Y. J.; Collado-Mateo, D.; Dahodwala, N.; Do, H. P.; Edessa, D.; Endres, M.; Fereshtehnejad, S.-M.; Foreman, K. J.; Gankpe, F. G.; Gupta, R.; Hankey, G. J.; Hay, S. I.; Hegazy, M. I.; Hibstu, D. T.; Kasaeian, A.; Khader, Y.; Khalil, I.; Khang, Y.-H.; Kim, Y. J.; Kokubo, Y.; Logroscino, G.; Massano, J.; Mohamed Ibrahim, N.; Mohammed, M. A.; Mohammadi, A.; Moradi-Lakeh, M.; Naghavi, M.; Nguyen, B. T.; Nirayo, Y. L.; Ogbo, F. A.; Owolabi, M. O.; Pereira, D. M.; Postma, M. J.; Qorbani, M.; Rahman, M. A.; Roba, K. T.; Safari, H.; Safiri, S.; Satpathy, M.; Sawhney, M.; Shafieesabet, A.; Shiferaw, M. S.; Smith, M.; Szoeke, C. E. I.; Tabarés-Seisdedos, R.; Truong, N. T.; Ukwaja, K. N.; Venketasubramanian, N.; Villafaina, S.; weldegwergs, K. g.; Westerman, R.; Wijeratne, T.; Winkler, A. S.; Xuan, B. T.; Yonemoto, N.; Feigin, V. L.; Vos, T.; Murray, C. J. L., Global, regional, and national burden of Parkinson's disease, 1990-2016: a systematic analysis for the Global Burden of Disease Study 2016. *The Lancet Neurology* **2018,** 17, (11), 939-953.

[7]   Jankovic, J., Parkinson's disease: clinical features and diagnosis. *J. Neurol. Neurosurg. Psychiatry* **2008,** 79, (4), 368-76.

[8]   Alexander, G. E., Biology of Parkinson's disease: pathogenesis and pathophysiology of a multisystem neurodegenerative disorder. *Dialogues Clin. Neurosci.* **2004,** 6, (3), 259-80.

[9]   Berardelli, A.; Rothwell, J. C.; Thompson, P. D.; Hallett, M., Pathophysiology of bradykinesia in Parkinson's disease. *Brain* **2001,** 124, (Pt 11), 2131-46.

[10]   Armstrong, M. J.; Okun, M. S., Diagnosis and Treatment of Parkinson Disease: A Review. *JAMA* **2020,** 323, (6), 548-560.

[11]   Giguère, N.; Burke Nanni, S.; Trudeau, L. E., On Cell Loss and Selective Vulnerability of Neuronal Populations in Parkinson's Disease. *Front. Neurol.* **2018,** 9, 455.

[12]   Albin, R. L.; Young, A. B.; Penney, J. B., The functional anatomy of basal ganglia disorders. *Trends Neurosci.* **1989,** 12, (10), 366-375.

[13]   DeLong, M. R., Primate models of movement disorders of basal ganglia origin. *Trends Neurosci.* **1990,** 13, (7), 281-285.

[14]   Gerfen, C. R.; Engber, T. M.; Mahan, L. C.; Susel, Z.; Chase, T. N.; Monsma, F. J.; Sibley, D. R., D1 and D2 dopamine receptor-regulated gene expression of striatonigral and striatopallidal neurons. *Science* **1990,** 250, (4986), 1429-1432.

[15]   Surmeier, D. J.; Song, W.-J.; Yan, Z., Coordinated expression of dopamine receptors in neostriatal medium spiny neurons. *J. Neurosci.* **1996,** 16, (20), 6579-6591.

[16]   Gertler, T. S.; Chan, C. S.; Surmeier, D. J., Dichotomous anatomical properties of adult striatal medium spiny neurons. *J. Neurosci.* **2008,** 28, (43), 10814-10824.

[17]   Beiser, D. G.; Hua, S. E.; Houk, J. C., Network models of the basal ganglia. *Curr. Opin. Neurobiol.* **1997,** 7, (2), 185-190.

[18]   Gillespie, R. J.; Bamford, S. J.; Botting, R.; Comer, M.; Denny, S.; Gaur, S.; Griffin, M.; Jordan, A. M.; Knight, A. R.; Lerpiniere, J.; Leonardi, S.; Lightowler, S.; McAteer, S.; Merrett, A.; Misra, A.; Padfield, A.; Reece, M.; Saadi, M.; Selwood, D. L.; Stratton, G. C.; Surry, D.; Todd, R.; Tong, X.; Ruston, V.; Upton, R.; Weiss, S. M., Antagonists of the Human A2A Adenosine Receptor. 4. Design, Synthesis, and Preclinical Evaluation of 7-Aryltriazolo[4,5-d]pyrimidines. *J. Med. Chem.* **2009,** 52, (1), 33-47.

[19]   Armentero, M. T.; Pinna, A.; Ferre, S.; Lanciego, J. L.; Muller, C. E.; Franco, R., Past, present and future of A(2A) adenosine receptor antagonists in the therapy of Parkinson's disease. *Pharmacol. Ther.* **2011,** 132, (3), 280-99.

[20]   Abercrombie ED, Z. M., Modification of Central Catecholaminergic Systems by Stress and Injury In *Psychopharmacology: the fourth generation of progress*, Bloom EJ, K. D., Ed. New York:Raven Pres: 1995; pp 355–362.

[21]   Zigmond, M. J., Chemical transmission in the brain: homeostatic regulation and its functional implications. *Prog. Brain Res.* **1994,** 100, 115-22.

[22]   Zigmond, M. J.; Berger, T. W.; Grace, A. A.; Stricker, E. M., Compensatory responses to nigrostriatal bundle injury. *Mol. Chem. Neuropathol.* **1989,** 10, (3), 185-200.

[23]   Ascherio, A.; Schwarzschild, M. A., The epidemiology of Parkinson's disease: risk factors and prevention. *The Lancet Neurology* **2016,** 15, (12), 1257-1272.

[24]   parkinson.org Types of Parkinsonisms. https://www.parkinsons.org.uk/information-and-support/types-parkinsonism (3/2019),

[25]   Polymeropoulos, M. H.; Lavedan, C.; Leroy, E.; Ide, S. E.; Dehejia, A.; Dutra, A.; Pike, B.; Root, H.; Rubenstein, J.; Boyer, R.; Stenroos, E. S.; Chandrasekharappa, S.; Athanassiadou, A.; Papapetropoulos, T.; Johnson, W. G.; Lazzarini, A. M.; Duvoisin, R. C.; Di Iorio, G.; Golbe, L. I.; Nussbaum, R. L., Mutation in the α-Synuclein Gene Identified in Families with Parkinson's Disease. *Science* **1997,** 276, (5321), 2045-2047.

[26]   Espay, A. J.; Vizcarra, J. A.; Marsili, L.; Lang, A. E.; Simon, D. K.; Merola, A.; Josephs, K. A.; Fasano, A.; Morgante, F.; Savica, R.; Greenamyre, J. T.; Cambi, F.; Yamasaki, T. R.; Tanner, C. M.; Gan-Or, Z.; Litvan, I.; Mata, I. F.; Zabetian, C. P.; Brundin, P.; Fernandez, H. H.; Standaert, D. G.; Kauffman, M. A.; Schwarzschild, M. A.; Sardi, S. P.; Sherer, T.; Perry, G.; Leverenz, J. B., Revisiting protein aggregation as pathogenic in sporadic Parkinson and Alzheimer diseases. *Neurology* **2019,** 92, (7), 329.

[27]   Singleton, A. B.; Farrer, M.; Johnson, J.; Singleton, A.; Hague, S.; Kachergus, J.; Hulihan, M.; Peuralinna, T.; Dutra, A.; Nussbaum, R.; Lincoln, S.; Crawley, A.; Hanson, M.; Maraganore, D.; Adler, C.; Cookson, M. R.; Muenter, M.; Baptista, M.; Miller, D.; Blancato, J.; Hardy, J.; Gwinn-Hardy, K., α-Synuclein Locus Triplication Causes Parkinson's Disease. *Science* **2003,** 302, (5646), 841.

[28]   Tan, E. K.; Khajavi, M.; Thornby, J. I.; Nagamitsu, S.; Jankovic, J.; Ashizawa, T., Variability and validity of polymorphism association studies in Parkinson's disease. *Neurology* **2000,** 55, (4), 533.

[29]   Kalia, L. V., Diagnostic biomarkers for Parkinson's disease: focus on α-synuclein in cerebrospinal fluid. *Parkinsonism Relat. Disord.* **2019,** 59, 21-25.

[30]   Jankovic, J.; Tan, E. K., Parkinson's disease: etiopathogenesis and treatment. *Journal of Neurology, Neurosurgery & Psychiatry* **2020,** 91, (8), 795-808.

[31]   Chauhan, A.; Jeans, A. F., Is Parkinson's Disease Truly a Prion-Like Disorder? An Appraisal of Current Evidence. *Neurol. Res. Int.* **2015,** 2015, 345285.

[32]   Kim, W. S.; Kågedal, K.; Halliday, G. M., Alpha-synuclein biology in Lewy body diseases. *Alzheimers Res. Ther.* **2014,** 6, (5), 73.

[33]   Stefanis, L., α-Synuclein in Parkinson's disease. *Cold Spring Harb. Perspect. Med.* **2012,** 2, (2), a009399.

[34]   Gomperts, S. N.; Locascio, J. J.; Rentz, D.; Santarlasci, A.; Marquie, M.; Johnson, K. A.; Growdon, J. H., Amyloid is linked to cognitive decline in patients with Parkinson disease without dementia. *Neurology* **2013,** 80, (1), 85-91.

[35]   Marques, O.; Outeiro, T. F., Alpha-synuclein: from secretion to dysfunction and death. *Cell Death Dis.* **2012,** 3, (7), e350-e350.

[36]   Anna, O.; Wojciech, K.; Margarita, L.; Jolanta, D., Mutations in PRKN and SNCA Genes Important for the Progress of Parkinson's Disease. *Curr. Genomics* **2013,** 14, (8), 502-517.

[37]   Deng, H.; Wang, P.; Jankovic, J., The genetics of Parkinson disease. *Ageing Research Reviews* **2018,** 42, 72-85.

[38]   Blauwendraat, C.; Nalls, M. A.; Singleton, A. B., The genetic architecture of Parkinson's disease. *Lancet Neurol.* **2020,** 19, (2), 170-178.

[39]   Chan, N. C.; Salazar, A. M.; Pham, A. H.; Sweredoski, M. J.; Kolawa, N. J.; Graham, R. L. J.; Hess, S.; Chan, D. C., Broad activation of the ubiquitin–proteasome system by Parkin is critical for mitophagy. *Hum. Mol. Genet.* **2011,** 20, (9), 1726-1737.

[40]   Schlossmacher, M. G.; Frosch, M. P.; Gai, W. P.; Medina, M.; Sharma, N.; Forno, L.; Ochiishi, T.; Shimura, H.; Sharon, R.; Hattori, N.; Langston, J. W.; Mizuno, Y.; Hyman, B. T.; Selkoe, D. J.; Kosik, K. S., Parkin Localizes to the Lewy Bodies of Parkinson Disease and Dementia with Lewy Bodies. *Am. J. Pathol.* **2002,** 160, (5), 1655-1667.

[41]   Shimura, H.; Hattori, N.; Kubo, S.-i.; Mizuno, Y.; Asakawa, S.; Minoshima, S.; Shimizu, N.; Iwai, K.; Chiba, T.; Tanaka, K.; Suzuki, T., Familial Parkinson disease gene product, parkin, is a ubiquitin-protein ligase. *Nat. Genet.* **2000,** 25, (3), 302-305.

[42]   Shimura, H.; Schlossmacher, M. G.; Hattori, N.; Frosch, M. P.; Trockenbacher, A.; Schneider, R.; Mizuno, Y.; Kosik, K. S.; Selkoe, D. J., Ubiquitination of a new form of alpha-synuclein by parkin from human brain: implications for Parkinson's disease. *Science* **2001,** 293, (5528), 263.

[43]   Dauer, W.; Przedborski, S., Parkinson's Disease: Mechanisms and Models. *Neuron* **2003,** 39, (6), 889-909.

[44]   Ariga, H.; Takahashi-Niki, K.; Kato, I.; Maita, H.; Niki, T.; Iguchi-Ariga, S. M. M., Neuroprotective Function of DJ-1 in Parkinson's Disease. *Oxid. Med. Cell. Longev.* **2013,** 2013, 683920.

[45]   Canet-Avilés, R. M.; Wilson, M. A.; Miller, D. W.; Ahmad, R.; McLendon, C.; Bandyopadhyay, S.; Baptista, M. J.; Ringe, D.; Petsko, G. A.; Cookson, M. R., The Parkinson's disease protein DJ-1 is neuroprotective due to cysteine-sulfinic acid-driven mitochondrial localization. *Proc. Nat. Acad. Sci.* **2004,** 101, (24), 9103.

[46]   Cardinale, A.; Chiesa, R.; Sierks, M., Protein Misfolding and Neurodegenerative Diseases. *Int. J. Cell Biol.* **2014,** 2014, 217371.

[47]   Ibáñez, C. F.; Andressoo, J.-O., Biology of GDNF and its receptors — Relevance for disorders of the central nervous system. *Neurobiol. Dis.* **2017,** 97, 80-89.

[48]   Bonifati, V.; Rizzu, P.; van Baren, M. J.; Schaap, O.; Breedveld, G. J.; Krieger, E.; Dekker, M. C.; Squitieri, F.; Ibanez, P.; Joosse, M.; van Dongen, J. W.; Vanacore, N.; van Swieten, J. C.; Brice, A.; Meco, G.; van Duijn, C. M.; Oostra, B. A.; Heutink, P., Mutations in the DJ-1 gene associated with autosomal recessive early-onset parkinsonism. *Science* **2003,** 299, (5604), 256-9.

[49]   Niu, J.; Yu, M.; Wang, C.; Xu, Z., Leucine-rich repeat kinase 2 disturbs mitochondrial dynamics via Dynamin-like protein. *J. Neurochem.* **2012,** 122, (3), 650-8.

[50]   Chan, S. L.; Tan, E.-K., Targeting LRRK2 in Parkinson's disease: an update on recent developments. *Expert Opin. Ther. Targets* **2017,** 21, (6), 601-610.

[51]   Balestrino, R.; Schapira, A. H. V., Parkinson disease. *Eur. J. Neurol.* **2020,** 27, (1), 27-42.

[52] Klein, C.; Westenberger, A., Genetics of Parkinson's Disease. *Cold Spring Harb. Perspect. Med.* **2012,** 2, (1).

[53] Chahine, L. M.; Qiang, J.; Ashbridge, E.; Minger, J.; Yearout, D.; Horn, S.; Colcher, A.; Hurtig, H. I.; Lee, V. M. Y.; Van Deerlin, V. M.; Leverenz, J. B.; Siderowf, A. D.; Trojanowski, J. Q.; Zabetian, C. P.; Chen-Plotkin, A., Clinical and Biochemical Differences in Patients Having Parkinson Disease With vs Without GBA Mutations. *JAMA Neurology* **2013,** 70, (7), 852-858.

[54] Sidransky, E.; Nalls, M. A.; Aasly, J. O.; Aharon-Peretz, J.; Annesi, G.; Barbosa, E. R.; Bar-Shira, A.; Berg, D.; Bras, J.; Brice, A.; Chen, C. M.; Clark, L. N.; Condroyer, C.; De Marco, E. V.; Dürr, A.; Eblan, M. J.; Fahn, S.; Farrer, M. J.; Fung, H. C.; Gan-Or, Z.; Gasser, T.; Gershoni-Baruch, R.; Giladi, N.; Griffith, A.; Gurevich, T.; Januario, C.; Kropp, P.; Lang, A. E.; Lee-Chen, G. J.; Lesage, S.; Marder, K.; Mata, I. F.; Mirelman, A.; Mitsui, J.; Mizuta, I.; Nicoletti, G.; Oliveira, C.; Ottman, R.; Orr-Urtreger, A.; Pereira, L. V.; Quattrone, A.; Rogaeva, E.; Rolfs, A.; Rosenbaum, H.; Rozenberg, R.; Samii, A.; Samaddar, T.; Schulte, C.; Sharma, M.; Singleton, A.; Spitz, M.; Tan, E. K.; Tayebi, N.; Toda, T.; Troiano, A. R.; Tsuji, S.; Wittstock, M.; Wolfsberg, T. G.; Wu, Y. R.; Zabetian, C. P.; Zhao, Y.; Ziegler, S. G., Multicenter Analysis of Glucocerebrosidase Mutations in Parkinson's Disease. *New Engl. J. Med.* **2009,** 361, (17), 1651-1661.

[55] Velayati, A.; Yu, W. H.; Sidransky, E., The Role of Glucocerebrosidase Mutations in Parkinson Disease and Lewy Body Disorders. *Curr. Neurol. Neurosci. Rep.* **2010,** 10, (3), 190-198.

[56] Wu, H.-Y.; Chen, S.-F.; Hsieh, J.-Y.; Chou, F.; Wang, Y.-H.; Lin, W.-T.; Lee, P.-Y.; Yu, Y.-J.; Lin, L.-Y.; Lin, T.-S.; Lin, C.-L.; Liu, G.-Y.; Tzeng, S.-R.; Hung, H.-C.; Chan, N.-L., Structural basis of antizyme-mediated regulation of polyamine homeostasis. *Proc. Nat. Acad. Sci.* **2015,** 112, (36), 11229.

[57] Dias, V.; Junn, E.; Mouradian, M. M., The role of oxidative stress in Parkinson's disease. *J. Parkinsons Dis.* **2013,** 3, (4), 461-491.

[58] Huot, P.; Sgambato-Faure, V.; Fox, S. H.; McCreary, A. C., Serotonergic Approaches in Parkinson's Disease: Translational Perspectives, an Update. *ACS Chem. Neurosci.* **2017,** 8, (5), 973-986.

[59] Ansah, T. A.; Ferguson, M. C.; Nayyar, T.; Deutch, A. Y., Age- and duration-dependent effects of MPTP on cortical serotonin systems. *Neurosci. Lett.* **2011,** 504, (2), 160-164.

[60] Maiti, P.; Gregg, L. C.; McDonald, M. P., MPTP-induced executive dysfunction is associated with altered prefrontal serotonergic function. *Behav. Brain Res.* **2016,** 298, 192-201.

[61] Tan, S. K. H.; Hartung, H.; Sharp, T.; Temel, Y., Serotonin-dependent depression in Parkinson's disease: A role for the subthalamic nucleus? *Neuropharmacology* **2011,** 61, (3), 387-399.

[62] Sánchez, M. G.; Morissette, M.; Di Paolo, T., Estradiol and brain serotonin reuptake transporter in long-term ovariectomized parkinsonian monkeys. *Prog. Neuro-Psychopharmacol. Biol. Psychiatry* **2013,** 45, 170-177.

[63] Doder, M.; Rabiner, E. A.; Turjanski, N.; Lees, A. J.; Brooks, D. J., Tremor in Parkinson's disease and serotonergic dysfunction. *Neurology* **2003,** 60, (4), 601.

[64] Haapaniemi, T. H.; Ahonen, A.; Torniainen, P.; Sotaniemi, K. A.; Myllylä, V. V., [123I]β-CIT SPECT demonstrates decreased brain dopamine and serotonin transporter levels in untreated parkinsonian patients. *Mov. Disord.* **2001,** 16, (1), 124-130.

[65] Guttman, M.; Boileau, I.; Warsh, J.; Saint-Cyr, J. A.; Ginovart, N.; McCluskey, T.; Houle, S.; Wilson, A.; Mundo, E.; Rusjan, P.; Meyer, J.; Kish, S. J., Brain serotonin transporter binding in non-depressed patients with Parkinson's disease. *Eur. J. Neurol.* **2007,** 14, (5), 523-528.

[66] Liu, A. K. L.; Chang, R. C.-C.; Pearce, R. K. B.; Gentleman, S. M., Nucleus basalis of Meynert revisited: anatomy, history and differential involvement in Alzheimer's and Parkinson's disease. *Acta Neuropathol.* **2015,** 129, (4), 527-540.

[67] Tagliavini, F.; Pilleri, G., Basal nucleus of meynert: A neuropathological study in Alzheimer's disease, simple senile dementia, Pick's disease and Huntington's chorea. *J. Neurol. Sci.* **1983,** 62, (1), 243-260.

[68] Liu, A. K.; Chang, R. C.; Pearce, R. K.; Gentleman, S. M., Nucleus basalis of Meynert revisited: anatomy, history and differential involvement in Alzheimer's and Parkinson's disease. *Acta Neuropathol.* **2015,** 129, (4), 527-40.

[69] Allaman, I.; Bélanger, M.; Magistretti, P. J., Astrocyte-neuron metabolic relationships: for better and for worse. *Trends Neurosci.* **2011,** 34, (2), 76-87.

[70] Hurley, M. J.; Brandon, B.; Gentleman, S. M.; Dexter, D. T., Parkinson's disease is associated with altered expression of CaV1 channels and calcium-binding proteins. *Brain* **2013,** 136, (7), 2077-2097.

[71] Błaszczyk, J. W., Parkinson's Disease and Neurodegeneration: GABA-Collapse Hypothesis. *Front. Neurosci.* **2016,** 10, 269.

[72] Rodriguez, M.; Obeso, J.; Olanow, C. W., Subthalamic nucleus-mediated excitotoxicity in Parkinson's disease: a target for neuroprotection. *Ann. Neurol.* **1998,** 44, (S1 1), S175-S188.

[73] Dong, X.-x.; Wang, Y.; Qin, Z.-h., Molecular mechanisms of excitotoxicity and their relevance to pathogenesis of neurodegenerative diseases. *Acta Pharmacol. Sin.* **2009,** 30, (4), 379-387.

[74] Mark, L. P.; Prost, R. W.; Ulmer, J. L.; Smith, M. M.; Daniels, D. L.; Strottmann, J. M.; Brown, W. D.; Hacein-Bey, L., Pictorial review of glutamate excitotoxicity: fundamental concepts for neuroimaging. *Am. J. Neuroradiol.* **2001,** 22, (10), 1813-1824.

[75] Perier, C.; Vila, M., Mitochondrial biology and Parkinson's disease. *Cold Spring Harb. Perspect. Med.* **2012,** 2, (2), a009332.

[76] Bjørling-Poulsen, M.; Andersen, H. R.; Grandjean, P., Potential developmental neurotoxicity of pesticides used in Europe. *Environ. Health* **2008,** 7, (1), 1-22.

[77] Bové, J.; Prou, D.; Perier, C.; Przedborski, S., Toxin-induced models of Parkinson's disease. *NeuroRx* **2005,** 2, (3), 484-94.

[78] Iovino, L.; Tremblay, M. E.; Civiero, L., Glutamate-induced excitotoxicity in Parkinson's disease: The role of glial cells. *J. Pharmacol. Sci.* **2020,** 144, (3), 151-164.

[79] Jones, D. P., Radical-free biology of oxidative stress. *American Journal of Physiology-Cell Physiology* **2008,** 295, (4), C849-C868.

[80] Pisoschi, A. M.; Pop, A., The role of antioxidants in the chemistry of oxidative stress: A review. *Eur. J. Med. Chem.* **2015,** 97, 55-74.

[81] Dias, V.; Junn, E.; Mouradian, M. M., The role of oxidative stress in Parkinson's disease. *J. Parkinsons Dis.* **2013,** 3, (4), 461-91.

[82] Hirsch, E. C.; Hunot, S., Neuroinflammation in Parkinson's disease: a target for neuroprotection? *Lancet Neurol.* **2009,** 8, (4), 382-97.

[83] Venkateshappa, C.; Harish, G.; Mythri, R. B.; Mahadevan, A.; Bharath, M. S.; Shankar, S., Increased oxidative damage and decreased antioxidant function in aging human substantia nigra compared to striatum: implications for Parkinson's disease. *Neurochem. Res.* **2012,** 37, (2), 358-369.

[84] Liberatore, G. T.; Jackson-Lewis, V.; Vukosavic, S.; Mandir, A. S.; Vila, M.; McAuliffe, W. G.; Dawson, V. L.; Dawson, T. M.; Przedborski, S., Inducible nitric oxide synthase stimulates dopaminergic neurodegeneration in the MPTP model of Parkinson disease. *Nat. Med.* **1999,** 5, (12), 1403-9.

[85] Gao, H.-M.; Liu, B.; Zhang, W.; Hong, J.-S., Critical role of microglial NADPH oxidase-derived free radicals in the in vitro MPTP model of Parkinson's disease. *The FASEB Journal* **2003,** 17, (13), 1-22.

[86] Choi, D.-K.; Pennathur, S.; Perier, C.; Tieu, K.; Teismann, P.; Wu, D.-C.; Jackson-Lewis, V.; Vila, M.; Vonsattel, J.-P.; Heinecke, J. W., Ablation of the inflammatory enzyme myeloperoxidase mitigates features of Parkinson's disease in mice. *J. Neurosci.* **2005,** 25, (28), 6594-6600.

[87] Chalimoniuk, M.; Lukacova, N.; Marsala, J.; Langfort, J., Alterations of the expression and activity of midbrain nitric oxide synthase and soluble guanylyl cyclase in 1-methyl-4-phenyl-1, 2, 3, 6-tetrahydropyridine-induced Parkinsonism in mice. *Neuroscience* **2006,** 141, (2), 1033-1046.

[88] Zhou, C.; Huang, Y.; Przedborski, S., Oxidative stress in Parkinson's disease: a mechanism of pathogenic and therapeutic significance. *Ann. N. Y. Acad. Sci.* **2008,** 1147, 93.

[89] Maki, R. A.; Holzer, M.; Motamedchaboki, K.; Malle, E.; Masliah, E.; Marsche, G.; Reynolds, W. F., Human myeloperoxidase (hMPO) is expressed in neurons in the substantia nigra in Parkinson's disease and in the hMPO-α-synuclein-A53T mouse model, correlating with increased nitration and aggregation of α-synuclein and exacerbation of motor impairment. *Free Radical Biol. Med.* **2019,** 141, 115-140.

[90] Wu, D.-C.; Teismann, P.; Tieu, K.; Vila, M.; Jackson-Lewis, V.; Ischiropoulos, H.; Przedborski, S., NADPH oxidase mediates oxidative stress in the 1-methyl-4-phenyl-1, 2, 3, 6-tetrahydropyridine model of Parkinson's disease. *Proc. Nat. Acad. Sci.* **2003,** 100, (10), 6145-6150.

[91] Luo, S.; Kang, S. S.; Wang, Z.-H.; Liu, X.; Day, J. X.; Wu, Z.; Peng, J.; Xiang, D.; Springer, W.; Ye, K., Akt phosphorylates NQO1 and triggers its degradation, abolishing its antioxidative activities in Parkinson's disease. *J. Neurosci.* **2019,** 39, (37), 7291-7305.

[92] Sharma, N.; Rao, S. P.; Kalivendi, S. V., The deglycase activity of DJ-1 mitigates α-synuclein glycation and aggregation in dopaminergic cells: Role of oxidative stress mediated downregulation of DJ-1 in Parkinson's disease. *Free Radical Biol. Med.* **2019,** 135, 28-37.

[93] Russo, I.; Kaganovich, A.; Ding, J.; Landeck, N.; Mamais, A.; Varanita, T.; Biosa, A.; Tessari, I.; Bubacco, L.; Greggio, E., Transcriptome analysis of LRRK2 knock-out microglia cells reveals alterations of inflammatory-and oxidative stress-related pathways upon treatment with α-synuclein fibrils. *Neurobiol. Dis.* **2019,** 129, 67-78.

[94] Kurosaki, H.; Yamaguchi, K.; Man-Yoshi, K.; Muramatsu, S.-i.; Hara, S.; Ichinose, H., Administration of tetrahydrobiopterin restored the decline of dopamine in the striatum induced by an acute action of MPTP. *Neurochem. Int.* **2019,** 125, 16-24.

[95] Chew, K. C.; Ang, E.-T.; Tai, Y. K.; Tsang, F.; Lo, S. Q.; Ong, E.; Ong, W.-Y.; Shen, H.-M.; Lim, K.-L.; Dawson, V. L., Enhanced autophagy from chronic toxicity of iron and mutant A53T α-synuclein: implications for neuronal cell death in Parkinson disease. *J. Biol. Chem.* **2011,** 286, (38), 33380-33389.

[96] Tenkorang, M. A.; Duong, P.; Cunningham, R. L., NADPH Oxidase Mediates Membrane Androgen Receptor–Induced Neurodegeneration. *Endocrinology* **2019,** 160, (4), 947-963.

[97] Hare, D. J.; Double, K. L., Iron and dopamine: a toxic couple. *Brain* **2016,** 139, (Pt 4), 1026-35.

[98] Kurnik-Łucka, M.; Panula, P.; Bugajski, A.; Gil, K., Salsolinol: an Unintelligible and Double-Faced Molecule—Lessons Learned from In Vivo and In Vitro Experiments. *Neurotox. Res.* **2018,** 33, (2), 485-514.

[99] Johnson, J. A.; Johnson, D. A.; Kraft, A. D.; Calkins, M. J.; Jakel, R. J.; Vargas, M. R.; Chen, P. C., The Nrf2-ARE pathway: an indicator and modulator of oxidative stress in neurodegeneration. *Ann. N. Y. Acad. Sci.* **2008,** 1147, 61-9.

[100] Tufekci, K. U.; Bayin, E.; Genc, S.; Genc, K., The Nrf2/ARE Pathway: A Promising Target to Counteract Mitochondrial Dysfunction in Parkinson's Disease. *Parkinsons Dis.* **2011,** 2011, 314082.

[101] Belarbi, K.; Cuvelier, E.; Destée, A.; Gressier, B.; Chartier-Harlin, M.-C., NADPH oxidases in Parkinson's disease: a systematic review. *Mol. Neurodegener.* **2017,** 12, (1), 84.

[102] Nikolova, S.; Lee, Y. S.; Lee, Y.-S.; Kim, J.-a., Rac1-NADPH oxidase-regulated generation of reactive oxygen species mediates glutamate-induced apoptosis in SH-SY5Y human neuroblastoma cells. *Free Radical Res.* **2005,** 39, (12), 1295-1304.

[103] Chung, Y. C.; Bok, E.; Huh, S. H.; Park, J.-Y.; Yoon, S.-H.; Kim, S. R.; Kim, Y.-S.; Maeng, S.; Park, S. H.; Jin, B. K., Cannabinoid receptor type 1 protects nigrostriatal dopaminergic neurons against MPTP neurotoxicity by inhibiting microglial activation. *J. Immunol.* **2011,** 187, (12), 6508-6517.

[104] Heneka, M. T.; Feinstein, D. L., Expression and function of inducible nitric oxide synthase in neurons. *J. Neuroimmunol.* **2001,** 114, (1-2), 8-18.

[105] Ghafourifar, P.; Colton, C. A., Mitochondria and nitric oxide. Mary Ann Liebert, Inc.: 2003.

[106] Yao, D.; Gu, Z.; Nakamura, T.; Shi, Z.-Q.; Ma, Y.; Gaston, B.; Palmer, L. A.; Rockenstein, E. M.; Zhang, Z.; Masliah, E., Nitrosative stress linked to sporadic Parkinson's disease: S-nitrosylation of parkin regulates its E3 ubiquitin ligase activity. *Proc. Nat. Acad. Sci.* **2004,** 101, (29), 10810-10814.

[107] Kavya, R.; Saluja, R.; Singh, S.; Dikshit, M., Nitric oxide synthase regulation and diversity: implications in Parkinson's disease. *Nitric Oxide* **2006,** 15, (4), 280-294.

[108] Rathnayake, D.; Chang, T.; Udagama, P., Selected serum cytokines and nitric oxide as potential multi-marker biosignature panels for Parkinson disease of varying durations: a case-control study. *BMC Neurol.* **2019,** 19, (1), 56.

[109] Yeung, P. K.; Lai, A. K.; Son, H. J.; Zhang, X.; Hwang, O.; Chung, S. S.; Chung, S. K., Aldose reductase deficiency leads to oxidative stress-induced dopaminergic neuronal loss and autophagic abnormality in an animal model of Parkinson's disease. *Neurobiol. Aging* **2017,** 50, 119-133.

[110] Liberatore, G. T.; Jackson-Lewis, V.; Vukosavic, S.; Mandir, A. S.; Vila, M.; McAuliffe, W. G.; Dawson, V. L.; Dawson, T. M.; Przedborski, S., Inducible nitric oxide synthase stimulates dopaminergic neurodegeneration in the MPTP model of Parkinson disease. *Nat. Med.* **1999,** 5, (12), 1403-1409.

[111] Beckman, J. S.; Koppenol, W. H., Nitric oxide, superoxide, and peroxynitrite: the good, the bad, and ugly. *American Journal of Physiology-Cell Physiology* **1996,** 271, (5), C1424-C1437.

[112] Halliwell, B.; Gutteridge, J. M., [1] Role of free radicals and catalytic metal ions in human disease: an overview. *Methods Enzymol.* **1990,** 186, 1-85.

[113] Dehmer, T.; Lindenau, J.; Haid, S.; Dichgans, J.; Schulz, J. B., Deficiency of inducible nitric oxide synthase protects against MPTP toxicity in vivo. *J. Neurochem.* **2000,** 74, (5), 2213-2216.

[114] Hirsch, E. C.; Vyas, S.; Hunot, S., Neuroinflammation in Parkinson's disease. *Parkinsonism Relat. Disord.* **2012,** 18, S210-S212.

[115] Damier, P.; Kastner, A.; Agid, Y.; Hirsch, E. C., Does monoamine oxidase type B play a role in dopaminergic nerve cell death in Parkinson's disease? *Neurology* **1996,** 46, (5), 1262-1262.

[116] Ward, R. J.; Zucca, F. A.; Duyn, J. H.; Crichton, R. R.; Zecca, L., The role of iron in brain ageing and neurodegenerative disorders. *Lancet Neurol.* **2014,** 13, (10), 1045-60.

[117] Bilgic, B.; Pfefferbaum, A.; Rohlfing, T.; Sullivan, E. V.; Adalsteinsson, E., MRI estimates of brain iron concentration in normal aging using quantitative susceptibility mapping. *NeuroImage* **2012,** 59, (3), 2625-35.

[118] Ayton, S.; Lei, P.; Hare, D. J.; Duce, J. A.; George, J. L.; Adlard, P. A.; McLean, C.; Rogers, J. T.; Cherny, R. A.; Finkelstein, D. I., Parkinson's disease iron deposition caused by nitric oxide-induced loss of β-amyloid precursor protein. *J. Neurosci.* **2015,** 35, (8), 3591-3597.

[119] Fasano, M.; Bergamasco, B.; Lopiano, L., Is neuromelanin changed in Parkinson's disease? Investigations by magnetic spectroscopies. *J. Neural Transm.* **2006,** 113, (6), 769-774.

[120] Singh, N.; Haldar, S.; Tripathi, A.; Horback, K.; Wong, J.; Sharma, D.; Beserra, A.; Suda, S.; Anbalagan, C.; Dev, S.; Mukhopadhyay, C., Brain Iron Homeostasis: From Molecular Mechanisms To Clinical Significance and Therapeutic Opportunities. *Antioxidants & redox signaling* **2013,** 20.

[121] Cole, N. B.; Murphy, D. D.; Lebowitz, J.; Di Noto, L.; Levine, R. L.; Nussbaum, R. L., Metal-catalyzed oxidation of α-synuclein: helping to define the relationship between oligomers, protofibrils, and filaments. *J. Biol. Chem.* **2005,** 280, (10), 9678-9690.

[122] Zhang, X.; Xie, W.; Qu, S.; Pan, T.; Wang, X.; Le, W., Neuroprotection by iron chelator against proteasome inhibitor-induced nigral degeneration. *Biochem. Biophys. Res. Commun.* **2005,** 333, (2), 544-549.

[123] Carboni, E.; Lingor, P., Insights on the interaction of alpha-synuclein and metals in the pathophysiology of Parkinson's disease. *Metallomics* **2015,** 7, (3), 395-404.

[124] Medeiros, M. S.; Schumacher-Schuh, A.; Cardoso, A. M.; Bochi, G. V.; Baldissarelli, J.; Kegler, A.; Santana, D.; Chaves, C. M. M. B. S.; Schetinger, M. R. C.; Moresco, R. N., Iron and oxidative stress in Parkinson's disease: an observational study of injury biomarkers. *PLoS One* **2016,** 11, (1), e0146129.

[125] Gangania, M. K.; Batra, J.; Kushwaha, S.; Agarwal, R., Role of Iron and Copper in the Pathogenesis of Parkinson's Disease. *Indian J. Clin. Biochem.* **2017,** 32, (3), 353-356.

[126] Moos, T.; Rosengren Nielsen, T.; Skjørringe, T.; Morgan, E. H., Iron trafficking inside the brain. *J. Neurochem.* **2007,** 103, (5), 1730-40.

[127] Rouault, T. A., The role of iron regulatory proteins in mammalian iron homeostasis and disease. *Nat. Chem. Biol.* **2006,** 2, (8), 406-414.

[128] LaVaute, T.; Smith, S.; Cooperman, S.; Iwai, K.; Land, W.; Meyron-Holtz, E.; Drake, S. K.; Miller, G.; Abu-Asab, M.; Tsokos, M.; Switzer, R., 3rd; Grinberg, A.; Love, P.; Tresser, N.; Rouault, T. A., Targeted deletion of the gene encoding iron regulatory protein-2 causes misregulation of iron metabolism and neurodegenerative disease in mice. *Nat. Genet.* **2001,** 27, (2), 209-14.

[129] Faucheux, B. A.; Martin, M. E.; Beaumont, C.; Hunot, S.; Hauw, J. J.; Agid, Y.; Hirsch, E. C., Lack of up-regulation of ferritin is associated with sustained iron regulatory protein-1 binding activity in the substantia nigra of patients with Parkinson's disease. *J. Neurochem.* **2002,** 83, (2), 320-30.

[130] Rhodes, S. L.; Buchanan, D. D.; Ahmed, I.; Taylor, K. D.; Loriot, M.-A.; Sinsheimer, J. S.; Bronstein, J. M.; Elbaz, A.; Mellick, G. D.; Rotter, J. I.; Ritz, B., Pooled analysis of iron-related genes in Parkinson's disease: Association with transferrin. *Neurobiol. Dis.* **2014,** 62, 172-178.

[131] Mastroberardino, P. G.; Hoffman, E. K.; Horowitz, M. P.; Betarbet, R.; Taylor, G.; Cheng, D.; Na, H. M.; Gutekunst, C. A.; Gearing, M.; Trojanowski, J. Q.; Anderson, M.; Chu, C. T.; Peng, J.; Greenamyre, J. T., A novel transferrin/TfR2-mediated

mitochondrial iron transport system is disrupted in Parkinson's disease. *Neurobiol. Dis.* **2009,** 34, (3), 417-31.

[132] Jellinger, K.; Paulus, W.; Grundke-Iqbal, I.; Riederer, P.; Youdim, M. B. H., Brain iron and ferritin in Parkinson's and Alzheimer's diseases. *Journal of Neural Transmission - Parkinson's Disease and Dementia Section* **1990,** 2, (4), 327-340.

[133] Licker, V.; Turck, N.; Kövari, E.; Burkhardt, K.; Côte, M.; Surini-Demiri, M.; Lobrinus, J. A.; Sanchez, J. C.; Burkhard, P. R., Proteomic analysis of human substantia nigra identifies novel candidates involved in Parkinson's disease pathogenesis. *Proteomics* **2014,** 14, (6), 784-94.

[134] Dexter, D. T.; Carayon, A.; Javoy-Agid, F.; Agid, Y.; Wells, F. R.; Daniel, S. E.; Lees, A. J.; Jenner, P.; Marsden, C. D., Alterations in the levels of iron, ferritin and other trace metals in Parkinson's disease and other neurodegenerative diseases affecting the basal ganglia. *Brain* **1991,** 114 (Pt 4), 1953-75.

[135] James, S. A.; Roberts, B. R.; Hare, D. J.; de Jonge, M. D.; Birchall, I. E.; Jenkins, N. L.; Cherny, R. A.; Bush, A. I.; McColl, G., Direct in vivo imaging of ferrous iron dyshomeostasis in ageing Caenorhabditis elegans. *Chemical Science* **2015,** 6, (5), 2952-2962.

[136] Hirsch, E.; Graybiel, A. M.; Agid, Y. A., Melanized dopaminergic neurons are differentially susceptible to degeneration in Parkinson's disease. *Nature* **1988,** 334, (6180), 345-348.

[137] Zucca, F. A.; Segura-Aguilar, J.; Ferrari, E.; Muñoz, P.; Paris, I.; Sulzer, D.; Sarna, T.; Casella, L.; Zecca, L., Interactions of iron, dopamine and neuromelanin pathways in brain aging and Parkinson's disease. *Prog. Neurobiol.* **2017,** 155, 96-119.

[138] Wong, B. X.; Tsatsanis, A.; Lim, L. Q.; Adlard, P. A.; Bush, A. I.; Duce, J. A., β-Amyloid precursor protein does not possess ferroxidase activity but does stabilize the cell surface ferrous iron exporter ferroportin. *PLoS One* **2014,** 9, (12), e114174.

[139] Hastings, T. G.; Zigmond, M. J., Loss of dopaminergic neurons in parkinsonism: possible role of reactive dopamine metabolites. *J. Neural Transm. Suppl.* **1997,** 49, 103-10.

[140] Bisaglia, M.; Filograna, R.; Beltramini, M.; Bubacco, L., Are dopamine derivatives implicated in the pathogenesis of Parkinson's disease? *Ageing Res Rev* **2014,** 13, 107-14.

[141] Napolitano, A.; Pezzella, A.; Prota, G., New Reaction Pathways of Dopamine under Oxidative Stress Conditions: Nonenzymatic Iron-Assisted Conversion to Norepinephrine and the Neurotoxins 6-Hydroxydopamine and 6,7-Dihydroxytetrahydroisoquinoline. *Chem. Res. Toxicol.* **1999,** 12, (11), 1090-1097.

[142] Zhang, L.; Yagnik, G.; Jiang, D.; Shi, S.; Chang, P.; Zhou, F., Separation of intermediates of iron-catalyzed dopamine oxidation reactions using reversed-phase ion-pairing chromatography coupled in tandem with UV-visible and ESI-MS detections. *J. Chromatogr. B Analyt. Technol. Biomed. Life Sci.* **2012,** 911, 55-8.

[143] Hare, D. J.; Adlard, P. A.; Doble, P. A.; Finkelstein, D. I., Metallobiology of 1-methyl-4-phenyl-1,2,3,6-tetrahydropyridine neurotoxicity. *Metallomics* **2013,** 5, (2), 91-109.

[144] Stokes, A. H.; Hastings, T. G.; Vrana, K. E., Cytotoxic and genotoxic potential of dopamine. *J. Neurosci. Res.* **1999,** 55, (6), 659-65.

[145] Liu, X.; Yamada, N.; Maruyama, W.; Osawa, T., Formation of dopamine adducts derived from brain polyunsaturated fatty acids: mechanism for Parkinson disease. *J. Biol. Chem.* **2008,** 283, (50), 34887-95.

[146] Chen, L.; Hambright, W. S.; Na, R.; Ran, Q., Ablation of the Ferroptosis Inhibitor Glutathione Peroxidase 4 in Neurons Results in Rapid Motor Neuron Degeneration and Paralysis. *J. Biol. Chem.* **2015,** 290, (47), 28097-106.

[147] Hauser, D. N.; Dukes, A. A.; Mortimer, A. D.; Hastings, T. G., Dopamine quinone modifies and decreases the abundance of the mitochondrial selenoprotein glutathione peroxidase 4. *Free Radic. Biol. Med.* **2013,** 65, 419-427.

[148] Segura-Aguilar, J.; Paris, I.; Muñoz, P.; Ferrari, E.; Zecca, L.; Zucca, F. A., Protective and toxic roles of dopamine in Parkinson's disease. *J. Neurochem.* **2014,** 129, (6), 898-915.

[149] Herrera, A.; Muñoz, P.; Steinbusch, H. W. M.; Segura-Aguilar, J., Are Dopamine Oxidation Metabolites Involved in the Loss of Dopaminergic Neurons in the Nigrostriatal System in Parkinson's Disease? *ACS Chem. Neurosci.* **2017,** 8, (4), 702-711.

[150] Segura-Aguilar, J.; Muñoz, P.; Paris, I., Aminochrome as New Preclinical Model to Find New Pharmacological Treatment that Stop the Development of Parkinson's Disease. *Curr. Med. Chem.* **2016,** 23, (4), 346-59.

[151] Monteiro, H. P.; Winterbourn, C. C., 6-Hydroxydopamine releases iron from ferritin and promotes ferritin-dependent lipid peroxidation. *Biochem. Pharmacol.* **1989,** 38, (23), 4177-82.

[152] Double, K. L.; Maywald, M.; Schmittel, M.; Riederer, P.; Gerlach, M., In vitro studies of ferritin iron release and neurotoxicity. *J. Neurochem.* **1998,** 70, (6), 2492-9.

[153] Zhou, Z. D.; Lan, Y. H.; Tan, E. K.; Lim, T. M., Iron species-mediated dopamine oxidation, proteasome inhibition, and dopaminergic cell demise: implications for iron-related dopaminergic neuron degeneration. *Free Radic. Biol. Med.* **2010,** 49, (12), 1856-71.

[154] Przedborski, S.; Kostic, V.; Jackson-Lewis, V.; Naini, A. B.; Simonetti, S.; Fahn, S.; Carlson, E.; Epstein, C. J.; Cadet, J. L., Transgenic mice with increased Cu/Zn-superoxide dismutase activity are resistant to N-methyl-4-phenyl-1,2,3,6-tetrahydropyridine-induced neurotoxicity. *J. Neurosci.* **1992,** 12, (5), 1658-67.

[155] Klivenyi, P.; St Clair, D.; Wermer, M.; Yen, H. C.; Oberley, T.; Yang, L.; Flint Beal, M., Manganese superoxide dismutase overexpression attenuates MPTP toxicity. *Neurobiol. Dis.* **1998,** 5, (4), 253-8.

[156] Filograna, R.; Godena, V. K.; Sanchez-Martinez, A.; Ferrari, E.; Casella, L.; Beltramini, M.; Bubacco, L.; Whitworth, A. J.; Bisaglia, M., Superoxide Dismutase (SOD)-mimetic M40403 Is Protective in Cell and Fly Models of Paraquat Toxicity: IMPLICATIONS FOR PARKINSON DISEASE. *J. Biol. Chem.* **2016,** 291, (17), 9257-67.

[157] De Lazzari, F.; Bubacco, L.; Whitworth, A. J.; Bisaglia, M., Superoxide Radical Dismutation as New Therapeutic Strategy in Parkinson's Disease. *Aging Dis.* **2018,** 9, (4), 716-728.

[158] Yakunin, E.; Kisos, H.; Kulik, W.; Grigoletto, J.; Wanders, R. J.; Sharon, R., The regulation of catalase activity by PPAR γ is affected by α-synuclein. *Annals of clinical and translational neurology* **2014,** 1, (3), 145-59.

[159] GRAHAM, D. G., Oxidative pathways for catecholamines in the genesis of neuromelanin and cytotoxic quinones. *Mol. Pharmacol.* **1978,** 14, (4), 633-643.

[160] Dinkova-Kostova, A. T.; Abramov, A. Y., The emerging role of Nrf2 in mitochondrial function. *Free Radical Biol. Med.* **2015,** 88, 179-188.

[161] Zenkov, N. K.; Menshchikova, E. B.; Tkachev, V. O., Keap1/Nrf2/ARE redox-sensitive signaling system as a pharmacological target. *Biochemistry (Mosc.)* **2013,** 78, (1), 19-36.

[162] Prestera, T.; Talalay, P.; Alam, J.; Ahn, Y. I.; Lee, P. J.; Choi, A. M., Parallel induction of heme oxygenase-1 and chemoprotective phase 2 enzymes by electrophiles and antioxidants: regulation by upstream antioxidant-responsive elements (ARE). *Molecular medicine (Cambridge, Mass.)* **1995,** 1, (7), 827-837.

[163] Wang, B.; Williamson, G., Detection of a nuclear protein which binds specifically to the antioxidant responsive element (ARE) of the human NAD(P) H:quinone oxidoreductase gene. *Biochim. Biophys. Acta* **1994,** 1219, (3), 645-52.

[164] Sun, J.; Ren, X.; Simpkins, J. W., Sequential Upregulation of Superoxide Dismutase 2 and Heme Oxygenase 1 by tert-Butylhydroquinone Protects Mitochondria during Oxidative Stress. *Mol. Pharmacol.* **2015,** 88, (3), 437.

[165] Rushmore, T. H.; Pickett, C. B., Transcriptional regulation of the rat glutathione S-transferase Ya subunit gene. Characterization of a xenobiotic-responsive element controlling inducible expression by phenolic antioxidants. *J. Biol. Chem.* **1990,** 265, (24), 14648-53.

[166] Mulcahy, R. T.; Gipp, J. J., Identification of a Putative Antioxidant Response Element in the 5′-Flanking Region of the Human γ-Glutamylcysteine Synthetase Heavy Subunit Gene. *Biochem. Biophys. Res. Commun.* **1995,** 209, (1), 227-233.

[167] Im, J.-Y.; Lee, K.-W.; Woo, J.-M.; Junn, E.; Mouradian, M. M., DJ-1 induces thioredoxin 1 expression through the Nrf2 pathway. *Hum. Mol. Genet.* **2012,** 21, (13), 3013-3024.

[168] Murata, H.; Takamatsu, H.; Liu, S.; Kataoka, K.; Huh, N.-h.; Sakaguchi, M., NRF2 Regulates PINK1 Expression under Oxidative Stress Conditions. *PLoS One* **2015,** 10, (11), e0142438.

[169] Xiao, L.; Xu, X.; Zhang, F.; Wang, M.; Xu, Y.; Tang, D.; Wang, J.; Qin, Y.; Liu, Y.; Tang, C.; He, L.; Greka, A.; Zhou, Z.; Liu, F.; Dong, Z.; Sun, L., The mitochondria-targeted antioxidant MitoQ ameliorated tubular injury mediated by mitophagy in diabetic kidney disease via Nrf2/PINK1. *Redox Biology* **2017,** 11, 297-311.

[170] Liu, Y.; Yan, J.; Sun, C.; Li, G.; Li, S.; Zhang, L.; Di, C.; Gan, L.; Wang, Y.; Zhou, R.; Si, J.; Zhang, H., Ameliorating mitochondrial dysfunction restores carbon ion-induced cognitive deficits via co-activation of NRF2 and PINK1 signaling pathway. *Redox Biology* **2018,** 17, 143-157.

[171] Kuroda, Y.; Mitsui, T.; Kunishige, M.; Shono, M.; Akaike, M.; Azuma, H.; Matsumoto, T., Parkin enhances mitochondrial biogenesis in proliferating cells. *Hum. Mol. Genet.* **2006,** 15, (6), 883-895.

[172] Rothfuss, O.; Fischer, H.; Hasegawa, T.; Maisel, M.; Leitner, P.; Miesel, F.; Sharma, M.; Bornemann, A.; Berg, D.; Gasser, T.; Patenge, N., Parkin protects mitochondrial genome integrity and supports mitochondrial DNA repair. *Hum. Mol. Genet.* **2009,** 18, (20), 3832-3850.

[173] Wang, Q.; Li, W. X.; Dai, S. X.; Guo, Y. C.; Han, F. F.; Zheng, J. J.; Li, G. H.; Huang, J. F., Meta-Analysis of Parkinson's Disease and Alzheimer's Disease Revealed Commonly Impaired Pathways and Dysregulation of NRF2-Dependent Genes. *J. Alzheimers Dis.* **2017,** 56, (4), 1525-1539.

[174] Chao, Y.; Wong, S. C.; Tan, E. K., Evidence of inflammatory system involvement in Parkinson's disease. *BioMed research international* **2014,** 2014, 308654.

[175] Moehle, M. S.; West, A. B., M1 and M2 immune activation in Parkinson's Disease: Foe and ally? *Neuroscience* **2015,** 302, 59-73.

[176] Jankovic, J., Pathogenesis-targeted therapeutic strategies in Parkinson's disease. *Mov. Disord.* **2019,** 34, (1), 41-44.

[177] Kam, T.-I.; Hinkle, J. T.; Dawson, T. M.; Dawson, V. L., Microglia and astrocyte dysfunction in parkinson's disease. *Neurobiol. Dis.* **2020,** 144, 105028.

[178] Tan, E.-K.; Chao, Y.-X.; West, A.; Chan, L.-L.; Poewe, W.; Jankovic, J., Parkinson disease and the immune system—associations, mechanisms and therapeutics. *Nat. Rev. Neurol.* **2020,** 16, (6), 303-318.

[179] Bae, E.-J.; Lee, H.-J.; Rockenstein, E.; Ho, D.-H.; Park, E.-B.; Yang, N.-Y.; Desplats, P.; Masliah, E.; Lee, S.-J., Antibody-aided clearance of extracellular α-synuclein prevents cell-to-cell aggregate transmission. *J. Neurosci.* **2012,** 32, (39), 13454-13469.

[180] Fellner, L.; Irschick, R.; Schanda, K.; Reindl, M.; Klimaschewski, L.; Poewe, W.; Wenning, G. K.; Stefanova, N., Toll-like receptor 4 is required for α-synuclein dependent activation of microglia and astroglia. *Glia* **2013,** 61, (3), 349-60.

[181] Doorn, K. J.; Moors, T.; Drukarch, B.; van de Berg, W.; Lucassen, P. J.; van Dam, A. M., Microglial phenotypes and toll-like receptor 2 in the substantia nigra and hippocampus of incidental Lewy body disease cases and Parkinson's disease patients. *Acta neuropathologica communications* **2014,** 2, 90.

[182] Duffy, M. F.; Collier, T. J.; Patterson, J. R.; Kemp, C. J.; Luk, K. C.; Tansey, M. G.; Paumier, K. L.; Kanaan, N. M.; Fischer, D. L.; Polinski, N. K.; Barth, O. L.; Howe, J. W.; Vaikath, N. N.; Majbour, N. K.; El-Agnaf, O. M. A.; Sortwell, C. E., Correction to: Lewy body-like alpha-synuclein inclusions trigger reactive microgliosis prior to nigral degeneration. *J. Neuroinflammation* **2018,** 15, (1), 169-169.

[183] Harms, A. S.; Delic, V.; Thome, A. D.; Bryant, N.; Liu, Z.; Chandra, S.; Jurkuvenaite, A.; West, A. B., α-Synuclein fibrils recruit peripheral immune cells in the rat brain prior to neurodegeneration. *Acta neuropathologica communications* **2017,** 5, (1), 85-85.

[184] Guo, H.; Callaway, J. B.; Ting, J. P. Y., Inflammasomes: mechanism of action, role in disease, and therapeutics. *Nat. Med.* **2015,** 21, (7), 677-687.

[185] Panicker, N.; Sarkar, S.; Harischandra, D. S., Fyn kinase regulates misfolded α-synuclein uptake and NLRP3 inflammasome activation in microglia. *The journal of experimental medicine* **2019,** 216, (6), 1411-1430.

[186] Yun, S. P.; Kam, T.-I.; Panicker, N.; Kim, S.; Oh, Y.; Park, J.-S.; Kwon, S.-H.; Park, Y. J.; Karuppagounder, S. S.; Park, H.; Kim, S.; Oh, N.; Kim, N. A.; Lee, S.; Brahmachari, S.; Mao, X.; Lee, J. H.; Kumar, M.; An, D.; Kang, S.-U.; Lee, Y.; Lee, K. C.; Na, D. H.; Kim, D.; Lee, S. H.; Roschke, V. V.; Liddelow, S. A.; Mari, Z.; Barres, B. A.; Dawson, V. L.; Lee, S.; Dawson, T. M.; Ko, H. S., Block of A1 astrocyte conversion by microglia is neuroprotective in models of Parkinson's disease. *Nat. Med.* **2018,** 24, (7), 931-938.

[187] Hinkle, J. T.; Dawson, V. L.; Dawson, T. M., The A1 astrocyte paradigm: New avenues for pharmacological intervention in neurodegeneration. *Mov. Disord.* **2019,** 34, (7), 959-969.

[188] Liddelow, S. A.; Guttenplan, K. A.; Clarke, L. E.; Bennett, F. C.; Bohlen, C. J.; Schirmer, L.; Bennett, M. L.; Münch, A. E.; Chung, W.-S.; Peterson, T. C.; Wilton, D. K.; Frouin, A.; Napier, B. A.; Panicker, N.; Kumar, M.; Buckwalter, M. S.; Rowitch, D. H.; Dawson, V. L.; Dawson, T. M.; Stevens, B.; Barres, B. A., Neurotoxic reactive astrocytes are induced by activated microglia. *Nature* **2017,** 541, (7638), 481-487.

[189] Lin, C.-H.; Chen, C.-C.; Chiang, H.-L.; Liou, J.-M.; Chang, C.-M.; Lu, T.-P.; Chuang, E. Y.; Tai, Y.-C.; Cheng, C.; Lin, H.-Y.; Wu, M.-S., Altered gut microbiota and inflammatory cytokine responses in patients with Parkinson's disease. *J. Neuroinflammation* **2019,** 16, (1), 129.

[190] Mogi, M.; Harada, M.; Narabayashi, H.; Inagaki, H.; Minami, M.; Nagatsu, T., Interleukin (IL)-1 beta, IL-2, IL-4, IL-6 and transforming growth factor-alpha levels are elevated in ventricular cerebrospinal fluid in juvenile parkinsonism and Parkinson's disease. *Neurosci. Lett.* **1996,** 211, (1), 13-6.

[191] Brodacki, B.; Staszewski, J.; Toczyłowska, B.; Kozłowska, E.; Drela, N.; Chalimoniuk, M.; Stepien, A., Serum interleukin (IL-2, IL-10, IL-6, IL-4), TNFalpha, and INFgamma concentrations are elevated in patients with atypical and idiopathic parkinsonism. *Neurosci. Lett.* **2008,** 441, (2), 158-62.

[192] Bauernfeind, F. G.; Horvath, G.; Stutz, A.; Alnemri, E. S.; MacDonald, K.; Speert, D.; Fernandes-Alnemri, T.; Wu, J.; Monks, B. G.; Fitzgerald, K. A.; Hornung, V.; Latz, E., Cutting edge: NF-kappaB activating pattern recognition and cytokine receptors license NLRP3 inflammasome activation by regulating NLRP3 expression. *Journal of immunology (Baltimore, Md. : 1950)* **2009,** 183, (2), 787-791.

[193] Lee, P. P.; Lobato-Márquez, D.; Pramanik, N.; Sirianni, A.; Daza-Cajigal, V.; Rivers, E.; Cavazza, A.; Bouma, G.; Moulding, D.; Hultenby, K.; Westerberg, L. S., Wiskott-Aldrich syndrome protein regulates autophagy and inflammasome activity in innate immune cells. *Nature communications* **2017,** 8, (1), 1576.

[194] Wang, W.; Nguyen, L. T.; Burlak, C.; Chegini, F.; Guo, F.; Chataway, T.; Ju, S.; Fisher, O. S.; Miller, D. W.; Datta, D.; Wu, F.; Wu, C. X.; Landeru, A.; Wells, J. A.; Cookson, M. R.; Boxer, M. B.; Thomas, C. J.; Gai, W. P.; Ringe, D.; Petsko, G. A.; Hoang, Q. Q., Caspase-1 causes truncation and aggregation of the Parkinson's disease-associated protein α-synuclein. *Proc. Natl. Acad. Sci. U. S. A.* **2016,** 113, (34), 9587-92.

[195] Codolo, G.; Ploteghcr, N.; Pozzobon, T.; Brucale, M.; Tessari, I.; Bubacco, L.; de Bernard, M., Triggering of inflammasome by aggregated α-synuclein, an inflammatory response in synucleinopathies. *PLoS One* **2013,** 8, (1), e55375.

[196] Lee, S. J., Origins and effects of extracellular alpha-synuclein: implications in Parkinson's disease. *J. Mol. Neurosci.* **2008,** 34, (1), 17-22.

[197] Bartels, A. L.; Leenders, K. L., Cyclooxygenase and neuroinflammation in Parkinson's disease neurodegeneration. *Curr. Neuropharmacol.* **2010,** 8, (1), 62-68.

[198] Brioschi, S.; Colonna, M., The CNS Immune-Privilege Goes Down the Drain(age). *Trends Pharmacol. Sci.* **2019,** 40, (1), 1-3.

[199] Louveau, A.; Herz, J.; Alme, M. N.; Salvador, A. F.; Dong, M. Q.; Viar, K. E.; Herod, S. G.; Knopp, J.; Setliff, J. C.; Lupi, A. L.; Da Mesquita, S.; Frost, E. L.; Gaultier, A.; Harris, T. H.; Cao, R.; Hu, S.; Lukens, J. R.; Smirnov, I.; Overall, C. C.; Oliver, G.; Kipnis, J., CNS lymphatic drainage and neuroinflammation are regulated by meningeal lymphatic vasculature. *Nat. Neurosci.* **2018,** 21, (10), 1380-1391.

[200] Johnson, M. E.; Stecher, B.; Labrie, V.; Brundin, L.; Brundin, P., Triggers, Facilitators, and Aggravators: Redefining Parkinson's Disease Pathogenesis. *Trends Neurosci.* **2019,** 42, (1), 4-13.

[201] Harms, A. S.; Cao, S.; Rowse, A. L.; Thome, A. D.; Li, X.; Mangieri, L. R.; Cron, R. Q.; Shacka, J. J.; Raman, C.; Standaert, D. G., MHCII is required for α-synuclein-induced activation of microglia, CD4 T cell proliferation, and dopaminergic neurodegeneration. *J. Neurosci.* **2013,** 33, (23), 9592-600.

[202] Waisman, A.; Johann, L., Antigen-presenting cell diversity for T cell reactivation in central nervous system autoimmunity. *J. Mol. Med.* **2018,** 96, (12), 1279-1292.

[203] Williams, G. P.; Schonhoff, A. M.; Jurkuvenaite, A.; Thome, A. D.; Standaert, D. G.; Harms, A. S., Targeting of the class II transactivator attenuates inflammation and neurodegeneration in an alpha-synuclein model of Parkinson's disease. *J. Neuroinflammation* **2018,** 15, (1), 244.

[204] Kempuraj, D.; Selvakumar, G. P.; Zaheer, S.; Thangavel, R.; Ahmed, M. E.; Raikwar, S.; Govindarajan, R.; Iyer, S.; Zaheer, A., Cross-Talk between Glia, Neurons and Mast Cells in Neuroinflammation Associated with Parkinson's Disease. *J. Neuroimmune Pharmacol.* **2018,** 13, (1), 100-112.

[205] Jones, M. K.; Nair, A.; Gupta, M., Mast Cells in Neurodegenerative Disease. *Front. Cell. Neurosci.* **2019,** 13, 171-171.

[206] Shao, W.; Zhang, S. Z.; Tang, M.; Zhang, X. H.; Zhou, Z.; Yin, Y. Q.; Zhou, Q. B.; Huang, Y. Y.; Liu, Y. J.; Wawrousek, E.; Chen, T.; Li, S. B.; Xu, M.; Zhou, J. N.; Hu, G.; Zhou, J. W., Suppression of neuroinflammation by astrocytic dopamine D2 receptors via αB-crystallin. *Nature* **2013,** 494, (7435), 90-4.

[207] Maiti, P.; Manna, J.; Dunbar, G. L., Current understanding of the molecular mechanisms in Parkinson's disease: Targets for potential treatments. *Transl. Neurodegener.* **2017,** 6, 28-28.

[208] Schapira, A. H.; Cooper, J. M.; Dexter, D.; Clark, J. B.; Jenner, P.; Marsden, C. D., Mitochondrial complex I deficiency in Parkinson's disease. *J. Neurochem.* **1990,** 54, (3), 823-7.

[209] Bindoff, L.; Birch-Machin, M.; Cartlidge, N.; Parker, W.; Turnbull, D., Mitochondrial function in Parkinson's disease. *The Lancet* **1989,** 334, (8653), 49.

[210] Schapira, A.; Cooper, J.; Dexter, D.; Jenner, P.; Clark, J.; Marsden, C., Mitochondrial complex I deficiency in Parkinson's disease. *The Lancet* **1989,** 333, (8649), 1269.

[211] Maiti, P.; Manna, J.; Dunbar, G. L., Current understanding of the molecular mechanisms in Parkinson's disease: Targets for potential treatments. *Transl. Neurodegener.* **2017,** 6, (1), 28.

[212] Murphy, M. P., How mitochondria produce reactive oxygen species. *Biochem. J.* **2009,** 417, (1), 1-13.

[213] Tretter, L.; Sipos, I.; Adam-Vizi, V., Initiation of neuronal damage by complex I deficiency and oxidative stress in Parkinson's disease. *Neurochem. Res.* **2004,** 29, (3), 569-77.

[214] Burbulla, L. F.; Song, P.; Mazzulli, J. R.; Zampese, E.; Wong, Y. C.; Jeon, S.; Santos, D. P.; Blanz, J.; Obermaier, C. D.; Strojny, C., Dopamine oxidation mediates mitochondrial and lysosomal dysfunction in Parkinson's disease. *Science* **2017,** 357, (6357), 1255-1261.

[215] Rubinsztein, D. C., The roles of intracellular protein-degradation pathways in neurodegeneration. *Nature* **2006,** 443, (7113), 780-786.

[216] Larsen, K. E.; Sulzer, D., Autophagy in neurons a review. *Histol. Histopathol.* **2002**.

[217] Ciechanover, A.; Kwon, Y. T., Degradation of misfolded proteins in neurodegenerative diseases: therapeutic targets and strategies. *Exp. Mol. Med.* **2015,** 47, (3), e147-e147.

[218] Pukaß, K.; Richter-Landsberg, C., Inhibition of UCH-L1 in oligodendroglial cells results in microtubule stabilization and prevents α-synuclein aggregate formation by activating the autophagic pathway: implications for multiple system atrophy. *Front. Cell. Neurosci.* **2015,** 9, 163.

[219] McNaught, K. S. P.; Mytilineou, C.; JnoBaptiste, R.; Yabut, J.; Shashidharan, P.; Jenner, P.; Olanow, C. W., Impairment of the ubiquitin-proteasome system causes dopaminergic cell death and inclusion body formation in ventral mesencephalic cultures. *J. Neurochem.* **2002,** 81, (2), 301-306.

[220] Rideout, H. J.; Lang-Rollin, I. C.; Savalle, M.; Stefanis, L., Dopaminergic neurons in rat ventral midbrain cultures undergo selective apoptosis and form inclusions, but do not up-regulate iHSP70, following proteasomal inhibition. *J. Neurochem.* **2005,** 93, (5), 1304-1313.

[221] McNaught, K. S. P.; Olanow, C. W.; Halliwell, B.; Isacson, O.; Jenner, P., Failure of the ubiquitin–proteasome system in Parkinson's disease. *Nature Reviews Neuroscience* **2001,** 2, (8), 589-594.

[222] Ding, Q.; Dimayuga, E.; Martin, S.; Bruce-Keller, A. J.; Nukala, V.; Cuervo, A. M.; Keller, J. N., Characterization of chronic low-level proteasome inhibition on neural homeostasis. *J. Neurochem.* **2003,** 86, (2), 489-497.

[223] Sullivan, P. G.; Dragicevic, N. B.; Deng, J.-H.; Bai, Y.; Dimayuga, E.; Ding, Q.; Chen, Q.; Bruce-Keller, A. J.; Keller, J. N., Proteasome inhibition alters neural mitochondrial homeostasis and mitochondria turnover. *J. Biol. Chem.* **2004,** 279, (20), 20699-20707.

[224] Saigoh, K.; Wang, Y.-L.; Suh, J.-G.; Yamanishi, T.; Sakai, Y.; Kiyosawa, H.; Harada, T.; Ichihara, N.; Wakana, S.; Kikuchi, T.; Wada, K., Intragenic deletion in the gene

encoding ubiquitin carboxy-terminal hydrolase in gad mice. *Nat. Genet.* **1999,** 23, (1), 47-51.

[225] Goldberg, M. S.; Fleming, S. M.; Palacino, J. J.; Cepeda, C.; Lam, H. A.; Bhatnagar, A.; Meloni, E. G.; Wu, N.; Ackerson, L. C.; Klapstein, G. J., Parkin-deficient mice exhibit nigrostriatal deficits but not loss of dopaminergic neurons. *J. Biol. Chem.* **2003,** 278, (44), 43628-43635.

[226] Greene, J. C.; Whitworth, A. J.; Kuo, I.; Andrews, L. A.; Feany, M. B.; Pallanck, L. J., Mitochondrial pathology and apoptotic muscle degeneration in Drosophila parkin mutants. *Proc. Nat. Acad. Sci.* **2003,** 100, (7), 4078-4083.

[227] Cha, G.-H.; Kim, S.; Park, J.; Lee, E.; Kim, M.; Lee, S. B.; Kim, J. M.; Chung, J.; Cho, K. S., Parkin negatively regulates JNK pathway in the dopaminergic neurons of Drosophila. *Proc. Nat. Acad. Sci.* **2005,** 102, (29), 10345-10350.

[228] Dokladny, K.; Myers, O. B.; Moseley, P. L., Heat shock response and autophagy—cooperation and control. *Autophagy* **2015,** 11, (2), 200-213.

[229] Maiti, P.; Manna, J.; Veleri, S.; Frautschy, S., Molecular chaperone dysfunction in neurodegenerative diseases and effects of curcumin. *BioMed research international* **2014,** 2014.

[230] Karunanithi, S.; Brown, I. R., Heat shock response and homeostatic plasticity. *Front. Cell. Neurosci.* **2015,** 9, 68.

[231] Bercovich, B.; Stancovski, I.; Mayer, A.; Blumenfeld, N.; Laszlo, A.; Schwartz, A. L.; Ciechanover, A., Ubiquitin-dependent degradation of certain protein substrates in vitro requires the molecular chaperone Hsc70. *J. Biol. Chem.* **1997,** 272, (14), 9002-9010.

[232] Wyttenbach, A., Role of heat shock proteins during polyglutamine neurodegeneration. *J. Mol. Neurosci.* **2004,** 23, (1), 69-95.

[233] Kaushik, S.; Cuervo, A., Chaperone-mediated autophagy. In *Autophagosome and Phagosome*, Springer: 2008; pp 227-244.

[234] Auluck, P. K.; Chan, H. E.; Trojanowski, J. Q.; Lee, V. M.-Y.; Bonini, N. M., Chaperone suppression of α-synuclein toxicity in a Drosophila model for Parkinson's disease. *Science* **2002,** 295, (5556), 865-868.

[235] Tantucci, M.; Mariucci, G.; Taha, E.; Spaccatini, C.; Tozzi, A.; Luchetti, E.; Calabresi, P.; Ambrosini, M., Induction of heat shock protein 70 reduces the alteration of striatal electrical activity caused by mitochondrial impairment. *Neuroscience* **2009,** 163, (3), 735-740.

[236] Flower, T. R.; Chesnokova, L. S.; Froelich, C. A.; Dixon, C.; Witt, S. N., Heat shock prevents alpha-synuclein-induced apoptosis in a yeast model of Parkinson's disease. *J. Mol. Biol.* **2005,** 351, (5), 1081-1100.

[237] Cuervo, A. M.; Stefanis, L.; Fredenburg, R.; Lansbury, P. T.; Sulzer, D., Impaired degradation of mutant α-synuclein by chaperone-mediated autophagy. *Science* **2004,** 305, (5688), 1292-1295.

[238] Levine, B.; Klionsky, D. J., Development by self-digestion: molecular mechanisms and biological functions of autophagy. *Dev. Cell* **2004,** 6, (4), 463-477.

[239] Crotzer, V. L.; Blum, J. S., Autophagy and intracellular surveillance: Modulating MHC class II antigen presentation with stress. *Proc. Nat. Acad. Sci.* **2005,** 102, (22), 7779.

[240] Jankovic, J., Motor fluctuations and dyskinesias in Parkinson's disease: clinical manifestations. *Movement disorders: official journal of the Movement Disorder Society* **2005,** 20, (S11), S11-S16.

[241] Pan, T.; Kondo, S.; Le, W.; Jankovic, J., The role of autophagy-lysosome pathway in neurodegeneration associated with Parkinson's disease. *Brain* **2008,** 131, (8), 1969-1978.

[242] Anglade, P.; Vyas, S.; Javoy-Agid, F.; Herrero, M.; Michel, P.; Marquez, J.; Mouatt-Prigent, A.; Ruberg, M.; Hirsch, E.; Agid, Y., Apoptosis and autophagy in nigral neurons of patients with Parkinson's disease. *Histol. Histopathol.* **1997**.

[243] Toulorge, D.; Schapira, A. H.; Hajj, R., Molecular changes in the postmortem parkinsonian brain. *J. Neurochem.* **2016**, 139, 27-58.

[244] Tanji, K.; Mori, F.; Kakita, A.; Takahashi, H.; Wakabayashi, K., Alteration of autophagosomal proteins (LC3, GABARAP and GATE-16) in Lewy body disease. *Neurobiol. Dis.* **2011**, 43, (3), 690-697.

[245] Murphy, K. E.; Gysbers, A. M.; Abbott, S. K.; Spiro, A. S.; Furuta, A.; Cooper, A.; Garner, B.; Kabuta, T.; Halliday, G. M., Lysosomal-associated membrane protein 2 isoforms are differentially affected in early Parkinson's disease. *Mov. Disord.* **2015**, 30, (12), 1639-1647.

[246] Alvarez-Erviti, L.; Rodriguez-Oroz, M. C.; Cooper, J. M.; Caballero, C.; Ferrer, I.; Obeso, J. A.; Schapira, A. H., Chaperone-mediated autophagy markers in Parkinson disease brains. *Arch. Neurol.* **2010**, 67, (12), 1464-1472.

[247] Dijkstra, A. A.; Ingrassia, A.; de Menezes, R. X.; van Kesteren, R. E.; Rozemuller, A. J.; Heutink, P.; van de Berg, W. D., Evidence for immune response, axonal dysfunction and reduced endocytosis in the substantia nigra in early stage Parkinson's disease. *PLoS One* **2015**, 10, (6), e0128651.

[248] Trenkwalder, C.; Kuoppamäki, M.; Vahteristo, M.; Müller, T.; Ellmén, J., Increased dose of carbidopa with levodopa and entacapone improves "off" time in a randomized trial. *Neurology* **2019**, 92, (13), e1487-e1496.

[249] Espay, A. J.; Morgante, F.; Merola, A.; Fasano, A.; Marsili, L.; Fox, S. H.; Bezard, E.; Picconi, B.; Calabresi, P.; Lang, A. E., Levodopa-induced dyskinesia in Parkinson disease: current and evolving concepts. *Ann. Neurol.* **2018**, 84, (6), 797-811.

[250] Latt, M. D.; Lewis, S.; Zekry, O.; Fung, V. S., Factors to consider in the selection of dopamine agonists for older persons with Parkinson's disease. *Drugs Aging* **2019**, 36, (3), 189-202.

[251] Group, P. M. C., Long-term effectiveness of dopamine agonists and monoamine oxidase B inhibitors compared with levodopa as initial treatment for Parkinson's disease (PD MED): a large, open-label, pragmatic randomised trial. *The Lancet* **2014**, 384, (9949), 1196-1205.

[252] Rascol, O.; Brooks, D. J.; Korczyn, A. D.; De Deyn, P. P.; Clarke, C. E.; Lang, A. E., A five-year study of the incidence of dyskinesia in patients with early Parkinson's disease who were treated with ropinirole or levodopa. *New Engl. J. Med.* **2000**, 342, (20), 1484-1491.

[253] Warren, N.; O'Gorman, C.; Lehn, A.; Siskind, D., Dopamine dysregulation syndrome in Parkinson's disease: a systematic review of published cases. *J. Neurol. Neurosurg. Psychiatry* **2017**, 88, (12), 1060-1064.

[254] Lees, A. J.; Ferreira, J.; Rascol, O.; Poewe, W.; Rocha, J.-F.; McCrory, M.; Soares-da-Silva, P.; Investigators, B.-S., Opicapone as adjunct to levodopa therapy in patients with Parkinson disease and motor fluctuations: a randomized clinical trial. *JAMA neurology* **2017**, 74, (2), 197-206.

[255] Ferreira, J. J.; Lees, A. J.; Poewe, W.; Rascol, O.; Rocha, J.-F.; Keller, B.; Soares-da-Silva, P., Effectiveness of opicapone and switching from entacapone in fluctuating Parkinson disease. *Neurology* **2018**, 90, (21), e1849-e1857.

[256] Schapira, A. H.; Fox, S. H.; Hauser, R. A.; Jankovic, J.; Jost, W. H.; Kenney, C.; Kulisevsky, J.; Pahwa, R.; Poewe, W.; Anand, R., Assessment of safety and efficacy of safinamide as a levodopa adjunct in patients with Parkinson disease and motor fluctuations: a randomized clinical trial. *JAMA neurology* **2017**, 74, (2), 216-224.

[257] Torti, M.; Vacca, L.; Stocchi, F., Istradefylline for the treatment of Parkinson's disease: is it a promising strategy? *Expert Opin. Pharmacother.* **2018,** 19, (16), 1821-1828.

[258] Weaver, F. M.; Follett, K.; Stern, M.; Hur, K.; Harris, C.; Marks, W. J.; Rothlind, J.; Sagher, O.; Reda, D.; Moy, C. S., Bilateral deep brain stimulation vs best medical therapy for patients with advanced Parkinson disease: a randomized controlled trial. *JAMA* **2009,** 301, (1), 63-73.

[259] Follett, K. A.; Weaver, F. M.; Stern, M.; Hur, K.; Harris, C. L.; Luo, P.; Marks Jr, W. J.; Rothlind, J.; Sagher, O.; Moy, C., Pallidal versus subthalamic deep-brain stimulation for Parkinson's disease. *New Engl. J. Med.* **2010,** 362, (22), 2077-2091.

[260] Schuepbach, W.; Rau, J.; Knudsen, K.; Volkmann, J.; Krack, P.; Timmermann, L.; Hälbig, T.; Hesekamp, H.; Navarro, S.; Meier, N., Neurostimulation for Parkinson's disease with early motor complications. *New Engl. J. Med.* **2013,** 368, (7), 610-622.

[261] Henderson, E. J.; Lord, S. R.; Brodie, M. A.; Gaunt, D. M.; Lawrence, A. D.; Close, J. C.; Whone, A.; Ben-Shlomo, Y., Rivastigmine for gait stability in patients with Parkinson's disease (ReSPonD): a randomised, double-blind, placebo-controlled, phase 2 trial. *Lancet Neurol.* **2016,** 15, (3), 249-258.

[262] van Laar, T.; De Deyn, P. P.; Aarsland, D.; Barone, P.; Galvin, J. E., Effects of cholinesterase inhibitors in Parkinson's disease dementia: a review of clinical data. *CNS Neurosci. Ther.* **2011,** 17, (5), 428-441.

[263] Seppi, K.; Ray Chaudhuri, K.; Coelho, M.; Fox, S. H.; Katzenschlager, R.; Perez Lloret, S.; Weintraub, D.; Sampaio, C.; and the collaborators of the Parkinson's Disease Update on Non-Motor Symptoms Study Group on behalf of the Movement Disorders Society Evidence-Based Medicine, C., Update on treatments for nonmotor symptoms of Parkinson's disease—an evidence-based medicine review. *Mov. Disord.* **2019,** 34, (2), 180-198.

[264] Shotbolt, P.; Samuel, M.; David, A., Quetiapine in the treatment of psychosis in Parkinson's disease. *Ther. Adv. Neurol. Disord.* **2010,** 3, (6), 339-350.

[265] Cummings, J.; Isaacson, S.; Mills, R.; Williams, H.; Chi-Burris, K.; Corbett, A.; Dhall, R.; Ballard, C., Pimavanserin for patients with Parkinson's disease psychosis: a randomised, placebo-controlled phase 3 trial. *The Lancet* **2014,** 383, (9916), 533-540.

[266] Palma, J. A.; Kaufmann, H., Treatment of autonomic dysfunction in Parkinson disease and other synucleinopathies. *Mov. Disord.* **2018,** 33, (3), 372-390.

[267] Sánchez-Ferro, A.; Benito-León, J.; Gómez-Esteban, J. C., The management of orthostatic hypotension in Parkinson's disease. *Front. Neurol.* **2013,** 4, 64-64.

[268] Bharucha, A. E.; Wald, A. In *Chronic constipation*, Mayo Clin. Proc., 2019; Elsevier: pp 2340-2357.

[269] Lang, A. E.; Espay, A. J., Disease Modification in Parkinson's Disease: Current Approaches, Challenges, and Future Considerations. *Mov. Disord.* **2018,** 33, (5), 660-677.

[270] Colombo, D.; Pnevmatikou, P.; Melloni, E.; Keywood, C., Therapeutic innovation in Parkinson's disease: a 2020 update on disease-modifying approaches. *Expert Rev. Neurother.* **2020,** 20, (10), 1047-1064.

[271] Wang, B.; Liu, Q.; Shan, H.; Xia, C.; Liu, Z., Nrf2 inducer and cncC overexpression attenuates neurodegeneration due to α-synuclein in Drosophila. *Biochem. Cell Biol.* **2015,** 93, (4), 351-8.

[272] Kim, S.; Indu Viswanath, A. N.; Park, J. H.; Lee, H. E.; Park, A. Y.; Choi, J. W.; Kim, H. J.; Londhe, A. M.; Jang, B. K.; Lee, J.; Hwang, H.; Lim, S. M.; Pae, A. N.; Park, K. D., Nrf2 activator via interference of Nrf2-Keap1 interaction has antioxidant and anti-inflammatory properties in Parkinson's disease animal model. *Neuropharmacology* **2020,** 167, 107989.

[273] Barber, P. S. R. M. A. H. S. Therapeutics for neurological disorders. WO2010046710, 2010.

[274] Jeong, J. S.; Piao, Y.; Kang, S.; Son, M.; Kang, Y. C.; Du, X. F.; Ryu, J.; Cho, Y. W.; Jiang, H.-H.; Oh, M. S.; Hong, S.-P.; Oh, Y. J.; Pak, Y. K., Triple herbal extract DA-9805 exerts a neuroprotective effect via amelioration of mitochondrial damage in experimental models of Parkinson's disease. *Sci. Rep.* **2018,** 8, (1), 15953.

[275] Yu, C.; Kim, B.-s.; Kim, E., FAF1 mediates regulated necrosis through PARP1 activation upon oxidative stress leading to dopaminergic neurodegeneration. *Cell Death Differ.* **2016,** 23, (11), 1873-1885.

[276] Park, H. S.; Song, Y. S.; Moon, B. S.; Yoo, S.-E.; Lee, J. M.; Chung, Y.-T.; Kim, E.; Lee, B. C.; Kim, S. E., Neurorestorative Effects of a Novel Fas-Associated Factor 1 Inhibitor in the MPTP Model: An [18F]FE-PE2I Positron Emission Tomography Analysis Study. *Front. Pharmacol.* **2020,** 11, (953).

[277] Ghosh, A.; Tyson, T.; George, S.; Hildebrandt, E. N.; Steiner, J. A.; Madaj, Z.; Schulz, E.; Machiela, E.; McDonald, W. G.; Escobar Galvis, M. L.; Kordower, J. H.; Van Raamsdonk, J. M.; Colca, J. R.; Brundin, P., Mitochondrial pyruvate carrier regulates autophagy, inflammation, and neurodegeneration in experimental models of Parkinson's disease. *Sci. Transl. Med.* **2016,** 8, (368), 368ra174.

[278] Athauda, D.; Maclagan, K.; Skene, S. S.; Bajwa-Joseph, M.; Letchford, D.; Chowdhury, K.; Hibbert, S.; Budnik, N.; Zampedri, L.; Dickson, J.; Li, Y.; Aviles-Olmos, I.; Warner, T. T.; Limousin, P.; Lees, A. J.; Greig, N. H.; Tebbs, S.; Foltynie, T., Exenatide once weekly versus placebo in Parkinson's disease: a randomised, double-blind, placebo-controlled trial. *Lancet* **2017,** 390, (10103), 1664-1675.

[279] Athauda, D.; Foltynie, T., The glucagon-like peptide 1 (GLP) receptor as a therapeutic target in Parkinson's disease: mechanisms of action. *Drug Discov. Today* **2016,** 21, (5), 802-18.

[280] Chen, S.; Yu, S. J.; Li, Y.; Lecca, D.; Glotfelty, E.; Kim, H. K.; Choi, H. I.; Hoffer, B. J.; Greig, N. H.; Kim, D. S.; Wang, Y., Post-treatment with PT302, a long-acting Exendin-4 sustained release formulation, reduces dopaminergic neurodegeneration in a 6-Hydroxydopamine rat model of Parkinson's disease. *Sci. Rep.* **2018,** 8, (1), 10722.

[281] Ikeda-Matsuo, Y.; Miyata, H.; Mizoguchi, T.; Ohama, E.; Naito, Y.; Uematsu, S.; Akira, S.; Sasaki, Y.; Tanabe, M., Microsomal prostaglandin E synthase-1 is a critical factor in dopaminergic neurodegeneration in Parkinson's disease. *Neurobiol. Dis.* **2019,** 124, 81-92.

[282] pipeline, G. p. http://gntpharma.com/en/pipeline/aad-2004-neurological-diseases/

[283] Insight, A. Crisdesalazine - GNT Pharma. https://adisinsight.springer.com/drugs/800032805

[284] Olson, K. E.; Kosloski-Bilek, L. M.; Anderson, K. M.; Diggs, B. J.; Clark, B. E.; Gledhill, J. M.; Shandler, S. J.; Mosley, R. L.; Gendelman, H. E., Selective VIP Receptor Agonists Facilitate Immune Transformation for Dopaminergic Neuroprotection in MPTP-Intoxicated Mice. *J. Neurosci.* **2015,** 35, (50), 16463.

[285] Mosley, R. L.; Lu, Y.; Olson, K. E.; Machhi, J.; Yan, W.; Namminga, K. L.; Smith, J. R.; Shandler, S. J.; Gendelman, H. E., A Synthetic Agonist to Vasoactive Intestinal Peptide Receptor-2 Induces Regulatory T Cell Neuroprotective Activities in Models of Parkinson's Disease. *Front. Cell. Neurosci.* **2019,** 13, 421-421.

[286] Delgado, M.; Ganea, D., Neuroprotective effect of vasoactive intestinal peptide (VIP) in a mouse model of Parkinson's disease by blocking microglial activation. *The FASEB Journal* **2003,** 17, (8), 1-18.

[287] Yuille, S.; Reichardt, N.; Panda, S., Human gut bacteria as potent class I histone deacetylase inhibitors in vitro through production of butyric acid and valeric acid. *PLoS One* **2018,** 13, (7), e0201073.

[288] Ahmed, S.; Busetti, A.; Fotiadou, P.; Vincy Jose, N.; Reid, S.; Georgieva, M.; Brown, S.; Dunbar, H.; Beurket-Ascencio, G.; Delday, M. I.; Ettorre, A.; Mulder, I. E., In vitro Characterization of Gut Microbiota-Derived Bacterial Strains With Neuroprotective Properties. *Front. Cell. Neurosci.* **2019,** 13, (402).

[289] Inc., C. P. Cantabio Pharmaceuticals to Present Latest Positive In Vivo Results From its DJ-1 Targeting Small Molecule Drug Development Program for Parkinson's Disease at the Milner Therapeutics Symposium at the University of Cambridge, UK. https://www.globenewswire.com/news-release/2018/10/01/1587841/0/en/Cantabio-Pharmaceuticals-to-Present-Latest-Positive-In-Vivo-Results-From-its-DJ-1-Targeting-Small-Molecule-Drug-Development-Program-for-Parkinson-s-Disease-at-the-Milner-Therapeuti.html

[290] Hertz, N. T.; Berthet, A.; Sos, M. L.; Thorn, K. S.; Burlingame, A. L.; Nakamura, K.; Shokat, K. M., A neo-substrate that amplifies catalytic activity of parkinson's-disease-related kinase PINK1. *Cell* **2013,** 154, (4), 737-47.

[291] Duong, T.; Kim, J.; Ruley, H. E.; Jo, D., Cell-Permeable Parkin Proteins Suppress Parkinson Disease-Associated Phenotypes in Cultured Cells and Animals. *PLoS One* **2014,** 9, (7), e102517.

[292] Fischer, T.; Sardi, S. P.; Shihabuddin, L.; Rudin, D.; Sharma, J.; Araujo, R.; Li, J.; Peterschmitt, M. J., Evaluation of Glucosylceramide Synthase (GCS) Inhibition for GBA-Associated Parkinson's Disease (P3.051). *Neurology* **2018,** 90, (15 Supplement), P3.051.

[293] Fischer, T.; Gasser, T.; Isaacson, S.; Kulisevsky, J.; Mir, P.; Simuni, T.; Wills, A. M.; Guedes, L. C.; Svenningsson, P.; Waters, C.; Ji, A.; Li, J.; Minini, P.; Nembo, B.; Sardi, S. P.; Saubadu, S.; Sharma, J.; Peterschmitt, M. J., Safety, tolerability and pharmacokinetics of oral venglustat in Parkinson's disease patients with a GBA mutation (S4.002). *Neurology* **2019,** 92, (15 Supplement), S4.002.

[294] Sidransky, E.; Arkadir, D., Substrate reduction therapy for GBA1-associated Parkinsonism: Are we betting on the wrong mouse? *Mov. Disord.* **2020,** 35, (2), 228-230.

[295] Mazzulli, J. R.; Zunke, F.; Tsunemi, T.; Toker, N. J.; Jeon, S.; Burbulla, L. F.; Patnaik, S.; Sidransky, E.; Marugan, J. J.; Sue, C. M.; Krainc, D., Activation of β-Glucocerebrosidase Reduces Pathological α-Synuclein and Restores Lysosomal Function in Parkinson's Patient Midbrain Neurons. *The Journal of neuroscience : the official journal of the Society for Neuroscience* **2016,** 36, (29), 7693-7706.

[296] Pipeline, A. Advancing on Neurodegeneration and Chemo-Resistant Cancer. https://azymustherapeutics.com/pipeline/

[297] Fuji, R. N.; Flagella, M.; Baca, M.; Baptista, M. A.; Brodbeck, J.; Chan, B. K.; Fiske, B. K.; Honigberg, L.; Jubb, A. M.; Katavolos, P.; Lee, D. W.; Lewin-Koh, S. C.; Lin, T.; Liu, X.; Liu, S.; Lyssikatos, J. P.; O'Mahony, J.; Reichelt, M.; Roose-Girma, M.; Sheng, Z.; Sherer, T.; Smith, A.; Solon, M.; Sweeney, Z. K.; Tarrant, J.; Urkowitz, A.; Warming, S.; Yaylaoglu, M.; Zhang, S.; Zhu, H.; Estrada, A. A.; Watts, R. J., Effect of selective LRRK2 kinase inhibition on nonhuman primate lung. *Sci. Transl. Med.* **2015,** 7, (273), 273ra15.

[298] Estrada, A. A.; Liu, X.; Baker-Glenn, C.; Beresford, A.; Burdick, D. J.; Chambers, M.; Chan, B. K.; Chen, H.; Ding, X.; DiPasquale, A. G.; Dominguez, S. L.; Dotson, J.; Drummond, J.; Flagella, M.; Flynn, S.; Fuji, R.; Gill, A.; Gunzner-Toste, J.; Harris, S. F.; Heffron, T. P.; Kleinheinz, T.; Lee, D. W.; Le Pichon, C. E.; Lyssikatos, J. P.; Medhurst, A. D.; Moffat, J. G.; Mukund, S.; Nash, K.; Scearce-Levie, K.; Sheng, Z.; Shore, D. G.; Tran, T.; Trivedi, N.; Wang, S.; Zhang, S.; Zhang, X.; Zhao, G.; Zhu, H.; Sweeney, Z. K., Discovery of Highly Potent, Selective, and Brain-Penetrable Leucine-

Rich Repeat Kinase 2 (LRRK2) Small Molecule Inhibitors. *J. Med. Chem.* **2012,** 55, (22), 9416-9433.

[299] Denali_Therapeutics_Inc. Denali Therapeutics Announces Positive Clinical Results From LRRK2 Inhibitor Program for Parkinson's Disease. https://www.globenewswire.com/news-release/2018/08/01/1545852/0/en/Denali-Therapeutics-Announces-Positive-Clinical-Results-From-LRRK2-Inhibitor-Program-for-Parkinson-s-Disease.html

[300] Zhao, H. T.; John, N.; Delic, V.; Ikeda-Lee, K.; Kim, A.; Weihofen, A.; Swayze, E. E.; Kordasiewicz, H. B.; West, A. B.; Volpicelli-Daley, L. A., LRRK2 Antisense Oligonucleotides Ameliorate α-Synuclein Inclusion Formation in a Parkinson's Disease Mouse Model. *Molecular therapy. Nucleic acids* **2017,** 8, 508-519.

[301] ClinicalTrials.gov A Study to Evaluate the Safety, Tolerability, and Pharmacokinetics of BIIB094 in Adults With Parkinson's Disease. https://clinicaltrials.gov/ct2/show/NCT03976349?id=NCT03976349&draw=2&rank=1&load=cart

[302] Brahmachari, S.; Karuppagounder, S. S.; Ge, P.; Lee, S.; Dawson, V. L.; Dawson, T. M.; Ko, H. S., c-Abl and Parkinson's Disease: Mechanisms and Therapeutic Potential. *J. Parkinsons Dis.* **2017,** 7, (4), 589-601.

[303] Brahmachari, S.; Ge, P.; Lee, S. H.; Kim, D.; Karuppagounder, S. S.; Kumar, M.; Mao, X.; Shin, J. H.; Lee, Y.; Pletnikova, O.; Troncoso, J. C.; Dawson, V. L.; Dawson, T. M.; Ko, H. S., Activation of tyrosine kinase c-Abl contributes to α-synuclein-induced neurodegeneration. *J. Clin. Invest.* **2016,** 126, (8), 2970-88.

[304] Karuppagounder, S. S.; Brahmachari, S.; Lee, Y.; Dawson, V. L.; Dawson, T. M.; Ko, H. S., The c-Abl inhibitor, nilotinib, protects dopaminergic neurons in a preclinical animal model of Parkinson's disease. *Sci. Rep.* **2014,** 4, 4874.

[305] Sun_Pharma_Advanced_Research_Company_pipeline SCC - 138. https://www.sparc.life/research-programs/scc-138

[306] Pagan, F.; Hebron, M.; Valadez, E. H.; Torres-Yaghi, Y.; Huang, X.; Mills, R. R.; Wilmarth, B. M.; Howard, H.; Dunn, C.; Carlson, A.; Lawler, A.; Rogers, S. L.; Falconer, R. A.; Ahn, J.; Li, Z.; Moussa, C., Nilotinib Effects in Parkinson's disease and Dementia with Lewy bodies. *J. Parkinsons Dis.* **2016,** 6, (3), 503-17.

[307] Pagan, F. L.; Hebron, M. L.; Wilmarth, B.; Torres-Yaghi, Y.; Lawler, A.; Mundel, E. E.; Yusuf, N.; Starr, N. J.; Arellano, J.; Howard, H. H.; Peyton, M.; Matar, S.; Liu, X.; Fowler, A. J.; Schwartz, S. L.; Ahn, J.; Moussa, C., Pharmacokinetics and pharmacodynamics of a single dose Nilotinib in individuals with Parkinson's disease. *Pharmacol. Res. Perspect.* **2019,** 7, (2), e00470.

[308] Pagan, F. L.; Hebron, M. L.; Wilmarth, B.; Torres-Yaghi, Y.; Lawler, A.; Mundel, E. E.; Yusuf, N.; Starr, N. J.; Anjum, M.; Arellano, J.; Howard, H. H.; Shi, W.; Mulki, S.; Kurd-Misto, T.; Matar, S.; Liu, X.; Ahn, J.; Moussa, C., Nilotinib Effects on Safety, Tolerability, and Potential Biomarkers in Parkinson Disease: A Phase 2 Randomized Clinical Trial. *JAMA Neurol* **2020,** 77, (3), 309-317.

[309] Simuni, T.; Fiske, B.; Merchant, K.; Coffey, C. S.; Klingner, E.; Caspell-Garcia, C.; Lafontant, D.-E.; Matthews, H.; Wyse, R. K.; Brundin, P.; Simon, D. K.; Schwarzschild, M.; Weiner, D.; Adams, J.; Venuto, C.; Dawson, T. M.; Baker, L.; Kostrzebski, M.; Ward, T.; Rafaloff, G., Nilotinib in Patients with Advanced Parkinson's Disease: A Randomized Phase 2A Study (NILO-PD). *medRxiv* **2020**, 2020.05.11.20093146.

[310] Goldfine, A.; Faulkner, R.; Sadashivam, V.; Omidvar, O.; Hill, J.; Jagadeesan, S.; Sharma, A.; Yao, S.-L., Results of a Phase 1 Dose-Ranging Trial, and Design of a Phase 2 Trial, of K0706, a Novel C-Abl Tyrosine Kinase Inhibitor for Parkinson's Disease. (P2.8-047). *Neurology* **2019,** 92, (15 Supplement), P2.8-047.

[311] ClinicalTrials.gov PROSEEK: A Phase 2 Study In Early Parkinson's Disease Patients Evaluating The Safety And Efficacy Of Abl Tyrosine Kinase Inhibition Using K0706. https://clinicaltrials.gov/ct2/show/NCT03655236

[312] Hunot, S.; Vila, M.; Teismann, P.; Davis, R. J.; Hirsch, E. C.; Przedborski, S.; Rakic, P.; Flavell, R. A., JNK-mediated induction of cyclooxygenase 2 is required for neurodegeneration in a mouse model of Parkinson's disease. *Proc. Natl. Acad. Sci. U. S. A.* **2004,** 101, (2), 665-70.

[313] Pan, J.; Qian, J.; Zhang, Y.; Ma, J.; Wang, G.; Xiao, Q.; Chen, S.; Ding, J., Small peptide inhibitor of JNKs protects against MPTP-induced nigral dopaminergic injury via inhibiting the JNK-signaling pathway. *Lab. Invest.* **2010,** 90, (2), 156-167.

[314] Probst, G. D.; Bowers, S.; Sealy, J. M.; Truong, A. P.; Hom, R. K.; Galemmo, R. A., Jr.; Konradi, A. W.; Sham, H. L.; Quincy, D. A.; Pan, H.; Yao, N.; Lin, M.; Tóth, G.; Artis, D. R.; Zmolek, W.; Wong, K.; Qin, A.; Lorentzen, C.; Nakamura, D. F.; Quinn, K. P.; Sauer, J. M.; Powell, K.; Ruslim, L.; Wright, S.; Chereau, D.; Ren, Z.; Anderson, J. P.; Bard, F.; Yednock, T. A.; Griswold-Prenner, I., Highly selective c-Jun N-terminal kinase (JNK) 2 and 3 inhibitors with in vitro CNS-like pharmacokinetic properties prevent neurodegeneration. *Bioorg. Med. Chem. Lett.* **2011,** 21, (1), 315-9.

[315] Decressac, M.; Björklund, A., mTOR inhibition alleviates L-DOPA-induced dyskinesia in parkinsonian rats. *J. Parkinsons Dis.* **2013,** 3, (1), 13-7.

[316] GlobeNewsWire resTORbio Announces Initiation of Phase 1b/2a Trial of RTB101 in Parkinson's Disease. https://www.globenewswire.com/news-release/2019/04/02/1795088/0/en/resTORbio-Announces-Initiation-of-Phase-1b-2a-Trial-of-RTB101-in-Parkinson-s-Disease.html

[317] Douglas, M. R.; Lewthwaite, A. J.; Nicholl, D. J., Genetics of Parkinson's disease and parkinsonism. *Expert Rev. Neurother.* **2007,** 7, (6), 657-66.

[318] Chesselet, M. F., In vivo alpha-synuclein overexpression in rodents: a useful model of Parkinson's disease? *Exp. Neurol.* **2008,** 209, (1), 22-7.

[319] Fleming, S. M.; Fernagut, P. O.; Chesselet, M. F., Genetic mouse models of parkinsonism: strengths and limitations. *NeuroRx* **2005,** 2, (3), 495-503.

[320] Fernagut, P. O.; Chesselet, M. F., Alpha-synuclein and transgenic mouse models. *Neurobiol. Dis.* **2004,** 17, (2), 123-30.

[321] Fleming, S. M.; Salcedo, J.; Hutson, C. B.; Rockenstein, E.; Masliah, E.; Levine, M. S.; Chesselet, M. F., Behavioral effects of dopaminergic agonists in transgenic mice overexpressing human wildtype alpha-synuclein. *Neuroscience* **2006,** 142, (4), 1245-53.

[322] Chesselet, M.-F.; Fleming, S.; Mortazavi, F.; Meurers, B., Strengths and limitations of genetic mouse models of Parkinson's disease. *Parkinsonism Relat. Disord.* **2008,** 14 Suppl 2, (Suppl 2), S84-S87.

[323] Fernagut, P. O.; Hutson, C. B.; Fleming, S. M.; Tetreaut, N. A.; Salcedo, J.; Masliah, E.; Chesselet, M. F., Behavioral and histopathological consequences of paraquat intoxication in mice: effects of alpha-synuclein over-expression. *Synapse* **2007,** 61, (12), 991-1001.

[324] Lang, A. E.; Obeso, J. A., Time to move beyond nigrostriatal dopamine deficiency in Parkinson's disease. *Ann. Neurol.* **2004,** 55, (6), 761-5.

[325] Segura-Aguilar, J., Can we conclude a potential therapeutic action for Parkinson's disease by using postmortem tissue and a preclinical model based on an exogenous neurotoxin? *Cell Death Dis.* **2018,** 9, (7), 748.

[326] Biedler, J. L.; Roffler-Tarlov, S.; Schachner, M.; Freedman, L. S., Multiple neurotransmitter synthesis by human neuroblastoma cell lines and clones. *Cancer Res.* **1978,** 38, (11 Part 1), 3751-3757.

[327] Ciccarone, V.; Spengler, B. A.; Meyers, M. B.; Biedler, J. L.; Ross, R. A., Phenotypic diversification in human neuroblastoma cells: expression of distinct neural crest lineages. *Cancer Res.* **1989,** 49, (1), 219-25.

[328] Arun, P.; Madhavarao, C. N.; Moffett, J. R.; Namboodiri, A. M. A., Antipsychotic drugs increase N-acetylaspartate and N-acetylaspartylglutamate in SH-SY5Y human neuroblastoma cells. *J. Neurochem.* **2008,** 106, (4), 1669-1680.

[329] Ross, R. A.; Biedler, J. L., Presence and regulation of tyrosinase activity in human neuroblastoma cell variants in vitro. *Cancer Res.* **1985,** 45, (4), 1628-1632.

[330] Takahashi, T.; Deng, Y.; Maruyama, W.; Dostert, P.; Kawai, M.; Naoi, M., Uptake of a neurotoxin-candidate, (R)-1,2-dimethyl-6,7-dihydroxy-1,2,3,4-tetrahydroisoquinoline into human dopaminergic neuroblastoma SH-SY5Y cells by dopamine transport system. *J. Neural Transm.* **1994,** 98, (2), 107-118.

[331] Påhlman, S.; Ruusala, A.-I.; Abrahamsson, L.; Mattsson, M. E.; Esscher, T., Retinoic acid-induced differentiation of cultured human neuroblastoma cells: a comparison with phorbolester-induced differentiation. *Cell Differ.* **1984,** 14, (2), 135-144.

[332] Krishna, A.; Biryukov, M.; Trefois, C.; Antony, P. M.; Hussong, R.; Lin, J.; Heinäniemi, M.; Glusman, G.; Köglsberger, S.; Boyd, O., Systems genomics evaluation of the SH-SY5Y neuroblastoma cell line as a model for Parkinson's disease. *BMC Genomics* **2014,** 15, (1), 1-21.

[333] Agholme, L.; Lindström, T.; Kågedal, K.; Marcusson, J.; Hallbeck, M., An in vitro model for neuroscience: differentiation of SH-SY5Y cells into cells with morphological and biochemical characteristics of mature neurons. *J. Alzheimer's Dis.* **2010,** 20, (4), 1069-1082.

[334] Encinas, M.; Iglesias, M.; Liu, Y.; Wang, H.; Muhaisen, A.; Cena, V.; Gallego, C.; Comella, J. X., Sequential treatment of SH-SY5Y cells with retinoic acid and brain-derived neurotrophic factor gives rise to fully differentiated, neurotrophic factor-dependent, human neuron-like cells. *J. Neurochem.* **2000,** 75, (3), 991-1003.

[335] Melino, G.; Thiele, C. J.; Knight, R. A.; Piacentini, M., Retinoids and the control of growth/death decisions in human neuroblastoma cell lines. *J. Neurooncol.* **1997,** 31, (1), 65-83.

[336] Adem, A.; Mattsson, M. E.; Nordberg, A.; Påhlman, S., Muscarinic receptors in human SH-SY5Y neuroblastoma cell line: regulation by phorbol ester and retinoic acid-induced differentiation. *Dev. Brain Res.* **1987,** 33, (2), 235-242.

[337] Lopes, F. M.; Schröder, R.; da Frota Júnior, M. L. C.; Zanotto-Filho, A.; Müller, C. B.; Pires, A. S.; Meurer, R. T.; Colpo, G. D.; Gelain, D. P.; Kapczinski, F., Comparison between proliferative and neuron-like SH-SY5Y cells as an in vitro model for Parkinson disease studies. *Brain Res.* **2010,** 1337, 85-94.

[338] Cheung, Y.-T.; Lau, W. K.-W.; Yu, M.-S.; Lai, C. S.-W.; Yeung, S.-C.; So, K.-F.; Chang, R. C.-C., Effects of all-trans-retinoic acid on human SH-SY5Y neuroblastoma as in vitro model in neurotoxicity research. *Neurotoxicology* **2009,** 30, (1), 127-135.

[339] Kovalevich, J.; Langford, D., Considerations for the Use of SH-SY5Y Neuroblastoma Cells in Neurobiology. In *Neuronal Cell Culture: Methods and Protocols*, Amini, S.; White, M. K., Eds. Humana Press: Totowa, NJ, 2013; pp 9-21.

[340] Presgraves, S. P.; Ahmed, T.; Borwege, S.; Joyce, J. N., Terminally differentiated SH-SY5Y cells provide a model system for studying neuroprotective effects of dopamine agonists. *Neurotox. Res.* **2003,** 5, (8), 579-598.

[341] Xin, W.; Emadi, S.; Williams, S.; Liu, Q.; Schulz, P.; He, P.; Alam, N. B.; Wu, J.; Sierks, M. R., Toxic oligomeric alpha-synuclein variants present in human Parkinson's disease brains are differentially generated in mammalian cell models. *Biomolecules* **2015,** 5, (3), 1634-1651.

[342] Xicoy, H.; Wieringa, B.; Martens, G. J. M., The SH-SY5Y cell line in Parkinson's disease research: a systematic review. *Mol. Neurodegener.* **2017,** 12, (1), 10.

[343] Goldie, B. J.; Barnett, M. M.; Cairns, M. J., BDNF and the maturation of posttranscriptional regulatory networks in human SH-SY5Y neuroblast differentiation. *Front. Cell. Neurosci.* **2014,** 8, 325.

[344] Ioannidis, J. P., Extrapolating from animals to humans. *Sci. Transl. Med.* **2012,** 4, (151), 151ps15-151ps15.

[345] Glinka, Y.; Gassen, M.; Youdim, M. B., Mechanism of 6-hydroxydopamine neurotoxicity. *J. Neural Transm. Suppl.* **1997,** 50, 55-66.

[346] Iglesias-González, J.; Sánchez-Iglesias, S.; Méndez-Álvarez, E.; Rose, S.; Hikima, A.; Jenner, P.; Soto-Otero, R., Differential toxicity of 6-hydroxydopamine in SH-SY5Y human neuroblastoma cells and rat brain mitochondria: protective role of catalase and superoxide dismutase. *Neurochem. Res.* **2012,** 37, (10), 2150-60.

[347] Vroegop, S. M.; Decker, D. E.; Buxser, S. E., Localization of damage induced by reactive oxygen species in cultured cells. *Free Radical Biol. Med.* **1995,** 18, (2), 141-151.

[348] Glinka, Y.; Tipton, K. F.; Youdim, M. B., Nature of inhibition of mitochondrial respiratory complex I by 6-Hydroxydopamine. *J. Neurochem.* **1996,** 66, (5), 2004-10.

[349] Glinka, Y. Y.; Youdim, M. B., Inhibition of mitochondrial complexes I and IV by 6-hydroxydopamine. *European Journal of Pharmacology: Environmental Toxicology and Pharmacology* **1995,** 292, (3-4), 329-332.

[350] Decker, D. E.; Althaus, J. S.; Buxser, S. E.; VonVoigtlander, P. F.; Ruppel, P. L., Competitive irreversible inhibition of dopamine uptake by 6-hydroxydopamine. *Res. Commun. Chem. Pathol. Pharmacol.* **1993,** 79, (2), 195-208.

[351] SANER, A.; THOENEN, H., Model Experiments on the Molecular Mechanism of Action of 6-Hydroxydopamine. *Mol. Pharmacol.* **1971,** 7, (2), 147-154.

[352] Glinka, Y. Y.; Youdim, M. B., Inhibition of mitochondrial complexes I and IV by 6-hydroxydopamine. *Eur. J. Pharmacol.* **1995,** 292, (3-4), 329-32.

[353] Tao, K.; Wang, B.; Feng, D.; Zhang, W.; Lu, F.; Lai, J.; Huang, L.; Nie, T.; Yang, Q., Salidroside Protects Against 6-Hydroxydopamine-Induced Cytotoxicity by Attenuating ER Stress. *Neurosci. Bull.* **2016,** 32, (1), 61-69.

[354] Alvarez-Fischer, D.; Henze, C.; Strenzke, C.; Westrich, J.; Ferger, B.; Höglinger, G. U.; Oertel, W. H.; Hartmann, A., Characterization of the striatal 6-OHDA model of Parkinson's disease in wild type and α-synuclein-deleted mice. *Exp. Neurol.* **2008,** 210, (1), 182-193.

[355] Vila, M.; Przedborski, S., Targeting programmed cell death in neurodegenerative diseases. *Nature Reviews Neuroscience* **2003,** 4, (5), 365-375.

[356] Javitch, J. A.; D'Amato, R. J.; Strittmatter, S. M.; Snyder, S. H., Parkinsonism-inducing neurotoxin, N-methyl-4-phenyl-1, 2, 3, 6-tetrahydropyridine: uptake of the metabolite N-methyl-4-phenylpyridine by dopamine neurons explains selective toxicity. *Proc. Nat. Acad. Sci.* **1985,** 82, (7), 2173-2177.

[357] Jackson-Lewis, V.; Vila, M.; Tieu, K.; Teismann, P.; Vadseth, C.; Choi, D.-K.; Ischiropoulos, H.; Przedborski, S., Blockade of microglial activation is neuroprotective in the 1-methyl-4-phenyl-1, 2, 3, 6-tetrahydropyridine mouse model of Parkinson disease. *J. Neurosci.* **2002,** 22, (5), 1763-1771.

[358] Selvaraj, S.; Sun, Y.; Watt, J. A.; Wang, S.; Lei, S.; Birnbaumer, L.; Singh, B. B., Neurotoxin-induced ER stress in mouse dopaminergic neurons involves downregulation of TRPC1 and inhibition of AKT/mTOR signaling. *J. Clin. Invest.* **2012,** 122, (4), 1354-67.

[359] Hisahara, S.; Shimohama, S., Toxin-induced and genetic animal models of Parkinson's disease. *Parkinsons Dis.* **2010,** 2011, 951709-951709.

[360] Uversky, V. N., Neurotoxicant-induced animal models of Parkinson's disease: understanding the role of rotenone, maneb and paraquat in neurodegeneration. *Cell Tissue Res.* **2004,** 318, (1), 225-241.

[361] Bové, J.; Prou, D.; Perier, C.; Przedborski, S., Toxin-induced models of Parkinson's disease. *NeuroRx* **2005,** 2, (3), 484-494.

[362] Gao, H. M.; Liu, B.; Hong, J. S., Critical role for microglial NADPH oxidase in rotenone-induced degeneration of dopaminergic neurons. *J. Neurosci.* **2003,** 23, (15), 6181-7.

[363] Wang, T.; Li, C.; Han, B.; Wang, Z.; Meng, X.; Zhang, L.; He, J.; Fu, F., Neuroprotective effects of Danshensu on rotenone-induced Parkinson's disease models in vitro and in vivo. *BMC complement. med. ther.* **2020,** 20, (1), 20.

[364] Chou, A.; Li, S.; Fitzmaurice, A.; Bronstein, J., Mechanisms of Rotenone-induced Proteasome Inhibition. *Neurotoxicology* **2010,** 31, 367-72.

[365] Cantu, D.; Fulton, R. E.; Drechsel, D. A.; Patel, M., Mitochondrial aconitase knockdown attenuates paraquat-induced dopaminergic cell death via decreased cellular metabolism and release of iron and H_2O_2. *J. Neurochem.* **2011,** 118, (1), 79-92.

[366] Shimizu, K.; Matsubara, K.; Ohtaki, K.; Fujimaru, S.; Saito, O.; Shiono, H., Paraquat induces long-lasting dopamine overflow through the excitotoxic pathway in the striatum of freely moving rats. *Brain Res.* **2003,** 976, (2), 243-52.

[367] Manning-Bog, A. B.; McCormack, A. L.; Li, J.; Uversky, V. N.; Fink, A. L.; Di Monte, D. A., The herbicide paraquat causes up-regulation and aggregation of alpha-synuclein in mice: paraquat and alpha-synuclein. *J. Biol. Chem.* **2002,** 277, (3), 1641-4.

[368] Moran, J. M.; Gonzalez-Polo, R. A.; Ortiz-Ortiz, M. A.; Niso-Santano, M.; Soler, G.; Fuentes, J. M., Identification of genes associated with paraquat-induced toxicity in SH-SY5Y cells by PCR array focused on apoptotic pathways. *J. Toxicol. Environ. Health A* **2008,** 71, (22), 1457-67.

[369] Sandler, M.; Carter, S. B.; Hunter, K.; Stern, G., Tetrahydroisoquinoline alkaloids: in vivo metabolites of L-dopa in man. *Nature* **1973,** 241, (5390), 439-443.

[370] Collins, M. A.; Nijm, W. P.; Borge, G. F.; Teas, G.; Goldfarb, C., Dopamine-related tetrahydroisoquinolines: significant urinary excretion by alcoholics after alcohol consumption. *Science* **1979,** 206, (4423), 1184-1186.

[371] Collins, M. A.; Bigdeli, M. G., Tetrahydroisoquinolines in vivo. I. Rat brain formation of salsolinol, a condensation product of dopamine and acetaldehyde, under certain conditions during ethanol intoxication. *Life Sci.* **1975,** 16, (4), 573-583.

[372] Naoi, M.; Maruyama, W.; Dostert, P.; Kohda, K.; Kaiya, T., A novel enzyme enantio-selectively synthesizes (R)salsolinol, a precursor of a dopaminergic neurotoxin, N-methyl(R)salsolinol. *Neurosci. Lett.* **1996,** 212, (3), 183-186.

[373] Chen, X.; Zheng, X.; Ali, S.; Guo, M.; Zhong, R.; Chen, Z.; Zhang, Y.; Qing, H.; Deng, Y., Isolation and Sequencing of Salsolinol Synthase, an Enzyme Catalyzing Salsolinol Biosynthesis. *ACS Chem. Neurosci.* **2018,** 9, (6), 1388-1398.

[374] Musshoff, F.; Schmidt, P.; Dettmeyer, R.; Priemer, F.; Wittig, H.; Madea, B., A systematic regional study of dopamine and dopamine-derived salsolinol and norsalsolinol levels in human brain areas. *Forensic Sci. Int.* **1999,** 105, (1), 1-11.

[375] Musshoff, F.; Lachenmeier, D.; Kroener, L.; Schmidt, P.; Dettmeyer, R.; Madea, B., Simultaneous gas chromatographic-mass spectrometric determination of dopamine, norsalsolinol and salsolinol enantiomers in brain samples of a large human collective. *Cell. Mol. Biol. (Noisy-le-grand)* **2003,** 49, (5), 837-849.

[376] Musshoff, F.; Lachenmeier, D. W.; Schmidt, P.; Dettmeyer, R.; Madea, B., Systematic regional study of dopamine, norsalsolinol, and (R/S)-salsolinol levels in human brain areas of alcoholics. *Alcoholism: Clinical and Experimental Research* **2005,** 29, (1), 46-52.

[377] Musshoff, F.; Schmidt, P.; Dettmeyer, R.; Priemer, F.; Jachau, K.; Madea, B., Determination of dopamine and dopamine-derived (R)-/(S)-salsolinol and norsalsolinol in various human brain areas using solid-phase extraction and gas chromatography/mass spectrometry. *Forensic Sci. Int.* **2000,** 113, (1-3), 359-366.

[378] Riggin, R. M.; Kissinger, P. T., Identification of salsolinol as a phenolic component in powdered cocoa and cocoa-based products. *J. Agric. Food Chem.* **1976,** 24, (4), 900-900.

[379] Duncan, M.; Smythe, G., Salsolinol and dopamine in alcoholic beverages. *The Lancet* **1982,** 319, (8277), 904-905.

[380] Duncan, M. W.; Smythe, G. A.; Nicholson, M. V.; Clezy, P. S., Comparison of high-performance liquid chromatography with electrochemical detection and gas chromatography—mass fragmentography for the assay of salsolinol, dopamine and dopamine metabolites in food and beverage samples. *J. chromatogr., B, Biomed. sci. appl.* **1984,** 336, (1), 199-209.

[381] Deng, Y.; Maruyama, W.; Kawai, M.; Dostert, P.; Yamamura, H.; Takahashi, T.; Naoi, M., Assay for the (R)-and (S)-enantiomers of salsolinols in biological samples and foods with ion-pair high-performance liquid chromatography using β-cyclodextrin as a chiral mobile phase additive. *J. chromatogr., B, Biomed. sci. appl.* **1997,** 689, (2), 313-320.

[382] Naoi, M.; Matsuura, S.; Takahashi, T.; Nagatsu, T., A N-methyltransferase in human brain catalyses N-methylation of 1, 2, 3, 4-tetrahydroisoquinoline into N-methyl-1, 2, 3, 4-tetrahydroisoquinoline, a precursor of a dopaminergic neurotoxin, N-methylisoquinolinium ion. *Biochem. Biophys. Res. Commun.* **1989,** 161, (3), 1213-1219.

[383] Maruyama, W.; Nakahara, D.; Ota, M.; Takahashi, T.; Takahashi, A.; Nagatsu, T.; Naoi, M., N-Methylation of dopamine-derived 6, 7-dihydroxy-1, 2, 3, 4-tetrahydroisoquinoline,(R)-salsolinol, in rat brains: in vivo microdialysis study. *J. Neurochem.* **1992,** 59, (2), 395-400.

[384] Maruyama, W.; Dostert, P.; Naoi, M., Dopamine-derived 1-methyl-6, 7-dihydroxyisoquinolines as hydroxyl radical promoters and scavengers in the rat brain: in vivo and in vitro studies. *J. Neurochem.* **1995,** 64, (6), 2635-2643.

[385] Naoi, M.; Maruyama, W.; Zhang, J. H.; Takahashi, T.; Deng, Y.; Dostert, P., Enzymatic oxidation of the dopaminergic neurotoxin, 1(R), 2(N)-dimethyl-6,7-dihydroxy-1,2,3,4-tetrahydroisoquinoline, into 1,2(N)-dimethyl-6,7-dihydroxyisoquinolinium ion. *Life Sci.* **1995,** 57, (11), 1061-6.

[386] Morikawa, N.; Naoi, M.; Maruyama, W.; Ohta, S.; Kotake, Y.; Kawai, H.; Niwa, T.; Dostert, P.; Mizuno, Y., Effects of various tetrahydroisoquinoline derivatives on mitochondrial respiration and the electron transfer complexes. *J Neural Transm (Vienna)* **1998,** 105, (6-7), 677-88.

[387] Wanpen, S.; Kooncumchoo, P.; Shavali, S.; Govitrapong, P.; Ebadi, M., Salsolinol, an endogenous neurotoxin, activates JNK and NF-kappaB signaling pathways in human neuroblastoma cells. *Neurochem. Res.* **2007,** 32, (3), 443-50.

[388] Storch, A.; Kaftan, A.; Burkhardt, K.; Schwarz, J., 1-Methyl-6, 7-dihydroxy-1, 2, 3, 4-tetrahydroisoquinoline (salsolinol) is toxic to dopaminergic neuroblastoma SH-SY5Y cells via impairment of cellular energy metabolism. *Brain Res.* **2000,** 855, (1), 67-75.

[389] Bollimuntha, S.; Ebadi, M.; Singh, B. B., TRPC1 protects human SH-SY5Y cells against salsolinol-induced cytotoxicity by inhibiting apoptosis. *Brain Res.* **2006,** 1099, (1), 141-149.

[390] Maruyama, W.; Boulton, A.; Davis, B.; Dostert, P.; Naoi, M., Enantio-specific induction of apoptosis by an endogenous neurotoxin, N-methyl (R) salsolinol, in dopaminergic SH-SY5Y cells: suppression of apoptosis by N-(2-heptyl)-N-methylpropargylamine. *J. Neural Transm.* **2001,** 108, (1), 11-24.

[391] Zhang, Y.; Ma, H.; Xie, B.; Han, C.; Wang, C.; Qing, H.; Deng, Y., Alpha-synuclein overexpression induced mitochondrial damage by the generation of endogenous neurotoxins in PC12 cells. *Neurosci. Lett.* **2013,** 547, 65-69.

[392] Kang, J. H., Salsolinol, a tetrahydroisoquinoline catechol neurotoxin, induces human Cu,Zn-superoxidie dismutase modificaiton. *J. Biochem. Mol. Biol.* **2007,** 40, (5), 684-9.

[393] Martinez-Alvarado, P.; Dagnino-Subiabre, A.; Paris, I.; Metodiewa, D.; Welch, C. J.; Olea-Azar, C.; Caviedes, P.; Caviedes, R.; Segura-Aguilar, J., Possible role of salsolinol quinone methide in the decrease of RCSN-3 cell survival. *Biochem. Biophys. Res. Commun.* **2001,** 283, (5), 1069-1076.

[394] Kim, H.-J.; Yoon, H.-R.; Washington, S.; Chang, I. I.; Oh, Y. J.; Surh, Y.-J., DNA strand scission and PC12 cell death induced by salsolinol and copper. *Neurosci. Lett.* **1997,** 238, (3), 95-98.

[395] Kim, H.-J.; Soh, Y.; Jang, J.-H.; Lee, J.-S.; Oh, Y. J.; Surh, Y.-J., Differential cell death induced by salsolinol with and without copper: possible role of reactive oxygen species. *Mol. Pharmacol.* **2001,** 60, (3), 440-449.

[396] Kang, J., Oxidative Modification of Neurofilament-L Induced by Endogenous Neurotoxin, Salsolinol. *Bull. Korean Chem. Soc* **2011,** 32329.

[397] Huang, L.-s.; Sun, G.; Cobessi, D.; Wang, A. C.; Shen, J. T.; Tung, E. Y.; Anderson, V. E.; Berry, E. A., 3-Nitropropionic Acid Is a Suicide Inhibitor of Mitochondrial Respiration That, upon Oxidation by Complex II, Forms a Covalent Adduct with a Catalytic Base Arginine in the Active Site of the Enzyme *J. Biol. Chem.* **2006,** 281, (9), 5965-5972.

[398] Colle, D.; Santos, D. B.; Hartwig, J. M.; Godoi, M.; Engel, D. F.; de Bem, A. F.; Braga, A. L.; Farina, M., Succinobucol, a Lipid-Lowering Drug, Protects Against 3-Nitropropionic Acid-Induced Mitochondrial Dysfunction and Oxidative Stress in SH-SY5Y Cells via Upregulation of Glutathione Levels and Glutamate Cysteine Ligase Activity. *Mol. Neurobiol.* **2016,** 53, (2), 1280-1295.

[399] Túnez, I.; Tasset, I.; Pérez-De La Cruz, V.; Santamaría, A., 3-Nitropropionic acid as a tool to study the mechanisms involved in Huntington's disease: past, present and future. *Molecules* **2010,** 15, (2), 878-916.

[400] Rosenstock, T.; Carvalho, A.; Jurkiewicz, A.; Frussa-Filho, R.; Smaili, S., Mitochondrial calcium, oxidative stress and apoptosis in a neurodegenerative disease model induced by 3-nitropropionic acid. *J. Neurochem.* **2004,** 88, 1220-8.

[401] Kritis, A. A.; Stamoula, E. G.; Paniskaki, K. A.; Vavilis, T. D., Researching glutamate - induced cytotoxicity in different cell lines: a comparative/collective analysis/study. *Front. Cell. Neurosci.* **2015,** 9, 91-91.

[402] Salter, M. W., Src, N-methyl-D-aspartate (NMDA) receptors, and synaptic plasticity. *Biochem. Pharmacol.* **1998,** 56, (7), 789-98.

[403] Lu, S.; Lu, C.; Han, Q.; Li, J.; Du, Z.; Liao, L.; Zhao, R. C., Adipose-derived mesenchymal stem cells protect PC12 cells from glutamate excitotoxicity-induced apoptosis by upregulation of XIAP through PI3-K/Akt activation. *Toxicology* **2011,** 279, (1-3), 189-95.

[404] Yang, J. L.; Sykora, P.; Wilson, D. M., 3rd; Mattson, M. P.; Bohr, V. A., The excitatory neurotransmitter glutamate stimulates DNA repair to increase neuronal resiliency. *Mech. Ageing Dev.* **2011,** 132, (8-9), 405-11.

[405] Cheng, B.; Martinez, A. A.; Morado, J.; Scofield, V.; Roberts, J. L.; Maffi, S. K., Retinoic acid protects against proteasome inhibition associated cell death in SH-SY5Y cells via the AKT pathway. *Neurochem. Int.* **2013,** 62, (1), 31-42.

[406] Nicholls, D. G.; Budd, S. L., Neuronal excitotoxicity: the role of mitochondria. *BioFactors* **1998,** 8, (3-4), 287-99.

[407] Boyce, M.; Yuan, J., Cellular response to endoplasmic reticulum stress: a matter of life or death. *Cell Death Differ.* **2006,** 13, (3), 363-73.

[408] Kulikov, A. V.; Rzhaninova, A. A.; Goldshtein, D. V.; Boldyrev, A. A., Expression of NMDA receptors in multipotent stromal cells of human adipose tissue under conditions of retinoic acid-induced differentiation. *Bull. Exp. Biol. Med.* **2007,** 144, (4), 626-9.

[409] Christnacher, A.; Sommer, B., Alternative splicing of AMPA receptor subunits: regulation in clonal cell lines. *FEBS Lett.* **1995,** 373, (1), 93-6.

[410] Sun, Z. W.; Zhang, L.; Zhu, S. J.; Chen, W. C.; Mei, B., Excitotoxicity effects of glutamate on human neuroblastoma SH-SY5Y cells via oxidative damage. *Neurosci. Bull.* **2010,** 26, (1), 8-16.

[411] Sun, X.; Shi, X.; Lu, L.; Jiang, Y.; Liu, B., Stimulus-dependent neuronal cell responses in SH-SY5Y neuroblastoma cells. *Mol Med Rep* **2016,** 13, (3), 2215-20.

[412] Gonzalez, G.; Grúz, J.; D'Acunto, C. W.; Kaňovský, P.; Strnad, M., Cytokinin Plant Hormones Have Neuroprotective Activity in In Vitro Models of Parkinson's Disease. *Molecules* **2021,** 26, (2).

[413] Gonzalez, G.; Hodoň, J.; Kazakova, A.; D'Acunto, C. W.; Kaňovský, P.; Urban, M.; Strnad, M., Novel pentacyclic triterpenes exhibiting strong neuroprotective activity in SH-SY5Y cells in salsolinol- and glutamate-induced neurodegeneration models. *Eur. J. Med. Chem.* **2021,** 213, 113168.

[414] Rárová, L.; Steigerová, J.; Kvasnica, M.; Bartůněk, P.; Křížová, K.; Chodounská, H.; Kolář, Z.; Sedlák, D.; Oklestkova, J.; Strnad, M., Structure activity relationship studies on cytotoxicity and the effects on steroid receptors of AB-functionalized cholestanes. *J. Steroid Biochem. Mol. Biol.* **2016,** 159, 154-169.

[415] Tammam, M. A.; Rárová, L.; Kvasnicová, M.; Gonzalez, G.; Emam, A. M.; Mahdy, A.; Strnad, M.; Ioannou, E.; Roussis, V., Bioactive Steroids from the Red Sea Soft Coral Sinularia polydactyla. *Mar. Drugs* **2020,** 18, (12), 632.

[416] Stone, W. L.; Qui, M.; Smith, M., Lipopolysaccharide enhances the cytotoxicity of 2-chloroethyl ethyl sulfide. *BMC Cell Biol.* **2003,** 4, 1-1.

[417] Kim, M. S.; Seo, J. Y.; Oh, J.; Jang, Y. K.; Lee, C. H.; Kim, J. S., Neuroprotective Effect of Halophyte Salicornia herbacea L. Is Mediated by Activation of Heme Oxygenase-1 in Mouse Hippocampal HT22 Cells. *J. Med. Food* **2017,** 20, (2), 140-151.

[418] Carrasco, R. A.; Stamm, N. B.; Patel, B. K. R., One-step cellular caspase-3/7 assay. *BioTechniques* **2003,** 34, (5), 1064-1067.

[419] Riley, J. S.; Quarato, G.; Lopez, J.; O'Prey, J.; Pearson, M.; Chapman, J.; Sesaki, H.; Carlin, L. M.; Passos, J. F.; Wheeler, A. P.; Oberst, A.; Ryan, K. M.; Tait, S. W. G., Activated BAX/BAK enable mitochondrial inner membrane permeabilisation and mtDNA release during cell death. *EMBO J.* **2018**, 272104.

[420] Kiełczewska, U.; Jorda, R.; Gonzalez, G.; Morzycki, J. W.; Ajani, H.; Svrčková, K.; Štěpánková, Š.; Wojtkielewicz, A., The synthesis and cholinesterase inhibitory activities of solasodine analogues with seven-membered F ring. *J. Steroid Biochem. Mol. Biol.* **2021,** 205, 105776.

[421] Maková, B.; Mik, V.; Lišková, B.; Gonzalez, G.; Vítek, D.; Medvedíková, M.; Monfort, B.; Ručilová, V.; Kadlecová, A.; Khirsariya, P.; Gándara Barreiro, Z.; Havlíček, L.; Zatloukal, M.; Soural, M.; Paruch, K.; D'Autréaux, B.; Hajdúch, M.; Strnad, M.; Voller, J., Cytoprotective activities of kinetin purine isosteres. *Biorg. Med. Chem.* **2021,** 33, 115993.

[422] Hammer, O.; Harper, D.; Ryan, P., PAST: Paleontological Statistics Software Package for Education and Data Analysis. *Palaeontol. Electron.* **2001,** 4, 1-9.

[423] Buko, V.; Kuzmitskaya, I.; Kirko, S.; Belonovskaya, E.; Naruta, E.; Lukivskaya, O.; Shlyahtun, A.; Ilyich, T.; Zakreska, A.; Zavodnik, I., Betulin attenuated liver damage

by prevention of hepatic mitochondrial dysfunction in rats with alcoholic steatohepatitis. *Physiol Int* **2019,** 106, (4), 323-334.

Supplementary material I.

Gonzalez, G.; Grúz, J.; D'Acunto, C.W.; Kaňovský, P.; Strnad, M. Cytokinin Plant Hormones Have Neuroprotective Activity in In Vitro Models of Parkinson's Disease. *Molecules* **2021**, *26*, **361.**

Article

Cytokinin Plant Hormones Have Neuroprotective Activity in In Vitro Models of Parkinson's Disease

Gabriel Gonzalez [1,2] **, Jiří Grúz** [1] **, Cosimo Walter D'Acunto** [1] **, Petr Kaňovský** [2] **and Miroslav Strnad** [1,2,*]

1   Laboratory of Growth Regulators, Institute of Experimental Botany of the Czech Academy of Sciences, and Faculty of Science, Palacký University, Šlechtitelů 27, CZ-78371 Olomouc, Czech Republic; Gonzalez.gabriel@seznam.cz (G.G.); jiri.gruz@upol.cz (J.G.); waldacun@gmail.com (C.W.D.)
2   Department of Neurology, University Hospital Olomouc and Faculty of Medicine and Dentistry, Palacký University Olomouc, CZ-775 20 Olomouc, Czech Republic; Petr.Kanovsky@fnol.cz
*   Correspondence: miroslav.strnad@upol.cz; Tel.: +420-585-634-850

Abstract: Cytokinins are adenine-based phytohormones that regulate key processes in plants, such as cell division and differentiation, root and shoot growth, apical dominance, branching, and seed germination. In preliminary studies, they have also shown protective activities against human neurodegenerative diseases. To extend knowledge of the protection (protective activity) they offer, we investigated activities of natural cytokinins against salsolinol (SAL)-induced toxicity (a Parkinson's disease model) and glutamate (Glu)-induced death of neuron-like dopaminergic SH-SY5Y cells. We found that kinetin-3-glucoside, *cis*-zeatin riboside, and N^6-isopentenyladenosine were active in the SAL-induced PD model. In addition, *trans*-, *cis*-zeatin, and kinetin along with the iron chelator deferoxamine (DFO) and the necroptosis inhibitor necrostatin 1 (NEC-1) significantly reduced cell death rates in the Glu-induced model. Lactate dehydrogenase assays revealed that the cytokinins provided lower neuroprotective activity than DFO and NEC-1. Moreover, they reduced apoptotic caspase-3/7 activities less strongly than DFO. However, the cytokinins had very similar effects to DFO and NEC-1 on superoxide radical production. Overall, they showed protective activity in the SAL-induced model of parkinsonian neuronal cell death and Glu-induced model of oxidative damage mainly by reduction of oxidative stress.

Keywords: cytokinin; phytohormone; neuroprotection; neuron-like SH-SY5Y cells; cytotoxicity; salsolinol; glutamate; oxidative stress; Parkinson's disease

1. Introduction

Parkinson's disease (PD) is the second most common motor-related neurodegenerative disease, and numbers of globally diagnosed cases are expected to rise from 6 million in 2015 to more than 12 million by 2040 [1]. It is characterized by motor symptoms linked with specific degeneration and loss of approximately 30–70% of dopaminergic (DA) neurons in the substantia nigra pars compacta and their projections to the striatum [2,3]. Some, of many, known molecular hallmarks of PD include enhanced oxidative and nitrosative stress, mitochondrial dysfunction [4–7], excitotoxicity [8], ubiquitin/proteasomal system dysfunction [9], and neuroinflammation [10]. Current treatments have various adverse side-effects and only offer symptomatic relief [11], so there are intense efforts to develop drugs with efficient curative effects on degenerating DA neurons. Resources that may aid such efforts include natural compounds that tend to have fewer side effects. Inter alia, substances from *Ginkgo biloba* (ginkgetin, ginkgolide, bilobalide), ginseng (ginsenosides), and flavonoids (baicalein, kaempferol, rutin and luteolin) have demonstrated broad protective activity in several in vitro models (including the human neuroblastoma cell line SH-SY5Y) and in vivo models of PD induced by 1,1'-dimethyl-4,4'-bipyridinium dichloride (paraquat), 1-methyl-4-phenyl-1,2,3,6-tetrahydropyridine (MPTP), 1-methyl-4-phenylpyridinium (MPP+), and 6-hydroxydopamine (6-OHDA) [12].
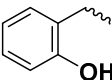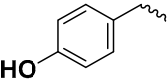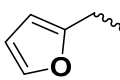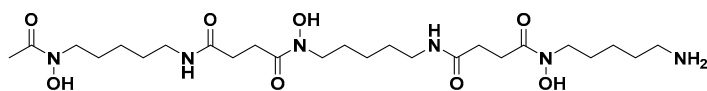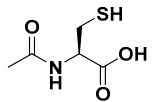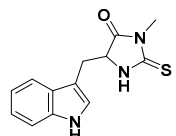
The study presented here focused on effects of a class of natural phytohormones called cytokinins (CKs), and their metabolites, which are well known regulators of cell division, growth, differentiation, and leaf senescence in plants [13]. Structurally, CKs are adenine derivatives substituted at the N^6-position with either a prenyl (isopentenyl) or aromatic sidechain. Natural forms include 6-(E)-4-hydroxy-3-methylbut-2-enylaminopurine (*trans*-zeatin, ***t*Z**), its 6-(Z)-isomer (*cis*-zeatin, ***c*Z**), N^6-isopentenyladenine (**iP**), 6-benzylaminopurine (**BAP**), 6-furfurylaminopurine (kinetin, **K**), and *ortho*-, *meta*-, and *para*-hydroxylated or methoxylated derivatives of **BAP**, called topolins (***o*T**, ***m*T**, ***p*T**, **Me*o*T**, **Me*m*T**, **Me*p*T**). Various 9-ribosides, 9-nucleotides, as well as 7-, 9, and O-glucosides of these forms also commonly occur, as shown in Table 1. In addition to their native roles in plants, CKs have shown potent ant-oxidant activity towards reactive oxygen species (ROS) that provides protection in several in vitro stress models of aging-associated disorders [14].

Table 1. Structures of cytokinins and the positive control agents.
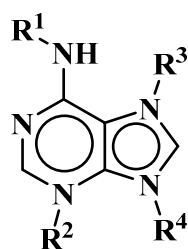
R¹	R²	R³	R⁴	Trivial Name	Abbreviation
(isopentenyl)	-	-	H	N^6-isopentenyladenine	iP
	-	-	ribosyl	N^6-isopentenyladenosine	iPR
HO (trans-zeatin sidechain)	-	-	H	*trans*-zeatin	*t*Z
	-	-	ribosyl	*t*-zeatin riboside	*t*ZR
	-	glycosyl	-	*t*-zeatin-7-glucoside	*t*Z7G
	-	-	glycosyl	*t*-zeatin-9-glucoside	*t*Z9G
	-	-	ribonucleotide	tZR-5′-monophosphate	*t*ZMP
Gluc-O (sidechain)	-	-	-	*t*-zeatin-O-glucoside	*t*ZOG
HO (cis-zeatin sidechain)	-	-	H	*cis*-zeatin	*c*Z
	-	-	ribosyl	*c*-zeatin riboside	*c*ZR
HO (cis-zeatin sidechain)	-	-	glycosyl	*c*-zeatin-9-glucoside	cZ9G
	-	-	ribonucleotide	cZR-5′-monophosphate	cZMP
glucose-O (sidechain)	-	-	-	*c*-zeatin-O-glucoside	cZOG
(benzyl)	-	-	H	6-benzylaminopurine	BAP
(meta-hydroxybenzyl)	-	-	H	*meta*-topolin	*m*T
OH	-	-	ribosyl	*meta*-topolin riboside	*m*TR

Table 1. *Cont.*

R^1	R^2	R^3	R^4	Trivial Name	Abbreviation
	-	-	H	*ortho*-topolin	*o*T
	-	-	ribosyl	*ortho*-topolin riboside	*o*TR
	-	-	H	*para*-topolin	*p*T
	-	-	ribosyl	*para*-topolin riboside	*p*TR
	-	-	H	kinetin	K
	-	-	ribosyl	kinetin riboside	KR
	-	-	ribotide	KR-5'-monophosphate	KMP
	glycosyl	-	-	kinetin-3-glucoside	K3G
	-	-	glycosyl	kinetin-9-glucoside	K9G
				Deferoxamine	DFO
				N-acetylcysteine	NAC
				Necrostatin 1	NEC-1

In particular, CKs reportedly have cytoprotective activity in models such as H$_2$O$_2$-induced cell death of human fibroblasts [15] and D-galactose-induced glycoxidative stress in rat astrocytes [16]. More importantly, in this context, they have shown neuroprotective effects in models related to neurodegenerative diseases such as familial PD, proteasome inhibitor MG 132-induced or H$_2$O$_2$-induced toxicity in SH-SY5Y cells [17], Glu-induced oxidative damage of HT22 mouse hippocampal neuronal cells [18], and the PC12 cell model of Huntington's disease [19]. Other studies indicate that CKs' protective activities involve both direct [20,21] and indirect [15,16,22] modulation of cellular redox systems. In addition to CKs' characteristic antioxidant activities, they reportedly have regulatory effects in mitochondria that enhance neuronal viability [17]. Moreover, **K** can stabilize mitochondrial membrane potential and increase ATP production, thereby mitigating Glu-induced death of HT22 cells [18]. However, despite findings regarding their effects in several models, there is limited knowledge of CKs' protective activity in the most common (sporadic) form of PD.

To address the knowledge gap described above, we systematically evaluated effects of natural CKs and their metabolites in two in vitro models: A salsolinol (SAL)-induced model of PD and glutamate (Glu)-induced model of oxidative damage in neuron-like SH-SY5Y cells. This line was used because of its dopaminergic phenotype, sensitivity to dopaminergic toxins such as SAL, and convenient formation of relatively stable populations of differentiated neuronal cells with reduced proliferation rates following 48 h exposure to 10 μM *all-trans* retinoic acid (ATRA) [23–25].

Neuron-like cells were exposed to the endo/exotoxin SAL to mimic PD pathology via dysfunction of cellular redox system: Depletion of the glutathione (GSH), and inhibition

of both anti-oxidant enzyme (Cu/Zn superoxide dismutase and catalase) activities and mitochondrial complexes (I and II), leading to apoptosis and necrosis [26]. In the other model, Glu induces potentially lethal oxidative damage by disruption of the redox system. Both models in the SH-SY5Y cell line have been previously used in neuroprotection studies [26,27].

Cytoprotective and/or antioxidant activities related to degenerative disorders of **K**, **iP**, **BAP**, **iPR**, **tZR**, and their free bases have been tested, and (as outlined above) some CKs have been found to have protective activities in neuronal cells. However, no previously published studies have examined the structure-neuroprotective activity relationship (SAR) of natural CKs (Table 1). Therefore, this study was undertaken to examine neuroprotective (anti-parkinsonian) activities of almost all known naturally occurring CKs in the selected SAL- and Glu-induced models of neurodegeneration. First, we evaluated each of the CKs' oxygen radical absorbance capacity (ORAC) and (in safety tests) cytotoxicity towards neuron-like SH-SY5Y cells. Then, we evaluated the compounds' neuroprotective effects and influence on oxidative stress levels by measuring superoxide ($O_2^{\cdot}$) production (dihydroethidium, DHE assay) and apoptotic caspase-3,7 activities. The results provide the first reported systematic indications of the relationships between natural CKs' structures and neuroprotective activities.

2. Results and Discussion

2.1. Cytokinins' Oxygen Radical Absorbance Capacity (ORAC)

As neurodegenerative diseases are associated with elevated oxidative stress, antioxidant activity plays a key role in defenses of neuronal cells. To assess CKs' biological potential in this respect, antioxidant capacity was determined by ORAC, which is commonly used to determine substances' antioxidant capacity [28]. Antioxidant capacity was expressed as Trolox equivalents (TE), which determines the effectiveness (lower to higher) of compounds than Trolox on equimolar basis. The results, presented in Table 1, show that topolins (**oT**, **mT** and **pT**) and their ribosides (**oTR**, **mTR**, **pTR**) have high antioxidant activities, which are probably closely related to the electron-rich system of their C6-hydroxybenzylamino substituent. Despite their high ORAC values, the topolins did not have high neuroprotective activity. However, several heteroaromatic CKs including **K** (N^6-furfurylaminopurine) and non-aromatic *cis*-zeatin-O-glucoside (**cZOG**), which has a 4-hydroxy-3-methylbut-2-en-1-yl)amino substituent, also showed high antioxidant capacity (Table 2). Other CK metabolites—including kinetin-3-glucoside (**K3G**), kinetin riboside 5′-monophosphate (**KMP**), kinetin-9-glucoside (**K9G**), and *trans*-zeatin riboside-5′-monophosphate (**tZMP**)—had moderate antioxidant activity. All the others had detectable capacity except **BAP**. These results confirm previous findings that **iP**, **pT**, **K** can act as direct radical scavengers, but conflict with previously reported activity of BAP in the ORAC test [20,21]. To conclude, these compounds have potential in the treatment of neurodegenerative diseases associated with increased oxidative stress [29].

2.2. Differentiation of SH-SY5Y Cells

To study CKs' neuroprotective effects, SH-SY5Y neuroblastoma cells (chosen for reasons already described [23]) were differentiated by exposure to 10 μM ATRA for 48 h as previously described [23,24]. They were then stained using a membrane staining kit to examine morphological differences between undifferentiated and differentiated cells. As shown in Figure 1A, the neuron-like differentiated cells grew less densely, were more prolonged, and produced more neurites (indicated by yellow arrows in the figure) than the undifferentiated cells. These morphological changes associated with differentiation have been previously observed, even after shorter exposure (24 h) to ATRA [24,30]. More importantly, the number of neurites rises dramatically to a level when they can create a neurite network. From this reason, cell viability was measured to compare the rate of proliferation of undifferentiated and differentiated SH-SY5Y cells. The viability of undifferentiated SH-SY5Y was taken as the maximum rate of proliferation. The results present in

Figure 1B show that proliferation rate (assessed by Calcein AM viability assay) of SH-SY5Y was reduced by 23% after 48 h ATRA treatment.
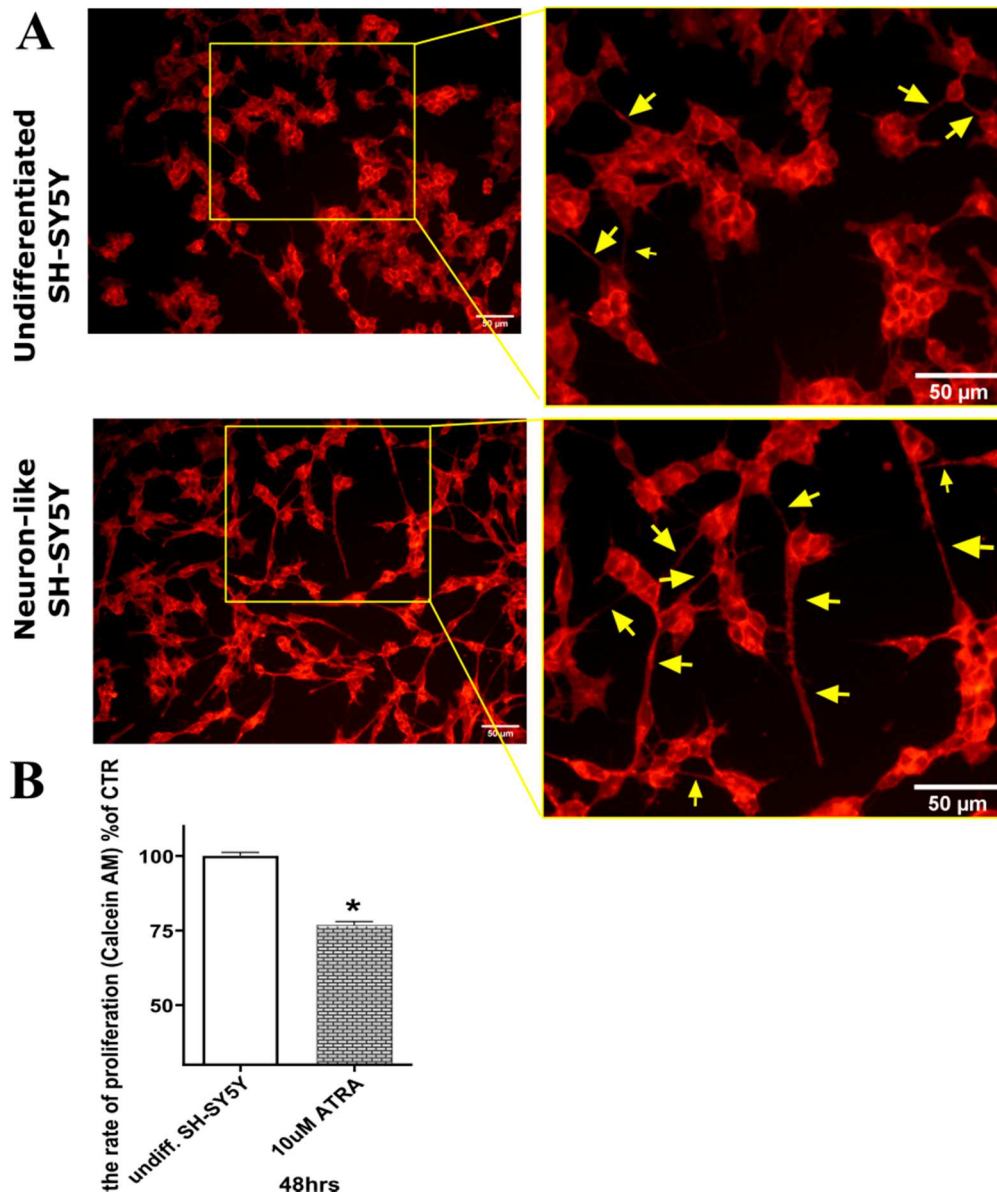

Figure 1. (**A**) Fluorescent micrographs of SH-SY5Y cells with membranes stained using a Neurite outgrowth kit (Invitrogen™): Control, undifferentiated cells (exposed to mock treatment solution: <0.1% DMSO); Cells differentiated by exposure to 10 μM all-trans retinoic acid (ATRA) for 48 h. Bars = 50 μm. (**B**) Proliferation rates of undifferentiated and differentiated SH-SY5Y cells: numbers of viable cells after 48 h exposure to <0.1% DMSO and 10 μM ATRA, respectively. Data were obtained from five independent experiments with triplicate cultures: asterisks show the significance of differences in numbers of viable cells (as percentages of numbers of undifferentiated cells) between the cultures: * $p < 0.05$.

Table 2. Oxygen radical absorbance capacity (ORAC) of the tested cytokinins (CKs) expressed as Trolox equivalents (TE) on an equimolar basis. Names, abbreviations, and structures of the CKs are presented in Figure 1.

	Average (TE)	SD (*n* = 3)		Average (TE)	SD (*n* = 3)
*t*Z	0.073	0.012	K	2.082	0.256
*t*ZR	0.13	0.012	KR	1.673	0.294
*t*ZMP	0.326	0.017	KMP	0.726	0.026
*t*Z7G	0.082	0.006	K3G	0.53	0.035
*t*Z9G	0.063	0.004	K9G	0.906	0.025
*t*ZOG	0.042	0.006	BAP	N/A *	N/A *
*c*Z	0.151	0.009	*o*T	7.026	1.179
*c*ZR	0.178	0.005	*o*TR	3.241	0.140
*c*ZMP	0.173	0.036	*m*T	4.509	0.687
*c*Z9G	0.085	0.009	*m*TR	3.171	0.239
*c*ZOG	3.301	0.036	*p*T	16.799	0.829
iP	0.384	0.005	*p*TR	4.147	0.238
iPR	0.224	0.024			

* N/A—no antioxidant capacity was detected.

2.3. Cytotoxicity of Cytokinins towards Neuron-like SH-SY5Y Cells

In tests of the CKs' potential cytotoxicity with the Calcein AM viability assay [31] most showed low toxicity towards the neuron-like SH-SY5Y cells. The decrease of viability below 90% was considered as threshold for neurotoxic effect. The only two exceptions were **KR** (11.9%) and *p***TR** (10.5%), in accordance with previous findings that some cytokinin metabolites, particularly ribosides, may have cytotoxic effects [32]. Other ribosides, such as *c***ZR**, **iPR**, *o***TR**, *m***TR**, caused no apparent reduction in the neuron-like SH-SY5Y cells' viability (Table 3). **DFO** [33,34] and **NEC-1** [35,36] used as positive controls in our in vitro model were also proved by other studies on SH-SY5Y cells to be non-toxic. In conclusion, mainly derivatives **KR** and *p***TR** showed lower viability than 90% and were therefore considered less interesting for further evaluation in both in vitro models of neurodegeneration.

Table 3. Cell viability of neuron-like SH-SY5Y cells after exposure to cytokinins for 24 h. Viability is expressed as percentage of DMSO control.

Compound	Viability [a]	Compound	Viability [a]
	(%, 10 µM)		(%, 10 µM)
*t*Z	102.3 ± 2.20	K	97.9 ± 1.81
*t*ZR	98.8 ± 1.82	KR	88.1 ± 3.09
*t*ZMP	101.5 ± 4.59	KMP	93.5 ± 3.57
*t*Z7G	101.4 ± 2.44	K3G	99.8 ± 1.13
*t*Z9G	97.6 ± 1.59	K9G	98.3 ± 1.11
*t*ZOG	94.3 ± 1.67	BAP	98.8 ± 1.40
*c*Z	104.0 ± 1.79	*o*T	95.5 ± 4.02
*c*ZR	100.0 ± 1.23	*o*TR	90.8 ± 3.81
*c*ZMP	93.8 ± 2.13	*m*T	90.4 ± 6.03
*c*Z9G	101.7 ± 2.08	*m*TR	99.5 ± 3.69
*c*ZOG	98.18 ± 1.59	*p*T	90.6 ± 3.25
iP	104.5 ± 0.97	*p*TR	89.5 ± 3.89
iPR	96.9 ± 3.25		
NAC (1 mM)	90.2 ± 5.06	DFO (100µM)	102.1 ± 4.22
NEC-1 (50 µM)	95,8 ± 3.75		

[a] viabilities are expressed as means ± SEM, compounds were tested in three independent experiments in triplicates.

2.4. Identification of Neuroprotective Cytokinins in the SAL-induced Model of PD

For these tests, neuronal SH-SY5Y cells were differentiated for 48 h then co-treated with 500 µM SAL and each CK at three concentrations (0.1, 1, 10 µM). As shown by the dot-

ted line in Figure 2A, application of the neurotoxin SAL at 500 μM reduced the viability of differentiated SH-SY5Y cells, according to the Calcein AM assay, by 30%. *N*-acetylcysteine (**NAC**) was used as a positive control in these tests due to its previously reported neuroprotective effect in the same SH-SY5Y cell-based in vitro model [37]. Concentrations of 10, 100, and 1000 μM **NAC** were used to induce partial or almost complete recovery in the SAL-model. **NAC** was able to increase cell viability at 100 μM and 1 mM concentration, corresponding to 83.39 ± 1.74% and 89.21 ± 2.89%, respectively. **NAC**'s protective activity at 100 μM (indicated by the dashed line in Figure 2A) was used as a potency threshold for selecting CKs for further tests. According to this setup, the biologically significant neuroprotective activities have been observed with **K3G** at 10 μM (81.84 ± 2.36%), *cZR* at 0.1 μM (81.14 ± 2.30%) and 1 μM (81.53 ± 2.24%) and *iPR* at 1 μM (82.43 ± 2.51%). Thus, **iPR** and **cZR** were effective neuroprotectants at lower micro or sub-micromolar concentrations than **NAC**. The cytokinin screening also revealed that many other metabolites can moderately increase the viability of differentiated SH-SY5Y cells exposed to SAL. However, some tested CKs (including *tZR*, *tZMP*, *m*T, *m*TR, *p*T, and *p*TR) had very little protective effect.
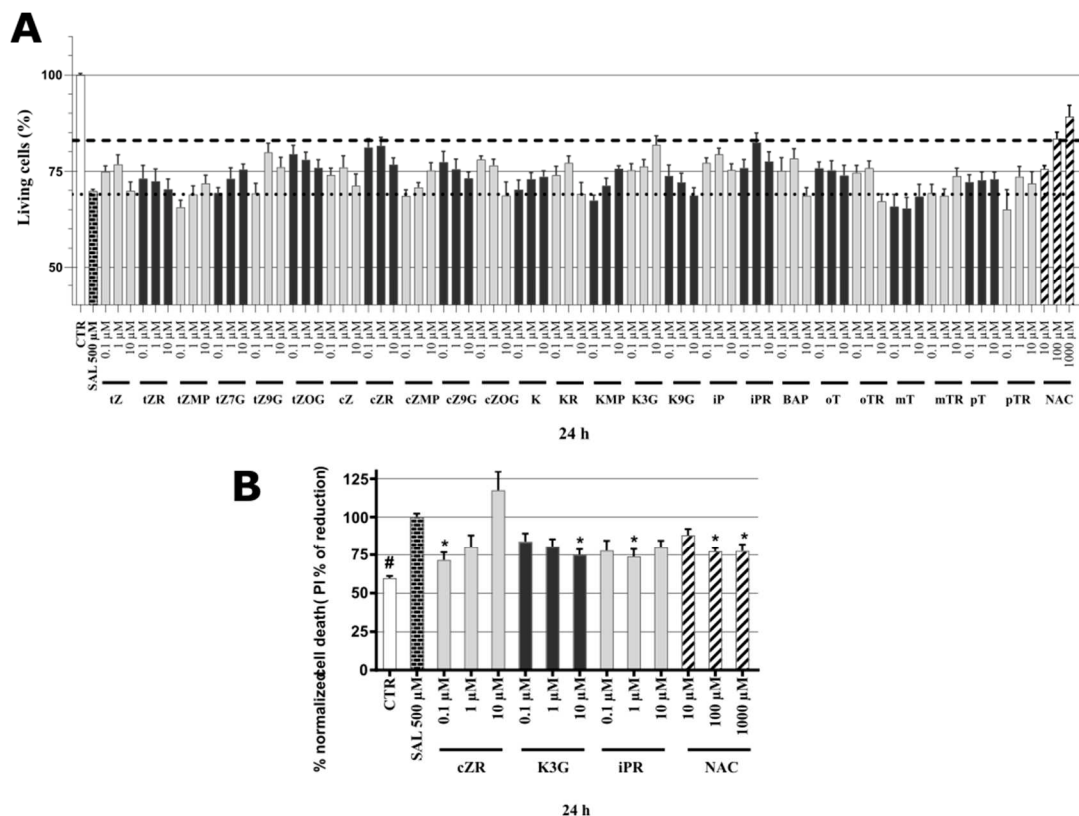
Figure 2. (**A**) Neuroprotective activity of cytokinins and *N*-acetylcystein (**NAC**) in SAL-induced model of PD on neuron-like SH-SY5Y cells. The dashed line shows the **NAC** effect threshold at which cytokinins were selected for further testing; the dotted line then counts the number of living cells in the Calcein AM assay after treating the cells with 500 μM SAL; healthy control cells (CTR, DMSO < 0.1%). Triplicates in at least three separated days. (**B**) Normalized SH-SY5Y cell death after propidium iodide staining. Triplicates in at least five independent days. * *P* compared with vehicle with 500 μM SAL, # *P* compared with vehicle without 500 μM SAL.

To confirm the most active natural CKs' anti-PD activities, overall cell death rates were quantified by propidium iodide (PI) staining, which (in contrast to cell metabolism-based viability tests) only labels cells with impaired membrane integrity, dying cells, and already dead cells [38]. Results were normalized with respect to the cell death rate following treatment with SAL alone (set as 100%). As shown in Figure 2B, the **NAC** positive control substance significantly reduced cell death rates at both 100 and 1000 μM (to 77.3 ± 2.21% and 77.5 ± 4.44%, respectively). Overall, **NAC** proved to be a neuroprotective agent with

comparable activities to those recorded in other studies in a dose-dependent manner (in the 50–500 μM range) for SH-SY5Y cells [37]. The PI assay also showed that the CKs *c*ZR, **K3G**, and **iPR** have protective activities, especially *c*ZR, which reduced the cell death rate to 71.6 ± 5.08% at 0.1 μM. In contrast to *c*ZR, **K3G** had reversed dose-dependent effects, with maximum activity at 10 μM (reducing the cell death rate to 75.0 ± 3.69%) and **iPR**'s activity peaked at 1 μM (reducing the rate to 73.9 ± 4.99%). Taken together, as shown in Figure 2, CKs provided comparable neuroprotective activity to 100 μM **NAC** according to both the viability and cytotoxicity assays. Moreover, effective concentrations of CKs such as *c*ZR and **iPR** were much lower than those of **NAC**, in the sub-micromolar and micromolar ranges. Previous observations obtained following double staining with PI and annexin V/PI indicate that **K** may reduce apoptosis [39], thus we also investigated effects of CKs and **NAC** on oxidative stress and caspase-3,7 activation (a well-known apoptosis marker).

2.5. Cytokinins Decrease SAL-induced Superoxide Radical Formation

Oxidative stress (OS) is a key pathological contributor to several neurodegenerative diseases, and both SAL (at > 100 μM) and tetrahydroisoquinolines are potent OS inducers [26,40]. Thus, we also measured formation of superoxide (a ROS and important OS marker) in the presence of SAL with and without selected CKs or **NAC**. To ensure that SAL caused sufficient OS damage in SH-SY5Y cells to detect responses, cells were exposed to 500 μM SAL for 24 h, as in previous work [37] and in accordance with findings presented above. The cells were then stained by dihydroethidium (DHE) to detect superoxide radical formation [41,42]. As can be seen in Figure 3A, cells were visually observed after labelling with DHE (which provides red fluorescence signals following reaction with superoxide). SAL induced a clear rise in DHE fluorescence, relative to levels in control and **NAC**-treated cells. Moreover, three CKs (*c*ZR, **K3G**, and **iPR**) had similar visual effects to **NAC** (100 μM) on DHE fluorescence. Furthermore, the spectrophotometric quantification with respect to levels detected in cells treated by SAL alone (set as 100%), was in line with microscopy observation. As shown in Figure 3B, the normalized superoxide level in healthy control cells (CTR) was less than 39%, and the positive control substance **NAC** provided moderate-to-complete reduction of SAL-induced ROS production at 100 and 1000 μM (to 76.3 ± 4.33 and 44.3 ± 5.12%), suggesting that glutathione (GSH) depletion plays a key role in the model [26]. Interestingly, SAL induced dramatic reductions in GSH contents of SH-SY5Y cells accompanied by elevation of OS, to levels similar to those previously observed in a study that also recorded **NAC**-mediated effects on cell viability, cell death, and glutathione contents [43]. Results presented here show that **NAC** also reduced superoxide radical formation to basal levels (i.e., levels in DMSO-treated controls). CK ribosides were tested at active concentrations (0.1–1 μM) along with **K3G**, and significantly reduced the cells' superoxide radical contents to the following levels (relative to those of cells treated with SAL alone): *c*ZR 80.34 ± 5.99% at 0.1 μM; **K3G** 77.1 ± 4.89% at 10 μM; **iPR** 79.2 ± 5.91% at 1 μM, comparable to the effects of 100 μM **NAC**. Collectively, the orthogonal demonstrations strongly indicate that potent anti-OS activity plays a key role in the protective effects of **NAC** and CKs in the SAL-induced PD model. A correlation between OS amelioration and neuroprotection has also been noted by other authors [29], and several studies have found that **K** and **BAP** can directly ameliorate OS activities [44] through formation of complexes with Cu^{2+} ions, resulting in superoxide dismutase-like activity [45,46]. However, CKs have also been described as indirect antioxidants with effects mediated by induction of the nuclear factor erythroid 2-related factor 2 (NRF2) antioxidant response pathway (**iPR**) [22] or partial restoration of glutathione peroxidase and SOD activities (**K**) [16]. In addition, **K** reportedly has neuroprotective activities against OS injury induced by H_2O_2 in SH-SY5Y cells [17]. Both types of reported anti-ROS activity of CKs could potentially explain to effects of *c*ZR, **K3G**, and **iPR** in reduction of superoxide radicals in the SAL-induced SH-SY5Y cell PD model [47–50].

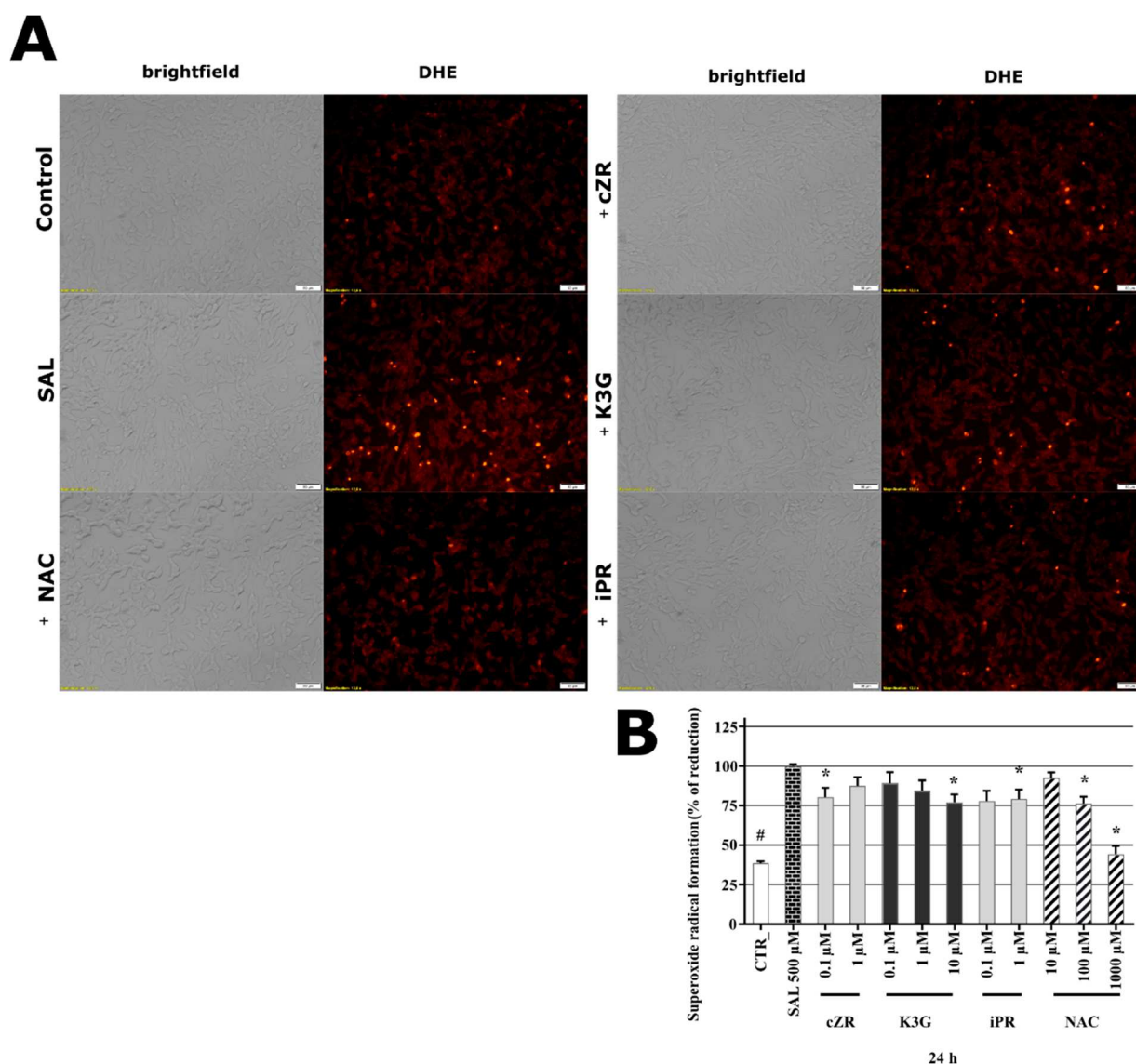**Figure 3.** (**A**) Microphotographs showing SAL-induced oxidative stress and oxidative stress-reducing activities of cytokinins in human differentiated neuron-like SH-SY5Y cells visualized by fluorescence microscopy following dihydroethidium (DHE) labelling. Bars = 50 μm. The images show cells treated with DMSO solution (controls), 500 μM salsolinol (SAL) alone, and combinations of 500 μM SAL and 1000 μM **NAC** (+**NAC**), 0.1 μM *c*ZR (+*c*ZR); 10 μM **K3G** (+**K3G**), 1μM **iPR** (+**iPR**) for 24 h before staining with DHE. (**B**) SAL-induced superoxide radical formation and cytokinin or *N*-acetylcysteine (**NAC**) protective activity. The graph shows the quantification of DHE stained cells using Infinite M200 Pro microplate reader (Tecan, Austria). Triplicates in at least five independent days. * *P* compared with vehicle with 500 μM SAL, # *P* compared with vehicle without 500 μM SAL.

2.6. Anti-Apoptotic Effects of Cytokinins Determined by Caspase-3/7 Activity Measurements

As shown by the PI staining assays described above, SAL induced increases in the SH-SY5Y cells' death rates. As SAL is associated with both apoptosis and necrosis [51] we also investigated the activation of caspase-3 and 7 (casp-3/7) as a specific marker of apoptosis (the execution phase) [52] after exposing the cells to CKs. Caspase-3/7 activities recorded following treatment with each of the test compounds were normalized with respect to those recorded following treatment with 500 μM SAL (set as 100%). As shown in Figure 4, the well-known caspase inhibitor **Ac-DEVD-CHO** (included as a specific, apoptosis-related control) strongly inhibited caspase-3/7 activity at sub-micromolar concentrations (to 36.3 ± 2.66 and 25.2 ± 2.69% of levels in cells treated with SAL alone

at 0.05 and 0.5 μM, respectively). Similar levels of inhibition have been previously observed [53] in different in vitro SH-SY5Y cell-based models of neurodegeneration. The positive control **NAC** also significantly reduced caspase-3/7 activity, to 88.7 ± 1.87% and 78.5 ± 2.56% of SAL-induced levels at 100 μM and 1000 μM, respectively. The tested CKs had a wide array of effects on caspase-3/7 activities. Interestingly from the CK ribosides, only *cZR* had significant effects on the activities at 0.1 μM (reducing them to 83.3 ± 4.33% of SAL-induced levels, respectively), while **iPR** at 1 μM did not significant reduction of casp-3,7. Finally, **K3G** decreased caspase-3/7 activity with maximum effect at 10 μM (to 81.7 ± 4.31% of the SAL-induced level). Overall, SAL-induced a 1.6-fold increase in caspase-3/7 activity compared to healthy control cells (CTR, Figure 4), in accordance with results of an earlier study, in which a similar SAL concentration (400 μM) and the same cell line were used [54]. **NAC** is known to influence caspase-3/7 activity in several models of neuronal death [55–58]. However, results presented here provide the first demonstration of their caspase-3/7 in an SH-SY5Y cell-based SAL-induced model of neuronal death. The positive control reduced the caspase-3/7 activity induced by 500 μM SAL in a similar manner to CKs, but *cZR* and **K3G** were effective even at sub-micromolar or micromolar concentrations. Other studies with stress models associated with PD (proteasome inhibitor MG 132- or H_2O_2-induced toxicity in SH-SY5Y cells [17] and fibroblasts [15]) and Huntington's disease (serum starvation model in PC12 cells [19]) have also shown that the CKs **K** and *tZR* can have anti-apoptotic (caspase-3) activities [17], and that both **K** and *tZR* can have anti-senescence activities [17,19]. Moreover, associations between decreasing of casp-3,7 activation and neuroprotective activity was reported for SAL and SAL-related models [54,59,60].
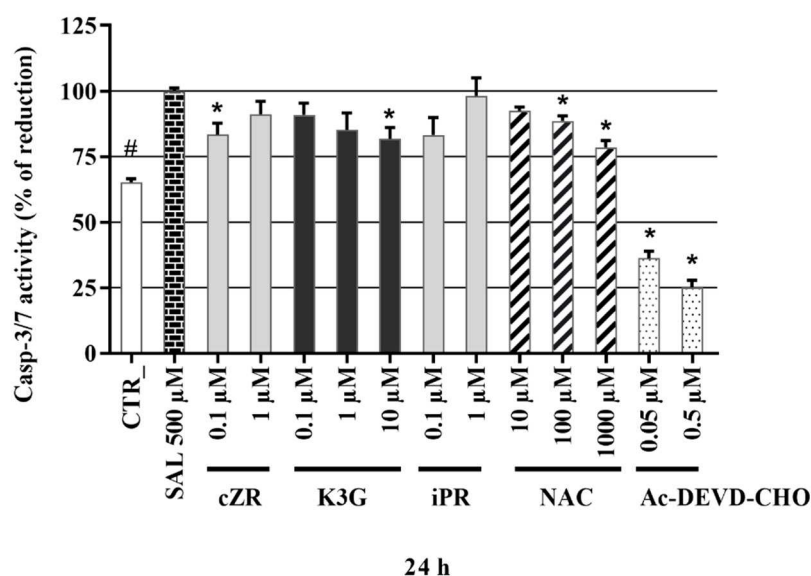
Figure 4. Caspase-3/7 activity in the SAL-induced model of PD. Triplicates in at least four independent days. * *P* compared with vehicle with 500 μM SAL, # *P* compared with vehicle without 500 μM SAL.

2.7. Identification of Cytokinin Neuroprotective Activity in the Glutamate-induced Cell Death Model

As SH-SY5Y cells do not express all NMDA receptor subunits [61], the most likely mechanism of glutamate (Glu) toxicity is blockage of the cystine/glutamate Xc-antiporter with massive induction of oxidative stress [62]. Previous authors have already demonstrated an association between glutamate-induced cell death and necroptosis in SH-SY5Y cells [63], and the importance of caspase-3 activation in glutamate-induced toxicity towards them [62,64]. Several studies have also shown the occurrence of iron-driven cell death (ferroptosis) after glutamate intoxication [62,65,66], and indicated the occurrence of three types of cell death (necroptosis, apoptosis, and ferroptosis) following blockade

of the Xc-antiporter system. In order to complete a comprehensive evaluation of the neu-roprotective potential of the tested cytokinins, the glutamate-induced cell death assay system was included in an analytical panel with the known neuroprotective iron chelator deferoxamine (**DFO**) and inhibitor of necroptosis necrostatin-1 (**NEC-1**) [67] as positive controls. Here, SH-SY5Y cells were differentiated for 48 h, then treated with 160 mM Glu or in co-treatment thereof with various cytokinin concentrations (0.1–10 μM) for 24 h and stained by PI. In this model, the effect of Glu on cell death was 100% PI signal, so the reduction in cell death by the test compounds was evaluated. Glu induced almost a 4-fold increase in cell death compared to healthy SH-SY5Y controls (26.1 $\pm$ 0.42%). Screening of positive controls and cytokinins revealed that both positive controls **NEC-1** (50 μM, 76.6 $\pm$ 2.51%) and **DFO** (10 μM, 84.2 $\pm$ 4.54%) decreased the cell death induced by glu-tamate. As shown in Figure 5A, from the panel of cytokinins, only three cytokinins were able to protect neuron-like SH-SY5Y cells in similar fashion as positive controls. The most active cytokinins were *trans*-zeatin (*t*Z) (0.1 μM, 79.5 $\pm$ 2.91%; 1 μM, 81.3 $\pm$ 2.77%) and cis-zeatin (*c*Z) (0.1 μM, 82.1 $\pm$ 3.29%; 1 μM, 86.2 $\pm$ 2.89%) and kinetin (**K**) (1 μM, 88.0 $\pm$ 3.76%; 10 μM, 79.9 $\pm$ 3.44%). To confirm their promising activity, an orthogonal assay was used to elucidate in more detail CKs' biological effects in this model: A lactate dehydrogenase (LDH)-release assay [68], which also showed a dramatic (4-fold) increase in toxicity following Glu treatment. Interestingly, the determination of LDH-release allowed us to differentiate between activities of CKs and the positive controls (**NEC-1** and **DFO**). The CKs had moderate but significant protective activity (*t*Z reduced the death rates to 91.9 $\pm$ 1.40% at 0.1 μM; *c*Z reduced them to 92.3 $\pm$ 1.15% at 0.1 μM and 91.7% $\pm$ 1.56% at 1 μM; **K** reduced them to 92.2 $\pm$ 1.06% at 1 μM). The positive controls **NEC-1** and **DFO** had stronger protective effects but were effective at much higher concentrations (reducing the rates to 76.9 $\pm$ 2.94% and 81.6 $\pm$ 3.74% at 50 and 10 μM, respectively) (Figure 5B). The LDH assay validated the indications obtained with PI staining and observed effects of the positive controls were consistent with published data [69,70]. Findings regarding effects of **K** in Glu-induced cell death model in HT22 cells [18] and our observations of effects of representative CKs such as *t*Z, *c*Z, and **K** show that CKs are promising candi-dates for treating neurodegenerative diseases associated with oxidative stress [71]. Finally, *t*Z and *c*Z were preferred because they were effective at lower concentrations and were selected, together with **K**, for further studies of their effects on levels of oxidative stress and caspase-3,7 activation.

2.8. Effects of Cytokinins on Glu-induced Oxidative Stress in SH-SY5Y cells

Unlike the previous model, Glu can induce oxidative stress in SH-SY5Y cells by differ-ent pathways. One is based on blockage of the Cystine/glutamate (Xc-) antiporter, which leads to glutathione (GSH) depletion and negative effects on superoxide dismutase (SOD) activity [62]. Glu-mediated cell death also putatively involves Rac-NADPH-oxidase-driven ROS (particularly superoxide radical) formation in SH-SY5Y cells [72]. These findings indicate that the primary cause of cell death in the Glu-induced model is OS. Within the model, neuron-like cells were co-treated with Glu and tested compounds, stained by DHE, and observed by fluorescence microscopy. As can be seen in Figure 6A, a dramatic rise in red DHE fluorescence was observed in Glu-treated cells, which was ameliorated by the positive control substances and tested CKs. Based on the microscopy observation, the quantification of superoxide levels was performed in Glu-induced cells in a similar manner, by the DHE assay, to those in SAL-induced cells. The results were normalized with respect to levels induced by Glu alone (set as 100%), which caused a dramatic, almost 3-fold increase in superoxide levels within just 4 h in neuron-like SH-SY5Y cells relative to levels in healthy control cells (CTR: 33.79 $\pm$ 1.45%). As shown in Figure 6B, CKs such as *t*Z, *c*Z, and **K** significantly reduced the superoxide level in Glu-intoxicated cells: 0.1 μM *t*Z, 0.1 μM *c*Z, 1 μM and 10 μM **K** reduced it to 81.0 $\pm$ 4.03, 80.6 $\pm$ 3.89, 81.8 $\pm$ 3.39 and 83.8 $\pm$ 2.32% of levels in cells treated with Glu alone. These levels are comparable to those obtained with the necroptosis inhibitor **NEC-1** (80.5 $\pm$ 3.19% at 5 μM and 80.4 $\pm$ 2.70%
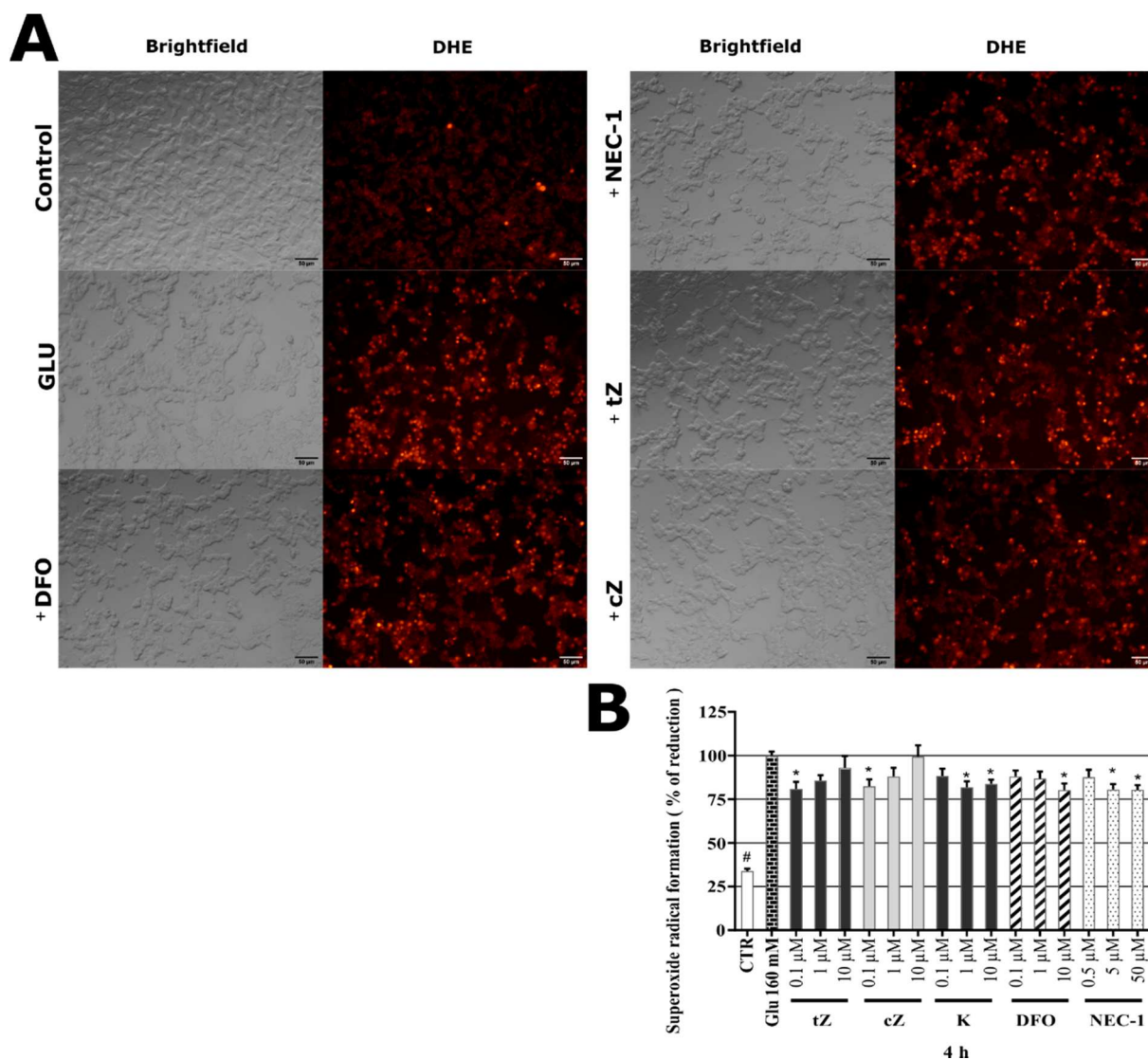
at 50 μM) and iron-chelator **DFO** (80.2 ± 3.80% at 10 μM). The results obtained with the Glu-induced cell death model, particularly the effects of positive controls, are consistent with previous reports [70,73]. Previous evidence that CKs have OS-reducing effects in Glu-induced or similar models is limited to a demonstration that **K** is a potent OS-reducing agent (at approximately 23 μM) in the HT22 cell-based Glu-induced cell death model [18]. We found that **K** had an OS-reducing effect at lower concentrations (1–10 μM) in our SH-SY5Y cells. In addition, beneficial long-term effects of *t*Z on human fibroblasts, including hydrogen peroxide-decomposing activity, have been observed [15], suggesting that *t*Z and *c*Z may have indirect OS-reducing effects in Glu-induced cell death models. Additionally, other reports pointed out the associations between CKs-mediated OS-reducing effect and protective activity [22,74–76]. Taken together, *t*Z, *c*Z, and **K** showed surprisingly strong OS-reducing effects, comparable to those of positive controls, despite differing strengths in overall neuroprotective effect.

Figure 5. (**A**) Death rate of neuron-like SH-SY5Y cells in glutamate (Glu)-induced model of cell death; (**B**) Glu-induced toxicity (LDH-release) of neuron-like SH-SY5Y cells. Triplicates in at least three independent days.* *P* compared with vehicle with 160 μM Glu, # *P* compared with vehicle without 160 μM Glu.

Figure 6. (**A**) Glu-induced oxidative stress (OS) and OS-reducing activity of indicated compounds in human neuron-like SH-SY5Y cells visualized by fluorescence microscopy following dihydroethidium (DHE) labelling. Bars = 50 μm. Images show neuron-like SH-SY5Y cells treated by DMSO (Control), 160 mM glutamate (Glu) alone, and together with: 10 μM deferoxaine (+**DFO**), 50 μM necrostatin-1 (+**NEC-1**), 0.1 μM *tZ* (+*tZ*) and 0.1μM *cZ* (+*cZ*) for 4 h, then stained by DHE. (**B**) Glu-induced superoxide radical formation in neuron-like SH-SY5Y cells after 4 h. The graph displays the quantification of DHE stained cells using Infinite M200 Pro microplate reader (Tecan, Austria). Triplicates in five independent days. * *P* compared with vehicle with 160 μM Glu, # *P* compared with vehicle without 160 μM Glu.

2.9. Effects of Cytokinins on Caspase-3/7 Activity in the Glu-induced Cell Death Model

Glu has similar toxic effects on SH-SY5Y cells to previously reported effects on HT22 cells associated with Xc-antiporter blockage. Thus, non-apoptotic cell death mechanisms (ferroptosis, necroptosis, etc.) are involved in both cases [62] although expression of caspase-3 and to some degree the NMDA subunit of NR1 may be more strongly occurred in SH-SY5Y cells [61]. Hence, final stages of cell death in the two cell lines may differ. A contributory role of caspase-3 activity has been observed in many studies in the Glu-induced model of cell death of SH-SY5Y cells [62,77–79]. In this assay, neuron-like SH-SY5Y cells were treated here with 160 mM Glu, which leads to elevation of caspase-3/7 activity. In efforts to elucidate the role of apoptosis in Glu-induced death of SH-SY5Y cells, a specific caspase-3/7 inhibitor, **Ac-DEVD-CHO**, was applied and found to have strong inhibitory effect: At 50 nM it reduced caspase-3,7 activity to 23.70 ± 1.01% of the level in cells treated

with Glu alone and at 0.5 µM it almost completely blocked the activity (reducing it to a normalized level of just 7.22 ± 1.05%; comparable to the level observed in healthy cells: 7.8 ± 0.39%), as shown in Figure 7. Application of positive controls resulted in a gradual dose-dependent decrease in caspase-3,7 activity. Interestingly, **NEC-1** had a slight effect with maximum effect at 50 µM and **DFO** had more robust inhibitory activity at 10 µM (reducing the activity to 80.5 ± 1.85 and 75.8 ± 3.00%, respectively). On the other hand, only slight, but significant effects on casp-3,7 were achieved by *tZ* at 1 µM (89.5 ± 2.50%), *cZ* at 0.1 µM (87.4 ± 1.62%) and **K** at 1 µM (91.0 ± 2.06%). Taken together, the results show that both positive controls had stronger caspase-3/7 activity-decreasing activity than the tested CKs, but the CKs had effects at much lower concentrations. Overall, the results indicate that modulation of caspase-3/7 activity plays a key role in the potent neuroprotective activity of agents such as **DFO** [58] in the Glu-induced model of cell death [79,80]. However, as shown in this section, **NEC-1** also had neuroprotective activity, suggesting that other types of cell death might be involved in Glu-induced death of neuron-like SH-SY5Y cells [63,67,81]. Indications that caspase-independent mechanisms are involved in Glu-induced cell death have also been obtained in analyses of effects of **NEC-1** [70], **DFO** [69], and K [18] on HT22 cells.
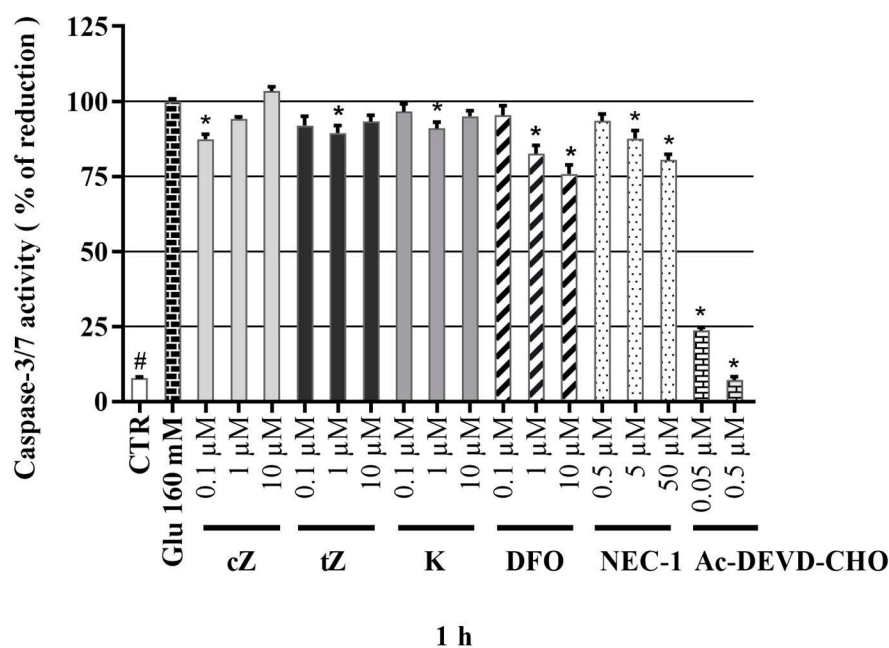
Figure 7. Caspase-3/7 activity in Glu-model of oxidative damage of neuron-like SH-SY5Y cells. Triplicates in at least four independent days. * *P* compared with vehicle with 160 µM Glu, # *P* compared with vehicle without 160 µM Glu.

3. Conclusions

In summary, our study revealed that CKs and their metabolites have neuroprotective activities in the SAL-induced model of Parkinson's disease and Glu-induced oxidative damage in human differentiated SH-SY5Y neuronal cells. **K3G**, *cZR*, and **iPR** were found to have biologically significant neuroprotective activities. Moreover, the active CKs were effective at lower (sub-micromolar and micromolar) concentrations than the positive control substance **NAC**. **K3G**, *cZR* and **iPR** also had positive effects on viability, cytotoxicity, oxidative stress and caspase-3,7 activity (except **iPR**). The orthogonal demonstrations strongly indicate that anti-oxidative stress activity plays a key role in CKs' protective effects in the SAL-induced cell death model. Only three metabolites in the tested panel of CKs (*tZ*, *cZ*, and **K**) protected neuron-like SH-SY5Y cells in the Glu-induced model of oxidative damage in a similar fashion to the iron chelator **NEC1** and necroptosis inhibitor **DFO**. To confirm their promising activity, we tested their effects in an orthogonal lactate dehydrogenase

(LDH)-release assay. The CKs had moderate but significant protective activity. This was weaker than corresponding activities of the control substances, but despite the differences in modulation of neuronal health, all three tested CKs stimulated potent reductions in superoxide radical formation, similarly to the positive control substances. The CKs also had comparable effects on Glu-induced oxidative stress in SH-SY5Y cells to those of **NEC1** and **DFO**, but these compounds had stronger inhibitory effects on caspase-3/7 activity than the CKs. As Glu-induced cell death does not rely on a caspase-dependent pathway, as shown in studies of effects of **DFO** and **NEC-1** on HT-22 cells [70], CKs can apparently modulate both caspase-dependent and -independent cell death by reducing oxidative stress [18,82]. In ongoing studies, the detailed mechanism of action of CKs and/or their mitochondrial effects on neuronal or astrocyte cells will be investigated.

4. Materials and Methods

4.1. Chemicals and Reagents

Cytokinin standards were obtained from OlChemIm (Olomouc, Czech Republic). Calcein AM (1 mg/mL solution), an LDH release kit and a Neurite outgrowth kit were purchased from ThermoFisher. Propidium iodide, dihydroethidium, components of caspase-3/7 assay buffer, DMEM/F12 1:1 medium, fetal bovine serum, trypsin, ATRA, salsolinol hydrobromide, glutamate monosodium salt, deferoxamine, *N*-acetylcysteine, Ac-DEVD-CHO, and DMSO for cell cultures were purchased from Sigma Aldrich (Merck). Ac-DEVD-AMC substrate was supplied by Enzo Life Science.

4.2. ORAC Radical Scavenging Activity Assays

Compounds' ability to scavenge free radicals in vitro was determined by the Oxygen Radical Absorbance Capacity (ORAC) assay. Briefly, fluorescein (100 µL, 500 mM) and 25 µL of tested compound solution was added to a 96-well microplate pre-incubated at 37 °C. Next, 25 µL of 250 mM 2,2′-azobis(2-amidino-propan)dihydrochloride (AAPH) was quickly added, the microplate was shaken for 5 s and red fluorescence (with 485 and 510 nm excitation and emission wavelengths, respectively) was measured every 3 min over 90 min using an Infinite 200 microplate reader (TECAN, Männedorf, Switzerland). NAUC (Net Area Under Curve) values were used to express antioxidant activities relative to that of Trolox (a synthetic hydrophilic analogue of α-tocopherol, vitamin E). Substances with ORAC values greater than zero are deemed to actively trap free radicals.

4.3. SH-SY5Y Cell Culture

The human neuroblastoma cell line SH-SY5Y purchased from ATCC (American Type Culture Collection, Manassas, VA, USA) was grown in Dulbecco's modified Eagle's Medium and Ham's F12 Nutrient Mixture (DMEM:F-12, 1:1), supplemented with 10% fetal bovine serum (FBS) and 1% penicillin and streptomycin at 37 °C in a humidified 5% CO_2 atmosphere. Cells were passaged up to 20 times and media were changed twice or thrice a week. Cell density was set as appropriate for the planned assay (5000, 7000, 10,000, or 20,000 cells per well) in 96-multiwell plates in 100 µL total volumes of medium for each experiment. The day after the seeding, ATRA in 1% FBS DMEM/F12 medium was added to the cells to a final concentration of 10 µM and incubation was continued for a further 48 h to induce differentiation, allow formation of longer neurites, and reduce proliferation.

4.4. Microscopy

Micrographs of neuron-like SH-SY5Y cells were obtained using a DM IL LED fluorescence microscope (Leica Microsystems, Mannheim, Germany) with an appropriate excitation filter for the assay, or a brightfield setup with a DP73 high-performance digital camera (Olympus, Tokyo, Japan). Since the signal-to-noise ratio for staining was moderate, the contrast was slightly adjusted in ImageJ software (Fiji) without affecting the resulting observation. Original images are included in the Supplementary Materials.

4.5. Cell Membrane Staining (Neurite Outgrowth kit, Invitrogen™)

Neuron-like SH-SY5Y cells (5000 cells per well) obtained by the 48 h differentiation procedure were stained by a Neurite outgrowth kit (Invitrogen™) according to the manufacturer's recommendations with minor modification. The cells were washed with PBS, labelled with a solution of the membrane staining dye supplied with the kit (following the protocol for 96 multiwell plates) in PBS for 20 min at 37 °C, washed again with PBS and viewed under a fluorescence microscope (with 533 and 585 nm excitation and emission wavelengths, respectively).

4.6. Cell Treatment

After the differentiation procedure, the differentiation media was changed to 1% DMEM/F12 medium supplemented with test compounds at concentrations of 0.1, 1, and 10 μM (with 7000 cells per well for cytotoxicity tests), or together with the toxin SAL at 500 μM (with 7000–10,000 cells per well) or 160 mM Glu (with 20,000 cells per well) for an appropriate duration for the assay type (viability, cell death, etc.). Control cells were treated with medium containing $\leq 0.1\%$ of DMSO.

4.7. Cell Viability and Cell Death

The viability of neuron-like SH-SY5Y cells growing in 96-well microplates (with ca. 7000 cells per well) after 24 h of treatments was evaluated by the Calcein AM assay with minor modification [31]. The Calcein AM solution in PBS used had 0.75 μM concentration and the incubation time was set to 50 min. The number of living cells in each well was determined using an Infinite M200 Pro microplate reader (Tecan, Austria), with 495 and 517 nm excitation and emission wavelengths, respectively.

Cell death of neuron-like cells (SAL model: 10,000 cells per well; Glu-model: 20,000 cells per well) was determined by PI assay as reported by Stone et al. 2003 with small modification [83]. Briefly, the medium of SAL-induced model was aspirated and changed to a 1 μg/mL solution of PI in PBS, but cells subjected to Glu-induction have weaker adherence so a 1 mg/mL solution of PI in PBS was added to give a final concentration of 1 μg/mL. In both cases, cells were incubated for a further 15–25 min at room temperature then PI fluorescence was measured by an Infinite M200 Pro reader (Tecan, Grödig, Austria) with 535 and 617 excitation and emission wavelengths, respectively. The resulting PI fluorescence obtained with toxins alone was set as 100% cell death.

4.8. Measurement of Oxidative Stress by the Dihydroethidium (DHE) assay

Cells were differentiated and treated as described in the previous section for SAL-induction (10,000 cells per well, 24 h or Glu-induction (20,000 cells per well, 4 h). After the treatments, cells were centrifuged at $500 \times g$ for 330 s, then the culture media were replaced (following aspiration) with 10 μM DHE solution in PBS. 96-multiwell plates with cells were incubated in the dark for 30 min at room temperature, then DHE fluorescence was measured by an Infinite M200 Pro microplate reader (Tecan, Grödig, Austria) with 500 and 580 nm excitation and emission wavelengths, respectively. The resulting DHE fluorescence obtained with SAL or Glu alone was set as 100% superoxide radical formation. Illustrative fluorescence microphotographs of DHE-stained cells were obtained after DHE measurement with the microplate reader.

4.9. Measurement of Caspase-3/7 Activity

One-step caspase-3/7 assays were performed according to a previously published procedure [84]. For cultures subjected to SAL-induction and Glu-induction, the reaction mixtures (caspase-3,7 buffer and components with cells in 96-multiwell plates) were incubated for 2 h and 3 h at 37 °C, respectively. Caspase-3/7 activity was then measured by an Infinite M200 Pro microplate reader (Tecan, Austria) with 346 and 438 nm excitation and emission wavelengths, respectively.

4.10. Statistical Analysis

Experiments were performed in triplicates and repeated in three to five (n = 3–5) independent days. All data are expressed as mean ± SEM. Values for all measured variables are expressed as means ± SEM, which were calculated using Prism 8.4.3 (GraphPad software, La Jolla, CA, USA), which was also used to generate the figures. The statistical analysis was carried by the PAST (ver. 1.97) software package [85]. For differentiation experiment the Student t test was used. The rest of experiments were evaluated by non-parametric Kruskal–Wallis test with Mann–Whitney *post hoc* test with sequential Bonferroni correction. A value of $p < 0.05$ was considered significant.

References

1. Dorsey, E.R.; Sherer, T.; Okun, M.S.; Bloem, B.R. The Emerging Evidence of the Parkinson Pandemic. *J. Parkinsons Dis.* **2018**, *8*, S3–S8. [CrossRef] [PubMed]
2. Rizek, P.; Kumar, N.; Jog, M.S. An update on the diagnosis and treatment of Parkinson disease. *CMAJ Can. Med Assoc. J.* **2016**, *188*, 1157–1165. [CrossRef] [PubMed]
3. Jankovic, J. Progression of Parkinson disease: Are we making progress in charting the course? *Arch. Neurol.* **2005**, *62*, 351–352. [CrossRef] [PubMed]
4. Sian, J.; Dexter, D.T.; Lees, A.J.; Daniel, S.; Agid, Y.; Javoy-Agid, F.; Jenner, P.; Marsden, C.D. Alterations in glutathione levels in Parkinson's disease and other neurodegenerative disorders affecting basal ganglia. *Ann. Neurol.* **1994**, *36*, 348–355. [CrossRef]
5. Alam, Z.I.; Daniel, S.E.; Lees, A.J.; Marsden, D.C.; Jenner, P.; Halliwell, B. A generalised increase in protein carbonyls in the brain in Parkinson's but not incidental Lewy body disease. *J. Neurochem.* **1997**, *69*, 1326–1329. [CrossRef]
6. Alam, Z.I.; Jenner, A.; Daniel, S.E.; Lees, A.J.; Cairns, N.; Marsden, C.D.; Jenner, P.; Halliwell, B. Oxidative DNA damage in the parkinsonian brain: An apparent selective increase in 8-hydroxyguanine levels in substantia nigra. *J. Neurochem.* **1997**, *69*, 1196–1203. [CrossRef]
7. Park, J.-S.; Davis, R.L.; Sue, C.M. Mitochondrial Dysfunction in Parkinson's Disease: New Mechanistic Insights and Therapeutic Perspectives. *Curr. Neurol. Neurosci. Rep.* **2018**, *18*, 21. [CrossRef]
8. Ambrosi, G.; Cerri, S.; Blandini, F. A further update on the role of excitotoxicity in the pathogenesis of Parkinson's disease. *J. Neural Transm.* **2014**, *121*, 849–859. [CrossRef]
9. Dantuma, N.P.; Bott, L.C. The ubiquitin-proteasome system in neurodegenerative diseases: Precipitating factor, yet part of the solution. *Front. Mol. Neurosci.* **2014**, *7*, 70. [CrossRef]
10. Cookson, M.R.; Bandmann, O. Parkinson's disease: Insights from pathways. *Hum. Mol. Genet.* **2010**, *19*, R21–R27. [CrossRef]
11. Rinne, U.K. Problems associated with long-term levodopa treatment of Parkinson's disease. *Acta Neurol. Scand. Suppl.* **1983**, *95*, 19–26. [CrossRef] [PubMed]
12. Corona, J.C. Natural Compounds for the Management of Parkinson's Disease and Attention-Deficit/Hyperactivity Disorder. *BioMed Res. Int.* **2018**, *2018*, 4067597. [CrossRef] [PubMed]

13. Kieber, J.J. Tribute to Folke Skoog: Recent Advances in our Understanding of Cytokinin Biology. *J. Plant Growth Regul.* **2002**, *21*, 1–2. [CrossRef] [PubMed]

14. Voller, J.; Maková, B.; Kadlecová, A.; Gonzalez, G.; Strnad, M. Plant Hormone Cytokinins for Modulating Human Aging and Age-Related Diseases. In *Hormones in Ageing and Longevity*; Rattan, S., Sharma, R., Eds.; Springer International Publishing: Cham, Switzerland, 2017; pp. 311–335.

15. Rattan, S.I.; Sodagam, L. Gerontomodulatory and youth-preserving effects of zeatin on human skin fibroblasts undergoing aging in vitro. *Rejuvenation Res* **2005**, *8*, 46–57. [CrossRef] [PubMed]

16. Liu, Y.; Zhang, Z.; Yang, X. Kinetin protects against lipid peroxidation and improves antioxidant status in cultured astrocytes and mouse brain exposed to D-galactose. *Afr. J. Biotechnol.* **2011**, *10*, 11721–11727.

17. Hertz, N.T.; Berthet, A.; Sos, M.L.; Thorn, K.S.; Burlingame, A.L.; Nakamura, K.; Shokat, K.M. A neo-substrate that amplifies catalytic activity of parkinson's-disease-related kinase PINK1. *Cell* **2013**, *154*, 737–747. [CrossRef]

18. Wei, Y.; Liu, D.; Zheng, Y.; Hao, C.; Li, H.; Ouyang, W. Neuroprotective Effects of Kinetin Against Glutamate-Induced Oxidative Cytotoxicity in HT22 Cells: Involvement of Nrf2 and Heme Oxygenase-1. *Neurotox. Res.* **2018**, *33*, 725–737. [CrossRef]

19. Lee, Y.-C.; Yang, Y.-C.; Huang, C.-L.; Kuo, T.-Y.; Lin, J.-H.; Yang, D.-M.; Huang, N.-K. When Cytokinin, a Plant Hormone, Meets the Adenosine A2A Receptor: A Novel Neuroprotectant and Lead for Treating Neurodegenerative Disorders? *PLoS ONE* **2012**, *7*, e38865. [CrossRef]

20. Brizzolari, A.; Marinello, C.; Carini, M.; Santaniello, E.; Biondi, P.A. Evaluation of the antioxidant activity and capacity of some natural N6-substituted adenine derivatives (cytokinins) by fluorimetric and spectrophotometric assays. *J. Chromatogr. B* **2016**, *1019*, 164–168. [CrossRef]

21. McDaniel, D.H.; Neudecker, B.A.; DiNardo, J.C.; Lewis Ii, J.A.; Maibach, H.I. Idebenone: A new antioxidant—Part I. Relative assessment of oxidative stress protection capacity compared to commonly known antioxidants. *J. Cosmet. Dermatol.* **2005**, *4*, 10–17. [CrossRef]

22. Dassano, A.; Mancuso, M.; Giardullo, P.; De Cecco, L.; Ciuffreda, P.; Santaniello, E.; Saran, A.; Dragani, T.A.; Colombo, F. N(6)-isopentenyladenosine and analogs activate the NRF2-mediated antioxidant response. *Redox Biol.* **2014**, *2*, 580–589. [CrossRef] [PubMed]

23. Forster, J.I.; Köglsberger, S.; Trefois, C.; Boyd, O.; Baumuratov, A.S.; Buck, L.; Balling, R.; Antony, P.M. Characterization of Differentiated SH-SY5Y as Neuronal Screening Model Reveals Increased Oxidative Vulnerability. *J. Biomol. Screen.* **2016**, *21*, 496–509. [CrossRef] [PubMed]

24. Dwane, S.; Durack, E.; Kiely, P.A. Optimising parameters for the differentiation of SH-SY5Y cells to study cell adhesion and cell migration. *BMC Res. Notes* **2013**, *6*, 366. [CrossRef] [PubMed]

25. Xicoy, H.; Wieringa, B.; Martens, G.J.M. The SH-SY5Y cell line in Parkinson's disease research: A systematic review. *Mol. Neurodegener.* **2017**, *12*, 10. [CrossRef]

26. Kurnik-Łucka, M.; Panula, P.; Bugajski, A.; Gil, K. Salsolinol: An Unintelligible and Double-Faced Molecule—Lessons Learned from In Vivo and In Vitro Experiments. *Neurotox. Res.* **2018**, *33*, 485–514. [CrossRef]

27. Li, C.; Chai, S.; Ju, Y.; Hou, L.; Zhao, H.; Ma, W.; Li, T.; Sheng, J.; Shi, W. Pu-erh Tea Protects the Nervous System by Inhibiting the Expression of Metabotropic Glutamate Receptor 5. *Mol. Neurobiol.* **2017**, *54*, 5286–5299. [CrossRef]

28. Ou, B.; Hampsch-Woodill, M.; Prior, R.L. Development and validation of an improved oxygen radical absorbance capacity assay using fluorescein as the fluorescent probe. *J. Agric. Food Chem.* **2001**, *49*, 4619–4626. [CrossRef]

29. McBean, G.J.; López, M.G.; Wallner, F.K. Redox-based therapeutics in neurodegenerative disease. *Br. J. Pharmacol.* **2017**, *174*, 1750–1770. [CrossRef]

30. Cheung, Y.-T.; Lau, W.K.-W.; Yu, M.-S.; Lai, C.S.-W.; Yeung, S.-C.; So, K.-F.; Chang, R.C.-C. Effects of all-trans-retinoic acid on human SH-SY5Y neuroblastoma as in vitro model in neurotoxicity research. *Neurotoxicology* **2009**, *30*, 127–135. [CrossRef]

31. Rárová, L.; Steigerová, J.; Kvasnica, M.; Bartůněk, P.; Křížová, K.; Chodounská, H.; Kolář, Z.; Sedlák, D.; Oklestkova, J.; Strnad, M. Structure activity relationship studies on cytotoxicity and the effects on steroid receptors of AB-functionalized cholestanes. *J. Steroid Biochem. Mol. Biol.* **2016**, *159*, 154–169. [CrossRef]

32. Voller, J.; Zatloukal, M.; Lenobel, R.; Dolezal, K.; Béres, T.; Krystof, V.; Spíchal, L.; Niemann, P.; Dzubák, P.; Hajdúch, M.; et al. Anticancer activity of natural cytokinins: A structure-activity relationship study. *Phytochemistry* **2010**, *71*, 1350–1359. [CrossRef] [PubMed]

33. Texel, S.J.; Zhang, J.; Camandola, S.; Unger, E.L.; Taub, D.D.; Koehler, R.C.; Harris, Z.L.; Mattson, M.P. Ceruloplasmin Deficiency Reduces Levels of Iron and BDNF in the Cortex and Striatum of Young Mice and Increases Their Vulnerability to Stroke. *PLoS ONE* **2011**, *6*, e25077. [CrossRef] [PubMed]

34. Guan, H.; Yang, H.; Yang, M.; Yanagisawa, D.; Bellier, J.-P.; Mori, M.; Takahata, S.; Nonaka, T.; Zhao, S.; Tooyama, I. Mitochondrial ferritin protects SH-SY5Y cells against H2O2-induced oxidative stress and modulates α-synuclein expression. *Exp. Neurol.* **2017**, *291*, 51–61. [CrossRef] [PubMed]

35. Hirayama, N.; Aki, T.; Funakoshi, T.; Noritake, K.; Unuma, K.; Uemura, K. Necrosis in human neuronal cells exposed to paraquat. *J. Toxicol. Sci.* **2018**, *43*, 193–202. [CrossRef]

36. Ito, K.; Eguchi, Y.; Imagawa, Y.; Akai, S.; Mochizuki, H.; Tsujimoto, Y. MPP+ induces necrostatin-1- and ferrostatin-1-sensitive necrotic death of neuronal SH-SY5Y cells. *Cell Death Discov.* **2017**, *3*, 17013. [CrossRef]

37. Wanpen, S.; Govitrapong, P.; Shavali, S.; Sangchot, P.; Ebadi, M. Salsolinol, a dopamine-derived tetrahydroisoquinoline, induces cell death by causing oxidative stress in dopaminergic SH-SY5Y cells, and the said effect is attenuated by metallothionein. *Brain Res.* **2004**, *1005*, 67–76. [CrossRef]

38. Dengler, W.A.; Schulte, J.; Berger, D.P.; Mertelsmann, R.; Fiebig, H.H. Development of a propidium iodide fluorescence assay for proliferation and cytotoxicity assays. *Anti-Cancer Drugs* **1995**, *6*, 522–532. [CrossRef]

39. Othman, E.M.; Naseem, M.; Awad, E.; Dandekar, T.; Stopper, H. The Plant Hormone Cytokinin Confers Protection against Oxidative Stress in Mammalian Cells. *PLoS ONE* **2016**, *11*, e0168386. [CrossRef]

40. Yap, Y.; Omasanggar, R.; Koh, Y.L.; Yew, M.Y.; Lai, H.T.; Ling, A.P.K.; Chye, S.M.; Ng, K.Y.; Koh, R.Y. Neurotoxic effect of salsolinol through oxidative stress induction and Nrf2-Keap1 signalling regulation. *J. Chem. Pharm. Res.* **2016**, *8*, 30–38.

41. Bindokas, V.P.; Jordan, J.; Lee, C.C.; Miller, R.J. Superoxide production in rat hippocampal neurons: Selective imaging with hydroethidine. *J. Neurosci.* **1996**, *16*, 1324–1336. [CrossRef]

42. Carter, W.O.; Narayanan, P.K.; Robinson, J.P. Intracellular hydrogen peroxide and superoxide anion detection in endothelial cells. *J. Leukoc. Biol.* **1994**, *55*, 253–258. [PubMed]

43. Wanpen, S.; Kooncumchoo, P.; Shavali, S.; Govitrapong, P.; Ebadi, M. Salsolinol, an endogenous neurotoxin, activates JNK and NF-kappaB signaling pathways in human neuroblastoma cells. *Neurochem. Res.* **2007**, *32*, 443–450. [CrossRef] [PubMed]

44. Jabłońska-Trypuć, A.; Matejczyk, M.; Czerpak, R. N6-benzyladenine and kinetin influence antioxidative stress parameters in human skin fibroblasts. *Mol. Cell. Biochem.* **2016**, *413*, 97–107. [CrossRef] [PubMed]

45. Goldstein, S.; Czapski, G. SOD-like activity studies of cytokinin-copper(II) complexes. *Free Radic. Res. Commun.* **1991**, *12*, 173–177. [CrossRef] [PubMed]

46. Štarha, P.; Trávníček, Z.; Herchel, R.; Popa, I.; Suchý, P.; Vančo, J. Dinuclear copper(II) complexes containing 6-(benzylamino)purines as bridging ligands: Synthesis, characterization, and in vitro and in vivo antioxidant activities. *J. Inorg. Biochem.* **2009**, *103*, 432–440. [CrossRef] [PubMed]

47. De Lazzari, F.; Bubacco, L.; Whitworth, A.J.; Bisaglia, M. Superoxide Radical Dismutation as New Therapeutic Strategy in Parkinson's Disease. *Aging Dis.* **2018**, *9*, 716–728. [CrossRef]

48. Lalkovičová, M.; Danielisová, V. Neuroprotection and antioxidants. *Neural Regen. Res.* **2016**, *11*, 865–874. [CrossRef]

49. Surendran, S.; Raja Sankar, S. Parkinson's disease: Oxidative stress and therapeutic approaches. *Neurol. Sci.* **2010**, *31*, 531–540. [CrossRef]

50. Lee, K.H.; Cha, M.; Lee, B.H. Neuroprotective Effect of Antioxidants in the Brain. *Int. J. Mol. Sci.* **2020**, *21*, 7152. [CrossRef]

51. Bollimuntha, S.; Ebadi, M.; Singh, B.B. TRPC1 protects human SH-SY5Y cells against salsolinol-induced cytotoxicity by inhibiting apoptosis. *Brain Res.* **2006**, *1099*, 141–149. [CrossRef]

52. Walsh, J.G.; Cullen, S.P.; Sheridan, C.; Lüthi, A.U.; Gerner, C.; Martin, S.J. Executioner caspase-3 and caspase-7 are functionally distinct proteases. *Proc. Natl. Acad. Sci. USA* **2008**, *105*, 12815. [CrossRef] [PubMed]

53. Jantas, D.; Piotrowski, M.; Lason, W. An Involvement of PI3-K/Akt Activation and Inhibition of AIF Translocation in Neuroprotective Effects of Undecylenic Acid (UDA) Against Pro-Apoptotic Factors-Induced Cell Death in Human Neuroblastoma SH-SY5Y Cells. *J. Cell. Biochem.* **2015**, *116*, 2882–2895. [CrossRef] [PubMed]

54. Brown, D.; Tamas, A.; Reglödi, D.; Tizabi, Y. PACAP Protects Against Salsolinol-Induced Toxicity in Dopaminergic SH-SY5Y Cells: Implication for Parkinson's Disease. *J. Mol. Neurosci.* **2013**, *50*, 600–607. [CrossRef] [PubMed]

55. Cheng, B.; Anand, P.; Kuang, A.; Akhtar, F.; Scofield, V.L. N-Acetylcysteine in Combination with IGF-1 Enhances Neuroprotection against Proteasome Dysfunction-Induced Neurotoxicity in SH-SY5Y Cells. *Parkinsons Dis.* **2016**, *2016*, 6564212. [CrossRef]

56. Li, J.; Meng, Z.; Zhang, G.; Xing, Y.; Feng, L.; Fan, S.; Fan, F.; Buren, B.; Liu, Q. N-acetylcysteine relieves oxidative stress and protects hippocampus of rat from radiation-induced apoptosis by inhibiting caspase-3. *Biomed. Pharmacother.* **2015**, *70*, 1–6. [CrossRef]

57. Rakshit, J.; Mallick, A.; Roy, S.; Sarbajna, A.; Dutta, M.; Bandyopadhyay, J. Iron-Induced Apoptotic Cell Death and Autophagy Dysfunction in Human Neuroblastoma Cell Line SH-SY5Y. *Biol. Trace Elem. Res.* **2019**, *193*, 138–151. [CrossRef]

58. Rakshit, J.; Priyam, A.; Gowrishetty, K.K.; Mishra, S.; Bandyopadhyay, J. Iron chelator Deferoxamine protects human neuroblastoma cell line SH-SY5Y from 6-Hydroxydopamine-induced apoptosis and autophagy dysfunction. *J. Trace Elem. Med. Biol.* **2020**, *57*, 126406. [CrossRef]

59. Ma, X.W.; Guo, R.Y. Dose-dependent effect of Curcuma longa for the treatment of Parkinson's disease. *Exp. Ther. Med.* **2017**, *13*, 1799–1805. [CrossRef]

60. Naoi, M.; Maruyama, W.; Takahashi, T.; Akao, Y.; Nakagawa, Y. Involvement of endogenous N-methyl(R)salsolinol in Parkinson's disease: Induction of apoptosis and protection by (-)deprenyl. In *Advances in Research on Neurodegeneration*; Mizuno, Y., Calne, D.B., Horowski, R., Poewe, W., Riederer, P., Youdim, M.B.H., Eds.; Springer: Vienna, Austria, 2000; pp. 111–121.

61. Kulikov, A.V.; Rzhaninova, A.A.; Goldshtein, D.V.; Boldyrev, A.A. Expression of NMDA receptors in multipotent stromal cells of human adipose tissue under conditions of retinoic acid-induced differentiation. *Bull. Exp. Biol. Med.* **2007**, *144*, 626–629. [CrossRef]

62. Kritis, A.A.; Stamoula, E.G.; Paniskaki, K.A.; Vavilis, T.D. Researching glutamate—Induced cytotoxicity in different cell lines: A comparative/collective analysis/study. *Front. Cell. Neurosci.* **2015**, *9*, 91. [CrossRef]

63. Sun, X.; Shi, X.; Lu, L.; Jiang, Y.; Liu, B. Stimulus-dependent neuronal cell responses in SH-SY5Y neuroblastoma cells. *Mol. Med. Rep.* **2016**, *13*, 2215–2220. [CrossRef] [PubMed]

64. Cunha, M.P.; Lieberknecht, V.; Ramos-Hryb, A.B.; Olescowicz, G.; Ludka, F.K.; Tasca, C.I.; Gabilan, N.H.; Rodrigues, A.L.S. Creatine affords protection against glutamate-induced nitrosative and oxidative stress. *Neurochem. Int.* **2016**, *95*, 4–14. [CrossRef] [PubMed]

65. Mou, Y.; Wang, J.; Wu, J.; He, D.; Zhang, C.; Duan, C.; Li, B. Ferroptosis, a new form of cell death: Opportunities and challenges in cancer. *J. Hematol. Oncol.* **2019**, *12*, 34. [CrossRef] [PubMed]

66. Zille, M.; Kumar, A.; Kundu, N.; Bourassa, M.W.; Wong, V.S.C.; Willis, D.; Karuppagounder, S.S.; Ratan, R.R. Ferroptosis in Neurons and Cancer Cells Is Similar But Differentially Regulated by Histone Deacetylase Inhibitors. *eNeuro* **2019**, *6*. [CrossRef]

67. Jantas, D.; Chwastek, J.; Grygier, B.; Lasoń, W. Neuroprotective Effects of Necrostatin-1 Against Oxidative Stress–Induced Cell Damage: An Involvement of Cathepsin D Inhibition. *Neurotox. Res.* **2020**, *37*, 525–542. [CrossRef]

68. Sun, Z.W.; Zhang, L.; Zhu, S.J.; Chen, W.C.; Mei, B. Excitotoxicity effects of glutamate on human neuroblastoma SH-SY5Y cells via oxidative damage. *Neurosci. Bull.* **2010**, *26*, 8–16. [CrossRef]

69. Chu, J.; Liu, C.-X.; Song, R.; Li, Q.-L. Ferrostatin-1 protects HT-22 cells from oxidative toxicity. *Neural Regen. Res.* **2020**, *15*, 528–536.

70. Xu, X.; Chua, C.C.; Kong, J.; Kostrzewa, R.M.; Kumaraguru, U.; Hamdy, R.C.; Chua, B.H. Necrostatin-1 protects against glutamate-induced glutathione depletion and caspase-independent cell death in HT-22 cells. *J. Neurochem.* **2007**, *103*, 2004–2014. [CrossRef]

71. Shirlee, T.; David, S.; Pamela, M. Oxytosis: A Novel Form of Programmed Cell Death. *Curr. Top. Med. Chem.* **2001**, *1*, 497–506. [CrossRef]

72. Nikolova, S.; Lee, Y.S.; Lee, Y.-S.; Kim, J.-A. Rac1-NADPH oxidase-regulated generation of reactive oxygen species mediates glutamate-induced apoptosis in SH-SY5Y human neuroblastoma cells. *Free Radic. Res.* **2005**, *39*, 1295–1304. [CrossRef]

73. Jelinek, A.; Heyder, L.; Daude, M.; Plessner, M.; Krippner, S.; Grosse, R.; Diederich, W.; Culmsee, C. Mitochondrial rescue prevents glutathione peroxidase-dependent ferroptosis. *Free Radic. Biol. Med.* **2018**, *117*, 45–57. [CrossRef]

74. Olsen, A.; Siboska, G.E.; Clark, B.F.C.; Rattan, S.I.S. N6-Furfuryladenine, Kinetin, Protects against Fenton Reaction-Mediated Oxidative Damage to DNA. *Biochem. Biophys. Res. Commun.* **1999**, *265*, 499–502. [CrossRef] [PubMed]

75. Sharma, S.P.; Kaur, J.; Rattan, S.I.S. Increased longevity of kinetin-fed Zaprionus fruitflies is accompanied by their reduced fecundity and enhanced catalase activity. *IUBMB Life* **1997**, *41*, 869–875. [CrossRef] [PubMed]

76. Choi, S.J.; Jeong, C.H.; Choi, S.G.; Chun, J.Y.; Kim, Y.J.; Lee, J.; Shin, D.H.; Heo, H.J. Zeatin prevents amyloid beta-induced neurotoxicity and scopolamine-induced cognitive deficits. *J. Med. Food* **2009**, *12*, 271–277. [CrossRef] [PubMed]

77. Yang, S.-J.; Han, A.R.; Kim, E.-A.; Yang, J.W.; Ahn, J.-Y.; Na, J.-M.; Cho, S.-W. KHG21834 attenuates glutamate-induced mitochondrial damage, apoptosis, and NLRP3 inflammasome activation in SH-SY5Y human neuroblastoma cells. *Eur. J. Pharmacol.* **2019**, *856*, 172412. [CrossRef] [PubMed]

78. Yuksel, T.N.; Yayla, M.; Halici, Z.; Cadirci, E.; Polat, B.; Kose, D. Protective effect of 5-HT7 receptor activation against glutamate-induced neurotoxicity in human neuroblastoma SH-SY5Y cells via antioxidative and antiapoptotic pathways. *Neurotoxicol. Teratol.* **2019**, *72*, 22–28. [CrossRef]

79. Lee, H.J.; Spandidos, D.A.; Tsatsakis, A.; Margina, D.; Izotov, B.N.; Yang, S.H. Neuroprotective effects of Scrophularia buergeriana extract against glutamate-induced toxicity in SH-SY5Y cells. *Int. J. Mol. Med.* **2019**, *43*, 2144–2152. [CrossRef]

80. Hu, Y.; Li, J.; Liu, P.; Chen, X.; Guo, D.-H.; Li, Q.-S.; Rahman, K. Protection of SH-SY5Y Neuronal Cells from Glutamate-Induced Apoptosis by 3,6′-Disinapoyl Sucrose, a Bioactive Compound Isolated from Radix Polygala. *J. Biomed. Biotechnol.* **2012**, *2012*, 728342. [CrossRef]

81. Geng, N.; Shi, B.J.; Li, S.L.; Zhong, Z.Y.; Li, Y.C.; Xua, W.L.; Zhou, H.; Cai, J.H. Knockdown of ferroportin accelerates erastin-induced ferroptosis in neuroblastoma cells. *Eur. Rev. Med. Pharmacol. Sci.* **2018**, *22*, 3826–3836.

82. Krishnamurthy, P.; Mays, J.; Bijur, G.; Johnson, G. Transient oxidative stress in SH-SY5Y human neuroblastoma cells results in caspase dependent and independent cell death and tau proteolysis. *J. Neurosci. Res.* **2000**, *61*, 515–523. [CrossRef]

83. Stone, W.L.; Qui, M.; Smith, M. Lipopolysaccharide enhances the cytotoxicity of 2-chloroethyl ethyl sulfide. *BMC Cell Biol.* **2003**, *4*, 1–7. [CrossRef] [PubMed]

84. Carrasco, R.A.; Stamm, N.B.; Patel, B.K.R. One-step cellular caspase-3/7 assay. *BioTechniques* **2003**, *34*, 1064–1067. [CrossRef] [PubMed]

85. Hammer, O.; Harper, D.; Ryan, P. PAST: Paleontological Statistics Software Package for Education and Data Analysis. *Palaeontol. Electron.* **2001**, *4*, 1–9.

Supplementary material II.

Gonzalez, G.; Hodoň, J.; Kazakova, A.; D'Acunto, C. W.; Kaňovský, P.; Urban, M.; Strnad, M., Novel pentacyclic triterpenes exhibiting strong neuroprotective activity in SH-SY5Y cells in salsolinol- and glutamate-induced neurodegeneration models. *European Journal of Medicinal Chemistry* **2021**, *213*, 113168

Research paper

Novel pentacyclic triterpenes exhibiting strong neuroprotective activity in SH-SY5Y cells in salsolinol- and glutamate-induced neurodegeneration models

Gabriel Gonzalez [a, b], Jiří Hodoň [c], Anna Kazakova [c], Cosimo Walter D'Acunto [a], Petr Kaňovský [b], Milan Urban [d, *], Miroslav Strnad [a, b, **]

[a] Laboratory of Growth Regulators, Faculty of Science, Palacký University and the Institute of Experimental Botany of the Czech Academy of Sciences, Šlechtitelů 27, CZ-78371, Olomouc, Czech Republic
[b] Department of Neurology, University Hospital Olomouc and Faculty of Medicine and Dentistry, Palacký University Olomouc, CZ-775 20, Olomouc, Czech Republic
[c] Department of Organic Chemistry, Faculty of Science, Palacky University, 17. Listopadu 1192/12, 771 46, Olomouc, Czech Republic
[d] Department of Medicinal Chemistry, Institute of Molecular and Translational Medicine, Faculty of Medicine and Dentistry, Palacky University in Olomouc, Hnevotinska 5, 779 00, Olomouc, Czech Republic

ARTICLE INFO

ABSTRACT

Novel triterpene derivatives were prepared and evaluated in salsolinol (SAL)- and glutamate (Glu)-induced models of neurodegeneration in neuron-like SH-SY5Y cells. Among the tested compounds, betulin triazole **4** bearing a tetraacetyl-β-D-glucose substituent showed a highly potent neuroprotective effect. Further studies revealed that removal of tetraacetyl-β-D-glucose part (free triazole derivative **10**) resulted in strong neuroprotection in the SAL model at 1 μM, but this derivative suffered from cytotoxicity at higher concentrations. Both compounds modulated oxidative stress and caspase-3,7 activity, but **10** showed a superior effect comparable to the Ac-DEVD-CHO inhibitor. Interestingly, while both **4** and **10** outperformed the positive controls in blocking mitochondrial permeability transition pore opening, only **4** demonstrated potent restoration of the mitochondrial membrane potential (MMP) in the model. Derivatives **4** and **10** also showed neuroprotection in the Glu model, with **10** exhibiting the strongest oxidative stress reducing effect among the tested compounds, while the neuroprotective activity of **4** was probably due recovery of the MMP.

© 2021 Elsevier Masson SAS. All rights reserved.

1. Introduction

In recent years, the incidence of neurodegenerative diseases has increased dramatically. Parkinson's disease (PD), with a 1% occurrence in populations over 60, is now the most common motor-related and second most frequent neurodegenerative disease [1–4]. Generally, PD is characterized by motor-associated symptoms, such as bradykinesia (lack or slowness of movements), rigidity, resting tremor and postural instability, which are tightly linked with the progressive and severe degeneration of dopaminergic neurons in the *Substantia nigra pars compacta* in the *Basal ganglia*. Appearance of early PD symptoms is linked with the degeneration and loss of about 50−80% of DA neurons [5–9]. Amongst many PD forms, idiopathic or sporadic PD is the most prevalent in diagnoses. There is no known specific cause for this form, making treatment of the disease problematic. On the other hand, several molecular hallmarks of PD, such as proteasomal and autophagy-lysosomal dysfunction [10], stress of the endoplasmic reticulum [11], synaptopathy [12], mitochondrial dysfunction [13],

* Corresponding author. Institute of Molecular and Translational Medicine, Faculty of Medicine and Dentistry, Palacký University in Olomouc, Hněvotínská 5, 779 00, Olomouc, Czech Republic.
** Corresponding author. Laboratory of Growth Regulators, Faculty of Science, Palacký University, and Institute of Experimental Botany of the Czech Academy of Sciences, Šlechtitelů 27, CZ-78371, Olomouc, Czech Republic.
E-mail addresses: milan.urban@upol.cz (M. Urban), miroslav.strnad@upol.cz (M. Strnad).

oxidative stress (OS) [14], disruption of calcium homeostasis [15,16] and neuroinflammation [17] have been identified in PD patient brains.

Currently, PD is managed by only symptomatic treatment, which is not effective at blocking or decreasing progression of the disease [18,19]. Therefore, drug development is currently focused on promising disease-modifying therapy approaches. Specifically, several natural [20] and synthetic compounds or already approved CNS drugs [21−25] have been shown to exhibit encouraging neuroprotective activity in *in vitro* and *in vivo* models of neurodegenerative diseases [22,26−28].

Pentacyclic triterpenes belong to the most abundant natural secondary metabolites found in higher plants, fungi, algae, and marine animals. A large number of triterpenes have been isolated from natural sources and many of them are biologically active [29]. There are many examples of cytotoxic [30−32], antibacterial [33], antifeedant [34], antiviral [35], anticariogenic [36], hepatoprotective [37], and cardioprotective [38] triterpenic compounds, and some have been reported to have neuroprotective or CNS-related activity [39−42], which was also identified in tenuigenin [43] or betulin [44−46]. Hundreds of new derivatives of betulinic acid (**1**) and betulin (**2**) (Fig. 1) have been prepared by our research group in previous research projects, but many of them were found to have low solubility in water, which may prevent sufficient adsorption from the gastro-intestinal tract. Based on this experience, a series of triterpene conjugates was prepared in an attempt to improve the solubility, but in some cases, coupling to other (polar) molecules caused a significant decrease in their cytotoxicity [47−50]. Such non-cytotoxic compounds may be successful in the screening of alternative biological activities.

In the present work, a series of pentacyclic triterpenes was prepared and evaluated in *in vitro* models of neurodegeneration in neuron-like SH-SY5Y cells [51−53]. The primary aim was to investigate the protective effect of new triterpenes in salsolinol- and glutamate-induced models of cell death mimicking aspects of PD. The results indicated that some of the triterpene derivatives displayed strong neuroprotective effects in both models. Subsequent studies of the most active representatives showed that the betulin derivatives were also potent in decreasing superoxide radical formation, caspase-3,7 activity and mitochondrial permeability transition pore formation.

2. Results and discussion

2.1. Chemistry

The first set of compounds for testing the potential
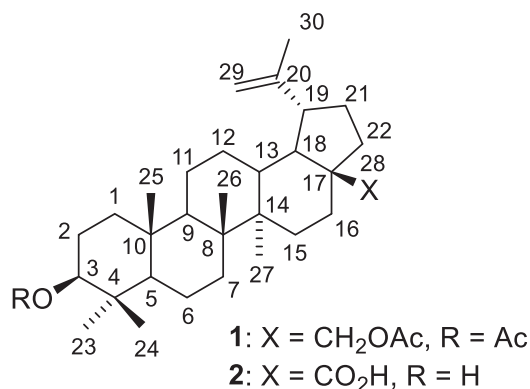
Fig. 1. Starting terpenes − betulin **1** and betulinic acid **2**.

neuroprotective activity comprised derivatives of pentacyclic triterpenes from our compound library exhibiting low cytotoxicity. From all tested compounds, derivatives **3**−**8** (Fig. 2) were selected as the most interesting. Among them, conjugates **3** and **4** (Fig. 2) showed the most significant neuroprotective activity in our models of neurodegeneration. The syntheses of compounds **3**, **4**, and **6** have not been reported previously, whereas derivatives **5a**, **5b**, **7**, and **8** have already been described [47,48,54,55]. Compounds **3** and **4** were prepared from betulin diacetate (**1**, Scheme 1) by its two-step oxidation at the position C-30 followed by the alkylation of the intermediate carboxylic acid **12** with propargyl bromide to give ester **9**. Huisgen cycloaddition of the resulting propargyl ester **9** with 2,3,4,6-tetra-*O*-acetyl-β-D-galactopyranosyl azide and 2,3,4,6-tetra-*O*-acetyl-β-D-glucopyranosyl azide (prepared according to the literature [56]) gave the final products **3** and **4**. Compound **6** was prepared by the selective bromination of the position 2 in allobetulon **11** followed by nucleophilic substitution of the intermediate bromoderivative with KCN, modified procedure from Ref. [57] was used. Both promising compounds **3** and **4** are conjugates containing triterpenoid part, 1,2,3-triazole, and acetylated sugar. In order to find out which part is responsible for the neuroprotective activity, compounds **10, 12** and **13** were prepared (they are substructures of compound **4**) (Scheme 1). In the case of preparation of the molecule **10**, ester **9** was subjected to cycloaddition with bis(4-methoxyphenyl)methyl azide (DoD-N$_3$) that serves as protected azide and the intermediate was deprotected by TFA. Conjugate **13** was prepared by the Huisgen cycloaddition of 1−2,3,4,6-tetra-*O*-acetyl-β-D-galactopyranosyl azide with propargyl alcohol in a modified manner from Ref. [58]. The derivatives **4** and **10** were selected for more advanced testing to reveal their mechanism of action because of their superior neuroprotective activities in the first screening.

2.2. Biology

2.2.1. In vitro neuroprotective and cytotoxic activity in neuron-like SH-SY5Y

In order to study a variety of biological effects of triterpenoids related to neuroprotective activity, the neuroblastoma cell line SH-SY5Y was treated by 10 μM all-trans retinoic acid (ATRA) for 48 h. After two days, SH-SY5Y cells displayed a characteristic neuronal phenotype, as described in other publications [59,60]. As shown in Fig. 3, untreated SH-SY5Y cells were characterized by a higher density and lower number of neurites, whereas differentiated cells displayed an elongated morphology, higher number of neurites (marked by yellow arrows) and lower density of cells. Such observations are consistent with published results [59,60].

To evaluate the potential neuroprotective effects of triterpene derivatives, the compounds were first screened in a cytotoxicity test. In this assay, neuron-like SH-SY5Y cells were exposed to the tested derivatives in a concentration range 0.1−10 μM for 24 h. A control group was treated by DMSO alone (≤0.1% v/v). Cell viability was determined by the calcein AM assay [61]. As shown in Table 1, almost all the derivatives displayed zero cytotoxic activity. Only four derivatives induced a decrease in cell viability at the highest concentration. For example, compound **8** exhibited a slight decrease at 10 μM (87.0% cell viability compared to control), while compounds **5b** (57.6%), **10** (30.5%) and **12** (11.6%) demonstrated a higher cytotoxic effect at the same concentration. The positive control cyclophilin D inhibitor cyclosporine A was also cytotoxic towards SH-SY5Y cells at 5 μM, whereas *N*-acetyl cysteine did not affect the cell viability even at 1000 μM. Thus, the compounds displaying cytotoxic effects at 5 or 10 μM were tested in *in vitro* models of neurodegeneration in a lower concentration range (0.1−1 μM).
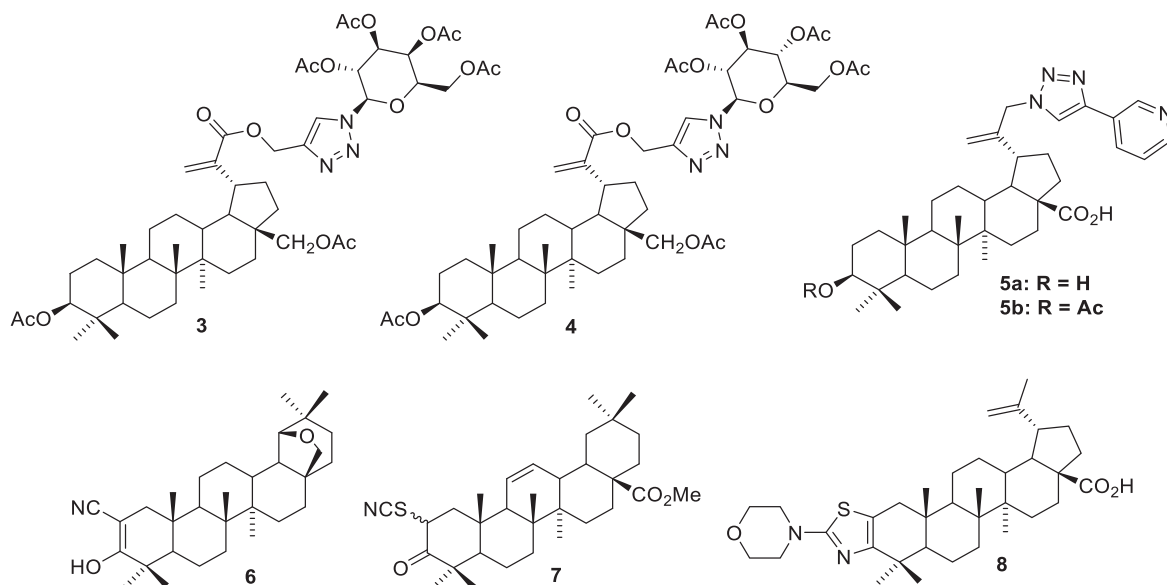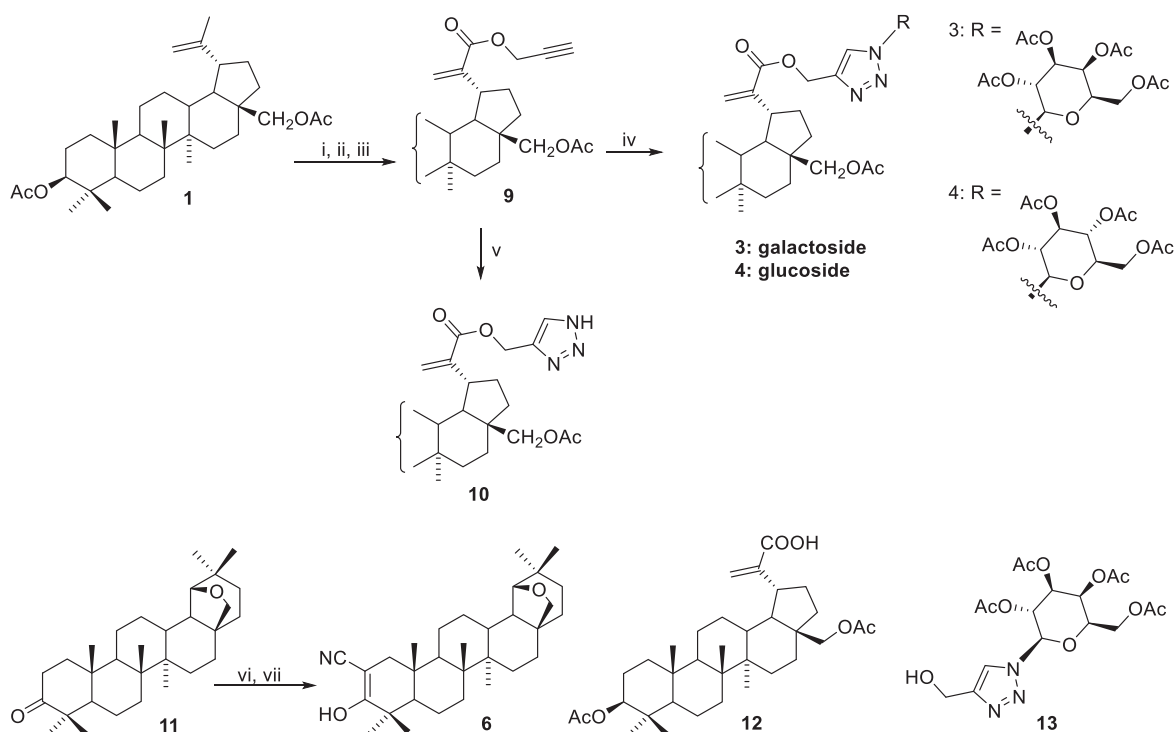
Fig. 2. Terpenoid structures tested for neuroprotective effects on neuron-like SH-SY5Y cells.

Scheme 1. Preparation of new compounds **3**, **4**, **6**, **9**, **10**. Reagents and conditions: (i) SeO$_2$, 2-methoxyethanol, refl. 3 h; (ii) Jones reagent, acetone, r.t., 6 h; (iii) propargyl bromide, K$_2$CO$_3$, THF, refl., 12 h; (iv) 2,3,4,6-tetra-*O*-acetyl-β-ᴅ-galactopyranosyl azide or 2,3,4,6-tetra-*O*-acetyl-β-ᴅ-glucopyranosyl azide, CuI, *N,N*-diisopropylethyl amine, THF, r.t., 24 h; (v) bis(4-methoxyphenyl)methyl azide (DoD-N$_3$), DIPEA, AcOH, CuI, DCM, 24 h, 20 °C, then 50% TFA/DCM, anisole, 1 h, 20 °C; (vi) Br$_2$, CHCl$_3$, r.t., 30 min; (vii) KCN, DMSO, 24 h.

2.2.2. Neuroprotective activity of pentacyclic triterpenes in salsolinol-induced model of PD

To evaluate the neuroprotective activity, neuronal SH-SY5Y were allowed to differentiate for 48 h and then were treated with 500 μM salsolinol (SAL) alone or in combination with the tested compounds at 0.1−1 − 10 μM concentration for 24 h. Within the model, N-acetyl cysteine (NAC) and cyclosporin A (CsA) were used as well-known positive neuroprotective controls [62,63]. The

viability of the treated cells was quantified by the calcein AM assay. As shown in Fig. 4A, treatment by 500 μM SAL resulted in a decrease in viability to 70.49 ± 0.51%. Both NAC (100 μM, 82.27 ± 1.30% and 1000 μM, 89.01 ± 2.34%) and CsA (0.5 μM, 99.32 ± 3.80%) demonstrated potent protective effects, in agreement with previously published data [62,63]. In the case of triterpene derivatives, protective activity value was at least at the same level or higher than 100 μM NAC suggesting a promising effect (green line in Fig. 4A).
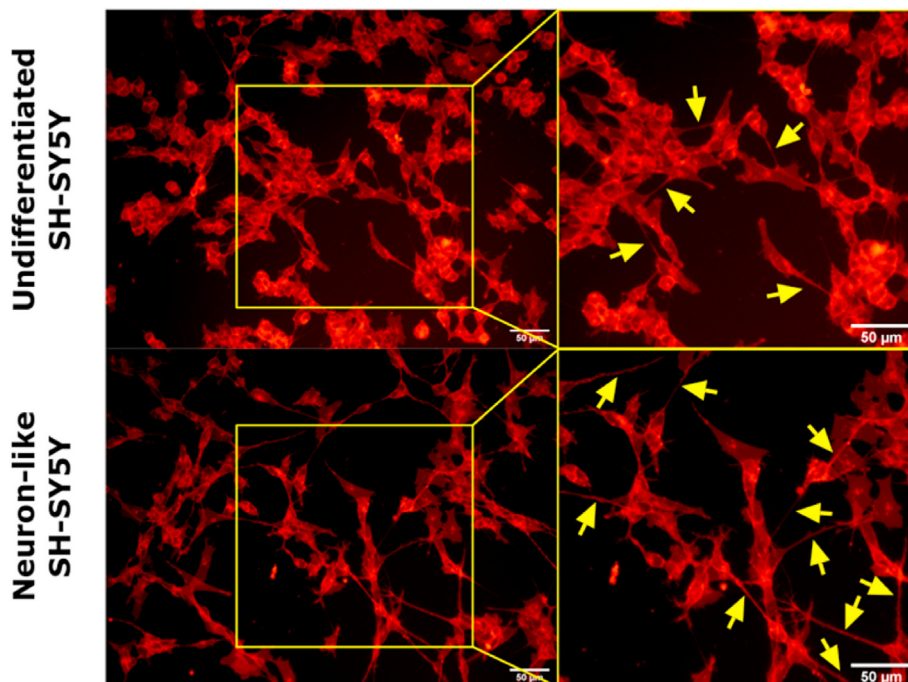
Fig. 3. Fluorescent microphotographs of membrane-stained (by neurite outgrowth kit Invitrogen™) SH-SY5Y cells viewed under a fluorescence microscope. Bar = 50 μm. The image shows undifferentiated and neuron-like SH-SY5Y cells treated for 48 h with 10 μM ATRA. The presence of neurites is indicated by yellow arrows.

Table 1
Cytotoxicity (% of DMSO control) of new pentacyclic triterpenes and positive controls *N*-acetyl cysteine (NAC) and cyclosporin A (CsA) at different concentrations after 24 h of treatment.

Viability						
Compound	0.1 μM	±SEM	1 μM	±SEM	10 μM	±SEM
3	139.7	4.877	139.3	2.98	129.6	4.42
4	114.6	3.69	138.2	2.70	127.6	2.86
5a	103.2	3.20	115.7	1.58	132.6	2.00
5b	106.1	2.96	124.0	2.69	57.6	3.99
6	93.1	1.29	93.8	1.16	98.8	1.44
7	100.1	2.93	107.3	2.45	99.2	3.70
8	91.3	2.44	90.01	0.99	87.0	3.39
12	102.2	2.90	102.0	3.45	11.6	1.37
13	108.9	4.89	106.8	3.98	100.2	4.26
10	97.4	3.72	118.6	3.10	30.5	3.021
***N*-acetyl cysteine (NAC)**	**10** μM	± **SEM**	**100** μM	± **SEM**	**1000** μM	± **SEM**
	107.9	3.87	114.4	3.65	120.0	4.67
Cyclosporin A (CsA)	**0.05** μM	± **SEM**	**0.5** μM	± **SEM**	**5** μM	± **SEM**
	103.6	3.17	120.7	3.35	57.4	3.87

[α] Viabilities are expressed as means ± SEM, compounds were tested in triplicate in three independent experiments.

Derivatives **3** and **4** were found to induce a potent neuroprotective effect with the strongest activity at 1 μM (**3**, 90.90 ± 2.06%; **4**, 91.69 ± 2.47%). In comparison to derivative **3**, compound **4** showed a better dose-dependent profile of the activity. The neuroprotective effects of derivatives **5a** and **5b** also peaked at 1 μM, represented by 81.72 ± 1.52% and 84.27 ± 4.33% of viable cells, respectively. Interestingly, a small modification by acetylation of the 3-OH group (A ring of compound **5a**) resulted in slightly better activity, although **5b** suffered from toxicity at higher concentrations, as shown in the previous section. Overall, triterpene derivatives **3** and **4** demonstrated a slightly better effect than 1000 μM NAC and their highest neuroprotective effect was achieved at orders of magnitude lower concentrations (100–1000 fold). From a structural viewpoint, both compounds share the same scaffold, but compound **3** was substituted with tetraacetyl-β-D-galactose, whereas compound **4** was substituted with tetraacetyl-β-D-glucose.

Subsequent investigations were performed to identify the specific part of triterpenoid molecules **3** and **4** responsible for their high neuroprotective activity, see Fig. 4B and C. Three different substructures (**13**, **12** and **10**), glucose and galactose were also tested for cytotoxicity and then in the SAL model. Surprisingly, derivative **10** showed the highest protective effect (at 1 μM, 97.91 ± 2.30%) of all the tested compounds. It mediated its protective effect also at low 0.1 μM concentration (81.41 ± 2.46%). Unfortunately, 10 μM **10** (without toxin) was associated with cytotoxic effects, as seen in Table 1. Substructures **12** and **13** showed only slight or zero improvements in cell viability at 1 μM in the SAL model, while **12** was also cytotoxic at 10 μM, as shown above. To conclude, the study of the substructures of triterpenoid **3** revealed that the triterpenic scaffold bearing triazole (compound **10**)
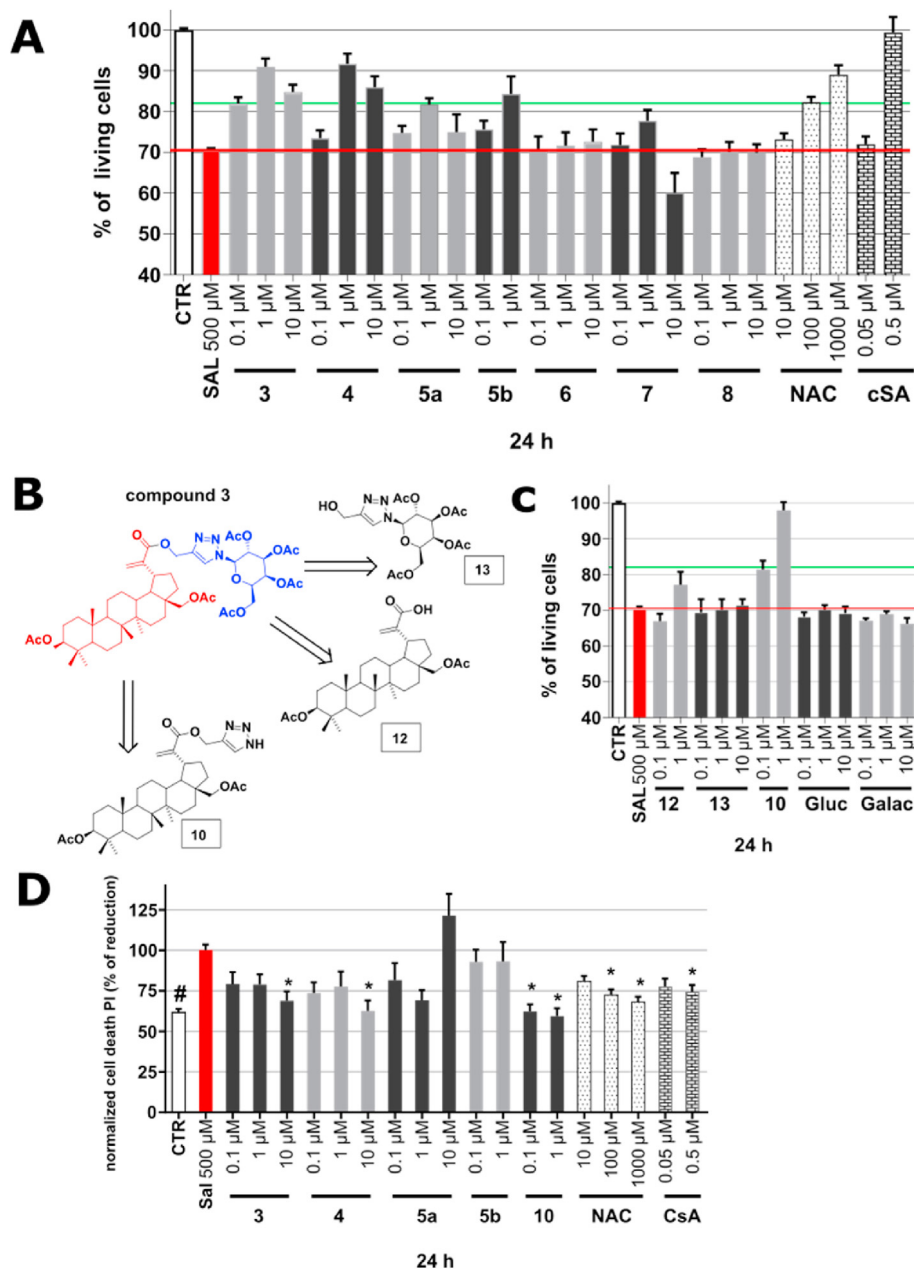
Fig. 4. (A) Evaluation of pentacyclic triterpene derivatives in a salsolinol (SAL)-induced model of Parkinson's disease on neuron-like SH-SY5Y cells. The threshold of protective activity comparable to positive controls is marked by the green line, whereas the red line indicates the viability after 500 μM SAL treatment for 24 h. The results are presented as mean ± standard error of the mean (SEM) from triplicates in at least three independent experiments. (B) Structure of derivative **3** and substructures **12**, **13** and **10**. (C) Evaluation of substructures **12**, **13**, **10** together with glucose (Gluc) and galactose (Galac). (D) Neuroprotective effects of selected triterpenes in the SAL-induced model of cell death using propidium iodide (PI) staining after 24 h. All results are presented as mean ± standard error of the mean (SEM) from triplicates in at least three independent experiments. *P compared with vehicle with 500 μM SAL, #P compared with vehicle without 500 μM SAL. A value of $P < 0.05$ was considered statistically significant.

exhibited the strongest protective effect at 0.1 μM and 1 μM, whilst the other parts were ineffective (**12**, **13**). Most importantly, using this approach, we found that derivatization of compound **10** by N-tetraacetylgalactose/glucose dramatically reduced the cytotoxicity.

To confirm the results acquired during the screening of cell viability, an orthogonal test with propidium iodide (PI) was used. In general, PI stains only cells with a damaged cell membrane or already dead cells [64–66]. As shown in Fig. 4D, SAL exposure resulted in cell death, which was considered as a 100% PI signal. Reduction in the cell death due to co-treatment with the tested compounds was then determined relative to this threshold. Only compounds **3** (10 μM, 68.7 ± 5.85%), **4** (10 μM, 62.6 ± 6.36%), and **10**

(0.1 μM, 62.3 ± 4.43%; 1 μM, 59.3 ± 4.97%) and the positive controls NAC (100 μM, 72.5 ± 3.42%; 1000 μM, 68.2 ± 3.14%) and CsA (0.5 μM, 74.5 ± 4.01%) demonstrated a statistically significant reduction of dead cells within the model. Other derivatives, i.e. **5a** and **5b**, showed an insignificant decrease of cell death.

Overall, based on both the viability/cell death assays, derivatives **3**, **4**, and **10** were identified as the most promising compounds with a neuroprotective effect comparable to the NAC and CsA controls. Because compounds **4** and **10** showed complete reduction in cell death due to SAL-induced toxicity, these derivatives were selected as the most suitable for further studies of OS, caspase-3,7 activity, mitochondrial membrane potential (MMP) and mitochondrial

permeability transition pore (mPTP) opening. These assays were used to determine the cellular mechanism of neuroprotection shown by the compounds. In addition, the selected compounds were also evaluated in the following glutamate-induced model of oxidative damage in neuron-like SH-SY5Y cells.

2.2.3. Effects of triterpene derivatives 4 and 10 on oxidative stress and caspase-3,7

OS is one of the molecular hallmarks of PD and other neuro-degenerative diseases. Therefore, superoxide radical production in the SAL-induced PD model was studied. It is already known that SAL is able to affect the redox homeostasis in SH-SY5Y cells [51,62]. In connection with these findings, the effect of SAL alone or in co-treatment with selected compounds was studied [52] using a dihydroethidium (DHE) fluorescence probe for detection of super-oxide radicals as markers of oxidative stress [67–69].

Similarly to the work presented in the previous section, the values obtained after application of SAL alone were considered as 100% against which the reduction of superoxide radical production in co-treatment experiments was determined. As shown in Fig. 5B, healthy cells produced relatively low levels of ROS ($39.9 \pm 0.89\%$ of SAL), in contrast to SAL treatment. As expected, NAC decreased levels of superoxide radical formation in a dose-dependent manner with a dramatic reduction at 1000 μM ($53.8 \pm 2.69\%$). Such results are consistent with other reports [70]. On the other hand, CsA showed only a very moderate effect at submicromolar concentrations (approx. 86.4%). Interestingly, compounds 4 and 10 displayed a better effect than CsA and 100 μM NAC. The strongest OS-reducing effect for derivative 4 occurred at 1–10 μM ($74.5 \pm 3.79\%$ and $77.2 \pm 3.14\%$) and for 10 at 0.1–1 μM ($83.7 \pm 3.02\%$ and $81.0 \pm 2.12\%$). Still, both compounds were less effective than NAC at the highest concentration tested. Furthermore, to support the results of DHE quantification by spectrophotometry, fluorescence microscopic observations were performed. As shown in Fig. 5A, the visual observations were in accordance with the results quantified by spectrophotometric measurements (Fig. 5B). As demonstrated by DHE staining (red fluorescence), compound 4 and NAC showed a strong visual decrease in fluorescence in comparison to SAL, whereas 10 and CsA exhibited a lower effect.

Taken together, the OS-reducing effect of NAC described in other models was confirmed in the SAL model. More importantly, the protective effect of NAC seemed to be mediated primarily by a reduction of superoxide radical formation (OS). On the other hand, CsA demonstrated only a partial OS-reducing effect but showed potent protective activity in the viability/cell death assays, suggesting that CsA-mediated protection relies on regulation of other processes linked with apoptosis or modulation of some processes in mitochondria, as described in other reports [63]. The tested tri-terpenes also demonstrated a strong OS-reducing effect, which was comparable or better than that of the positive controls (CsA and 100 μM NAC). Interestingly, derivative 10 displayed a lower OS-reducing activity than 4, despite showing a better protective effect on cell viability/death, suggesting that 4 and 10 could modulate different cellular processes leading to the overall neuroprotection.

2.2.4. Triterpenes regulate caspase-3,7 activity upon SAL intoxication of neuron-like SH-SY5Y cells

SAL is also known as a modulator of both necrotic and apoptotic cell death of SH-SY5Y cells, as demonstrated by other research groups [71]. Our results of overall cell death determined by PI showed its potent decrease after application of derivatives 4 and 10 within the model. To detect and demonstrate the presence of ongoing apoptosis after SAL exposure, activation of caspase-3 and 7 (casp-3,7) as a specific apoptotic marker was quantified. As before, neuron-like SH-SY5Y cells were treated with 500 μM SAL or co-

treatment of the tested compounds and then casp-3,7 activity was determined after 24 h using the specific substrate Ac-DEVD-AMC.

The casp-3,7 activity induced by SAL application was considered to be 100%, against which the reducing effect of compounds was subsequently determined. As shown in Fig. 5C, healthy cells showed only $65.7 \pm 1.04\%$ of casp-3,7 activity compared to the SAL control. Ac-DEVD-CHO, a nanomolar casp-3,7 inhibitor, caused a dramatic decrease in casp-3,7 activation at 0.05 μM ($36.9 \pm 3.11\%$) and 0.5 μM ($30.8 \pm 3.15\%$) concentration. These results are in close agreement with previously published data by another group [72]. As expected, NAC as a positive control significantly decreased casp-3,7 activity at the highest concentration tested (1000 μM NAC, $79.3 \pm 2.29\%$). On the other hand, cyclosporin A did not affect casp-3,7 within the model. Surprisingly, the selected triterpene derivatives showed different effects on the level of casp-3,7 activation after SAL exposure. Compound 4 induced a significant reduction in casp-3,7 activity comparable to NAC, achieving the most significant effect at 1 μM ($81.8 \pm 2.58\%$) and 10 μM ($79.5 \pm 4.13\%$), respectively. On the other hand, derivative 10 induced an enormous drop in casp-3,7 activity at 0.1 μM ($42.2 \pm 5.02\%$) to 1 μM ($24.3 \pm 5.21\%$) concentration, which was comparable to the effect of Ac-DEVD-CHO.

Taken together, these results show that the new triterpenes along with the positive controls induced a potent decrease in casp-3,7 activation. Interestingly, CsA did not influence apoptosis in this model, in partial contrast with observations of another research group studying the toxic effects of N-methyl-R-salsolinol (N-Met-R-SAL − a SAL metabolite) in the SH-SY5Y cell model [63]. Several previous studies have shown that N-Met-R-SAL and SAL may act differently. Whereas SAL is known to induce both necrosis and apoptosis, N-Met-R-SAL predominantly induces apoptosis [63,73], indicating that CsA probably regulates non-apoptotic cell death in SAL models. In comparison, both the triterpene derivatives 4 and 10 showed anti-apoptotic efficiency at lower concentrations than NAC. More importantly, the derivatives exhibited different levels of inhibitory effects on casp-3,7 activity. Whereas the effect of 4 was similar to that of NAC and indicated an association with a reduction in OS and consequent decrease of casp-3,7 activity, derivative 10 more likely displayed a direct action because its inhibitory effects on casp-3,7 inhibitory activity were comparable to those of the conventional Ac-DEVD-CHO inhibitor.

2.2.5. Triterpenes modulate mitochondria in the SAL-induced model of PD

It is known that mitochondrial dysfunction together with increased OS is one of the key hallmarks of all neurodegenerative diseases [74]. SAL has also been shown to be a potent mitochondrial disruptor via direct action towards mitochondrial complex I and II of the electron transport chain or impairment of cell redox systems [51]. To evaluate the effect of the triterpene derivatives 4 and 10 on mitochondria of neuron-like SH-SY5Y cells within the SAL model, the ratiometric JC10 assay was performed [75].

In this assay, mitochondria with a normal membrane potential usually form the polymeric JC10 form (red), whereas disrupted mitochondria or cells with ongoing apoptosis or necrosis are characterized by the prevalence of monomeric, i.e. green JC10 dye. The assay was monitored with the negative control carbonyl cyanide m-chlorophenyl hydrazone (CCCP), a proton gradient uncoupler and chemical inhibitor of oxidative phosphorylation, which was used as an inducer of mitochondrial depolarization [76]. As shown in Fig. 6A, application of 1 μM CCCP caused almost complete mitochondrial depolarization and a decrease of the JC10 red/green ratio to $6.3 \pm 1.05\%$ compared to the DMSO control. In relation to the PD model, treatment by SAL resulted in a decrease of the red/green
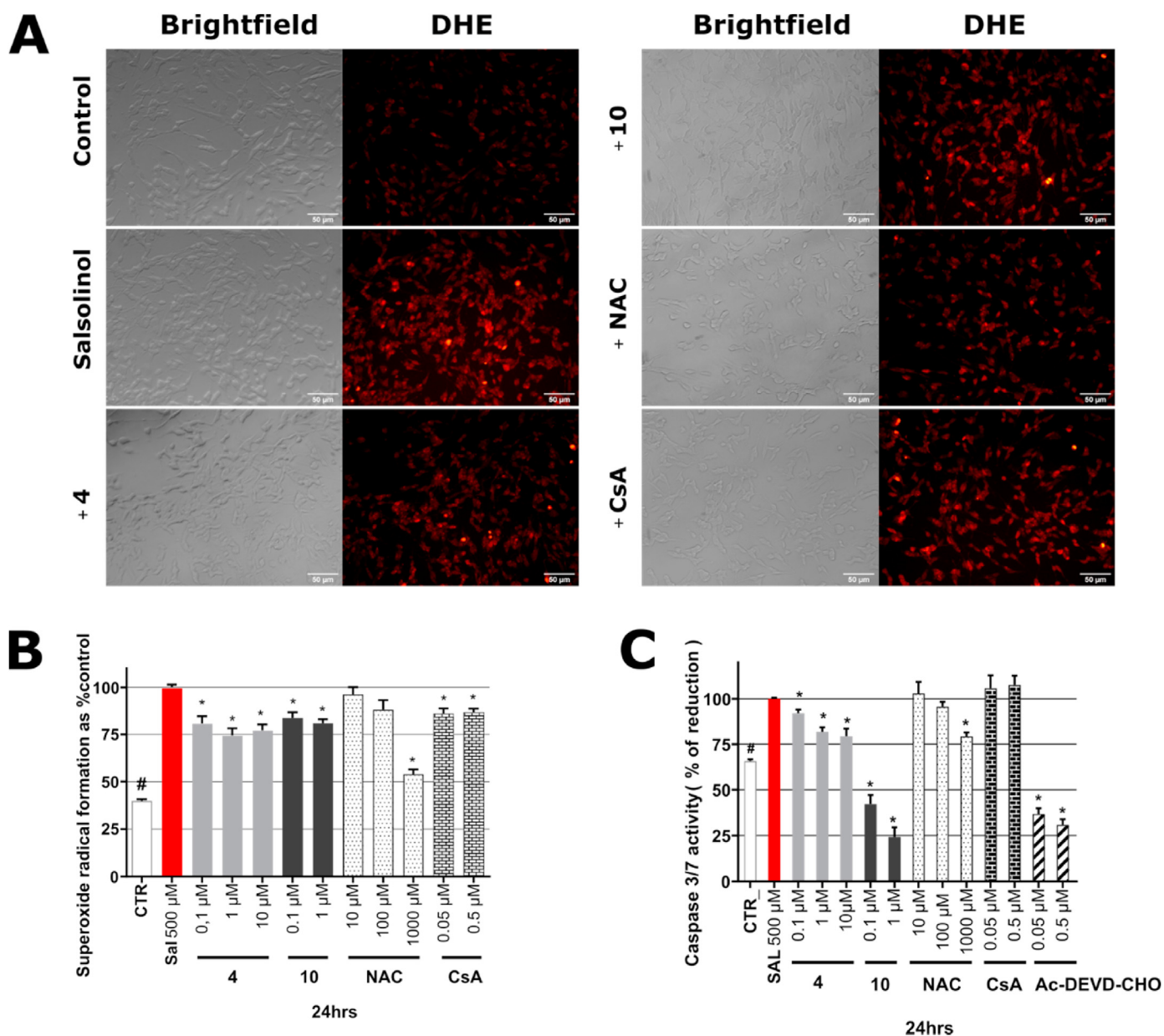
Fig. 5. (A) SAL-induced OS in human neuron-like SH-SY5Y cells visualized by fluorescence microscopy. Illustrative dihydroethidium (DHE) stained microphotographs are shown. Bar = 50 μm. Neuron-like SH-SY5Y cells treated by DMSO (control), salsolinol (SAL) and co-treatment of 500 μM SAL and 1 μM **4** (+4) or 1 μM **10** (+10) or 0.5 μM CsA (+CsA) or 1000 μM NAC (+NAC) for 24 h. (B) SAL-induced OS and triterpene anti-OS activity after 24 h. All results are presented as mean ± standard error of the mean (SEM) from at least five independent experiments performed in triplicate. (C) Caspase-3,7 activity in SAL-induced model of PD on neuron-like SH-SY5Y cells after 24 h. All results are presented as mean ± standard error of the mean (SEM) from at least four independent experiments performed in triplicate. *P compared with vehicle with 500 μM SAL, #P compared with vehicle without 500 μM SAL. A value of $P < 0.05$ was considered statistically significant.

JC10 ratio to 45.3 ± 2.09%. Both positive controls improved the MMP at 100 and 1000 μM NAC (66.4 ± 3.42% and 69.7 ± 4.66%), but not in case of CsA which show only slight non-significant effect. The tested triterpenes differed in their activity on mitochondria. Derivative **4** showed almost complete dose-dependent recovery of the mitochondrial potential with maximum effect at 10 μM (89.2 ± 4.07%). Surprisingly, triterpene **10** did not efficiently alter the MMP, but 0.1 μM concentration was associated with a slight but non-significant improvement of the potential. A possible explanation for the effect of **10** could be its toxicity at 10 μM.

To understand the relationships between the oxidative stress, mitochondrial depolarization, apoptotic/non-apoptotic cell death and effect of the tested compounds, we investigated mPTP after SAL

intoxication. As already reported by other groups, mPTP formation is known to be a key regulator of both apoptosis and necrosis [77]. In particular, a link between mPTP formation and inhibition of apoptosis has been described in *N*-Met-*R*-SAL-induced model of PD on SH-SY5Y cells [63].

Based on these findings, neuron-like cells were treated by 500 μM SAL or co-treatment with the tested compounds for 24 h. The cells were then stained by calcein AM/CoCl$_2$ to quantify the decrease/increase in fluorescence relative to mPTP opening or closing [78]. The presence of mPTP opening was associated with quenching of calcein fluorescence, whereas an increase in calcein AM indicated the inhibition of mPTP opening in mitochondria. The results of calcein AM/CoCl$_2$ staining are presented as a fold change
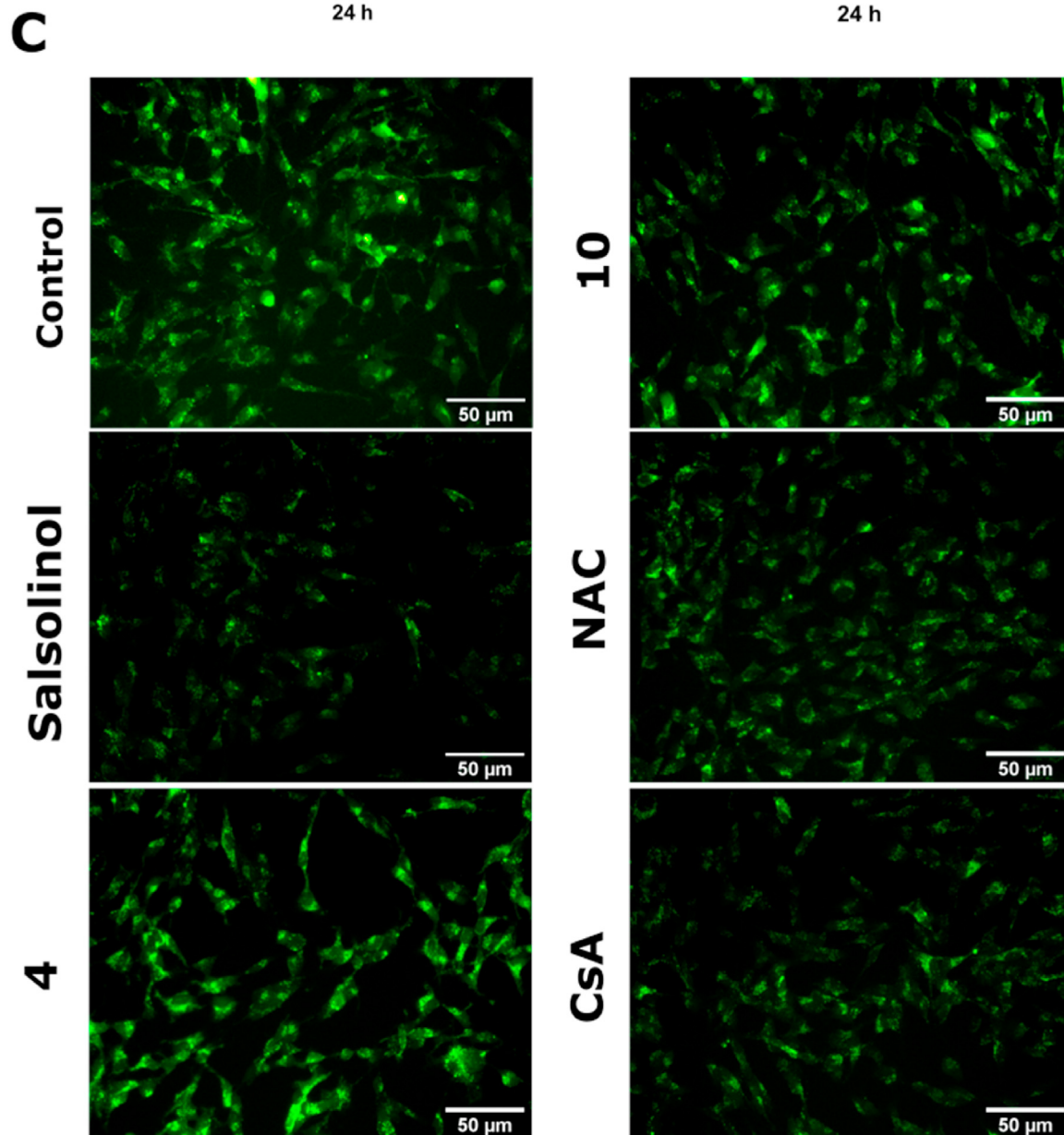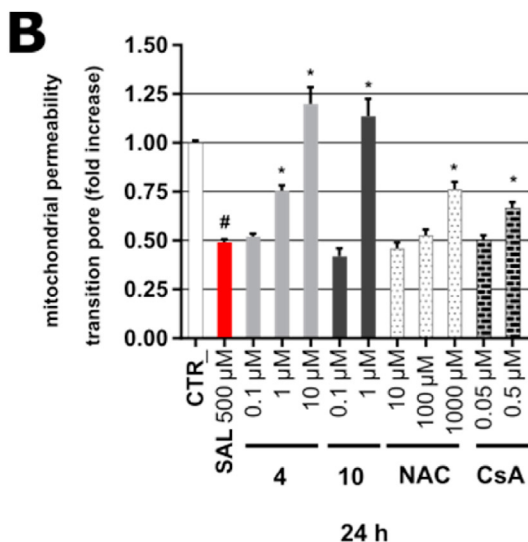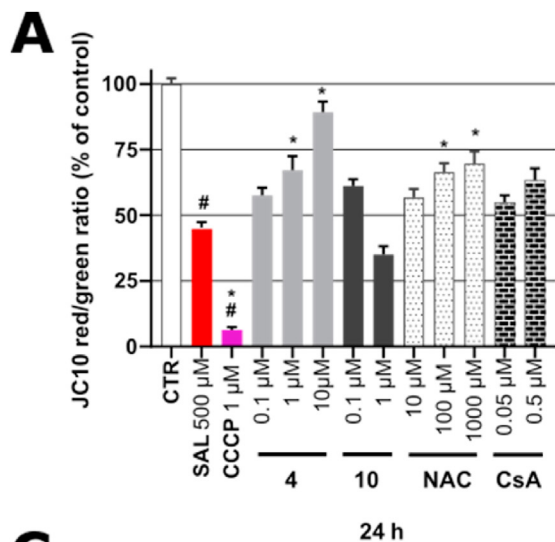
of calcein fluorescence relative to the value for the DMSO control set at 1. As depicted in Fig. 6B, SAL intoxication resulted in a decrease of calcein fluorescence to 0.49 ± 0.02. Interestingly and unexpectedly, CsA ($0.5 \mu M$, 0.67 ± 0.03 fold change) demonstrated a weaker effect on mPTP opening than NAC ($1000 \mu M$, 0.76 ± 0.04 fold change). These results indicate that the dramatic reduction of OS by NAC strongly influenced mPTP opening rather than direct inhibition afforded by CsA within the model. On the other hand, the triterpene derivatives **4** at $1-10 \mu M$ (0.75 ± 0.03; 1.20 ± 0.09 fold change) and **10** at $1 \mu M$ (1.14 ± 0.09 fold change) demonstrated complete blockade of mPTP opening after SAL intoxication. As shown in Fig. 6C, the results obtained by spectrophotometric quantification were supported by observations of calcein AM/CoCl$_2$ staining using fluorescent microscopy. A study by another group showed that the betulinic acid (lup-20 (29)-ene scaffold of compounds **4** and **10**) mediated blockade of the mPTP, and it was suggested to be one of the key processes responsible for the protective effect *in vivo* [79].

Taken together, the results showed that the new triterpenes had a stronger effect on mPTP opening than the positive controls. In addition, derivatives **4** and **10** showed some differences in mitochondrial regulation. More specifically, the strong blockade of mPTP opening mediated by **10** probably contributed strongly to the highly potent inhibition of caspase 3 and 7 activity since other studies have shown direct involvement of mPTP in apoptosis [63,77]. Moreover, compound **4** induced both a potent increase of MMP and blockade of mPTP, whereas derivative **10** only blocked mPTP opening without any beneficial effect on the MMP. Furthermore, substitution of the betulin derivative **10** by tetraacetylglucose (derivative **4**) eliminated its cytotoxicity and unfavourable effects on the MMP. Indeed, **4** showed potent protective effects at $10 \mu M$ in all observed parameters. In comparison to **10**, compound **4** was tightly connected with complete reversion of mitochondrial membrane potential.

2.2.6. Effect of triterpenes **4** and **10** on cell morphology after SAL intoxication

Since the SAL-induced model of PD on SH-SY5Y cells is associated with apoptosis and necrosis, as described by others [80], double staining by acridine orange (AO) and PI was performed. Generally, AO produces green fluorescence staining of all cells (viable and non-viable), whereas PI stains cells with impaired membrane integrity producing red fluorescence [81]. In this model, neuron-like SH-SY5Y cells were qualitatively evaluated regardless of whether triterpene treatment and positive controls affected the presence of apoptotic or necrotic cells. As shown in Fig. 7, the control (healthy cells, designated VI (green)) showed no or minimal of PI staining. In addition, the control cells were characterized by the formation of long neurites and neurite networks. On the other hand, the SAL-treated cells exhibited three types of damaged cells reflected by the presence of AO and/or PI stained cells. The first type, early apoptotic cells (EA, white arrows), were characterized by the presence of AO green cytoplasm and a PI red nucleus without any fragmentation. Late apoptotic cells (LA, orange arrows) showed nuclear fragmentation with minimal or complete disappearance of AO green staining. Finally, cells that underwent necrosis were rounded and PI stained in the absence of AO green staining and fragmentation. The fluorescent microscopy observations together

with spectrophotometric quantifications of overall cell death (PI assay) and apoptosis (caspase-3,7 assay) confirmed the presence of both apoptosis and necrosis of neuron-like SH-SY5Y cells, as published in the literature [51,80,82]. In the case of triterpenes, the general reduction of PI and cell death was quantified by a spectrophotometric assay (see details in previous section; Fig. 4D). As can be seen from Fig. 7, the neuron-like SH-SY5Y cells treated by **4** showed the presence of all types of damaged cells, whereas **10** was preferentially associated with the presence of necrotic cells. As with compound **4**, NAC-treated cells were associated with all types of damaged cells.

In contrast to NAC, CsA showed mainly the presence of late apoptotic cells and signs of necrotic cells. Overall, the observations after AO/PI double staining supported the results obtained by spectrophotometric quantification methods. In particular, in the case of derivative **10**, the preferential presence of necrotic cells highlighted its highly potent anti-apoptotic effect in the SAL-induced model of PD on neuron-like SH-SY5Y cells.

2.2.7. Triterpenes **4** and **10** display a protective effect against the Glu-induced model of oxidative injury on neuron-like SH-SY5Y cells by regulation of superoxide radical formation

As shown in the previous section, compounds **4** and **10** displayed a strong protective effect in the SAL model, including various pathological processes. To further study the protective effect of derivatives **4** and **10**, especially against increased OS and apoptosis, a model of glutamate (Glu)-induced oxidative damage was introduced. To evaluate the neuroprotective activity of new derivatives in the Glu model, SH-SY5Y cells were differentiated for 48 h and then exposed to 160 mM Glu [83] or co-treated with Glu and the tested compounds at standard concentrations. The iron chelator deferoxamine (DFO) and CsA were used as positive controls because they have been demonstrated to have a neuroprotective effect in *in vitro* models of Glu-induced cell death by other research groups [84,85].

After 24 h, the protective effect was assessed by PI staining as an indicator of cell death. Similarly to the SAL model, the effect generated by Glu was considered to be 100% so that the reduction of cell death by the test compounds was determined. As seen from Fig. 8A, the maximum reduction in PI staining was observed in the healthy control (to $25.5 \pm 0.63\%$ compared to the Glu control). In the case of the positive controls, a higher protective effect was demonstrated for DFO ($10 \mu M$, $79.5 \pm 4.75\%$), whereas CsA application ($0.5 \mu M$, $83.5 \pm 4.54\%$) led to a lower but significant activity. These observations are consistent with other literature reports [84,85]. Interestingly, derivative **4** at $10 \mu M$ exhibited the highest protective effect of all the compounds tested, representing a reduction in cell death to $75.1 \pm 2.36\%$. Lower concentrations of **4** were also associated with significant dose-dependent protection. On the other hand, derivative **10** at $1 \mu M$ ($85.0 \pm 2.77\%$ of reduction) showed a protective effect slightly better than CsA but less potent than DFO.

Because a stronger effect in neuroprotection was demonstrated by compound **4** and **10** than for the positive controls, we further investigated the effect of all compounds on OS (superoxide radical formation) and apoptosis (caspase-3,7 activity) in the Glu model. Also, as Glu has been shown to be a potent disruptor of redox homeostasis in various types of neuronal cell lines [53], the OS

Fig. 6. (A) Mitochondrial membrane potential determined in neuron-like SH-SY5Y cells by JC10 dye. (B) Mitochondrial permeability transition pore formation expressed as calcein quenching in the SAL-induced model of PD. All results are presented as mean $\pm$ standard error of the mean (SEM) from at least four independent experiments performed in triplicate. *P compared with vehicle with $500 \mu M$ SAL, #P compared with vehicle without $500 \mu M$ SAL. A value of $P < 0.05$ was considered statistically significant. (C) Mitochondrial permeability transition pore opening induced by SAL in human neuron-like SH-SY5Y cells visualized by fluorescence microscopy. Illustrative calcein AM/CoCl$_2$ stained microphotographs are shown. Bar $= 50 \mu m$. Neuron-like SH-SY5Y cells treated by DMSO (control), SAL alone (SAL), co-treatment of $500 \mu M$ SAL with $10 \mu M$ derivative **4** (+4), $1 \mu M$ **10** (+10); $1000 \mu M$ NAC (+NAC), $0.5 \mu M$ CsA (+CsA) for 24 h and stained by calcein AM/CoCl$_2$.
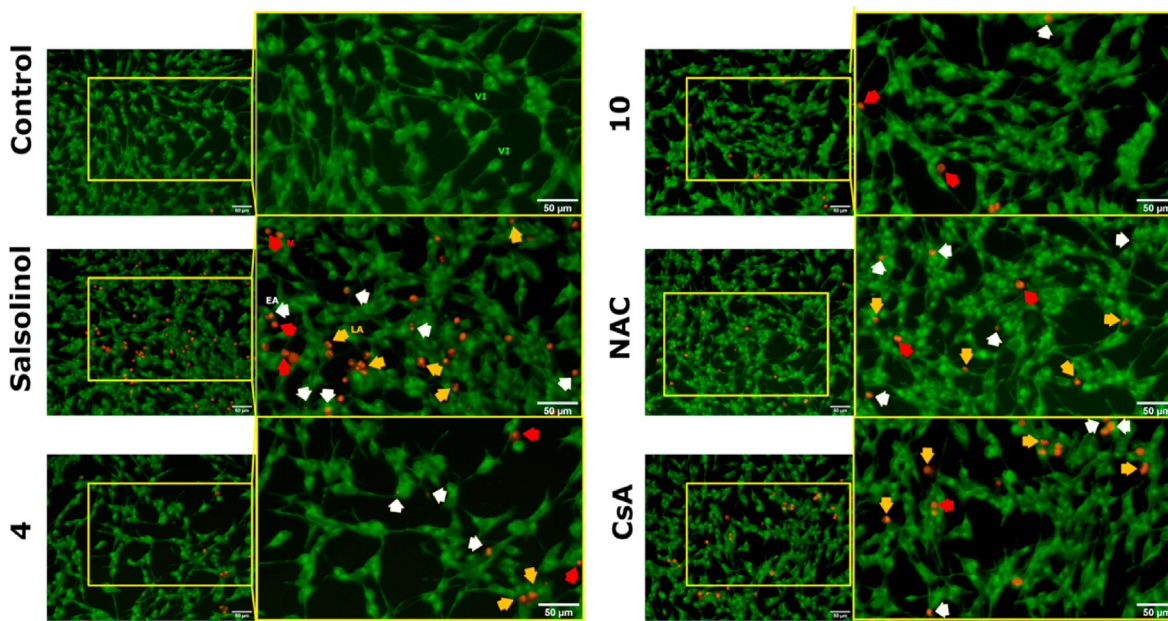
Fig. 7. Illustrative fluorescent images of acridine orange (AO)/propidium iodide (PI) double-stained human neuron-like SH-SY5Y cells viewed under fluorescence microscope. VI - viable cells, EA - early apoptosis, LA - late apoptosis, N - necrosis. The cells were treated with 500 μM SAL alone or in combination with 10 μM **4** (+4), 1 μM **10** (+10), 1000 μM N-acetylcystein (+NAC) or 0.5 μM cyclosporin A (CsA) for 24 h. Bar = 50 μm.

reducing activity of other compounds may play an important role in neuroprotection. In this model, neuron-like SH-SY5Y cells were treated for 4 h as described above and stained by DHE.

Similarly to PI staining, the Glu-induced rise of OS (superoxide radical formation) was considered as 100%, relative to which the OS reducing effect of the compounds was measured. As shown in Fig. 8B, the neuron-like SH-SY5Y cells suffered from an intense burst of OS after Glu application over a relatively short period of time. Interestingly, the positive controls behaved differently in OS-reducing activity. DFO showed better protective effects, leading to a reduction in OS at 10 μM to $87.2 \pm 2.19\%$ of the control, whereas the effect of CsA was similar at submicromolar concentrations (approx. 82%). Surprisingly, triterpene **10** demonstrated a significant reduction in OS at 1 and 0.1 μM ($72.2 \pm 3.18\%$ and $75.7 \pm 3.19\%$, respectively), whereas **4** demonstrated a comparable effect to CsA at 10 μM, reaching $82.2 \pm 3.12\%$. The different effects of derivatives **4** and **10** on OS suggest that compound **10** likely modulates the protective effect on neuronal cells mainly through its effects on superoxide radical formation in a straightforward manner. Such a direct action on radical scavenging by the structurally similar triterpene betulin was described in the literature [86]. To support the results obtained by spectrophotometric quantification of OS for derivative **10**, neuron-like SH-SY5Y cells were stained by DHE and observed under a fluorescent microscope. As shown in Figs. 8C, **10** induced a significant decrease in DHE staining, in contrast to glutamate- or DFO-treated cells.

2.2.8. Differential effects of triterpenoids in the regulation of apoptosis and mitochondrial depolarization after Glu intoxication

Many studies have shown a key role of caspase-3,7 (casp-3,7) activation in Glu-induced cell death in SH-SY5Y cells, suggesting that its regulation could play an important role in neuroprotection [53,87–89]. Owing to the significant reducing activity of the new terpenoids towards OS, the effect of derivatives **4** and **10** on ongoing apoptosis was therefore studied by evaluating the activity of caspase-3,7. Similarly to the SAL model, the casp-3,7 inhibitor Ac-DEVD-CHO was used as a positive control and the result obtained following 160 mM Glu treatment was set at 100%.

Interestingly, Glu caused a huge increase in casp-3,7 activity, whereas healthy cells were associated with only minor activity ($13.7 \pm 0.72\%$) (Fig. 9A). A strong reduction of casp-3,7 activation was also achieved by Ac-DEVD-CHO at 0.05 μM ($27.8 \pm 0.97\%$) and 0.5 μM ($13.7 \pm 0.53\%$), while DFO and CsA showed a moderate to low effect, reaching $77.4 \pm 2.35\%$ and $89.1 \pm 1.97\%$ at 10 μM DFO and 0.5 μM CsA, respectively. The effect of CsA on the level of casp-3,7 activity was in line with already published data [84]. Surprisingly, both triterpenes were not very effective, demonstrating only a slight effect on casp-3,7 activity: derivative **4** showed some effect at 10 μM ($90.9 \pm 1.26\%$) and **10** induced a reduction of casp-3,7 by around 6% only.

These results provide further support that the protective effect of compound **10** was mainly due to a strong reduction in OS, which in turn influenced the overall cell death of the neuron-like SH-SY5Y cells. On the other hand, derivative **4** showed a stronger neuroprotective effect compared to **10**, yet showed a weaker reduction in OS and a slightly better decrease in casp-3,7 activation. These observations suggest that other regulatory processes may be involved in the neuroprotection mediated by the derivative **4**. One of the potential regulatory effects was subsequently discovered by measuring the MMP of SH-SY5Y cells co-treated with 160 mM Glu and compound **4** or **10**.

As shown in Fig. 9B, mitochondrial membrane depolarization was observed over a similar time period as casp-3,7 activation, reaching $31.2 \pm 4.60\%$ in Glu-treated cells. Surprisingly, derivative **4** exhibited a highly potent effect in restoring the mitochondrial potential at 10 μM ($74.7 \pm 7.44\%$), whereas derivative **10** was not effective at all. Taken together, the results suggested that all compounds were able to reduce casp-3,7 activation due to Glu intoxication. In contrast to the positive controls, which showed low moderate (CsA) to moderate (DFO) casp-3,7 reducing activity,
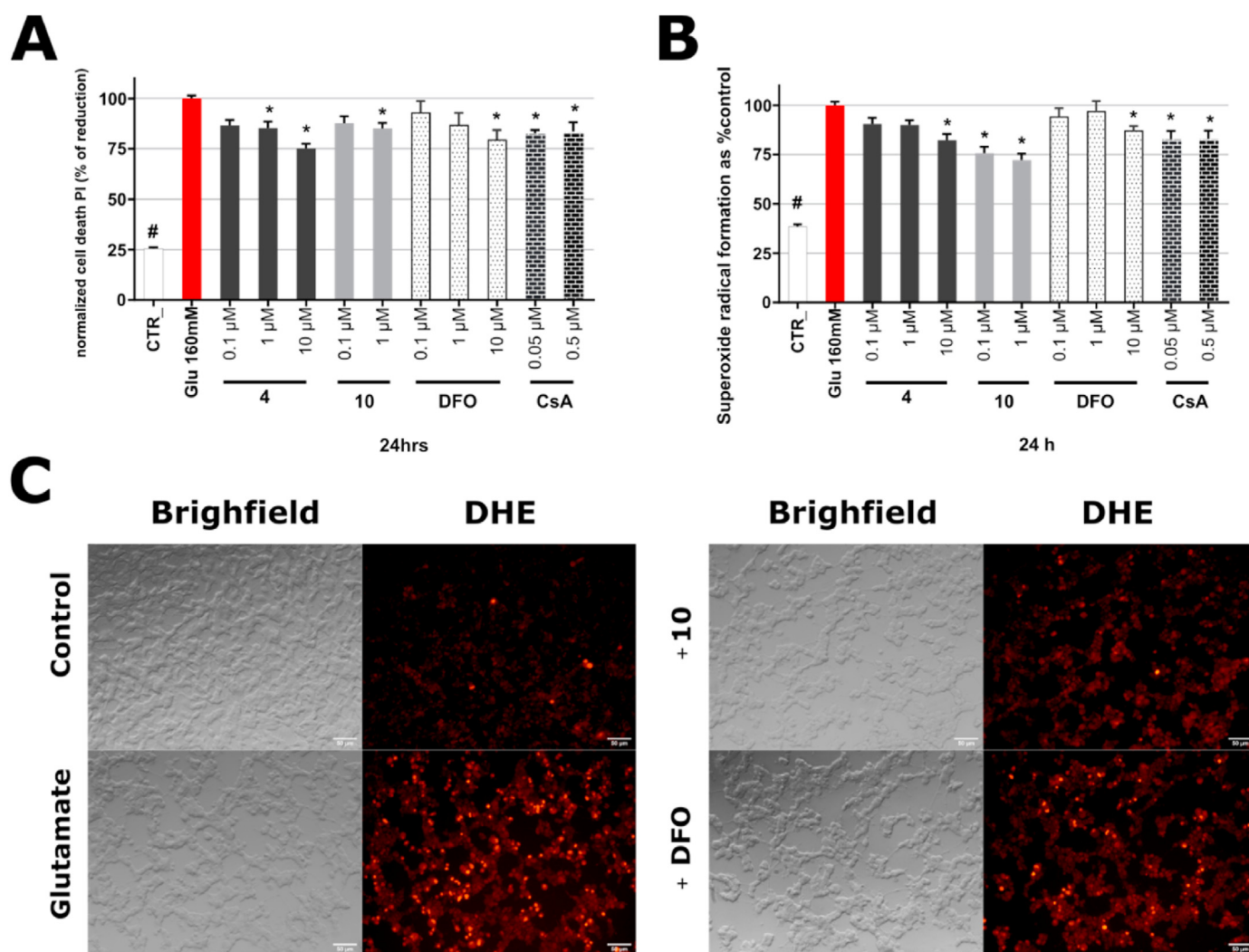
Fig. 8. (A) Neuroprotective effect of tested compounds in the glutamate (Glu)-induced model of cell death - PI staining. All results are presented as mean ± the standard error of the mean (SEM) from four independent experiments performed in triplicate. (B) Glu-induced OS and OS-reducing activity of triterpenes and positive controls. All results are presented as mean ± the standard error of the mean (SEM) from five independent experiments performed in triplicate. *P compared with vehicle with 160 mM Glu, #P compared with vehicle without 160 mM Glu. A value of $P < 0.05$ was considered statistically significant. (C) Glu-induced OS in human neuron-like SH-SY5Y cells visualized by fluorescence microscopy. Illustrative dihydroethidium (DHE) stained microphotographs are shown. Bar = 50 μm. Neuron-like SH-SY5Y cells treated by DMSO (Control), 160 mM Glu (Glutamate), co-treatment of 160 mM Glu with 1 μM 10 (+10) or 10 μM deferoxamine (+DFO) for 4 h and stained by DHE.

triterpenes **4** and **10** showed only a modest effect. More importantly, measurement of the MMP revealed that compound **4** mediated the protective effect mainly by restoring the MMP, whereas derivative **10** probably modulated Glu toxicity by a direct effect on superoxide radical formation.

2.2.8.1. Conclusion. In this study, a set of pentacyclic triterpenoids was studied for their potential neuroprotective effects. Some of the compounds were selected from existing non-toxic triterpenes from our library, whereas others were synthesized for the first time. Derivatives **3**, **4**, **5a** and **10** along with positive controls CsA and NAC were identified as neuroprotective in the SAL model. The most effective compounds **3** and **4** were broken down into substructures to find out which part of the molecules was responsible for the biological effects. We found that the substructure **10** (triterpene conjugated to an unsubstituted triazole) provided complete protection at 1 μM against SAL toxicity unlike the other substructures. Unfortunately, a higher concentration of **10** (10 μM) was found to be cytotoxic. Since compounds **3** and **4** had very similar effects, we

further tested only the original structure **4** and substructure **10**. The effects of derivatives **4** and **10** on OS, caspase 3,7 activation, and regulation of mitochondrial processes within the SAL-induced model of PD on neuron-like cells were extensively studied. Whereas the effect of both derivatives on OS reduction was comparable, **10** outperformed all the tested compounds in the inhibition of caspase-3,7. The effect of **10** was even comparable to nanomolar concentrations of the caspase 3,7 inhibitor Ac-DEVD-CHO. In subsequent evaluation of the MMP, compound **4** showed a dose-dependent recovery effect outperforming all other tested compounds. Conversely, derivative **10** did not demonstrate any improvement of MMP at an active concentration (1 μM), probably due to an unfavourable side effect on mitochondria. To explain the potent casp-3,7 inhibitory effect of derivative **10**, mPTP was evaluated as a key mediator of apoptosis and/or necrosis. The mPTP assay showed that both triterpenes were potent blockers and overcame the effect of NAC and CsA.

Based on these results, **4** and **10** were further tested in a Glu-induced model of oxidative damage on neuron-like SH-SY5Y cells.
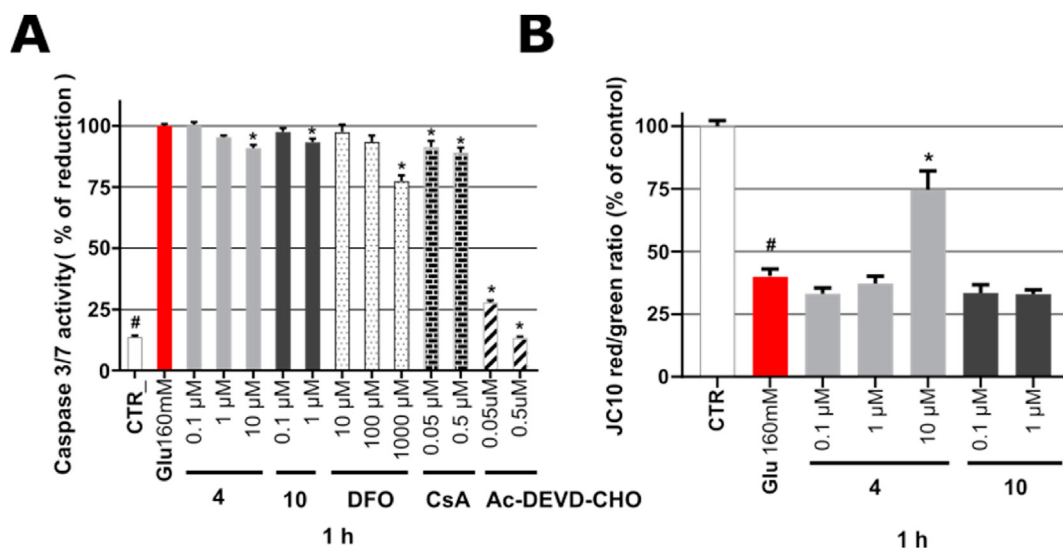
Fig. 9. (A) Caspase-3,7 activity in the Glu model of oxidative damage in neuron-like SH-SY5Y cells after 1 h of treatment. (B) Mitochondrial membrane potential in the Glu model after 1 h. All results represent mean ± the standard error of the mean (SEM) from four independent experiments performed in triplicate. *P compared with vehicle with 160 mM Glu, #P compared with vehicle without 160 mM Glu. A value of $P < 0.05$ was considered statistically significant.

In this model, the glycosylated derivative **4** demonstrated the strongest neuroprotective effect, whereas **10** was only slightly protective. Surprisingly, further evaluation of **10** in an OS assay revealed that it induced the strongest OS reducing effect of all the tested compounds, suggesting that **10** mediates neuroprotection *via* OS reduction.

Compound **4** showed only a moderate effect comparable with the positive controls. Finally, the evaluation of casp-3,7 activity resulted in only slight effects of **4** and **10**, indicating that other processes may be responsible for the induction of neuroprotection. To conclude, **10** was shown to be a potent OS-reducing agent, whereas **4**-mediated protection was associated with a strong restoring effect on the MMP in the Glu model. Based on these results, future work will focus on development of the lead structures **10** and **4** to include derivatization of the triazole part or substitution with another heterocycle, reduction of the allyl moiety (Michael acceptor) and derivatization with another sugar to reduce side effects and improve the neuroprotective activity (Fig. 10).

3. Experimental procedures

3.1. Chemistry

3.1.1. Instruments and methods

Melting points were determined using either Büchi B-545 or STUART SMP30 apparatus and were uncorrected. Infrared spectra were recorded on a Nicolet Avatar 370 FTIR and processed in OMNIC 9.8.372. DRIFT stands for Diffuse Reflectance Infrared Fourier Transform. ^{1}H and ^{13}C experiments were performed on Jeol ECX-500SS (500 MHz for ^{1}H), and Varian$^{\text{UNITY}}$ Inova 400 (400 MHz for ^{1}H) instruments using CDCl$_3$, DMSO-d_6, CD$_3$OD and THF-d_8 as solvents (25 °C). Chemical shifts (δ) were referenced to the residual signal of the solvent (CDCl$_3$, DMSO-d_6, CD$_3$OD or THF-d_8) and are reported in parts per million (ppm). Coupling constants (J) are reported in Hertz (Hz). NMR spectra were processed in ACD/NMR Processor Academic Edition 12.01, MestReNova 6.0.2−5475 or JEOL Delta v5.0.5.1 software. EI-MS spectra were recorded on an INCOS 50 (Finnigan MAT) spectrometer at 70 eV with an ion source
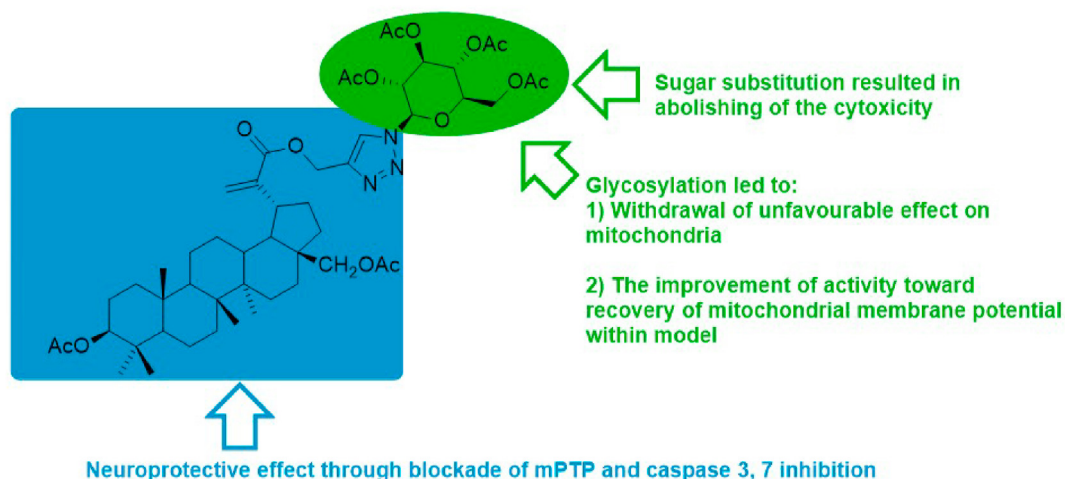

Fig. 10. Lead structures **4** and **10** and their effects in the SAL and Glu models.

temperature of 150 °C. The samples were introduced from a direct exposure probe at a heating rate of 10 mA/s. The relative abundances stated are related to the most abundant ion in the region $m/z > 180$. HRMS analysis was performed using an LC-MS Orbitrap Elite high-resolution mass spectrometer with electrospray ionization (Dionex Ultimate 3000, Thermo Exactive plus, MA, USA). Spectra were recorded in the positive and negative mode in the range 100–1000 m/z. The samples were dissolved in MeOH and injected into the mass spectrometer equipped with an autosampler after HPLC separation: precolumn Phenomenex Gemini (C18, 50 × 2 mm, 2.6 μm), mobile phase isocratic MeOH/water/HCOOH 95:5:0.1. The course of the reactions was monitored by TLC on Kieselgel 60 F$_{254}$ plates (Merck) detected first by UV light (254 nm) and then by spraying with 10% aqueous H$_2$SO$_4$ and heating to 150–200 °C. Purification was performed using column chromatography on Silica gel 60 (Merck 7734). Chemicals and reagents were purchased from Sigma-Aldrich and Lachner companies at the best available qualities. Betulin diacetate (**1**), betulinic acid (**2**), and allobetulon (**11**) were purchased from company Betulinines (www.betulinines.com).

3.1.2. Conjugate with peracetylated galactose (3)

2,3,4,6-Tetra-*O*-acetyl-β-D-galactopyranosyl azide (127 mg, 0.34 mmol), CuI (3.3 mg, 0.017 mmol) and Hünigs base (22 mg, 0.17 mmol) were added to a stirred solution of **9** (100 mg, 0.17 mmol) in THF (5 mL). The initially colourful solution changed immediately to brown-green, indicating the cycloaddition reaction. The reaction mixture was stirred for a further 24 h at r.t., and then the THF was evaporated under reduced pressure. Chromatography on silica gel (5 g) in cyclohexane/EtOAc 3:1 afforded pure **3**, which was then crystallized to give white crystals of **3** (90 mg, 55%). m.p. 120–126 °C (cyclohexane/EtOAc); IR ν (cm^{-1}): 1751 (C=O), 1628 (C=C). ^{1}H NMR (CDCl$_3$, 500 MHz) δ, ppm: 0.82 (3H, s); 0.83 (6H, s); 0.92 (3H, s); 1.01 (3H, s, 5 × CH$_3$); 1.87 (3H, s); 2.00 (3H, s); 2.03 (3H, s); 2.04 (3H, s); 2.05 (3H, s); 2.22 (3H, s, 6 × Ac); 2.76 (1H, td, J_1 = 11.2 Hz, J_2 = 5.2 Hz, H-19β); 3.84 (1H, d, J = 11.2 Hz); 4.10–4.30 (4H, m); 4.45 (1H, dd, J_1 = 10.0 Hz, J_2 = 6.0 Hz, H-3α); 5.20–5.35 (3H, m); 5.50–5.65 (3H, m, 5 × H–CH$_2$O, 1 × H-29 *pro E*); 5.84 (1H, d, J = 9.1 Hz, 1 × H–CH$_2$O); 6.11 (1H, bs, H-29 *pro Z*); 7.92 (1H, s triazole). ^{13}C NMR (CDCl$_3$, 500 MHz) δ, ppm: 14.75; 15.98; 16.14; 16.25; 16.62; 18.11; 20.34; 20.25; 20.45; 20.60; 20.65; 20.80; 20.99; 21.28; 23.64; 26.88; 26.96; 27.32; 27.90; 29.74; 30.89; 34.09; 34.19; 37.17; 37.32; 37.92; 38.35; 40.98; 42.75; 46.57; 50.22; 55.49; 57.74; 61.25; 62.71; 66.95; 67.99; 70.87; 74.27; 81.01; 86.47; 119.89; 122.47; 143.62; 145.98; 167.09; 169.09; 169.91; 169.10; 170.41; 170.13; 171.63. HRMS (ESI): m/z calcd for C$_{51}$H$_{73}$N$_3$O$_{15}$ [M+H]$^+$ 968.5114, found 968.5114.

3.1.3. Conjugate with peracetyl glucose (4)

2,3,4,6-Tetra-*O*-acetyl-β-D-glucopyranosyl azide (127 mg, 0.34 mmol), CuI (3.3 mg, 0.017 mmol) and Hünigs base (22 mg, 0.17 mmol) were added to a solution of **9** (100 mg, 0.17 mmol) in THF (5 mL). The initially colourless solution changed immediately into brown-green, indicating the cycloaddition reaction. The reaction mixture was stirred at r.t. For another 24 h, and then the THF was evaporated under reduced pressure. Chromatography on silica gel (5 g, cyclohexane/EtOAc 3:1) afforded pure **4**, which was then crystallized to give white crystals of **4** (121 mg, 74%). m.p. 122–126 °C (cyclohexane/EtOAc); IR ν (cm^{-1}): 1732 (C=O); 1635 (C=C). ^{1}H NMR (CDCl$_3$, 500 MHz) δ, ppm: 0.82 (3H, s); 0.83 (6H, s); 0.92 (3H, s); 1.02 (3H, s, 5 × CH$_3$); 1.85 (3H, s); 2.02 (3H, s); 2.03 (3H, s); 2.06 (3H, s); 2.08 (3H, s); 2.16 (3H, s, 6 × Ac); 2.76 (1H, td J_1 = 11.5 Hz, J_2 = 5.8 Hz, H-19β); 3.86 (1H, td, J = 10.8 Hz); 3.98–4.05 (1H, m); 4.09–4.35 (4H, m); 4.41 (1H, dd, J_1 = 10.1 Hz, J_2 = 5.2 Hz, H-3α); 5.20–5.35 (3H, m); 5.42 (2H, m); 5.58 (1H, m); 5.87 (1H, d,

J = 9.2 Hz); 6.11 (1H, s); 7.85 (1H, s, triazole). ^{13}C NMR (CDCl$_3$, 500 MHz) δ, ppm: 14.75; 16.14; 16.25; 16.62; 18.12; 20.08; 20.47; 20.50; 20.65; 20.69; 20.80; 20.99; 21.28; 23.64; 26.88; 26.96; 27.37; 27.91; 29.74; 30.89; 34.09; 34.17; 37.01; 37.16; 37.75; 38.34; 40.82; 42.59; 46.41; 50.04; 55.32; 57.67; 61.48; 62.53; 67.64; 70.24; 73.23; 75.38; 81.00; 85.93; 122.20; 122.25; 143.65; 143.81; 167.03; 168.91; 169.45; 170.02; 170.58; 171.12; 171.63. HRMS (ESI): m/z calcd for C$_{51}$H$_{73}$N$_3$O$_{15}$ [M+H]$^+$ 968.5114, found 968.5115.

3.1.4. Allobetulon-2β-carbonitrile 6

A modified procedure from Ref. [57] was used. 2-Bromoallobetulon (2.0 g; 3.3 mmol) was dissolved in DMSO (100 mL) and sodium cyanide (328 mg; 6.7 mmol) was added. The reaction progress was monitored by TLC in hexane/EtOAc 5:1. The reaction mixture was stirred for 24 h at r.t. The reaction was quenched by adding a double volume of water and the product was extracted into toluene. The organic phase was collected, washed with water and the solvents were removed *in vacuo*. Crude carbonitrile **6** was purified by chromatography on silica gel in toluene − toluene/Et$_2$O 10:1 and crystallized from cyclohexane to give white crystals of chromatographically uniform 2-carbonitrile **6** (700 mg; 45%). m.p. 268–270 °C (cyclohexane); [α]$_D$ +64.9° (c 0.47). IR ν (cm^{-1}): 2245 (CN), 1738 (C=O) cm^{-1}. ^{1}H NMR (500 MHz, CDCl$_3$) δ: 0.78–0.74 (1H, m); 0.79 (3H, s); 0.88 (3H, s); 0.93 (3H, s); 0.95 (3H, s); 0.97 (3H, s); 1.07 (3H, s); 1.34 (3H, s, 7 × CH$_3$); 1.67 (1H, d, J = 11.8 Hz, H-1b); 2.30 (1H, dd, J = 15.3, 1.7 Hz, H-1b); 3.44 (1H, d, J = 7.8 Hz, H-28a); 3.51 (1H, s, H-19β); 3.67 (1H, s, H-2); 3.75 (1H, d, J = 7.6 Hz, H-28-b). ^{13}C NMR (101 MHz, CDCl$_3$) δ: 13.52; 15.61; 17.35; 19.74; 21.41; 24.65; 26.27; 26.40; 26.45; 28.90; 29.58; 32.77; 33.16; 34.14; 34.40; 36.37; 36.81; 37.16; 37.76; 40.68; 40.92; 41.58; 46.83; 51.17; 52.29; 56.12; 61.65; 71.32; 77.36; 87.99; 118.62. HRMS (ESI-TOF) m/z calcd for C$_{31}$H$_{47}$NO$_2$ [M+H]$^+$ 466.3680, found 466.3678.

3.1.5. 3,28-Diacetoxylup-20(29)-en-30-oic acid (12)

Betulin diacetate was oxidized using SeO$_2$ in refluxing GLYM according to a previously published procedure to form 30-oxobetulin diacetate [90]. Jones reagent prepared from CrO$_3$ (110 mg, 1.1 mmol) was added to a solution of 30-oxobetulin diacetate (100 mg, 0.184 mmol) in acetone (5 mL) at 0 °C during 2 h. After another 8 h, the starting material was consumed (monitored by TLC in cyclohexane/EtOAc 2:1) and the reaction mixture was extracted between water and EtOAc. The crude product was chromatographed on silica gel (5 g) in cyclohexane/EtOAc 3:1. Pure **12** (46.4 mg, 45%) was obtained as white crystals. m.p. 140–144 °C (acetone/water). IR ν (cm^{-1}): 3450b (OH), 1631 (C=C). ^{1}H NMR (CDCl$_3$, 500 MHz) δ, ppm: 0.84 (3H, s); 0.85 (6H, s); 0.96 (3H, s); 1.04 (3H, s, 5 × CH$_3$); 2.04 (3H, s, Ac); 2.08 (3H, s, Ac); 2.15–2.24 (1H, m); 2.79 (1H, td, J_1 = 11.2 Hz, J_2 = 5.5 Hz, H-19β); 3.87 (1H, d, J = 11.2 Hz); 4.28 (1H, d, J = 4.9 Hz); 4.47 (1H, dd, J = 10.3 Hz, J = 5.2 Hz, H-3α); 5.69 (1H, s, H-29 *pro-E*); 6.27 (s, 1H, H-29 *pro-Z*). ^{13}C NMR (CDCl$_3$, 500 MHz) δ, ppm: 14.65; 16.00; 16.10; 16.47; 18.14; 20.86; 21.02; 21.28; 23.65; 24.45; 26.99; 27.45; 27.92; 29.76; 31.56; 34.11; 34.21; 37.02; 37.20; 37.77; 38.35; 40.07; 40.84; 42.61; 46.43; 50.07; 55.33; 62.63; 80.90; 125.39; 145.99; 171.58; 171.06, 171.94. HRMS (ESI): m/z calcd for C$_{34}$H$_{52}$O$_6$ [M+H]$^+$ 555.3680, found 555.3677.

3.1.6. Propargyl 3,28-diacetoxylup-20(29)-ene-30-oate (9)

Propargyl bromide (60 μL, 80% solution in THF, 0.54 mmol) was added to acid **12** (100 mg, 0.18 mmol) in THF (5 mL) followed by anhydrous K$_2$CO$_3$ (124 mg, 0.9 mmol). The reaction mixture was stirred under reflux for 24 h and then poured into water. The crude product was extracted into EtOAc and washed with water (twice). The crude compound was purified *via* chromatography on silica gel

(5 g) cyclohexane/EtOAc 3:1. Propargyl ester **9** was obtained as white crystals (92 mg, 86%). m.p. 134−138 °C (cyclohexane/EtOAc); IR ν (cm^{-1}): 3308 (C≡CH), 2250 (C≡C), 1728 (C=O), 1623 (C=C). ^{1}H NMR (CDCl$_3$, 500 MHz) δ, ppm: 0.83 (3H, s); 0.84 (6H, s); 0.94 (3H, s); 1.03 (3H, s, 5 × CH$_3$); 2.04 (3H, s, Ac); 2.08 (3H, s, Ac); 2.49 (1H, t, J = 2.3 Hz); 2.77 (1H, td, J_1 = 11.2 Hz, J_2 = 5.7 Hz, H-19β); 3.86 (1H, d, J = 10.9 Hz); 4.27 (1H, dd, J_1 = 11.2 Hz, J_2 = 1.2 Hz); 4.47 (1H, dd, J_1 = 10.3 Hz, J_2 = 5.4 Hz, H-3α); 4.76 (2H, m, H-28a, H-28b); 5.62 (1H, s, H-29 pro-E); 6.14 (1H, s, H-29 pro-Z); ^{13}C NMR (CDCl$_3$, 500 MHz) δ, ppm: 14.71; 16.09; 16.20; 16.57; 18.24; 20.91; 21.12; 21.39; 23.76; 27.07; 27.34; 28.01; 29.86; 30.41; 32.04; 34.20; 34.33; 37.12; 37.25; 37.88; 38.46; 40.93; 42.72; 46.52; 50.17; 51.04; 52.20; 55.44; 62.73; 74.90; 77.83; 80.96; 124.48; 145.98; 166.48; 171.09; 171.64. HRMS (ESI): *molecule did not ionize.*

3.1.7. 1H-1,2,3-triazol-4-ylmethyl 3β,28-diacetyloxylup-20(29)-en-30-oate (10)

CuI (4 mg, 0.02 mmol) was added to a solution of alkyne **9** (50 mg, 0.08 mmol), Dod-azide (bis [4-methoxyphenyl]methyl azide, 23 mg, 0.084 mmol), DIPEA (2 mg, 0.02 mmol), and HOAc (2 mg, 0.02 mmol) in CH$_2$Cl$_2$ (2 mL) under nitrogen at r.t. The reaction mixture was stirred for 24 h and then diluted with DCM and washed with 1 N HCl in water. The organic phase was dried over Na$_2$SO$_4$ and the solvent was evaporated under reduced pressure The residue was purified by column chromatography on silica gel (hexane/EtOAc, 3:1), giving the (1-(bis(4-methoxyphenyl)methyl)-1*H*-1,2,3-triazol-4-yl)methyl 3β,28-diacetyloxylup-20 (29)-en-30-oate (68 mg, 99% yield) as a white solid. R_f = 0.39 (Hexane − EtOAc, 3:2). IR ν (cm^{-1}): 1726 (C=O), 1628 (C=C). 1H NMR (CDCl3, 500 MHz) δ, ppm: 0.83 (6H, s), 0.84 (3H, s), 0.88 (3H, s), 1.01 (3H, s, 5 × Me), 2.04 (3H, s, Ac), 2.06 (3H, s, Ac), 2.73 (1H, td, $J1$ = 11.3 Hz, $J2$ = 5.6 Hz, H-19β), 3.80 (6H, s, MeO), 3.83 (1H, d, J = 11.3 Hz, H-28a), 4.25 (1H, d, $J1$ = 11.3 Hz, H-28b), 4.46 (1H, dd, $J1$ = 10.7 Hz, $J2$ = 5.5 Hz, H-3α), 5.25 (1H, d, $J1$ = 12.7 Hz, H-6'a), 5.29 (1H, d, $J1$ = 12.7 Hz, H-6'b), 5.55 (1H, s, H-29 pro-E), 6.09 (1H, s, H-29 pro-Z), 6.87 (4Harom, dd, J = 8.8 Hz, J = 0.9 Hz), 6.99 (1H, s H-1″), 7.02 (2Harom, d, J = 8.8 Hz), 7.03 (2Harom, d, J = 8.8 Hz), 7.46 (1H, s, H-5′). 13C NMR (CDCl3, 500 MHz) δ, ppm: 14.7, 16.1, 16.2, 16.6, 18.3, 21.0, 21.1, 21.4, 23.8, 27.1, 27.4, 28.1, 29.8, 29.9, 32.1, 34.25, 34.34, 37.2, 37.3, 37.9, 38.5, 41.0, 42.8, 46.6, 50.2, 51.0, 55.47 (2C), 55.49, 58.1, 62.7, 67.5, 81.0, 114.40 (2C), 114.41 (2C), 123.7, 124.3, 129.3 (2C), 129.4 (2C), 130.53, 130.55, 142.6, 146.2, 159.80, 159.81, 167.2, 171.1, 171.6. HRMS (ESI): *m/z* calcd for C$_{52}$H$_{70}$N$_3$O$_8$ [M+H]+ 864.5157, found 864.5164.

A 50% solution of TFA in CH$_2$Cl$_2$ (1 mL) was added to the intermediate (1-(bis(4-methoxyphenyl)methyl)-1*H*-1,2,3-triazol-4-yl) methyl 3β,28-diacetyloxylup-20 (29)-en-30-oate (66 mg, 0.08 mmol) and anisole (20 µL) in CH$_2$Cl$_2$ (1 mL) at r.t. The reaction mixture was stirred for 1 h and then diluted with water. The crude product was extracted with CHCl$_3$. The organic phase was washed with 5% NaHCO$_3$ in water, dried over Na$_2$SO$_4$ and the solvents were evaporated under reduced pressure. The residue was purified by column chromatography on silica gel (CHCl$_3$/MeOH, 3:1), giving the triazole **10** (34 mg, 71% yield) as a white solid. R_f = 0.62 (CHCl$_3$ − MeOH, 3:1). m.p. 118−120 °C (MeOH); IR ν (cm^{-1}): 3450 (NH), 1720 (C=O), 1631 (C=C). 1H NMR (CDCl3, 500 MHz) δ, ppm: 0.83 (6H, s), 0.84 (3H, s), 0.89 (3H, s), 1.01 (3H, s, 5 × Me), 1.78 (1H, d, $J1$ = 12.3 Hz, $J2$ = 8.0 Hz), 1.83−1.86 (2H, m), 2.04 (3H, s, Ac), 2.07 (3H, s, Ac), 2.12−2.16 (1H, m), 2.76 (1H, td, $J1$ = 11.3 Hz, $J2$ = 5.6 Hz, H-19β), 3.85 (1H, d, J = 11.0 Hz, H-28a), 4.25 (1H, d $J1$ = 11.0 Hz, H-28b), 4.46 (1H, dd, $J1$ = 10.9 Hz, $J2$ = 5.2 Hz, H-3α), 5.34 (2H, s, H-6′), 5.59 (1H, s, H-29 pro-E), 6.11 (1H, s, H-29 pro-Z), 7.78 (1H, s, H-5'). 13C NMR (CDCl3, 125 MHz) δ, ppm: 14.7, 16.1, 16.2, 16.6, 18.3, 20.9, 21.2, 21.5, 23.8, 27.1, 27.4, 28.1, 29.9, 32.1, 34.2, 34.3, 37.2, 37.3, 37.9, 38.5, 41.0, 42.7, 46.5, 50.2, 51.0, 53.5, 55.5, 57.4, 62.8, 81.2, 124.4,

146.2, 167.2, 171.4, 171.9. HRMS (ESI): *m/z* calcd for C$_{37}$H$_{56}$N$_3$O$_6$ [M+H]+ 638.4164, found 638.4162.

3.1.8. [1-(2′,3′,4′,6′-tetra-O-acetyl-β-D-galactopyranosyl)-1H-1,2,3-triazol-4-yl]-methanol

2,3,4,6-Tetra-*O*-acetyl-β-D-galactopyranosyl azide **(**280 mg, 0,75 mmol) was dissolved in *t*-BuOH (20 mL), then CuSO$_4$·5H$_2$O (93 mg, 0.37 mmol, 0.5 equiv.), sodium ascorbate (120 mg, 0.6 mmol, 0.8 equiv.) and distilled water (10 mL) were added. The heterogeneous reaction mixture was stirred vigorously for 5 min and propargyl alcohol (65 µL, 1.13 mmol, 1.5 equiv) was added. The mixture was heated to 50 °C for 24 h. The reaction was monitored by TLC. The reaction mixture was filtered and the solvents were lyophilized. The crude product was purified using reverse phase HPLC with PDA and MS detection and a mobile phase of 0.5% NaOAc in water: MeCN (gradient from 35% to 50% MeCN) to obtain **13** as a white solid. Yield 202 mg (63%); m.p. 155−157 °C (cyclohexane/MeOH); IR ν (cm^{-1}): 3469b (OH), 1700−1750 (C=O) cm^{-1}.^{1}H NMR and ^{13}C NMR are in agreement with the literature [58]. HRMS (ESI): *m/z* calcd for C$_{17}$H$_{23}$N$_3$O$_{11}$ ([M + H]$^+$), 430.1456, found 430.1456.

3.2. Biological evaluation

3.2.1. Drugs and reagents

Dulbecco's Modified Eagle Medium/Nutrient Mixture F-12 (DMEM/F-12), penicillin, streptomycin, fetal bovine serum, trypsin, propidium iodide, dihydroethidium, all-trans retinoic acid, *N*-acetylcysteine, defferoxamin, cyclosporin A, salsolinol hydrobromide, glutamate monosodium salt, buffer components for One-step caspase 3,7 assay, acridine orange, the mitochondrial membrane JC10 kit and cobalt (II) chloride were purchased from Sigma-Aldrich Merck. The neurite outgrowth kit (Invitrogen™) and Calcein AM were obtained from ThermoFisher. The caspase-3,7 substrate (Ac-DEVD-AMC) was purchased from Enzo Life Sciences, Inc.

3.2.2. SH-SY5Y cell culture

The SH-SY5Y human neuroblastoma cell line obtained from ATCC (American Type Culture Collection, Manassas, VA, USA) was cultivated in Dulbecco's modified Eagle's Medium and Ham's F12 Nutrient Mixture (DMEM:F-12, 1:1), supplemented with 10% fetal bovine serum (FBS) and 1% penicillin and streptomycin at 37 °C in a humidified atmosphere of 5% CO$_2$. The cell culture was used for all experiments until it reached passage 20. For each experiment, SH-SY5Y cells were seeded at a density according to the type of assay (5000, 7000, 10 000 and 20 000 cells/well) in 96-multiwell plates in 100 µl total volume of medium. The next day, all-*trans* retinoic acid in 1% FBS DMEM/F12 medium was added to the SH-SY5Y cells at a final concentration of 10 µM. The cells were kept under differentiated conditions for 48 h to achieve longer neurites and reduced proliferation.

3.2.3. Microscopy

Neuron-like SH-SY5Y cells were observed under a Leica DM IL LED (Leica Microsystems, Germany) fluorescence microscope with different excitation filters according to the type of assay or a brightfield setup. Images were captured using an Olympus DP73 high-performance digital camera (Olympus, Tokyo, Japan) and processed by ImageJ software (Fiji).

3.2.4. Cell membrane staining (neurite outgrowth kit, Invitrogen™)

SH-SY5Y cells (5000 cells/well) after 48 h of the differentiation procedure were stained by a neurite outgrowth kit (Invitrogen™) according to the manufacturer's protocol with small modifications. Briefly, cells were washed by PBS and stained with a solution of membrane staining dye (protocol for 96 multiwell plates) in PBS for

20 min at 37 °C. After 20 min, the dye in PBS was aspirated and replaced by fresh PBS. Microphotographs of the cells were recorded under the fluorescence microscope.

3.2.5. Cell treatment

After 48 h differentiation, the old differentiation medium was replaced by fresh 1% DMEM/F12 medium containing the tested compounds at 0.1, 1 and 10 μM concentration (7000 cells/well − cytotoxicity) as a co-treatment with 500 μm SAL (7000−10 000 cells/well) or 160 mM Glu (20 000 cells/well) for a duration according to the assay type. Control cells were treated by medium containing ≤0.1% of DMSO.

3.2.6. Cell viability and cell death

After 24 h of treatment, the cell viability of neuron-like SH-SY5Y cells growing in 96-well plates (7000 cells/well) was evaluated by the calcein AM assay [61]. Calcein AM solution (Invitrogen™) was added to a final concentration of 0.75 μM, and cells were incubated for 50 min. The fluorescence of free intracellular calcein was measured at 495/517 nm (excitation/emission) using an Infinite M200 Pro (Tecan, Austria) microplate reader. The cell viability was calculated as a percentage of control (DMSO control cells). Cell death of the neuron-like cells (SAL model: 10 000 cells/well; Glu model: 20 000 cells/well) was determined by the PI assay according to Stone et al., 2003 [66]. Briefly, PI was diluted to a 1 mg/mL solution in DMSO. Basic solution was diluted in PBS and then added to cell medium to reach concentration 1 μg/mL (Glu-model). In the SAL model, the old medium was replaced with a PBS solution of PI (1 μg/mL). The cells were incubated for 15−25 min at r.t. PI stained cells were quantified at 535/617 nm (excitation/emission) using an Infinite M200 Pro reader (Tecan, Austria). The fluorescence after treatment with the toxins was considered to correspond to 100% cell death.

3.2.7. Measurement of oxidative stress by dihydroethidium (DHE) assay

Cells were left to differentiate and subjected to treatment protocols according to the model of study for 24 h (SAL, 10 000 cells/well) or 4 h (Glu, 20 000 cells/well) in a 96-well plate, as described above. Then, cells were centrifuged at 500 g for 5 min and 30 s, followed by replacement of the old medium with PBS solution containing 10 μM dihydroethidium (DHE). Afterwards, the plate with cells was kept in the dark at r.t. For 30 min, and then superoxide radical formation (DHE signal) was quantified at 500/580 nm (excitation/emission) using an Infinite M200 Pro (Tecan, Austria) microplate reader. The resulting fluorescence intensity of DHE after toxin treatment was considered to be 100% superoxide radical formation, relative to which the individual percentages for the co-treatments were calculated. For visualization, cell images were observed using fluorescence microscopy.

3.2.8. Measurement of caspase 3/7 activity

A one-step caspase 3/7 assay was performed according to Carrasco et al., 2003 [91] with small modifications. Neuron-like SH-SY5Y cells were co-treated by toxins and the tested compounds and then incubated for 24 h (SAL model) or 1 h (Glu model). Afterwards, a solution of 3x caspase-3,7 assay buffer (containing 150 mM HEPES pH 7.4, 450 mM NaCl, 150 mM KCl, 30 mM MgCl₂, 1.2 mM EGTA, 1.5% Nonidet P40, 0.3% CHAPS, 30% sucrose) with DTT (30 mM), PMSF (3 mM) and 75 μM Ac-DEVD-AMC (Enzo Life Sciences) was added to each well of a 96-well plate, and the plate was incubated at 37 °C. Caspase-3,7 activity was measured using an Infinite M200 Pro (Tecan, Austria) microplate reader at 346 nm/438 nm (excitation/emission) after 2 h (SAL model) and 3 h (Glu model). The fluorescence after treatment with the toxins was considered to correspond to 100% caspase 3/7 activity.

3.2.9. Measurement of mitochondrial membrane potential by JC10 assay

SH-SY5Y cells (20 000 cells/well) were subjected to the co-treatment procedure for 24 h (SAL model) and 4 h (Glu model). After incubation, neuron-like cells were evaluated by the JC10 assay according to the manufacturer's procedure (mitochondrial membrane potential kit MAK-159, Sigma Aldrich, Merck).

3.2.10. Measurement of mitochondrial permeability transition pore opening by calcein AM/CoCl₂ assay

Mitochondrial permeability transition pore opening was estimated by the calcein AM/CoCl₂ assay with modifications as described in another study [78]. Briefly, neuron-like SH-SY5Y cells (20 000 cells/well) intoxicated by SAL or its combination with the tested compounds for 24 h were centrifuged at 500 g for 5 min 30 s. Then, the medium was aspirated and a solution of 1 μM calcein AM and 2 mM CoCl₂ in Hank's balanced salt solution (HBSS) was added and incubated at 37 °C for 20 min in a 5% CO₂ atmosphere. After incubation, the fluorescence intensity was measured by an Infinite M200 Pro (Tecan, Austria) microplate reader at 488 nm/517 nm (excitation/emission). The resulting signals were calculated as percentages of the DMSO control. Images of the cells were observed using a fluorescence microscope with subsequent processing in ImageJ software. For detailed observation the region of interests was taken.

3.2.11. In vitro models of cell death − acridine orange (AO)/propidium iodide (PI) double staining

Neuron-like SH-SY5Y cells (10 000 cells/well) were treated according to the SAL model, and the cells were kept with toxin for 24 h. The next day, the cells were centrifuged at 500 g for 5.5 min and the medium was replaced by AO (0.5 μM)/PI (1 μg/mL) PBS solution. The cells were kept at r.t. For 25 min, and then representative fluorescence microphotographs were obtained.

3.2.12. Statistical analysis

All data are expressed as mean ± SEM calculated and visualized by GraphPad Prism 8.4.3 software (La Jolla, USA). For statistical analysis the PAST (ver. 1.97) software package [92] was used. The statistical significance was determined by non-parametric Kruskal-Wallis followed by Mann-Whitney post hoc test with sequential Bonferroni correction of p-values. A P < 0.05 value was considered as significant.

Authors' contributions

Gabriel Gonzalez: Methodology, Investigation, Visualization, Writing, Conceptualization - original draft, Software. Milan Urban: Investigation, Visualization, Methodology, Writing. Jiří Hodoň: Investigation, Methodology. Anna Kazakova: Investigation, Methodology. Cosimo Walter D'Acunto: Investigation, Writing - review & editing. Petr Kaňovský: Writing - review & editing, Funding acquisition. Miroslav Strnad: Writing - review & editing, Funding acquisition.

Declaration of competing interest

The authors declare that they have no known competing financial interests or personal relationships that could have appeared to influence the work reported in this paper.

Acknowledgment

The project was supported by the European Regional Development Fund - Project ENOCH (No. CZ.02.1.01/0.0/0.0/16_019/0000868) and by a grant of the Czech Science Foundation No. 20-15621S. Stipendia for J. Hodoň and Gabriel Gonzalez were paid from internal grants of Palacky University IGA_PrF_2020_012 and IGA_PrF_2020_021. The project was also supported by student grant from Endowment fund Palacký University 2017—2019 (G. Gonzalez). Authors would like to thank Dita Jordová and Jana Hrubešová for excellent technical support and Lucie Borkova and Pavel Zoufaly for their help with the synthetic part.

Appendix A. Supplementary data

Supplementary data to this article can be found online at https://doi.org/10.1016/j.ejmech.2021.113168.

References

[1] S.K. Van Den Eeden, C.M. Tanner, A.L. Bernstein, R.D. Fross, A. Leimpeter, D.A. Bloch, L.M. Nelson, Incidence of Parkinson's disease: variation by age, gender, and race/ethnicity, Am. J. Epidemiol. 157 (2003) 1015—1022, https://doi.org/10.1093/aje/kwg068.

[2] O.B. Tysnes, A. Storstein, Epidemiology of Parkinson's disease, J. Neural. Transm. 124 (2017) 901—905, https://doi.org/10.1007/s00702-017-1686-y.

[3] L.M.L. de Lau, M.M.B. Breteler, Epidemiology of Parkinson's disease, Lancet Neurol. 5 (2006) 525—535, https://doi.org/10.1016/S1474-4422(06)70471-9.

[4] A. Wood-Kaczmar, S. Gandhi, N.W. Wood, Understanding the molecular causes of Parkinson's disease, Trends Mol. Med. 12 (2006) 521—528, https://doi.org/10.1016/j.molmed.2006.09.007.

[5] R.J. Gillespie, S.J. Bamford, R. Botting, M. Comer, S. Denny, S. Gaur, M. Griffin, A.M. Jordan, A.R. Knight, J. Lerpiniere, S. Leonardi, S. Lightowler, S. McAteer, A. Merrett, A. Misra, A. Padfield, M. Reece, M. Saadi, D.L. Selwood, G.C. Stratton, D. Surry, R. Todd, X. Tong, V. Ruston, R. Upton, S.M. Weiss, Antagonists of the human A2A adenosine receptor. 4. Design, synthesis, and preclinical evaluation of 7-Aryltriazolo[4,5-d]pyrimidines, J. Med. Chem. 52 (2009) 33—47, https://doi.org/10.1021/jm800961g.

[6] M.T. Armentero, A. Pinna, S. Ferre, J.L. Lanciego, C.E. Muller, R. Franco, Past, present and future of A(2A) adenosine receptor antagonists in the therapy of Parkinson's disease, Pharmacol. Ther. 132 (2011) 280—299, https://doi.org/10.1016/j.pharmthera.2011.07.004.

[7] Z. M, E.D. Abercrombie, Modification of central catecholaminergic systems by stress and injury, in: K.D. Bloom, E. J (Eds.), Psychopharmacology: the Fourth Generation of Progress, Raven Pres, New York, 1995, pp. 355—362.

[8] M.J. Zigmond, Chemical transmission in the brain: homeostatic regulation and its functional implications, Prog. Brain Res. 100 (1994) 115—122, https://doi.org/10.1016/S0079-6123(08)60776-1.

[9] M.J. Zigmond, T.W. Berger, A.A. Grace, E.M. Stricker, Compensatory responses to nigrostriatal bundle injury, Mol. Chem. Neuropathol. 10 (1989) 185—200, https://doi.org/10.1007/BF03159728.

[10] T. Moors, S. Paciotti, D. Chiasserini, P. Calabresi, L. Parnetti, T. Beccari, W.D. van de Berg, Lysosomal dysfunction and α-synuclein aggregation in Parkinson's disease: diagnostic links, Mov. Disord. 31 (2016) 791—801, https://doi.org/10.1002/mds.26562.

[11] E. Colla, Linking the endoplasmic reticulum to Parkinson's disease and alpha-synucleinopathy, Front. Neurosci. 13 (2019) 560, https://doi.org/10.3389/fnins.2019.00560.

[12] J.C. Bridi, F. Hirth, Mechanisms of α-synuclein induced synaptopathy in Parkinson's disease, Front. Neurosci. 12 (2018) 80, https://doi.org/10.3389/fnins.2018.00080.

[13] H.E. Moon, S.H. Paek, Mitochondrial dysfunction in Parkinson's disease, Exp. Neurobiol. 24 (2015) 103—116, https://doi.org/10.5607/en.2015.24.2.103.

[14] Z. Wei, X. Li, X. Li, Q. Liu, Y. Cheng, Oxidative stress in Parkinson's disease: a systematic review and meta-analysis, Front. Mol. Neurosci. 11 (2018) 236, https://doi.org/10.3389/fnmol.2018.00236.

[15] S.V. Zaichick, K.M. McGrath, G. Caraveo, The role of Ca(2+) signaling in Parkinson's disease, Dis. Model. Mech. 10 (2017) 519—535, https://doi.org/10.1242/dmm.028738.

[16] D.J. Surmeier, P.T. Schumacker, Calcium, bioenergetics, and neuronal vulnerability in Parkinson's disease, J. Biol. Chem. 288 (2013) 10736—10741, https://doi.org/10.1074/jbc.R112.410530.

[17] Q. Wang, Y. Liu, J. Zhou, Neuroinflammation in Parkinson's disease and its potential as therapeutic target, Transl. Neurodegener. 4 (2015) 19, https://doi.org/10.1186/s40035-015-0042-0.

[18] U.K. Rinne, Problems associated with long-term levodopa treatment of Parkinson's disease, Acta Neurol. Scand. Suppl. 95 (1983) 19—26, https://doi.org/10.1111/j.1600-0404.1983.tb01513.x.

[19] M.W. Hayes, V.S. Fung, T.E. Kimber, J.D. O'Sullivan, Updates and advances in the treatment of Parkinson disease, Med. J. Aust. 211 (2019) 277—283, https://doi.org/10.5694/mja2.50224.

[20] M. Solayman, M.A. Islam, F. Alam, M.I. Khalil, M.A. Kamal, S.H. Gan, Natural products combating neurodegeneration: Parkinson's disease, Curr. Drug Metabol. 18 (2017) 50—61, https://doi.org/10.2174/1389200217666160709204826.

[21] M. Carbone, S. Duty, M. Rattray, Riluzole neuroprotection in a Parkinson's disease model involves suppression of reactive astrocytosis but not GLT-1 regulation, BMC Neurosci. 13 (2012), https://doi.org/10.1186/1471-2202-13-38, 38-38.

[22] A.H. Schapira, C.W. Olanow, Neuroprotection in Parkinson disease: mysteries, myths, and misconceptions, J. Am. Med. Assoc. 291 (2004) 358—364, https://doi.org/10.1001/jama.291.3.358.

[23] E. Arias, S. Gallego-Sandín, M. Villarroya, A.G. García, M.G. López, Unequal neuroprotection afforded by the acetylcholinesterase inhibitors galantamine, donepezil, and rivastigmine in SH-SY5Y neuroblastoma cells: role of nicotinic receptors, J. Pharmacol. Exp. Therapeut. 315 (2005) 1346—1353, https://doi.org/10.1124/jpet.105.090365.

[24] J.R. Das, Y. Tizabi, Additive protective effects of donepezil and nicotine against salsolinol-induced cytotoxicity in SH-SY5Y cells, Neurotox. Res. 16 (2009) 194—204, https://doi.org/10.1007/s12640-009-9040-2.

[25] Y. Tian, Y. He, W. Song, E. Zhang, X. Xia, Neuroprotective effect of deferoxamine on N-methyl-d-aspartate-induced excitotoxicity in RGC-5 cells, Acta Biochim. Biophys. Sin. 49 (2017) 827—834, https://doi.org/10.1093/abbs/gmx082.

[26] P. Jenner, Preclinical evidence for neuroprotection with monoamine oxidase-B inhibitors in Parkinson's disease, Neurology 63 (2004) S13—S22, https://doi.org/10.1212/wnl.63.7_suppl_2.s13.

[27] C.W. Olanow, A rationale for dopamine agonists as primary therapy for Parkinson's disease, Can. J. Neurol. Sci. 19 (2015) 108—112, https://doi.org/10.1017/S0317167100041469.

[28] N. Giladi, M.P. McDermott, S. Fahn, S. Przedborski, J. Jankovic, M. Stern, C. Tanner, Freezing of gait in PD: prospective assessment in the DATATOP cohort, Neurology 56 (2001) 1712—1721, https://doi.org/10.1212/wnl.56.12.1712.

[29] R.A. Hill, J.D. Connolly, Triterpenoids, Nat. Prod. Rep. 35 (2018) 1294—1329, https://doi.org/10.1039/c8np00029h.

[30] D.M. Zhang, H.G. Xu, L. Wang, Y.J. Li, P.H. Sun, X.M. Wu, G.J. Wang, W.M. Chen, W.C. Ye, Betulinic acid and its derivatives as potential antitumor agents, Med. Res. Rev. 35 (2015) 1127—1155, https://doi.org/10.1002/med.21353.

[31] M. Ali-Seyed, I. Jantan, K. Vijayaraghavan, S.N. Bukhari, Betulinic acid: recent advances in chemical modifications, effective delivery, and molecular mechanisms of a promising anticancer therapy, Chem. Biol. Drug Des. 87 (2016) 517—536, https://doi.org/10.1111/cbdd.12682.

[32] J. Hodon, L. Borkova, J. Pokorny, A. Kazakova, M. Urban, Design and synthesis of pentacyclic triterpene conjugates and their use in medicinal research, Eur. J. Med. Chem. 182 (2019) 111653, https://doi.org/10.1016/j.ejmech.2019.111653.

[33] D. Wojnicz, D. Tichaczek-Goska, K. Korzekwa, M. Kicia, A. Hendrich, Anti-enterococcal activities of pentacyclic triterpenes, Adv. Clin. Exp. Med. 26 (2017) 483—490, https://doi.org/10.17219/acem/62245.

[34] U.V. Mallavadhani, A. Mahapatra, S.S. Raja, C. Manjula, Antifeedant activity of some pentacyclic triterpene acids and their fatty acid ester analogues, J. Agric. Food Chem. 51 (2003) 1952—1955, https://doi.org/10.1021/jf020691d.

[35] S. Xiao, Z. Tian, Y. Wang, L. Si, L. Zhang, D. Zhou, Recent progress in the antiviral activity and mechanism study of pentacyclic triterpenoids and their derivatives, Med. Res. Rev. 38 (2018) 951—976, https://doi.org/10.1002/med.21484.

[36] D. Steinberg, H.D. Sgan-Cohen, A. Stabholz, S. Pizanty, R. Segal, M.N. Sela, The anticariogenic activity of glycyrrhizin: preliminary clinical trials, Isr. J. Dent. Sci. 2 (1989) 153—157.

[37] G.-B. Xu, Y.-H. Xiao, Q.-Y. Zhang, M. Zhou, S.-G. Liao, Hepatoprotective natural triterpenoids, Eur. J. Med. Chem. 145 (2018) 691—716, https://doi.org/10.1016/j.ejmech.2018.01.011.

[38] N.F. Sangweni, P.V. Dludla, R.A. Mosa, A.P. Kappo, A. Opoku, C.J.F. Muller, R. Johnson, Lanosteryl triterpenes from Protorhus longifolia as a cardioprotective agent: a mini review, Heart Fail. Rev. 24 (2019) 155—166, https://doi.org/10.1007/s10741-018-9733-9.

[39] L. Heller, M. Kahnt, A. Loesche, P. Grabandt, S. Schwarz, W. Brandt, R. Csuk, Amino derivatives of platanic acid act as selective and potent inhibitors of butyrylcholinesterase, Eur. J. Med. Chem. 126 (2017) 652—668, https://doi.org/10.1016/j.ejmech.2016.11.056.

[40] A. Loesche, M. Kahnt, I. Serbian, W. Brandt, R. Csuk, Triterpene-based carboxamides act as good inhibitors of butyrylcholinesterase, Molecules 24 (2019) 948, https://doi.org/10.3390/molecules24050948.

[41] S. Schwarz, S.D. Lucas, S. Sommerwerk, R. Csuk, Amino derivatives of glycyrrhetinic acid as potential inhibitors of cholinesterases, Biorg. Med. Chem. 22 (2014) 3370—3378, https://doi.org/10.1016/j.bmc.2014.04.046.

[42] M.J. Castro, V. Richmond, M.B. Faraoni, A.P. Murray, Oxidation at C-16 enhances butyrylcholinesterase inhibition in lupane triterpenoids, Bioorg. Chem. 79 (2018) 301—309, https://doi.org/10.1016/j.bioorg.2018.05.012.

[43] Z. Liang, F. Shi, Y. Wang, L. Lu, Z. Zhang, X. Wang, X. Wang, Neuroprotective effects of tenuigenin in a SH-SY5Y cell model with 6-OHDA-induced injury, Neurosci. Lett. 497 (2011) 104—109, https://doi.org/10.1016/j.neulet.2011.04.041.

[44] C.W. Tsai, R.T. Tsai, S.P. Liu, C.S. Chen, M.C. Tsai, S.H. Chien, H.S. Hung, S.Z. Lin, W.C. Shyu, R.H. Fu, Neuroprotective effects of betulin in pharmacological and transgenic Caenorhabditis elegans models of Parkinson's disease, Cell Transplant. 26 (2017) 1903–1918, https://doi.org/10.1177/0963689717738785.

[45] B.-H. Kim, J. Kwon, W. Mar, Neuroprotective effect of demethylsuberosin, a proteasome activator, against MPP+-induced cell death in human neuroblastoma SH-SY5Y cells, Planta Med. 2 (2015) 15–18, https://doi.org/10.1055/s-0035-1545936.

[46] D. Wang, P. Chen, L. Chen, F. Zeng, R. Zang, H. Liu, C. Lu, Betulinic acid protects the neuronal damage in new born rats from isoflurane-induced apoptosis in the developing brain by blocking FASL-FAS signaling pathway, Biomed. Pharmacother. 95 (2017) 1631–1635, https://doi.org/10.1016/j.biopha.2017.09.028.

[47] V. Sidova, P. Zoufaly, J. Pokorny, P. Dzubak, M. Hajduch, I. Popa, M. Urban, Cytotoxic conjugates of betulinic acid and substituted triazoles prepared by Huisgen Cycloaddition from 30-azidoderivatives, PloS One 12 (2017), e0171621, https://doi.org/10.1371/journal.pone.0171621.

[48] J. Pokorny, V. Horka, V. Sidova, M. Urban, Synthesis and characterization of new conjugates of betulin diacetate and bis(triphenysilyl)betulin with substituted triazoles, Monatsh. Chem. 149 (2018) 839–845, https://doi.org/10.1007/s00706-017-2113-7.

[49] P. Perlikova, M. Kvasnica, M. Urban, M. Hajduch, J. Sarek, 2-Deoxyglycoside conjugates of lupane triterpenoids with high cytotoxic activity—synthesis, activity, and pharmacokinetic profile, Bioconjugate Chem. 30 (2019) 2844–2858, https://doi.org/10.1021/acs.bioconjchem.9b00565.

[50] J. Pokorny, L. Borkova, M. Urban, Click reactions in chemistry of triterpenes - advances towards development of potential therapeutics, Curr. Med. Chem. 25 (2018) 636–658, https://doi.org/10.2174/0929867324666171009122612.

[51] M. Kurnik-Łucka, P. Panula, A. Bugajski, K. Gil, Salsolinol: an unintelligible and double-faced molecule-lessons learned from in vivo and in vitro experiments, Neurotox. Res. 33 (2018) 485–514, https://doi.org/10.1007/s12640-017-9818-6.

[52] S. Wanpen, P. Govitrapong, S. Shavali, P. Sangchot, M. Ebadi, Salsolinol, a dopamine-derived tetrahydroisoquinoline, induces cell death by causing oxidative stress in dopaminergic SH-SY5Y cells, and the said effect is attenuated by metallothionein, Brain Res. 1005 (2004) 67–76, https://doi.org/10.1016/j.brainres.2004.01.054.

[53] A.A. Kritis, E.G. Stamoula, K.A. Paniskaki, T.D. Vavilis, Researching glutamate - induced cytotoxicity in different cell lines: a comparative/collective analysis/study, Front. Cell. Neurosci. 9 (2015), https://doi.org/10.3389/fncel.2015.00091, 91-91.

[54] L. Borkova, R. Adamek, P. Kalina, P. Drašar, P. Dzubak, S. Gurska, J. Rehulka, M. Hajduch, M. Urban, J. Sarek, Synthesis and cytotoxic activity of triterpenoid thiazoles derived from allobetulin, methyl betulonate, methyl oleanonate, and oleanonic acid, ChemMedChem 12 (2017) 390–398, https://doi.org/10.1002/cmdc.201600626.

[55] L. Borková, I. Frydrych, N. Jakubcová, R. Adámek, B. Lišková, S. Gurská, M. Medvedíková, M. Hajdúch, M. Urban, Synthesis and biological evaluation of triterpenoid thiazoles derived from betulonic acid, dihydrobetulonic acid, and ursonic acid, Eur. J. Med. Chem. 185 (2020) 111806, https://doi.org/10.1016/j.ejmech.2019.111806.

[56] D. Cuffaro, C. Camodeca, F. D'Andrea, E. Piragine, L. Testai, V. Calderone, E. Orlandini, E. Nuti, A. Rossello, Matrix metalloproteinase-12 inhibitors: synthesis, structure-activity relationships and intestinal absorption of novel sugar-based biphenylsulfonamide carboxylates, Biorg. Med. Chem. 26 (2018) 5804–5815, https://doi.org/10.1016/j.bmc.2018.10.024.

[57] H.-O.T. Kim, G.A. Tolstikov, M.I. Goryaev, Izvestiya akademii nauk kazakhskoi SSSR, Seriya Khimicheskaya 20 (1970) 49–54.

[58] I. Carvalho, P. Andrade, V.L. Campo, P.M.M. Guedes, R. Sesti-Costa, J.S. Silva, S. Schenkman, S. Dedola, L. Hill, M. Rejzek, S.A. Nepogodiev, R.A. Field, 'Click chemistry' synthesis of a library of 1,2,3-triazole-substituted galactose derivatives and their evaluation against Trypanosoma cruzi and its cell surface trans-sialidase, Biorg. Med. Chem. 18 (2010) 2412–2427, https://doi.org/10.1016/j.bmc.2010.02.053.

[59] Y.-T. Cheung, W.K.-W. Lau, M.-S. Yu, C.S.-W. Lai, S.-C. Yeung, K.-F. So, R.C.-C. Chang, Effects of all-trans-retinoic acid on human SH-SY5Y neuroblastoma as in vitro model in neurotoxicity research, Neurotoxicology 30 (2009) 127–135, https://doi.org/10.1016/j.neuro.2008.11.001.

[60] S. Dwane, E. Durack, P.A. Kiely, Optimising parameters for the differentiation of SH-SY5Y cells to study cell adhesion and cell migration, BMC Res. Notes 6 (2013), https://doi.org/10.1186/1756-0500-6-366, 366-366.

[61] L. Rárová, J. Steigerová, M. Kvasnica, P. Bartůněk, K. Křížová, H. Chodounská, Z. Kolář, D. Sedlák, J. Oklestkova, M. Strnad, Structure activity relationship studies on cytotoxicity and the effects on steroid receptors of AB-functionalized cholestanes, J. Steroid Biochem. Mol. Biol. 159 (2016) 154–169, https://doi.org/10.1016/j.jsbmb.2016.03.017.

[62] S. Wanpen, P. Govitrapong, S. Shavali, P. Sangchot, M. Ebadi, Salsolinol, a dopamine-derived tetrahydroisoquinoline, induces cell death by causing oxidative stress in dopaminergic SH-SY5Y cells, and the said effect is attenuated by metallothionein, Brain Res. 1005 (2004) 67–76, https://doi.org/10.1016/j.brainres.2004.01.054.

[63] Y. Akao, W. Maruyama, S. Shimizu, H. Yi, Y. Nakagawa, M. Shamoto-Nagai, M.B. Youdim, Y. Tsujimoto, M. Naoi, Mitochondrial permeability transition mediates apoptosis induced by N-methyl(R)salsolinol, an endogenous neurotoxin, and is inhibited by Bcl-2 and rasagiline, N-propargyl-1(R)-

[64] W.A. Dengler, J. Schulte, D.P. Berger, R. Mertelsmann, H.H. Fiebig, Development of a propidium iodide fluorescence assay for proliferation and cytotoxicity assays, Anti Canc. Drugs 6 (1995) 522–532, https://doi.org/10.1097/00001813-199508000-00005.

[65] L. Zhang, K. Mizumoto, N. Sato, T. Ogawa, M. Kusumoto, H. Niiyama, M. Tanaka, Quantitative determination of apoptotic death in cultured human pancreatic cancer cells by propidium iodide and digitonin, Canc. Lett. 142 (1999) 129–137, https://doi.org/10.1016/s0304-3835(99)00107-x.

[66] W.L. Stone, M. Qui, M. Smith, Lipopolysaccharide enhances the cytotoxicity of 2-chloroethyl ethyl sulfide, BMC Cell Biol. 4 (2003), https://doi.org/10.1186/1471-2121-4-1, 1-1.

[67] V.P. Bindokas, J. Jordan, C.C. Lee, R.J. Miller, Superoxide production in rat hippocampal neurons: selective imaging with hydroethidine, J. Neurosci. 16 (1996) 1324–1336, https://doi.org/10.1523/JNEUROSCI.16-04-01324.1996.

[68] G. Rothe, G. Valet, Flow cytometric analysis of respiratory burst activity in phagocytes with hydroethidine and 2',7'-dichlorofluorescin, J. Leukoc. Biol. 47 (1990) 440–448, https://doi.org/10.1002/jlb.47.5.440.

[69] W.O. Carter, P.K. Narayanan, J.P. Robinson, Intracellular hydrogen peroxide and superoxide anion detection in endothelial cells, J. Leukoc. Biol. 55 (1994) 253–258, https://doi.org/10.1002/jlb.55.2.253.

[70] J.H. Kang, Salsolinol, a catechol neurotoxin, induces oxidative modification of cytochrome c, BMB Rep 46 (2013) 119–123, https://doi.org/10.5483/bmbrep.2013.46.2.220.

[71] B.S. Cummings, R.G. Schnellmann, Measurement of cell death in mammalian cells (Chapter 12), Curr. Protoc. Pharmacol. 25 (1) (2004) 12.8.1–12.8.22, https://doi.org/10.1002/0471141755.ph1208s25.

[72] D. Jantas, M. Piotrowski, W. Lason, An involvement of PI3-K/akt activation and inhibition of AIF translocation in neuroprotective effects of undecylenic acid (UDA) against pro-apoptotic factors-induced cell death in human neuroblastoma SH-SY5Y cells, J. Cell. Biochem. 116 (2015) 2882–2895, https://doi.org/10.1002/jcb.25236.

[73] W. Maruyama, M. Naoi, T. Kasamatsu, Y. Hashizume, T. Takahashi, K. Kohda, P. Dostert, An endogenous dopaminergic neurotoxin, N-methyl-(R)-salsolinol, induces DNA damage in human dopaminergic neuroblastoma SH-SY5Y cells, J. Neurochem. 69 (1997) 322–329, https://doi.org/10.1046/j.1471-4159.1997.69010322.x.

[74] A. Johri, M.F. Beal, Mitochondrial dysfunction in neurodegenerative diseases, J. Pharmacol. Exp. Therapeut. 342 (2012) 619–630, https://doi.org/10.1124/jpet.112.192138.

[75] X. Wu, X. Li, Y. Liu, N. Yuan, C. Li, Z. Kang, X. Zhang, Y. Xia, Y. Hao, Y. Tan, Hydrogen exerts neuroprotective effects on OGD/R damaged neurons in rat hippocampal by protecting mitochondrial function via regulating mitophagy mediated by PINK1/Parkin signaling pathway, Brain Res. 1698 (2018) 89–98, https://doi.org/10.1016/j.brainres.2018.06.028.

[76] Y.S. Park, S.E. Choi, H.C. Koh, PGAM5 regulates PINK1/Parkin-mediated mitophagy via DRP1 in CCCP-induced mitochondrial dysfunction, Toxicol. Lett. 284 (2018) 120–128, https://doi.org/10.1016/j.toxlet.2017.12.004.

[77] J.J. Lemasters, T.P. Theruvath, Z. Zhong, A.-L. Nieminen, Mitochondrial calcium and the permeability transition in cell death, Biochim. Biophys. Acta 1787 (2009) 1395–1401, https://doi.org/10.1016/j.bbabio.2009.06.009.

[78] J.S. Riley, G. Quarato, J. Lopez, J. O'Prey, M. Pearson, J. Chapman, H. Sesaki, L.M. Carlin, J.F. Passos, A.P. Wheeler, A. Oberst, K.M. Ryan, S.W.G. Tait, Activated BAX/BAK enable mitochondrial inner membrane permeabilisation and mtDNA release during cell death, EMBO J. (2018) 272104, https://doi.org/10.1101/272104.

[79] V. Buko, I. Kuzmitskaya, S. Kirko, E. Belonovskaya, E. Naruta, O. Lukivskaya, A. Shlyahtun, T. Ilyich, A. Zakreska, I. Zavodnik, Betulin attenuated liver damage by prevention of hepatic mitochondrial dysfunction in rats with alcoholic steatohepatitis, Phys. Int. 106 (2019) 323–334, https://doi.org/10.1556/2060.106.2019.26.

[80] S. Bollimuntha, M. Ebadi, B.B. Singh, TRPC1 protects human SH-SY5Y cells against salsolinol-induced cytotoxicity by inhibiting apoptosis, Brain Res. 1099 (2006) 141–149, https://doi.org/10.1016/j.brainres.2006.04.104.

[81] D. Baskić, S. Popović, P. Ristić, N.N. Arsenijević, Analysis of cycloheximide-induced apoptosis in human leukocytes: fluorescence microscopy using annexin V/propidium iodide versus acridin orange/ethidium bromide, Cell Biol. Int. 30 (2006) 924–932, https://doi.org/10.1016/j.cellbi.2006.06.016.

[82] A.T. Peana, M. Rosas, S. Porru, E. Acquas, From ethanol to salsolinol: role of ethanol metabolites in the effects of ethanol, J. Exp. Neurosci. 10 (2016) 137–146, https://doi.org/10.4137/JEN.S25099.

[83] C. Li, S. Chai, Y. Ju, L. Hou, H. Zhao, W. Ma, T. Li, J. Sheng, W. Shi, Pu-erh tea protects the nervous system by inhibiting the expression of metabotropic glutamate receptor 5, Mol. Neurobiol. 54 (2017) 5286–5299, https://doi.org/10.1007/s12035-016-0064-3.

[84] M. Schultheiss, S. Schnichels, T. Mlynczak, J.H. Dipl-Ing, K.U. Bartz-Schmidt, P. Szurman, M.S. Spitzer, Cyclosporine a protects RGC-5 cells from excitotoxic cell death, J. Glaucoma 23 (2014) 219–224, https://doi.org/10.1097/ijg.0000000000000040.

[85] J. Chu, C.-X. Liu, R. Song, Q.-L. Li, Ferrostatin-1 protects HT-22 cells from oxidative toxicity, Neural Regen. Res. 15 (2020) 528–536, https://doi.org/10.4103/1673-5374.266060.

[86] L. Vidya, M.M. Malini, P. Varalakshmi, Effect of pentacyclic triterpenes on oxalate-induced changes in rat erythrocytes, Pharmacol. Res. 42 (2000)

313−316, https://doi.org/10.1006/phrs.2000.0691.

[87] S.-J. Yang, A.R. Han, E.-A. Kim, J.W. Yang, J.-Y. Ahn, J.-M. Na, S.-W. Cho, KHG21834 attenuates glutamate-induced mitochondrial damage, apoptosis, and NLRP3 inflammasome activation in SH-SY5Y human neuroblastoma cells, Eur. J. Pharmacol. 856 (2019) 172412, https://doi.org/10.1016/j.ejphar.2019.172412.

[88] T.N. Yuksel, M. Yayla, Z. Halici, E. Cadirci, B. Polat, D. Kose, Protective effect of 5-HT7 receptor activation against glutamate-induced neurotoxicity in human neuroblastoma SH-SY5Y cells via antioxidative and antiapoptotic pathways, Neurotoxicol. Teratol. 72 (2019) 22−28, https://doi.org/10.1016/j.ntt.2019.01.002.

[89] H.J. Lee, D.A. Spandidos, A. Tsatsakis, D. Margina, B.N. Izotov, S.H. Yang, Neuroprotective effects of Scrophularia buergeriana extract against glutamate-induced toxicity in SH-SY5Y cells, Int. J. Mol. Med. 43 (2019) 2144−2152, https://doi.org/10.3892/ijmm.2019.4139.

[90] M. Urban, J. Klinot, I. Tislerova, D. Biedermann, M. Hajduch, I. Cisarova, J. Sarek, Reactions of activated lupane oxo-compounds with diazomethane: an approach to new derivatives of cytotoxic triterpenes, Synthesis 2006 (2006) 3979−3986, https://doi.org/10.1055/s-2006-950327.

[91] R.A. Carrasco, N.B. Stamm, B.K.R. Patel, One-step cellular caspase-3/7 assay, Biotechniques 34 (2003) 1064−1067, https://doi.org/10.2144/03345dd02.

[92] O. Hammer, D. Harper, P. Ryan, PAST: paleontological statistics software package for education and data analysis, Palaeontol. Electron. 4 (2001) 1−9.

Supplementary material III.

Maková, B.; Mik, V.; Lišková, B.; Gonzalez, G.; Vítek, D.; Medvedíková, M.; Monfort, B.; Ručilová, V.; Kadlecová, A.; Khirsariya, P.; Gándara Barreiro, Z.; Havlíček, L.; Zatloukal, M.; Soural, M.; Paruch, K.; D'Autréaux, B.; Hajdúch, M.; Strnad, M.; Voller, J., Cytoprotective activities of kinetin purine isosteres. *Biorganic Medicinal Chemistry* 2021, *33*, 115993.

Cytoprotective activities of kinetin purine isosteres

Barbara Maková [a], Václav Mik [a], Barbora Lišková [b], Gabriel Gonzalez [a,g], Dominik Vítek [b], Martina Medvedíková [b], Beata Monfort [d], Veronika Ručilová [c], Alena Kadlecová [a], Prashant Khirsariya [e], Zoila Gándara Barreiro [a], Libor Havlíček [f], Marek Zatloukal [h], Miroslav Soural [c], Kamil Paruch [e], Benoit D'Autréaux [d], Marián Hajdúch [b], Miroslav Strnad [a], Jiří Voller [b,i,*]

[a] Department of Experimental Biology, Faculty of Science, Palacký University, Šlechtitelů 27, Olomouc CZ-78371, Czech Republic
[b] Institute of Molecular and Translational Medicine, Faculty of Medicine and Dentistry, Palacký University, Hněvotínská 3, Olomouc CZ-77515, Czech Republic
[c] Department of Organic Chemistry, Faculty of Science, Palacký University, 17. listopadu 1192/12, Olomouc CZ-783-71, Czech Republic
[d] Université Paris-Saclay, CEA, CNRS, Institute for Integrative Biology of the Cell (I2BC), 91198 Gif-sur-Yvette, France
[e] Department of Chemistry, CZ Openscreen, Faculty of Science, Masaryk University, Brno, Czech Republic
[f] Isotope Laboratory, The Czech Academy of Science, Institute of Experimental Botany, Vídeňská 1083, Praha 4 CZ-14220, Czech Republic
[g] Department of Neurology, Palacký University Olomouc, Faculty of Medicine and Dentistry and University Hospital, Olomouc, Czech Republic
[h] Department of Chemical Biolology and Genetics, Centre of the Region Hana for Biotechnological and Agricultural Research, Palacký University, Šlechtitelů 27, Olomouc CZ-78371, Czech Republic
[i] Laboratory of Growth Regulators, Palacký University & Institute of Experimental Botany AS CR, Šlechtitelů 27, Olomouc CZ-78371, Czech Republic

ARTICLE INFO

ABSTRACT

Kinetin (N^6-furfuryladenine), a plant growth substance of the cytokinin family, has been shown to modulate aging and various age-related conditions in animal models. Here we report the synthesis of kinetin isosteres with the purine ring replaced by other bicyclic heterocycles, and the biological evaluation of their activity in several *in vitro* models related to neurodegenerative diseases. Our findings indicate that kinetin isosteres protect Friedreich's ataxia patient-derived fibroblasts against glutathione depletion, protect neuron-like SH-SY5Y cells from glutamate-induced oxidative damage, and correct aberrant splicing of the ELP1 gene in fibroblasts derived from a familial dysautonomia patient. Although the mechanism of action of kinetin derivatives remains unclear, our data suggest that the cytoprotective activity of some purine isosteres is mediated by their ability to reduce oxidative stress. Further, the studies of permeation across artificial membrane and model gut and blood-brain barriers indicate that the compounds are orally available and can reach central nervous system. Overall, our data demonstrate that isosteric replacement of the kinetin purine scaffold is a fruitful strategy for improving known biological activities of kinetin and discovering novel therapeutic opportunities.

1. Introduction

Cytokinins, N^6-substituted adenines in chemical terms, are major regulators of plant growth and development but they also have activities in other organisms, including humans.[1] In plants, they occur as free cytokinin bases (the active forms) as well as ribosides and glucosides (transport and storage forms). The first studies of their pharmacological activity in humans focused on the anti-cancer activity of certain

---

cytokinin ribosides. Later research focused on cytokinin bases, for which diverse activities (including neuroprotective, antipsoriatic, and anti-aggregatory activities) have been reported, as reviewed by Kadlecová et al. in 2019.[2] In contrast to some cytokinin ribosides, cytokinin bases show no or limited toxicity toward human cells. The most intensively studied cytokinin base is kinetin (N^6-furfuryladenine), in large degree because it delays the aging of human cells *in vitro*[3] and may naturally occur in humans.[4] An important impetus for kinetin research was the discovery of its ability to correct the aberrant ELP1 and NF1 pre-mRNA splicing responsible for the neurodegenerative disorders familial dys-autonomia and neurofibromatosis type I, respectively.[5,6] Follow-up studies demonstrated that kinetin can increase the abundance of ELP1 wild-type transcripts in transgenic mouse familial dysautonomia models. The first human studies demonstrated that kinetin is orally available.[7] Recently, promising *in vitro* results have been reported for combination of kinetin and phoshatidylserine.[8] Other investigations showed that kinetin has protective activity in models of Parkinson's[9] and Huntington's diseases.[10]

In plants, cytokinin signaling is well characterized, from signal recognition by plasma membrane receptors (e.g., AHK2, AHK3 and AHK4 in the model plant *Arabidopsis thaliana)* to activation of the response genes.[11] In contrast, mechanisms of action of cytokinins, including kinetin, in human cells remain largely unknown. Studies of cytokinin bases often focus on their ability to protect biological mac-romolecules, cells, and tissues against stress by direct antioxidant ac-tivity or induction of antioxidant defenses, as reviewed by Kadlecová et al. in 2019.[2] Recent exciting studies have shown that kinetin riboside-5′-triphosphate, a metabolite of kinetin, acts as a neosubstrate of the mitoprotective kinase PINK1[9] and CK2 kinase, which phosphorylates huntingtin aggregates.[10] Perturbance of these kinases' activities plays major roles in Parkinson's and Huntington's diseases, respectively, so restoring or modulating their activities using kinetin could provide potent novel therapeutic options.

In contrast to cytokinin ribosides, for which several series of de-rivatives have been reported[12–19], studies of pharmacological activities of cytokinin bases have been largely limited to naturally occurring bases. However, a correction of aberrant splicing of ELP1 by 2-chlor-okinetin[20] and some 6,8-disubstituted purines[21] was reported and it was also demonstrated that 9-substituted derivatives of kinetin protect skin cells against UV light.[22] In those studies, effects of substitution of the purine ring or replacement of the furan moiety was explored. Pharma-cological activity of kinetin isosteres is subject of two recent US patents. Whereas 10676475[23] deals with effects on alternative pre-RNA splicing, 10167286[24] deals with PINK1 activation in the context of mitopro-tection and neuroprotection. Previously, kinetin isosteres were studied as plant hormones.[25–27]

Here, we report an evaluation of effects of replacing the purine moiety of kinetin (**1**) and 2-chlorokinetin (**2**) by other fused heterocycles (Table 1) on biological activities in several assays related to neurode-generative diseases.

2. Material and methods

2.1. Synthesis

The test compounds include both commercial compounds, from Olchemim (kinetin − **1**) and Molport (**14**–**23**), and prepared com-pounds. The synthesis of the latter is described in detail below. An exception is 2-chlorokinetin (**2**) that was provided by Dr. Mik (Palacký University) and its analytical data correspond to the previously pub-lished data.[28]

All chemicals and solvents for synthesis were purchased in analytical or HPLC grade quality from available suppliers and used without further purification. For microwave-assisted synthesis steps, reagents were placed in 10 mL closed vessels and subjected to treatment with a Discover SP microwave reactor (CEM Corporation) using dynamic mode

Table 1
Overview of the tested compounds.

No.	C2 Subst.	C6 substituent	Isostere core
1	-H	furfurylamino-	purine
2	-Cl	furfurylamino-	purine
3	-H	furfurylamino-	3*H*-imidazo[4,5-*b*]pyridine, 1-deazapurine
4	-Cl	furfurylamino-	3*H*-imidazo[4,5-*b*]pyridine, 1-deazapurine
5	-H	furfurylamino-	1*H*-imidazo[4,5-*c*]pyridine, 3-deazapurine
6	-Cl	furfurylamino-	1*H*-imidazo[4,5-*c*]pyridine, 3-deazapurine
7	-H	furfurylamino-	7*H*-pyrrolo[2,3-*d*]pyrimidine, 7-deazapurine
8	-Cl	furfurylamino-	7*H*-pyrrolo[2,3-*d*]pyrimidine 7-deazapurine
9	-H	furfurylamino-	5*H*-pyrrolo[3,2-*d*]pyrimidine, 9-deazapurine
10	-Cl	furfurylamino-	5*H*-pyrrolo[3,2-*d*]pyrimidine, 9-deazapurine
11	-H	furfurylamino-	3*H*-[1,2,3]triazolo[4,5-*d*]pyrimidine, 8-azapurine
12	-H	furfurylamino-	pyrazolo[1,5-*a*]pyrimidine
13	-H	furfurylamino-	pyrazolo[4,3-*d*]pyrimidine
14	-H	furfurylamino-	1-methyl-1*H*-pyrazolo[3,4-*d*]pyrimidine
15	-H	5-methylfurfurylamino-	1*H*-pyrazolo[3,4-*d*]pyrimidine
16	-H	(furfuryl)(methyl)amino-	1-methyl-1*H*-pyrazolo[3,4-*d*]pyrimidine
17	-H	(1-(5-methylfuran-2-yl)ethyl)amino-	1-methyl-1*H*-pyrazolo[3,4-*d*]pyrimidine
18	-H	(5-methylfurfuryl)(methyl)amino-	1-methyl-1*H*-pyrazolo[3,4-*d*]pyrimidine
19	-H	furfurylamino-	thieno[2,3-*d*]pyrimidine
20	-H	furfurylamino-	thieno[3,2-*d*]pyrimidine
21	-H	furfurylamino-	furo[2,3-*d*]pyrimidine
22	-H	furfurylamino-	5,6-dimethylfuro[2,3-*d*]pyrimidine
23	-H	furfurylamino-	quinazoline

and the following settings: stirring – high, power – 200 W, ramp time – 2 min, temperature 120 °C, hold time – 10 min cycles, powermax - on. Solid-phase synthesis was carried out in plastic reaction vessels (sy-ringes, each equipped with a porous disk) using a manually operated synthesizer. All reactions were carried out at ambient temperature (25 °C) unless stated otherwise. The volume of wash solvent was 10 mL per 1 g of resin. For washing, resin slurry was shaken with the fresh solvent for at least 1 min before changing the solvent. Resin-bound in-termediates were dried by a stream of nitrogen for prolonged storage and/or quantitative analysis.

For LC/MS analysis a sample of resin (~5 mg) was treated by TFA in DCM, the cleavage cocktail was evaporated by a stream of nitrogen, and cleaved compounds were extracted into 1 mL of MeCN/H2O (1:1). Prior to biological testing all the residual solvents were removed from the samples by careful lyophilization at −110 °C using a ScanVac Coolsafe 110-4 freeze-dryer. Thin layer chromatography (TLC) was performed on Silica gel 60 F254 plates (Merck) and migrating compounds were detected by 254 nm UV light and/or visualized by vanillin staining. Crude products were purified by column chromatography using 40–63 μm Silikagel (VWR). Compounds cleaved from the resin were purified chromatographically using a C18 reverse phase column (YMC Pack ODS-A, 20 × 100 mm, 5 μm particles), and mobile phase consisting of a gradient formed from 10 mM aqueous ammonium acetate and MeCN, with a flow rate of 15 mL/min.

The LC-MS analyses were performed following published protocols[29] and compounds synthesized on solid phase were analysed using a UHPLC-MS system consisting of an Acquity UHPLC chromatograph, coupled to a single quadrupole mass spectrometer (Waters), and equipped with a photodiode array detector and X-Select C18 column

maintained at 30 °C. The mobile liquid chromatography phase consisted of a linear gradient of 20–80% MeCN balanced with 0.01 M ammonium acetate in H_2O, over 2.5 min, followed by a hold at 80% MeCN for 1.5 min and re-equilibration with 20% B for 1 min (flow rate: 600 μL/min). The ESI I source of the MS was operated at discharge current of 5 μA, vaporizer temperature of 350 °C, and capillary temperature of 200 °C.

Melting points of synthesized compounds reported here were determined using a Kofler, Stuart SMP30 or Stuart SMP 40 melting point apparatus and are uncorrected. The elemental analysis of prepared compounds was performed on CHN-O Analyzer EA Flash 1112 Series (Thermo Finnigan). Analyses indicated by the symbols of the elements were within ±0.4% of the theoretical values

NMR spectra were recorded on Bruker Avance (300 or 500 MHz), Jeol ECA-500 MHz, and Jeol ECX500 spectrometers operating at 300 MHz (^{1}H), 75 MHz (^{13}C) or 500 MHz (^{1}H), and 125 MHz (^{13}C), frequencies, respectively. Samples were dissolved in DMSO-d_6 or CDCl3 and the chemical shifts (δ) reported in ppm were calibrated against a residual solvent peak (2.49 ppm for proton - DMSO-d_5, 7.26 ppm for proton – CHCl3) and DMSO-d_6 (39.5 ppm for carbon) or CDCl3 (77.0 ppm for carbon). The NMR spectra are available as Appendix A. Prepared compounds were subjected to HRMS analysis using Agilent 6224 Accurate-Mass TOF LC-MS with dual electrospray/chemical ionization mode with mass accuracy greater than 2 ppm or Dionex Ultimate 3000 chromatograph and Exactive Plus Orbitrap Elite high-resolution mass spectrometer (ThermoFisher, MA, USA) operating in positive full scan mode (120 000 FWMH) in the range of 100–1000 m/z The oven temperature and source voltage for electrospray ionization were set at 150 °C and 3.6 kV, respectively. The acquired data were internally calibrated with phthalate as a contaminant in MeOH (m/z 297.15909). Samples were diluted to a final concentration of 0.1 mg/mL in H_2O and MeOH (50:50, v/v). Before HPLC separation (using a Phenomenex Gemini, 50 × 2.00 mm, 3 μm particles, C18 column), the samples were injected by direct infusion into the LC-MS system using an autosampler. The mobile phase was isocratic MeCN/iPrOH/0.01 M ammonium acetate (40:5:55) with a flow rate of 0.3 mL/min.

2.1.1. Synthesis of 3H-imidazo[4,5-b]pyridine (1-deazapurine) derivatives (I-VII, 3, 4)

2.1.1.1. N-(furan-2-ylmethyl)-3H-imidazo[4,5-b]pyridin-7-amine (3).
Aminomethyl resin (1 g, 0.098 mmol/g) was washed 3× with DCM and 3× with DMF then 10% TEA in DMF (10 mL) was added. After shaking 10 min at rt, the resin was washed 5× with DMF and 4-(4-formyl-3,5-dimethoxyphenoxy)butanoic acid (524 mg), HOBt (229 mg) and DIC (300 mL) in DMF/DCM (1:1, 10 mL) were added. The resin was shaken for 16 h at rt, then washed 3× with DMF, 3× with DCM, 3× with anhydrous THF and 3× with anhydrous DMF. Furfurylamine (442 μL) was dissolved in 10% AcOH/anhydrous DMF (10 mL), the mixture was added to the resin and it was shaken for 16 h at rt. NaBH(OAc)3 (600 mg) was dissolved in 5% AcOH/anhydrous DMF (5 mL), and three equal portions of the solution were added at 1 h intervals to the reaction mixture. After the last addition, the resin was shaken for 16 h at rt, washed 5× with DMF, then shaken with 20% piperidine in DMF (10 mL) for 10 min at rt and washed 5× with DMF and 5× with DCM to obtain the resin **I**. The resin **I** (500 mg) was washed 3× with DMSO and shaken with a solution of 4,6-dichloro-3-nitropyridin-2-amine or 2,4-dichloro-3-nitropyridine (1.54 mmol) and EDIPA (436 μL) in DMSO (5 mL) for 16 h at rt. The resulting resins were washed 3× with DMF and 3× with DCM to obtain the intermediates **II** or **IV**. Resin **IV** was shaken with a solution of 25% aq·NH3 in DMSO for 16 h at 100 °C (in a sealed vial), washed 3× with DMF and 3× with DCM to obtain the resin **V**. Na2S2O4 (1050 mg), K2CO3 (960 mg) and TBAHS (170 mg) were dissolved in DCM/H2O (10 mL, 1:1), added to resins **III** or **V**, the resins were shaken for 16 h at rt, then washed 10× with MeOH/H2O (1:1), 3× with MeOH/DCM (1:1) and 3× with DCM. The resulting resins **VI**(H) or **VI**(Cl) were

washed 5× with DMSO, shaken with triethyl orthoformate/DMSO (5 mL, 1:1) for 16 h at 80 °C and washed 5× with DMSO and 5× with DCM. The resins **VII**(H) or **VII**(Cl) were shaken with TFA/DCM (5 mL, 1:1) for 90 min at rt, then washed 5× with TFA/DCM (1:1). TFA/DCM fractions were collected and evaporated with a stream of nitrogen. The crude products **3** or **4** were dissolved in MeCN (10 mL) and purified with semipreparative HPLC.

White solid, overall yield 20% (calculated from the loading of resin **II**). ^{1}H NMR (500 MHz, DMSO-d_6) δ (ppm): 4.62 (d, $J = 6.1$ Hz, 2H), 6.31 (d, $J = 2.9$ Hz, 1H), 6.37 (dd, $J = 3.2, 1.8$ Hz, 1H), 6.41 (d, $J = 5.6$ Hz, 1H), 7.08 (t, $J = 5.9$ Hz, 1H), 7.50–7.61 (m, 1H), 7.88 (d, $J = 5.6$ Hz, 1H), 8.06 (s, 1H). ^{13}C NMR (125 MHz, DMSO-d_6) δ (ppm): 99.0, 107.1, 110.4, 139.0, 142.1, 144.4, 145.2, 148.5, 152.8. HRMS (ESI-TOF): m/z calcd. for C11H10N4O [M+H]$^+$ 215.0927, found 215.0930.

2.1.1.2. 5-chloro-N-(furan-2-ylmethyl)-3H-imidazo[4,5-b]pyridin-7-amine (4).
White solid, overall yield 25% (calculated from the loading of resin **II**). ^{1}H NMR (500 MHz, DMSO-d_6) δ (ppm): 4.64 (bs, 2H), 6.32 (d, $J = 2.9$ Hz, 1H), 6.39 (dd, $J = 3.2, 1.8$ Hz, 1H), 6.42 (s, 1H), 7.27–7.47 (m, 1H), 7.58 (dd, $J = 1.8, 0.8$ Hz, 1H), 8.09 (s, 1H), 12.71 (bs, 1H). ^{13}C NMR (125 MHz, DMSO-d_6) δ (ppm): 39.1, 97.6, 106.9, 110.2, 139.1, 141.9, 145.5, 146.3, 152.1. HRMS (ESI-TOF): m/z calcd. for C11H9ClN4O [M+H]$^+$ 249.0538, found 249.0540.

2.1.2. Synthesis of 1H-imidazo[4,5-c]pyridine (3-deazapurine) derivatives (VIII-X, 5, 6)

Resin **II** (500 mg) was washed 5× with DMSO and shaken with 2-chloro-3-nitropyridin-4-amine or 2,6-dichloro-3-nitropyridin-4-amine (2.5 mmol) with EDIPA (436 μL) in DMSO (5 mL) for 16 h at rt, then washed 3× with DMSO and 3× with DCM. Na2S2O4 (1050 mg), K2CO3 (960 mg) and TBAHS (170 mg) were dissolved in DCM/H2O (10 mL, 1:1) and added to resins **VIII**(H) or **VIII**(Cl). The resins were shaken 16 h at rt, then washed 10× with MeOH/H2O (1:1), 3× with MeOH/DCM (1:1) and 3× with DCM. The resulting resins **IX**(H) or **IX**(Cl) were washed 5× with DMSO, shaken with triethyl orthoformate/DMSO (5 mL, 1:1) for 16 h at 100 °C and washed 5× with DMSO and 5× with DCM. The resins **X**(H) or **X**(Cl) were shaken with TFA/DCM (5 mL, 1:1) 90 min at rt, then washed 5× with TFA/DCM (1:1). TFA/DCM fractions were collected and evaporated with a stream of nitrogen. The crude products **5** or **6** were dissolved in MeCN (10 mL) and purified with semipreparative HPLC.

2.1.2.1. N-(furan-2-ylmethyl)-1H-imidazo[4,5-c]pyridin-4-amine (5).
White solid, overall yield 21% (calculated from the loading of resin **IV**). ^{1}H NMR (500 MHz, DMSO-d_6) δ (ppm): 4.69 (d, $J = 5.9$ Hz, 2H), 6.30–6.39 (m, 1H), 6.21 (s, 1H), 6.79 (d, $J = 4.9$ Hz, 1H), 6.98 (bs, 1H), 7.51 (s, 1H), 7.70 (d, $J = 5.8$ Hz, 1H), 8.08 (s, 1H), 12.50 (bs, 1H). ^{13}C NMR (125 MHz, DMSO-d_6) δ (ppm): 37.1, 99.2, 106.0, 110.1, 138.9, 139.6, 141.3, 147.6, 153.7. HRMS (ESI-TOF): m/z calcd. for C11H10N4O [M+H]$^+$ 215.0927, found 215.0929.

2.1.2.2. 6-chloro-N-(furan-2-ylmethyl)-1H-imidazo[4,5-c]pyridin-4-amine (6).
White solid, overall yield 28% (calculated from the loading of resin **IV**). ^{1}H NMR (500 MHz, DMSO-d_6) δ (ppm): 4.64 (bs, 2H), 6.25 (d, $J = 2.9$ Hz, 1H), 6.37 (dd, $J = 3.0, 1.9$ Hz, 1H), 6.79 (s, 1H), 7.41 (bs, 1H), 7.55 (d, $J = 0.9$ Hz, 1H), 8.15 (s, 1H). ^{13}C NMR (125 MHz, DMSO-d_6) δ (ppm): 37.1, 96.9, 106.7, 110.4, 124.2, 140.4, 140.7, 140.8, 141.7, 148.9, 153.3. HRMS (ESI-TOF): m/z calcd. for C11H9ClN4O [M+H]$^+$ 249.0538, found 249.0539.

2.1.3. Synthesis of 7H-pyrrolo[2,3-d]pyrimidine (7-deazapurine) derivatives (7, 8)

2.1.3.1. N-(furan-2-ylmethyl)-7H-pyrrolo[2,3-d]pyrimidin-4-amine (7).
A mixture of 4-chloro-7*H*-pyrrolo[2,3-*d*]pyrimidine (100 mg, 0.65

mmol), furfurylamine (90 µL, 0.98 mmol) and TEA (225 µL, 1.62 mmol) in dry MeOH (2.6 mL) was heated in a Discover SP microwave reactor in abovementioned conditions for four cycles. Solvent was evaporated under reduced pressure, the residue was treated with water (10 mL) and product was extracted by EtOAc (4 × 10 mL). Combined organic layers were washed with brine (10 mL), dried (Na2SO4) and concentrated *in vacuo*. Crude material was purified by silica gel column chromatography using CHCl3/MeOH as a mobile phase with a MeOH gradient. Yellow solid; yield 60%; ESI⁺-MS *m/z*: 215.4 [M+H]⁺. ¹H NMR (500 MHz, DMSO-d_6) δ (ppm): 4.68 (d, *J* = 5.8 Hz, 2H), 6.26 (dd, *J* = 3.2, 0.8 Hz, 1H), 6.37 (dd, *J* = 3.1, 1.8 Hz, 1H), 6.57 (dd, *J* = 3.4, 1.8 Hz, 1H), 7.06 (dd, *J* = 3.2, 2.3 Hz, 1H), 7.55 (dd, *J* = 1.7, 0.8 Hz, 1H), 7.84 (t, *J* = 5.7 Hz, 1H), 8.11 (s, 1H), 11.51 (bs, 1H). ¹³C NMR (125 MHz, DMSO-d_6) δ (ppm): 36.5, 98.6, 102.6, 106.8, 110.4, 121.0, 141.9, 150.2, 151.2, 153.1, 155.6. HRMS (ESI-TOF): *m/z* calcd. for C11H10N4O [M+H]⁺ 215.0927, found 215.0926.

2.1.3.2. 2-chloro-N-(furan-2-ylmethyl)-7H-pyrrolo[2,3-d]pyrimidin-4-amine (8). A mixture of 2,4-dichloro-7*H*-pyrrolo[2,3-*d*]pyrimidine (100 mg, 0.53 mmol), furfurylamine (74 µL, 0.8 mmol) and TEA (185 µL, 1.33 mmol) was refluxed in *n*PrOH (2.13 mL) for 4 h. After cooling at 4 °C for 2 h the resulting solid material was filtered, washed with cold *n*PrOH (3 × 1 mL), cold H2O (5 × 1 mL) and dried. Crude material was purified by silica gel column chromatography using CHCl3/MeOH as a mobile phase with a MeOH gradient. Yellow solid; yield 62%; ESI⁺-MS *m/z* (rel %): 249.4 [³⁵Cl-M+H]⁺ (1 0 0), 251.4 [³⁷Cl-M + H]⁺ (35). ¹H NMR (500 MHz, DMSO-d_6) δ (ppm): 4.63 (d, *J* = 5.5 Hz, 2H), 6.30 (dd, *J* = 3.2, 0.8 Hz, 1H), 6.40 (dd, *J* = 3.4, 1.8 Hz, 1H), 6.58 (dd, *J* = 3.4, 1.8 Hz, 1H), 7.08 (dd, *J* = 3.5, 2.3 Hz, 1H), 7.59 (dd, *J* = 1.8, 0.9 Hz, 1H), 8.32 (t, *J* = 5.7 Hz, 1H), 11.70 (bs, 1H). ¹³C NMR (125 MHz, DMSO-d_6) δ (ppm): 36.6, 99.1, 101.2, 107.3, 110.5, 121.6, 142.1, 150.8, 152.2, 152.3, 156.4. HRMS (ESI-TOF): *m/z* calcd. for C11H9ClN4O [M+H]⁺ 249.0538, found 249.0537.

2.1.4. Synthesis of 5H-pyrrolo[3,2-d]pyrimidine (9-deazapurine) derivatives (9, 10)

2.1.4.1. N-(furan-2-ylmethyl)-5H-pyrrolo[3,2-d]pyrimidin-4-amine (9). Compound **9** was prepared similarly to the 7-deazapurine analogue (see Section 2.1.3.1), except that five reaction cycles were needed. Yellow solid; yield 25%; ESI⁺-MS *m/z*: 216.4 [M+H]⁺. ¹H NMR (500 MHz, DMSO-d_6) δ (ppm): 4.71 (d, *J* = 5.5 Hz, 2H), 6.36 (d, *J* = 3.1 Hz, 2H), 6.41 (dd, *J* = 3.4, 1.8 Hz, 1H), 7.50 (d, *J* = 2.8 Hz, 2H), 7.61 (dd, *J* = 1.8, 0.9 Hz, 1H), 8.20 (s, 1H), 10.97 (bs, 1H). ¹³C NMR (125 MHz, DMSO-d_6) δ (ppm): 36.5, 101.2, 107.4, 110.6, 113.7, 127.9, 142.4, 146.1, 148.9, 149.8, 152.4. HRMS (ESI-TOF): *m/z* calcd. for C11H10N4O [M+H]⁺ 215.0927, found 215.0926

2.1.4.2. 2-chloro-N-(furan-2-ylmethyl)-5H-pyrrolo[3,2-d]pyrimidin-4-amine (10). Compound **10** was prepared similarly to the 7-deazapurine analogue (see Section 2.1.3.2). Pale yellow solid; yield 57%; ESI⁺-MS *m/z* (rel. %): 249.1 4 [³⁵Cl-M + H]⁺ (1 0 0), 251.0 [³⁷Cl-M + H]⁺ (31). ¹H NMR (500 MHz, DMSO-d_6) δ (ppm): 4.66 (d, *J* = 4.6 Hz, 2H), 6.32 (d, *J* = 3.1 Hz, 1H), 6.39 (dd, *J* = 3.2, 0.8 Hz, 1H), 6.43 (dd, *J* = 3.1, 1.8 Hz, 1H), 7.53 (d, *J* = 3.1 Hz, 1H), 7.63 (dd, *J* = 1.8, 0.9 Hz, 1H), 7.85 (bs, 1H), 11.03 (bs, 1H). ¹³C NMR (125 MHz, DMSO-d_6) δ (ppm): 36.6, 101.2, 107.8, 110.6, 112.4, 129.3, 142.6, 148.3, 149.9, 150.8, 151.6. HRMS (ESI-TOF): *m/z* calcd. for C11H9ClN4O [M+H]⁺ 249.0538, found 249.0537.

2.1.5. Synthesis of N-(furan-2-ylmethyl)-3H-[1,2,3]triazolo[4,5-d] pyrimidin-7-amine (XI-XV, 11)

2.1.5.1. Benzyl azide (XI). Benzyl bromide (17.84 mL, 0.15 mol) was added to a solution of NaN3 (11 g, 0.17 mol) in DMSO (300 mL) and the mixture was stirred in the dark at room temperature for 9 h. The reaction was quenched by adding ice cold water and the product was extracted by Et2O. Combined organic layers were carefully concentrated under reduced pressure to give an oily liquid that was used further without purification. Oily liquid; yield 79%. ¹H NMR (300 MHz, CDCl3) δ (ppm): 7.24–7.48 (m, 5H), 4.35 (s, 2H). ¹³C NMR (125 MHz, CDCl3) δ (ppm): 54.9, 128.4 (2 × C), 128.5, 129.0 (2 × C), 135.5.

2.1.5.2. 5-amino-1-benzyl-1H-1,2,3-triazole-4-carboxamide (XII). 2-Cyanoacetamide (11.83 g, 0.14 mol) was added to a solution of sodium ethoxide (Na − 3.23 g, 0.14 mol, EtOH – 190 mL) to give a white suspension. Benzyl azide (**XI**) (18.2 g, 0.13 mol) was added and the reaction mixture was heated at 90 °C overnight. The resulting solid was filtered, washed with EtOH, then water and dried. A second portion of product was obtained after concentration of the reaction mixture under reduced pressure and treatment with water. Off-white solid, yield 69%, m.p. 236–237 °C, ESI⁺-MS *m/z*: 217.8 [M+H]⁺ (1 0 0). ¹H NMR (500 MHz, DMSO-d_6) δ (ppm): 5.38 (s, 2H), 7.17. (d, *J* = 7.3 Hz, 2H), 7.26 (t, *J* = 7.3 Hz, 1H), 7.32 (t, *J* = 7.4 Hz, 2H). ¹³C NMR (125 MHz, DMSO-d_6) δ (ppm) 48.8, 122.2, 127.9 (2 × C), 128.2, 129.1 (2 × C), 136.5, 145.4, 164.8.

2.1.5.3. 3-Benzyl-3,6-dihydro-7H-[1,2,3]triazolo[4,5-d]pyrimidin-7-one (XIII). Ethyl formate (2.22 mL, 27.6 mmol) was added to a mixture of **XII** (2 g, 9.21 mmol) in sodium ethoxide solution (Na – 1.06 g, 46 mmol, EtOH – 50 mL). The mixture was heated in a pressure tube at 95 °C for 24 h. After cooling the pH of the reaction mixture was adjusted to 6, resulting in formation of solid material. The product was filtered off and recrystallized from ethanol. White solid; yield 84%; m.p. 194–195 °C. ESI⁺-MS *m/z*: 228.8 [M+H]⁺. ¹H NMR (500 MHz, DMSO-d_6) δ (ppm): 5.70 (s, 2H), 7.24–7.31 (m, 5H), 8.22 (s, 1H), 12.70 (s, 1H). ¹³C NMR (125 MHz, DMSO-d_6) δ (ppm): 50.3, 128.4 (2 × C), 128.7, 129.3 (2 × C), 130.2, 135.9, 149.1, 150.5, 155.9.

2.1.5.4. 3-Benzyl-7-chloro-3H-[1,2,3]triazolo[4,5-d]pyrimidine (XIV). A mixture of SOCl2 (10.13 mL, 139.6 mmol) and DMF (1.82 mL) was added to a solution of **XIII** (2.54 g, 11.17 mmol) in CHCl3 (100 mL). The reaction mixture was refluxed for 2 h then evaporated *in vacuo*. The residue was mixed with ice-cold water (30 mL) and the resulting mixture was extracted by Et2O (100 mL). After evaporation of Et2O, crude product was purified by silica column chromatography using petroleum ether/ethyl acetate (9:2, v/v) as a mobile phase. Off-white solid; yield 50%; m.p. 223–239 °C. ESI⁺-MS *m/z* (rel. %): 246.0 [M+H]⁺ (1 0 0). ¹H NMR (500 MHz, CDCl3) δ (ppm): 5.87 (s, 2H), 7.29–7.35 (m, 3H), 7.45 (dd, *J* = 7.9, 1.5 Hz, 2H), 8.91 (s, 1H). ¹³C NMR (125 MHz, CDCl3) δ (ppm): 51.5, 128.6 (2 × C), 129.0, 129.2 (2 × C), 133.9, 134.2, 149.8, 154.3, 155.7.

2.1.5.5. 3-Benzyl-N-(furan-2-ylmethyl)-3H-[1,2,3]triazolo[4,5-d]pyrimidin-7-amine (XV). A mixture of **XIV** (0.2 g, 0.81 mmol), furfurylamine (68 µL, 0.77 mmol) and EDIPA (0.7 mL, 40.7 mmol) in *i*PrOH (8 mL) was heated at 100 °C for 4.5 h. After cooling the product started to precipitate. The solid was filtered, washed with *i*PrOH (10 mL), then water (10 mL) and dried. Pale yellow solid; yield 84%; m.p. 169–170 °C. ESI⁺-MS *m/z* (rel. %): 306.8 [M+H]⁺ (1 0 0). ¹H NMR (500 MHz, CDCl3) δ (ppm): 4.88 (d, *J* = 5.8 Hz, 2H), 5.75 (s, 2H), 6.32 (s, 2H), 6.80 (s, 1H), 7.27–7.41 (m, 6H), 8.53 (s, 1H). ¹³C NMR (125 MHz, CDCl3) δ (ppm): 37.6, 50.6, 108.2, 110.6, 124.9, 128.4 (2 × C), 128.6, 129.0 (2 × C), 134.9, 142.7, 148.7, 150.6, 154.4, 157.1.

2.1.5.6. N-(furan-2-ylmethyl)-3H-[1,2,3]triazolo[4,5-d]pyrimidin-7-amine (11). Sodium (37 mg, 1.63 mmol) was added at −78 °C to liquid ammonia (25 mL) and stirred until complete dissolution. **XVII** (0.1 g, 0.33 mmol) was added and the reaction mixture was stirred at −78 °C for 1 h. After evaporation, the residue was treated with water and the pH

of the mixture adjusted to 5–6, resulting in precipitation of product. The solid was filtered off, washed with water and dried. Off-white solid; yield 62%; m.p. 244–245 °C. ESI$^+$-MS *m/z* (rel. %): 217.1 [M+H]$^+$ (1 0 0). ^{1}H NMR (500 MHz, DMSO-d_6) δ (ppm): 4.74 (d, $J = 5.8$ Hz, 2H), 6.29 (d, $J = 3.0$ Hz, 1H), 6.37 (d, $J = 1.8$ Hz, 1H), 7.56 (s, 1H), 8.38 (s, 1H), 9.28 (s, 1H). ^{13}C NMR (125 MHz, DMSO-d_6) δ (ppm): 37.0, 107.7, 111.0, 123.9, 142.6, 143.0, 152.4, 154.4, 156.7. HRMS (ESI-TOF): *m/z* calcd. for C9H8N6O [M+H]$^+$ 217.0838, found 249.0845.

2.1.6. Synthesis of N-(furan-2-ylmethyl)pyrazolo[1,5-a]pyrimidin-7-amine (12)

Furfurylamine (180 μL, 1.95 mmol) and K2CO3 (360 mg, 2.60 mmol) were added to a solution of 7-chloropyrazolo[1,5-*a*]pyrimidine (200 mg, 1.30 mmol) in anhydrous acetonitrile (8 mL) and DMF (2 mL) and the reaction mixture was stirred at 90 °C for 3 h. The solvents were evaporated under reduced pressure, the residue was mixed with H2O (30 mL), and the mixture was extracted with EtOAc (2 × 50 mL). Combined organic extracts were washed with brine (50 mL), dried over MgSO4 and concentrated under reduced pressure. The residue was purified by silica gel flash column chromatography using DCM/EtOAc (3:2) as a mobile phase. White solid; yield 34%; m.p. 120–122 °C. ^{1}H NMR (500 MHz, CDCl3) δ (ppm): 4.59 (d, $J = 5.8$ Hz, 2H), 6.06 (d, $J = 5.2$ Hz, 1H), 6.32–6.38 (m, 2H), 6.53 (d, $J = 2.3$ Hz, 1H), 6.84 (s, 1H), 7.35–7.45 (m, 1H), 8.00 (d, $J = 2.3$ Hz, 1H), 8.25 (d, $J = 5.2$ Hz, 1H). ^{13}C NMR (125 MHz, CDCl3) δ (ppm): 39.4, 85.3, 95.9, 108.6, 110.7, 143.0, 143.9, 146.9, 149.6, 149.7. HRMS (APCI): *m/z* calc. for C11H11N4O [M+H]$^+$ 215.0927, found 215.0925.

2.1.7. Synthesis of 1H-pyrazolo[4,3-d]pyrimidine derivative (XVI, XVII, 13)

2.1.7.1. 1H-pyrazolo[4,3-d]pyrimidine-7-thiol (XVI).
1*H*-pyrazolo[4,3-*d*]pyrimidine-7-thiol was prepared from 1*H*-pyrazolo[4,3-*d*]pyrimidin-7-ol according to the published procedure.[30]

2.1.7.2. 7-(methylthio)-1H-pyrazolo[4,3-d]pyrimidine (XVII).
A solution of MeI (144 mg, 1 mmol) in DMF (2.8 mL) was added dropwise at 0 °C to a mixture of **XVI** (153 mg, 1 mmol) and K2CO3 (152 mg, 1.1 mmol) in DMF (7.5 mL). The reaction mixture was allowed to warm to rt then stirred for an additional 10 min. After evaporation *in vacuo* the residue was partitioned between H2O and DCM. The product was finally obtained by crystallization from DCM. White solid; yield 84%; m.p. 195–200 °C; UV (nm): max. 308, sh 319. ESI$^-$-MS (*m/z*): 165.1 [M−H]$^-$.

2.1.7.3. N-(furan-2-ylmethyl)-1H-pyrazolo[4,3-d]pyrimidin-7-amine (13).
A mixture of **XVII** (93 mg, 0.56 mmol) in furfurylamine (3 mL) was heated at 125 °C for 8 h. After evaporation under reduced pressure the crude material was purified by silica gel column chromatography using stepwise increments of MeOH (3, 4, and 5%) in CHCl3. Product was finally obtained by crystallization from CHCl3. White solid; yield 66%, m.p. 182–185 °C; UV λ (nm): min. 253, max. 292, sh 305. ESI$^+$-MS (*m/z*): 216.1 [M+H]$^+$, ESI$^-$-MS (*m/z*): 214.1 [M+H]$^+$. ^{1}H NMR (500 MHz, DMSO-d_6) δ (ppm): 4.75 (bs, 2H), 6.38 (s, 1H), 6.41 (s, 1H), 7.61 (s, 1H), 7.93 (bs, 1H), 8.12 (s, 1H), 8.26 (s, 1H), 12.72 (bs, 1H). ^{13}C NMR (125 MHz, DMSO-d_6) δ (ppm): 36.4, 107.6, 110.5, 121.0, 133.1, 141.4, 142.4, 148.7, 151.7. Anal. (C10H9N5O) C,H,N.

2.2. Fibroblast cell culture

Skin fibroblasts GM04078 homozygous for the GAA expansion in the frataxin gene and skin fibroblast GM04663, which are homozygous for the 2507 + 6 T > C mutation in the ELP1 gene, were obtained from the Coriell repository. The cells were maintained in Dulbecco's modified Eagle's medium (DMEM) containing 5 g/L glucose, 2 mM L-glutamine, 100 U/mL penicillin, 100 μg/mL streptomycin and 10% fetal bovine serum (FBS) (Sigma) in standard culture conditions (5.5% CO2, 37 °C, 100% relative humidity). The cells were subcultured twice a week.

2.3. Fibroblast culture stress assays

GM04078 fibroblasts were trypsinized, diluted in DMEM medium with 10% FBS and seeded into 384-well plates (1500 cells in 30 μL medium/well). After 24 h incubation, the cells were pre-treated by the test compounds dissolved in DMSO using an Echo 555 system (Labcyte). DMSO vehicle served as a negative control. Stressors were added in 15 μL of the medium used for seeding after 8 h. After another 48 h, 15 μL of a 4-fold concentrated solution of resazurin (Sigma) in the culture medium was added to the cells to a final concentration of 0.0125 mg/mL. Fluorescence was measured after 3 h incubation using an M2 reader (Biotek) with excitation and emission wavelengths of 570 and 610 nm, respectively.

2.4. Reduced glutathione measurements

GM04078 fibroblasts were trypsinized, diluted in DMEM medium with 10% FBS and seeded into 384-well plates (1500 cells in 30 μL medium/well). After 24 h incubation, the cells were pre-treated by adding compound **6** dissolved in DMSO (final concentration 10 and 50 μM) using the Echo 555 system. DMSO vehicle served as a negative control. BSO was added (to serial concentrations of 10, 100 and 1000 μM) in 15 μL portions of medium after 8 h. The effect was evaluated after 24 h, when the medium was removed and, after a washing with 100 μL DMEM medium, replaced by DMEM medium containing 40 μM mono-bromobimane. After 40 min incubation, images were recorded, at 4× magnification using the blue channel of a Cell Voyager confocal imaging system. The intensity of the signal was evaluated by an image analysis tool in the Cell Profiler program. Control measurement using spectro-photometer (ex 395 nm, em 490 nm) was also performed.

2.5. Frataxin assay

To test the ability of compounds to replace frataxin (FXN) functionally, enzymatic assays were performed using mouse ISC machinery reconstituted *in vitro* with purified proteins [31]. The assays were performed under anaerobic conditions in Tris buffer (50 mM Tris, 150 mM NaCl, pH 8) containing 50 μM of apo-ISCU loaded with one equivalent of Fe^{2+}, 5 μM of the NFS1-ISD11-ACP complex, 5 μM of FDX2, 2 μM of FDXR and 100 μM of NADPH. Positive controls were prepared by adding 5 μM of FXN to the reaction mixture. Test compounds diluted in DMSO were added to the reaction mixture at concentrations of 30, 50, 100, 200 and 500 μM and supplementary DMSO was added to the reaction mixtures to keep its concentration the same in each reaction. Reference reaction mixtures were prepared with the same concentration of DMSO as the mixtures with test compounds. The reactions were initiated by adding 50 μM of L-cysteine and the formation of Fe-S clusters was monitored by UV–visible spectroscopy at 456 nm and 30 °C. Rates of the reactions were determined by linear regression of the slopes of the resulting curves in their linear domain between 2 and 10 min, using GraphPad Prism. The compounds' activities were calculated by dividing slopes of their reaction curves by those of the corresponding reference reactions, which yielded activation factors. Activation factors higher and lower than 1 indicate active and inactive compounds, respectively.

2.6. SH-SY5Y cultivation and differentiation

The SH-SY5Y human neuroblastoma cell line obtained from ATCC (American Type Culture Collection, Manassas, VA, USA) was cultivated in DMEM medium and Ham's F12 Nutrient Mixture (DMEM:F-12, 1:1), supplemented with 10% FBS and 1% of both penicillin and streptomycin at 37 °C in a humidified atmosphere of 5% CO2. Only the cells passaged less than 20 times were used in the experiments. The cells were seeded in

96-multiwell plates, in 100 µL total volume of medium per well. Next day, 10 µM of ATRA in DMEM/F12 medium with 1% FBS was added to each well to a final concentration 10 µM to induce neuronal differentiation. The cells were used for experiments 48 h later. The same protocol was used for the SH-SY5Y obtained from ECACC (European Collection of Authenticated Cell Culture).

2.7. Evaluation of compounds' cytoprotective activity toward differentiated SH-SY5Y cells

Portions of culture containing 20,000 SH-SY5Y cells were seeded into 96-well plates and differentiated by ATRA as outlined above. The differentiation medium was removed and replaced by fresh DMEM/F12 medium with 1% FBS containing test compounds at 0.1, 1 or 10 µM concentration. DMSO vehicle was used as a negative control. The differentiated cells were immediately exposed to glutamate (160 mM), and the frequency of dead cells was assessed using propidium iodide (PI) as a probe after another 24 h, following the published protocol[32] with modification. Briefly, PI (Sigma Aldrich) was diluted to 1 mg/mL in DMSO. This solution was further diluted in PBS then added to the cells' medium to a final concentration of 1 µg/mL, then the cells were incubated at rt for 15 min. Proportions of PI-stained cells were quantified using an Infinite M200 Pro reader (Tecan) with 535 excitation and emission wavelengths of 535 and 617 nm, respectively.

2.8. Measurement of caspase 3/7 activity

To assess the effects of test compounds on glutamate-induced apoptosis, SH-SY5Y cells were subjected to the differentiation and treatment steps described in the previous section, and then to the one-step caspase 3/7 assay described by Carrasco et al. in 2003[33] with modification of the caspase-3,7 substrate concentration, which was decreased to 75 µM. Caspase-3,7 activity was quantified using an Infinite M200 Pro (Tecan, Austria) microplate reader with excitation and emission wavelengths of 346 and 438 nm, respectively after 3-hour incubation. The average signal of the samples treated with glutamate corresponds to 100% caspase 3/7 activity.

2.9. Measurement of oxidative stress

To assess the effects of test compounds on glutamate-induced oxidative stress, SH-SY5Y cells were subjected to the differentiation and treatment steps described in the Section 3.5, and then the dihydroethidium assay described by Kim et al. in 2017[34] with the following modifications. After 4 h of exposure to glutamate, cells were centrifuged at 500 g for 330 s with subsequent replacement of media by PBS containing 10 µM dihydroethidium (DHE). Finally, plates with cells were kept at rt for 30 min, then superoxide radical formation (DHE) signal was quantified using an Infinite M200 Pro reader (Tecan) with excitation and emission wavelengths of 500 and 580 nm, respectively.

2.10. Evaluation of compounds' effects on alternative splicing of ELP1 transcripts

GM04663 cells in DMEM medium with 10% FBS were seeded in 10 cm Petri dishes (about 500,000 cells per dish) and grown overnight before treatment with the test compounds at 50 µM concentration to test their effects on alternative splicing of ELP1 transcripts. Kinetin (compound 1) and 2-chlorokinetin (compound 2) were used as positive controls. DMSO vehicle served as a negative control. After 24 h, total RNA was extracted from the cells using Trizol reagent. Isolated RNA was transcribed into cDNA using a High Capacity cDNA Reverse Transcription Kit (Applied Biosystems). The ELP1 cDNA segment between nucleotides 2194 and 2593 (numbering corresponding to the NM_003640.5 transcript) was amplified by the polymerase chain reaction using 5′-CAGGTGTCGCTTTTTCATCA-3′ and 5′-

CATTTCCAAGAAACACCTTAGGG-3′ primers[35] and JumpStart *Taq* DNA Polymerase with MgCl2 (Sigma-Aldrich). The temperature program involved: initial denaturation at 94 °C for 5 min followed by 34 cycles of denaturation at 94 °C for 40 s, annealing at 63.8 °C for 30 s and elongation at 72 °C for 90 s, with a final elongation step at 72 °C for 5 min. The PCR products corresponding to wild-type ELP1 transcript (422 bp) and transcript lacking exon 20 (348 bp) were separated by electrophoresis in 1.5% agarose gel and visualized by GelRed staining. For final comparison of the compounds identified as active during the initial screening, microfluidic electrophoresis (with an Agilent 2100 Bioanalyzer and 1000 LabChip kit) was used. A comparison with DNA standards of known size and concentration allowed precise quantification of the wild-type and aberrant transcripts' concentrations. The area under the peak calculations were carried out in the 2100 Expert Software.

2.11. Western blotting and immunodetection of frataxin

For this purpose, GM4078 cells in DMEM medium with 10% FBS were seeded in 10 cm Petri dishes (about 1.4 million cells per dish) and 24 h later treated with 10 and 50 µM of compound 6. The cells were harvested after 48 h. Medium was removed and the cell monolayer was washed twice with ice-cold PBS. The cells were scraped into 2 mL ice-cold PBS and centrifuged. The supernatant was removed and each pellet was flash-frozen by dipping the tube into liquid nitrogen. The samples were stored at −80 °C.

Total protein was extracted by direct cell lysis in Laemmli buffer (50 mM Tris-HCl, pH 6.8, 2% SDS, 10% glycerol, 0.04% bromophenol blue, and 250 mM mercaptoethanol). The protein concentrations in the samples were determined by Bradford's method and standardized. The samples were boiled for 10 min and stored at −20 °C.

The protein lysates (25–40 µg) were separated by SDS-PAGE (12.5% gel). Proteins were transferred to polyvinylidene difluoride membrane (Bio-Rad) pre-treated by incubation in a 5% solution of bovine serum albumin (BSA) with 1x PBS-Tween (PBS-T) for 2 h. The membrane was then incubated with anti-frataxin mouse antibody (18A5DB1 Abcam) in BSA for 2 h in PBS-T, followed by three washes with PBS-T. For loading standardization, a portion of the membrane was incubated with anti-actin antibody. The membrane was then incubated with a secondary (horseradish peroxidase-conjugated anti-mouse) antibody for 60 min followed by three washes with PBS-T. The immunoblots were then developed using Amersham ECL reagents.

2.12. In vitro permeability assays

Parallel artificial membrane permeability, chemical stability, stability in human plasma, microsomal stability and protein plasma binding assays were performed using methods described by Borková et al. In 2019.[36]

2.12.1. Quantification of test compounds in the permeability assays

Preparation of lyophilized samples for this analysis is described in the sections dedicated to the *in vitro* ADME assays. Test compounds in the samples were quantified using a RapidFire RF300 system (Agilent Technologies) interfaced with a QTRAP 5500 mass spectrometer fitted with an electrospray ionization source (AB Sciex, Concord, Canada) running in multiple-reaction monitoring mode.

Lyophilized samples were dissolved in the mobile phase (95% water, 5% acetonitrile, 0.1% formic acid) with respective internal standards. The dissolved samples were aspired directly from 96-well plates into a 10 µL sample loop and passed through a C4 cartridge (Agilent Technologies) with solvent A (95% water, 0.01% formic acid, 5% acetonitrile) at a flow rate of 1.5 mL/minute for 3 s. After the desalting step, the analyte retained on the cartridge was eluted with solvent B (95% acetonitrile, 5% 0.01% formic acid) into the mass spectrometer at a flow rate of 0.4 mL/minute for 7 s, where it was subjected to electrospray

ionization in the positive ion mode and daughter ion was identified.

2.12.2. Studies of transport across Caco-2 and MDCK-MDR1 cell monolayers

To generate cell monolayers for transport studies,[37,38] the cells were trypsinized and seeded on tissue culture polyester membrane filters with pore size 1 μm in 96-well Transwell® plates (Corning, NY, USA). Culture medium was added to both the donor and the acceptor compartments and the cells were allowed to differentiate and form monolayers. The culture medium was changed every other day.

MDR1-MCDK differentiated monolayers were used only if they were intact, as confirmed by the Lucifer Yellow Rejection Assay. Before each experiment, the cells were washed twice with Hank's balanced buffer solution (HBBS) (Gibco, Waltham, USA) and pre-equilibrated with HBSS buffered at pH 7.4 for 1 h. After removing the medium, MDCK-MDR1 cells were treated with test compounds at 10 μM in HBSS (pH 7.4) for 1 h, then samples were removed from both donor and acceptor compartments and lyophilized. All experiments were done in duplicates.

Apparent permeability coefficients were calculated as Papp = (dQ/dt)/(C0 × A), where dQ/dt is the rate of permeation of the test compound across the cell monolayer, C0 is the donor compartment concentration at time t = 0 and A is the area of the cell monolayer. The efflux ratio R was defined as the ratio PBA/PAB where PBA and /PAB are the apparent permeability coefficients of the test compound from the basal to apical and apical to basal sides of the cell monolayer, respectively. Compounds with an efflux ratio of ≥ 2 were considered potential P-gp substrates.

2.13. Data analysis

Statistical significance of the compound effect was evaluated by non-parametric Kruskal-Wallis test followed by post-hoc Man-Whitney test and sequential Bonferroni correction using the GrahpPad and PAST (ver. 1.97)[39] software packages. Differences with the corrected p-values < 0.05 were considered statistically significant. The error bars in graphs are standard errors, unless stated otherwise. Standard errors for drug efflux ratios were calculated by the Delta method described in[40] implemented in R.

3. Results and discussion

A series of kinetin (**1**) and 2-chlorokinetin (**2**) purine bioisosteres were prepared (Figs. 1, 2) and screened for their biological activity. Although the majority of the compounds is known in either peer reviewed literature or patents, synthesis and characterization was reported only for compounds **3, 5, 7** and **11**. Moreover, with exception of compound **7**, we used different synthetic routes as described below. We also evaluated biological effects of commercially available derivatives. Those included 1*H*-pyrazolo[3,4-*d*]pyrimidine analogues methylated on the *N*1 nitrogen atom and/or furfurylamino moiety (**14**–**18**) as well as thieno[2,3-*d*]pyrimidine (**19**), thieno[3,2-*d*]pyrimidine (**20**), furo[2,3-*d*]pyrimidine (**21, 22**), and quinazoline (**23**) (Fig. 3).
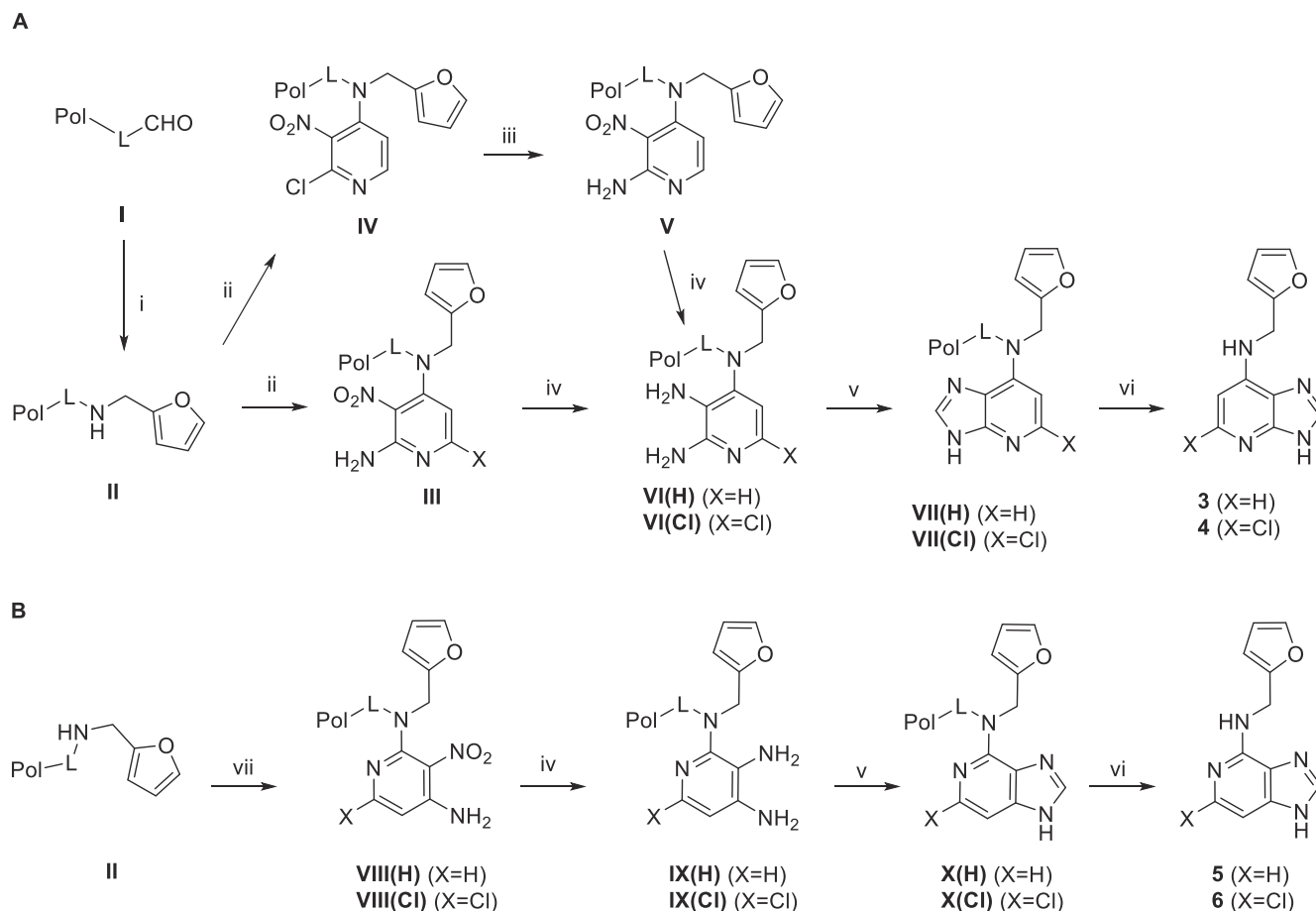
Fig. 1. Synthesis of 2-H and 2-Cl imidazo[4,5-*b*]pyridines (1-deazapurine, scheme A) and imidazo[4,5-*c*]pyridines (3-deazapurine, scheme B) kinetin isosteres. Reagents and conditions: (i) (a) furfurylamine, 10% AcOH in anh. DMF, 16 h, rt; (b) NaBH(OAc)₃, 5% AcOH in anh. DMF, 16 h, rt; (ii) 4,6-dichloro-3-nitropyridin-2-amine or 2,4-dichloro-3-nitropyridine, EDIPA, DMSO, 16 h, rt; (iii) DMSO, 25% aq.NH₃, 16 h, 100 °C; (iv) Na₂S₂O₄, K₂CO₃, TBAHS, DCM/H₂O, 16 h, rt; (v) triethyl orthoformate/DMSO (1:1), 16 h, 80 °C; (vi) TFA/DCM (1:1), 90 min, rt; (vii) 2-chloro-3-nitropyridin-4-amine or 2,6-dichloro-3-nitropyridin-4-amine, EDIPA, DMSO, 16 h, rt.
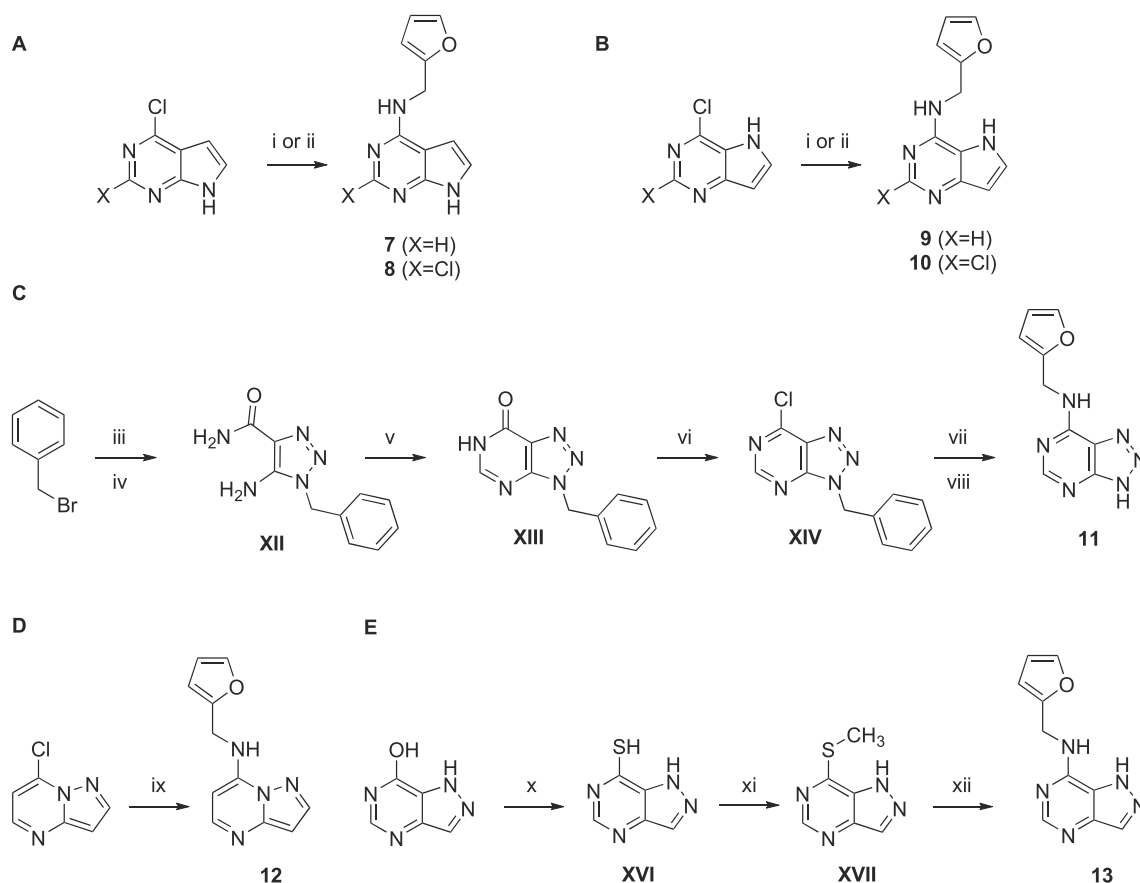
Fig 2. Synthesis of 2-H and 2-Cl pyrrolo[2,3-*d*]pyrimidines (7-dezapurines, scheme A), pyrrolo[3,2-*d*]pyrimidines (9-deazapurines, scheme B), triazolo[4,5-*d*]py-rimidine (8-azapurine, scheme C), pyrazolo[1,5-*a*]pyrimidine (scheme D), and pyrazolo[4,3-*d*]pyrimidine (scheme E) kinetin isosteres. Reagents and conditions: (i) furfurylamine, TEA, 120–170 °C, MW irradiation, 40–50 min; (ii) furfurylamine, TEA, *n*PrOH, reflux, 4 h; (iii) NaN$_3$, DMSO, rt (XI); (iv) 2-cyanoacetamide, EtONa, EtOH, 90 °C; (v) ethyl formate, EtONa, EtOH, 95 °C; (vi) SOCl$_2$, DMF/CHCl$_3$, reflux; (vii) furfurylamine, EDIPA, iPrOH, 100 °C, 4.5 h (XV); (viii) Na, NH$_3$, −78 °C, 1 h; (ix) furfurylamine, K$_2$CO$_3$, MeCN/DMF, 90 °C, 3 h; (x) P$_2$S$_5$, Py, reflux 3 h; (xi) MeI, K$_2$CO$_3$, DMF, 0 °C to rt, 10 min; (xii) furfurylamine, 125 °C, 8 h.
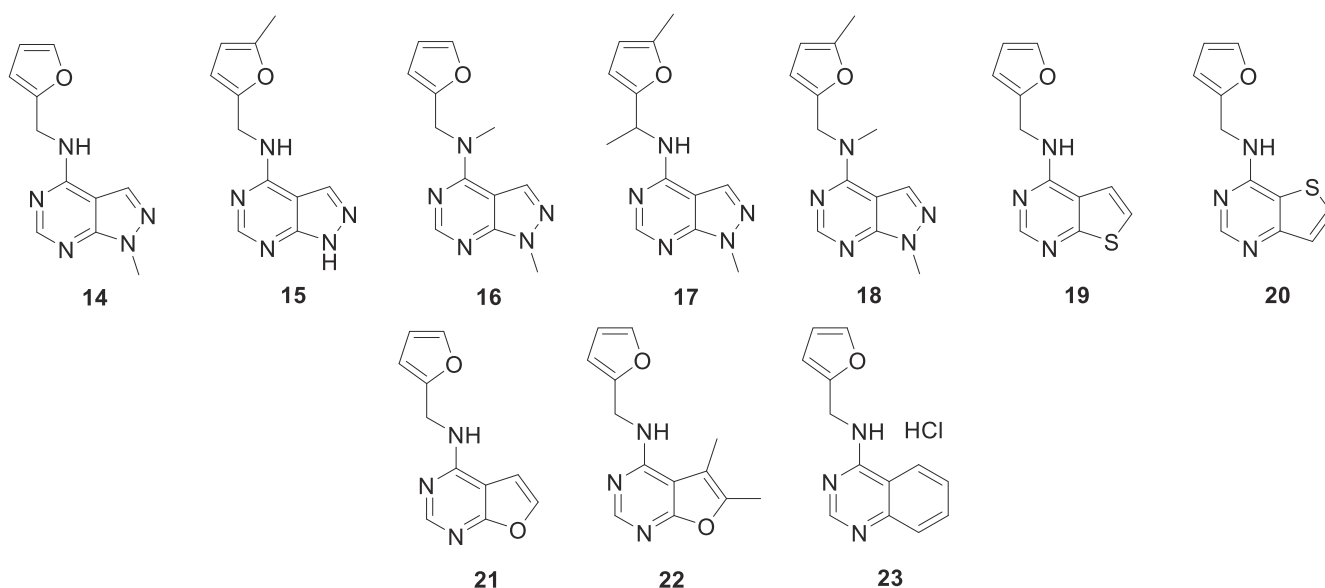
Fig. 3. Structures of commercially available kinetin isosteres.

3.1. Chemistry

Imidazo[4,5-*b*]pyridines (**3**, **4**) and imidazo[4,5-*c*]pyridines (**5**, **6**) were synthesized similarly to previously reported procedures[41,42] using

solid-phase synthesis (Fig. 1). Aminomethyl resin with acid-labile benzaldehyde linker **I** was reductively aminated with furfurylamine to give the resin **II**. To synthesize the chlorinated imidazo[4,5-*b*]pyridine **VII(Cl)**, the resin **II** was arylated with 4,6-dichloro-3-nitropyridin-2-

amine and intermediate **III** was obtained. After reduction with sodium dithionite, the resulting resin-bound intermediate **VI(Cl)** was cyclized with triethyl orthoformate, which afforded the polymer-supported imidazo[4,5-*b*]pyridine **VII(Cl)**. Final cleavage using trifluoroacetic acid yielded the desired product **4** (Fig. 1A).

The corresponding unsubstituted imidazo[4,5-*b*]pyridine **3** was prepared analogically using 2,4-dichloro-3-nitropyridine in the arylation step. The resin **IV** was subjected to amination with a mixture of aqueous ammonia and dimethylsulfoxide (DMSO) to obtain the resin **V** followed by the reduction and cyclization of the resin-bound intermediate **VI(H)** with triethyl orthoformate. Cleavage from the resin yielded crude imidazo[4,5-*b*]pyridine **3**. Cleaved compounds **3** and **4** were purified using semipreparative reverse-phase chromatography. Imidazo [4,5-*c*]pyridines **5** and **6** were prepared in a similar way using either 2-chloro-3-nitropyridin-4-amine or 2,6-dichloro-3-nitropyridin-4-amine to arylate the resin **II**. The rest of the reaction sequence was identical to preparation of imidazo[4,5-*b*]pyridines **3** and **4** (Fig. 1B). An alternative synthesis of compounds **3** and **5** using the substitution of the complete purine isostere ring with furfurylamine was reported.[27]

Unsubstituted pyrrolo[2,3-*d*]pyrimidine **7** and pyrrolo[3,2-*d*]pyrimidine **9** isosteres were prepared by microwave-assisted synthesis. A mixture of 4-chloro-7*H*-pyrrolo[2,3-*d*]pyrimidine or 4-chloro-5*H*-pyrrolo[3,2-*d*]pyrimidine with furfurylamine and triethylamine in methanol was subjected to focused microwave irradiation (MW) using a Discover SP reactor (Fig. 2A, B). Similar synthesis of compound **7** was reported by Davoll in 1960[25] but our protocol using MW provided much higher yields (60% vs. 26.2%)0.2-Cl Analogues (**8**, **10**) were prepared by conventionally heating starting material with furfurylamine, and triethylamine in refluxing *n*-propanol (Fig. 2A and B, respectively).

Synthesis of 8-azakinetin (**11**) was started by azidation of benzyl bromide with sodium azide in anhydrous DMSO to give **XI**, followed by cyclization of the triazole ring of **XII** with 2-cyanoacetamide. Pyrimidine ring closure was accomplished with ethyl formate and intermediate **XIII** was subsequently chlorinated by thionyl chloride to obtain compound **XIV**. Substitution of the chlorine atom with furfurylamine yielded compound **XV**. Final debenzylation was achieved by treating **XV** with sodium in liquid ammonia (Fig 2C). Pyrazolo[1,5-*a*]pyrimidine kinetin analogue (**12**) was prepared in just one step by reacting 7-chloropyrazolo[1,5-*a*]pyrimidine with furfurylamine (Fig. 2D), whereas synthesis of compound **13** required a three-step procedure. First, the hydroxy group of 1*H*-pyrazolo[4,3-*d*]pyrimidin-7-ol was converted to thiol by heating the starting compound with phosphorous pentasulfide according to a published protocol,[30] followed by methylation of **XVI** with methyl iodide. Finally, substitution of the methylsulfanyl group of **XVII** with furfurylamine furnished compound **13** (Fig. 2E). An alternative synthesis of compound **11** from 4-amino-6-chloro-5-nitropyrimidin was reported previously.[26]

3.2. Protection of fibroblasts derived from Friedreich ataxia patients against oxidative stress

Friedreich ataxia (FA) is a mitochondrial disease affecting the nervous system and heart caused by a homozygotic mutation in the gene encoding frataxin (FXN), a crucial protein for Fe-S cluster assembly. As a consequence, several essential proteins for mitochondrial energy production are affected, as reviewed by Bürk in 2017.[43] The current therapy only eases the symptoms without addressing the pathological changes of mitochondria and cells. Established screening protocols for candidate drugs exploit the increased sensitivity of FA fibroblasts to stress.[44–46] In a recent high-throughput screening campaign aimed at finding potential new treatments for FA based on evaluation of protection against glutathione depletion (Voller et al., in preparation), we identified 2-chloro-3-deazakinetin as a highly active derivative (compound **6** herein). We decided to further search the chemical space of kinetin derivatives for other active compounds using the same protocol. GM04078 FA fibroblasts were pretreated with the test compounds and then exposed to L-

buthionine sulfoximine (BSO), an inhibitor of glutathione *de novo* synthesis. The effect on cell viability was evaluated using the resazurin reduction assay.[47] Protective activity was observed not only for compound 6 but also for compound 5, an analogue with no 2-chloro substituent. Neither kinetin nor 2-chlorokinetin was active (data not shown). Follow-up experiments showed that both compounds **5** and **6** have dose-dependent effects (Fig. 4A), but the effect of compound **6** was much stronger. Compound **6** showed some protective activity at 10 or 50 μM against an even higher dose of BSO (Fig. 4B).

The protective effect of the compounds was not mediated by restoring levels of GSH, which were measured by quantifying fluorescent adducts with monobromobimane (not shown). We also addressed the possibility that the effect of compound **6** could be explained by restoration of FXN expression, but treating FA fibroblasts with the compound at 10 and 50 μM had no clear effects as assessed by western blotting and immunodetection (not shown). We also tested whether compounds **5** and **6** could directly replace the primary function of FXN in the stimulation of iron-sulfur cluster (ISC) biosynthesis.[48] To this end, we used functionally relevant reconstituted ISC machinery without frataxin to test effects of these compounds on the rate of Fe-S cluster synthesis.[31] At 200 μM, compound **5** slightly activated Fe-S cluster biosynthesis by a factor of 1.1, which is only about 0.5% of the activation afforded by FXN (see Appendix B – Fig. B.1). Such a small effect is not consistent with the compound's marked protective effect on BSO-treated cells. Moreover, compound **6**, which also protects against BSO toxicity in FA fibroblasts, slightly inhibits rather than stimulates Fe-S cluster synthesis. Therefore, compound **5** or **6** may influence secondary effects of the lack of FXN in FA fibroblasts rather than Fe-S cluster biosynthesis. Yet another mechanism that could potentially explain protective activity in FA models is iron chelation; however compound 6 had no effect in calcein quenching assay[49] (data not shown).

3.3. The effect on oxidative stress injury in SH-SY5Y cells

Observations of the protective activities of compounds 5 and 6 inspired us to test activities of kinetin isosteres in other disease models where glutathione depletion plays a role. The SH-SY5Y neuroblastoma cell line is often used in neuroprotection research, as reviewed by Xicoy et al. in 2017.[50] One of the frequently used stressors in SH-SY5Y studies is glutamate.[51] At high concentrations, it causes massive oxidative stress by inhibiting the cystine/glutamate Xc-antiporter which resulted in GSH depletion and negative regulation of superoxide dismutase (SOD).[51] Resulting phenotypes are complex; features of necroptosis, apoptosis, and ferroptosis may be present.[52] The changes are probably not triggered by glutamate excitotoxicity, as SH-SY5Y cells probably express only one of the NMDA receptor subunits.[53] However, some other mechanisms have been suggested including, for example, Rac-NADPH-oxidase-driven superoxide radical formation.[51]

We exposed SH-SY5Y cells from American Tissue Type Collection (ATTC) to 160 mM glutamate for 24 h – following enhancement of their differentiation and neuronal phenotype by 48 h treatment with 10 μM all-trans retinoic acid (ATRA) - and assessed the effect of kinetin isosteres on the proportion of dead cells by propidium iodide staining. The iron chelator deferoxamine was used as a positive control. Pilot experiments (not shown) allowed us to focus on several candidates for which protective activity was suspected. Significant activity was confirmed for compounds 6, 10 and 22 (Fig 5A). At 10 μM concentration, they reduced death-indicating propidium iodide signals in cells by more than 10%. However, their effect was lower than that of equimolar deferoxamine. We also assessed the possibility that those compounds may reduce oxidative stress, by quantifying superoxide radical production by dihydroethidium staining, and found that all the candidates had a dose-dependent effect (Fig. 5B).

Protective activity of compound **6** against glutamate-induced stress was further validated by testing in a SH-SY5Y cell line from European Collection of Authenticated Cell Culture (ECCAC) with a different
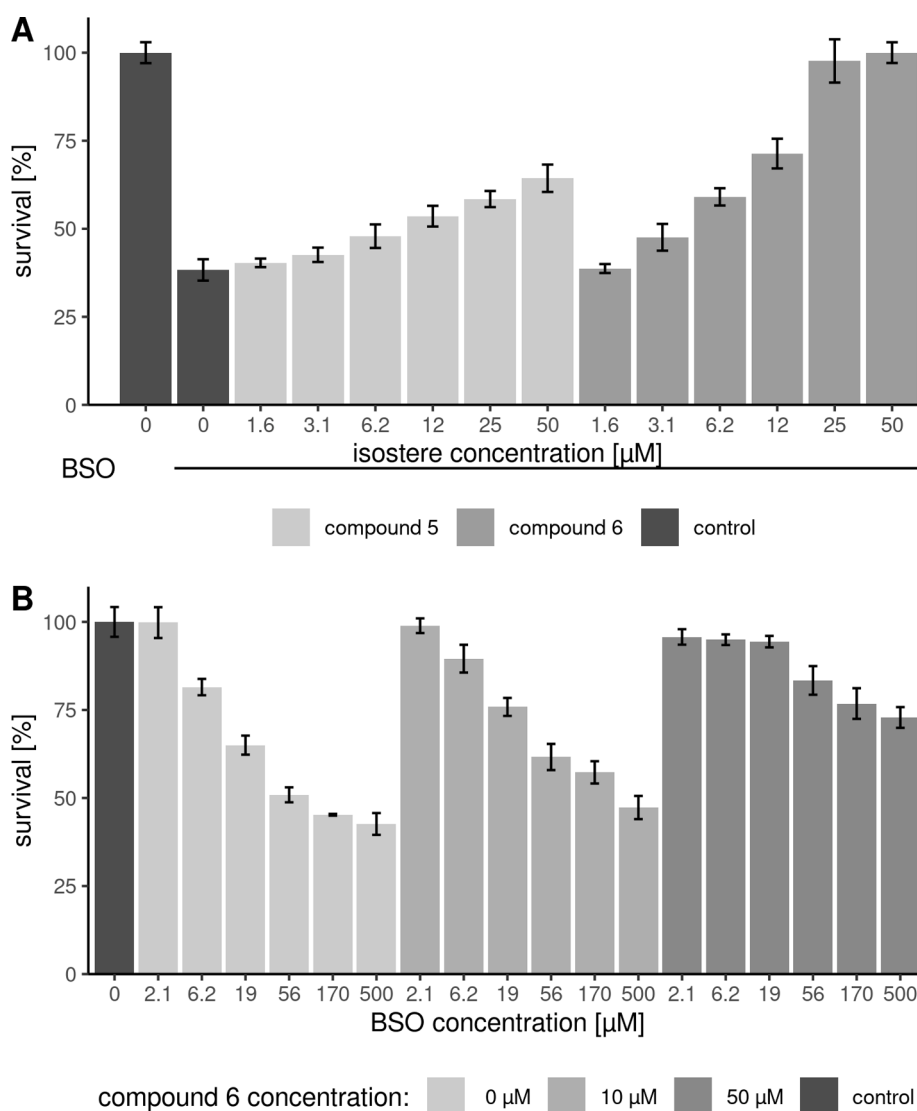
Fig. 4. The protective effect of compounds **5** and **6** against ʟ-buthionine sulfoximine (BSO) in FA-fibroblasts GM04078. Panel A: Pretreatment with serial concentrations of the compounds followed by exposure to 15 μM BSO. Panel B: Pretreatment with compound **6** at 10 or 50 μM followed by exposure to serial concentrations of BSO.

morphology and sensitivity to various toxins.[54] Compound **6** at 10 μM decreased oxidative stress and had a protective activity, albeit the effects were lower than those observed in the cells from ATTC. We also show that the protective effect was partially mediated by inhibition of caspase activation (see Appendix B Fig. B.2). A detailed study of kinetin's behaviour in neuron-like SH-SY5Y will be published separately (González et al., submitted to Molecules journal). Compounds 1-deaza and 3-deazakinetin showed a protective activity in undifferentiated SH-SY5Y against proteotoxic stress induced by MG-132 treatment according to the US patent 20170190704.[24] The effect is supposed to be mediated by PINK1 activation, however no supporting data are shown. As PINK1 activation by kinetin requires its conversion into the corresponding nucleoside monophosphate through the action of adenine phosphoribosyl transferase followed by further enzymatic phosphorylation,[9] the combination of purine ring modification with the presence of 2-chloro substitent suggests that compound **6** and **10** act by a different mechanism.

3.4. Effect of compounds on aberrant splicing of ELP1

We were also interested in the possibility that compound **6** and other

derivatives may have beneficial effects in models of neurodegenerative diseases in which kinetin (**1**) or 2-chlorokinetin (**2**) are active. One such disease is familial dysautonomia, a genetic disorder due (as already mentioned) to aberrant splicing of ELP1 transcripts.[20,55] It is known that patient-derived skin fibroblasts can be used for identification of compounds that increase exon 20 inclusion, as in wild-type splicing.

Here, we evaluated the effect of kinetin isosteres at 50 μM on the ratio of wild-type to mutant transcripts in the patient-derived skin fibroblast cell line GM04663. mRNA was reverse-transcribed and ELP1 DNA was amplified by PCR. During the screening phase of the study, the effect of the compounds was evaluated using standard agarose electrophoresis and GelRed staining (not shown). The activity of the hits was then validated by capillary electrophoresis (Fig. 6, Appendix B Fig. B.3).

The results demonstrate that replacement in either the pyrimidine or imidazole rings of the purine moiety can yield active compounds. However, some purine ring modifications led to loss of activity. 1-deaza derivatives of both kinetin and 2-chlorokinetin were active, but not their 3-deaza counterparts, suggesting that the *N3* nitrogen is crucial for the interaction with an unknown molecular target. The activity was retained if either *N*7 (compounds **7** and **8**) or *N*9-nitrogen (compounds **9** and **10**) were replaced by a carbon atom. The activity of 1-deaza, 7-deaza and 9-
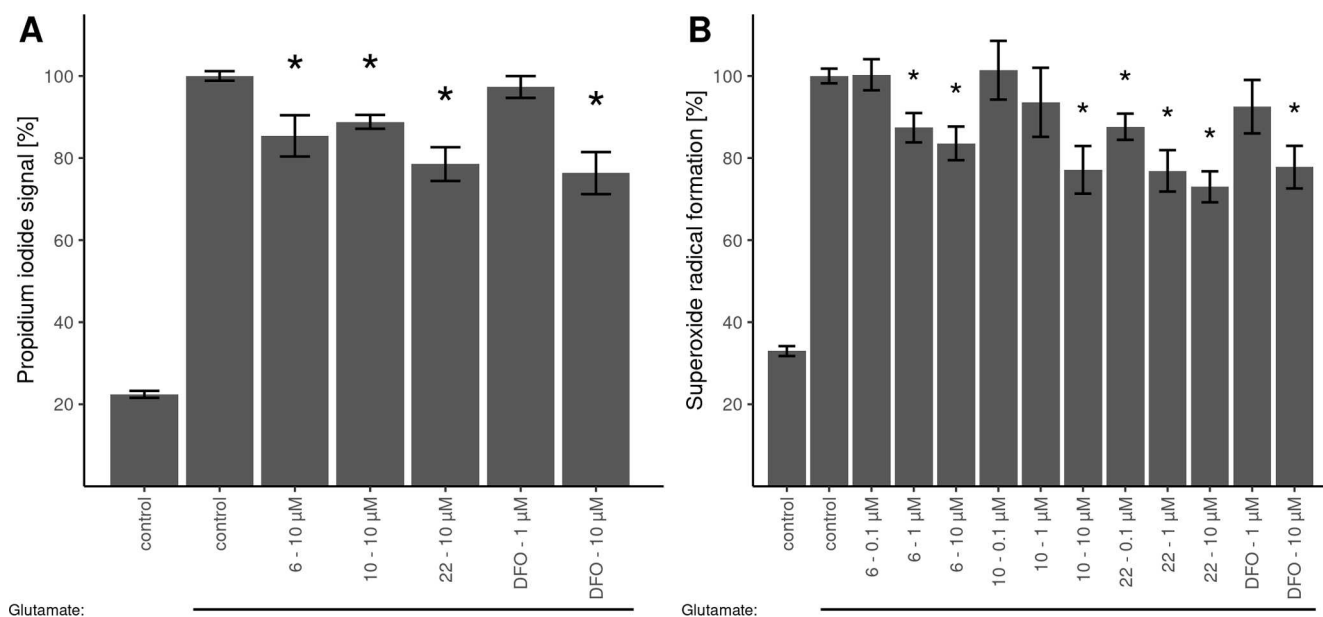
Fig. 5. Protective effects of selected kinetin isoters on glutamate-induced death (panel A) and oxidative stress (panel B) of SH-S5Y5 from ATCC collection. DFO – deferoxamine.
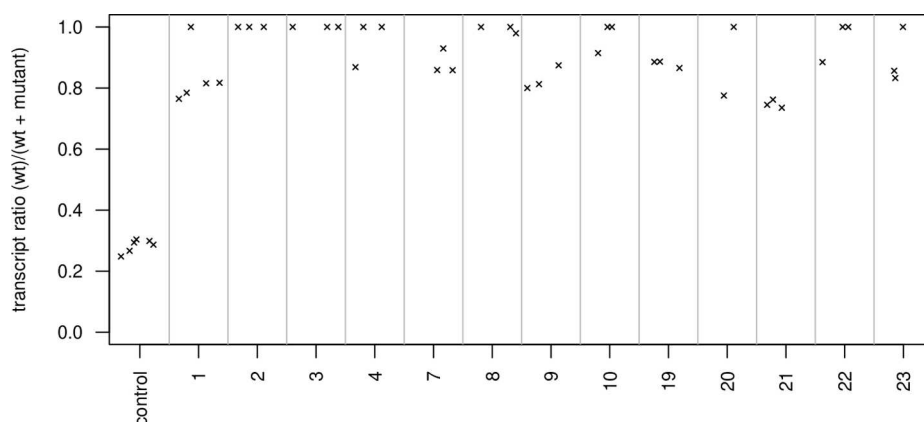

Fig. 6. Effects of the selected isosteres on alternative splicing of mutant ELP1 transcript: wild-type (wt)/wild-type + mutant transcript ratios.

deaza derivatives is also reported in US patent 10676475,[23] where a dual color luminiscence-based reporter system was used for the effect quantification. Activity can also be retained if the imidazole ring is replaced by other 5-membered heterocycles like furan (compound **21**) and thiophene (compound **19** and **20**). On the other hand, 8-aza (compound **11**) and 9-deaza-8-aza (compound **13**) derivatives were inactive. 7-deaza-8-azapurine derivatives substituted by a methyl group at position 9, the N^6-nitrogen or furan ring (compounds **15–18**) were also inactive. The binding site of the unknown target can accommodate even larger substituents, as demonstrated by the activity of the derivatives where the imidazole is replaced by either furan ring substituted by two methyl groups (compound **22**) or benzene (compound **23**). It has already been reported that the 2-chloro derivative of kinetin is an even more potent regulator of ELP1 splicing.[20] Similarly, 2-chloro- derivatives (where available) in our series of compounds retained the activity of their unsubstituted parent compounds.

3.5. In vitro ADME assays

Kinetin (**1**), 2-chlorokinetin (**2**) and their isosteres **3–13** and **19–23** were subjected to biochemical assays that can be used to predict absorption, distribution, metabolism and excretion (ADME)

properties.[56,57] The compounds selected for these assays excluded methylated derivatives, except **22**, where the substitution is on the purine ring.

The parallel artificial membrane permeability assay (PAMPA),[58] which measures compounds' permeation across hexadecane membranes, was used to estimate the selected compounds' absorption by passive diffusion. For this, we assessed their rates of transport across Caco-2 (human colon carcinoma cells with transport properties similar to enterocytes) and MDCK-MDR1 (dog kidney cells expressing a human efflux transporter) monolayers, which are reliable predictors of compounds' ability to cross intestinal[38] and blood-brain barriers (BBB)[37], respectively. Both apical-to-basal and basal-to-apical movements through the barriers were studied, in efforts to identify compounds that are subject to active efflux. Metabolization by human plasma and liver microsomal fractions was used to evaluate the selected compounds' stability. Finally, binding of the compounds to human plasma proteins was studied. The results of all the assays are summarized in Fig. 7.

The compounds showed good plasma stability (83–100% remaining after 2 h incubation) and most of them also had good microsomal stability (median 78% remaining after 1 h incubation). Degradation exceeded 50% only in two cases: **20** and **22.** Compound **22** was particularly prone to degradation, possibly because of the dimethyl
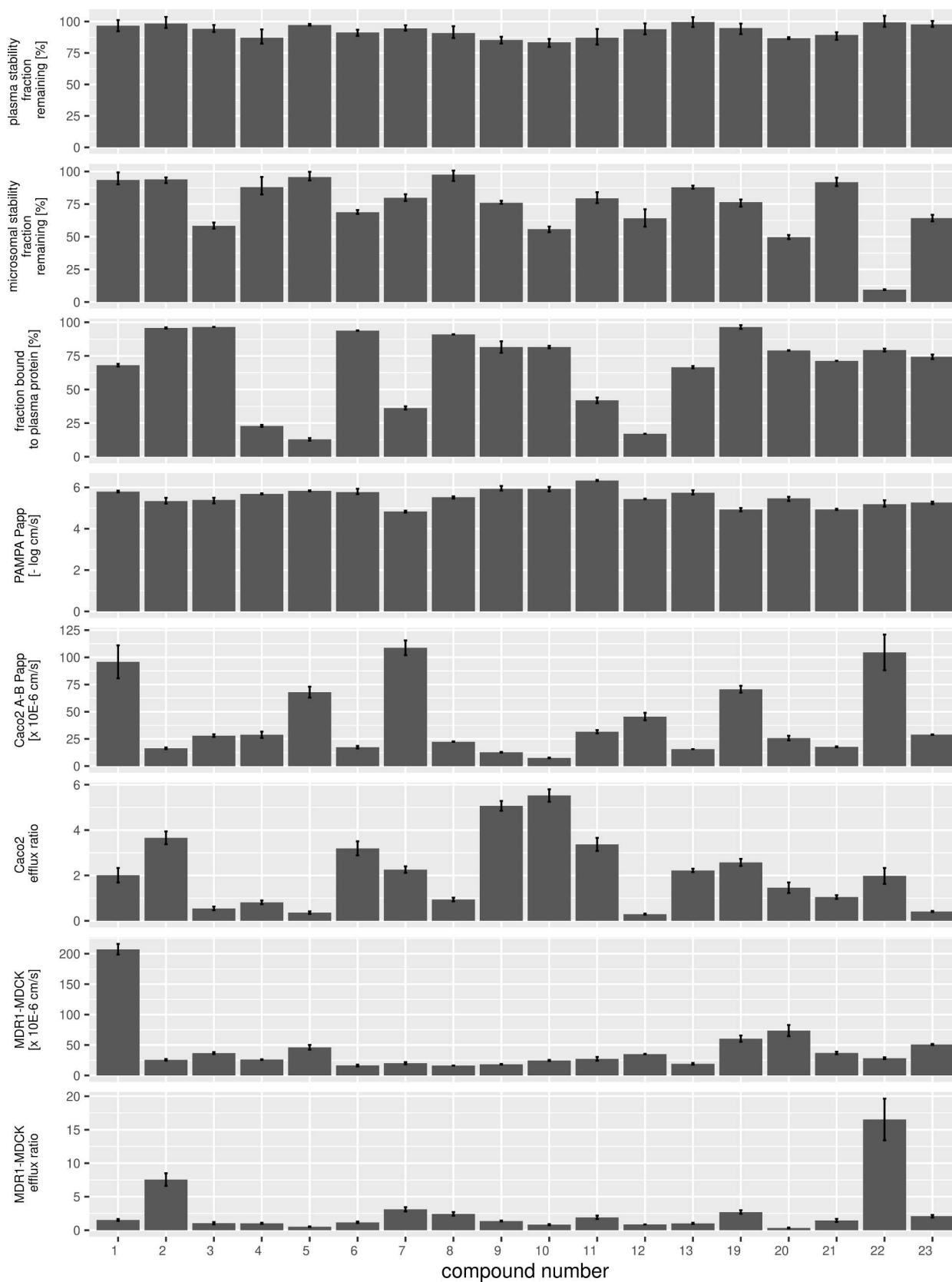
Fig. 7. Overview of the results of ADME *in vitro* assays. Error bars are ranges of values (triplicates in biochemical assays, duplicates in cell-based permeability assays). Standard errors calculated by the Delta method[40]) are only given for results of efflux ratio experiments.

substitution on the 5-membered ring of the purine moiety. Plasma protein binding was highly variable (12.9–96.6%, median 76.7%). Results of the PAMPA assays (log Papp −6.3 to −4.8 cm/s, 1st quartile −5.8 cm/s, median −5.5 cm/s, 3rd quartile −5.3 cm/s) indicate that majority of compounds can readily cross biological barriers by passive diffusion. Compounds with log Papp > −6 cm/s are classified as having high permeability. Results of the Caco-2 and MDCK-MDR1 assays (Papp = 7.6–108.8 and 16.3–207.3 in the units of 10^{-6} cm/s, respectively) are substantially higher than thresholds for high oral absorbance (5×10^{-6} cm/s) and BBB penetration (10×10^{-6} cm/s). Remarkably high values were obtained for kinetin, suggesting possible facilitated transport across the cell membrane. Comparably high absorption was observed for **5, 7, 19** and **22** in Caco-2, but not MDCK-MDR1 cells. The reason for this difference is unclear, although differences in the abundance and/or types of membrane transporters present could be responsible. Differences in compounds' efflux rates could also contribute to this effect, as three of these compounds are among those with the highest efflux rates from MDCK-MDR1 cells. However, compound fluxes are influenced by complex interactions of multiple factors, which would require substantial further elucidation.

3.6. Conclusion

Kinetin has been proposed as a potential therapeutic for diverse conditions and promotion of healthy aging (reviewed by Kadlecová et al. in 2019[2]). It even reached clinical trials for treating skin photoaging[59] and familial dysautonomia[7]. However, few previous peer reviewed studies have assessed pharmacological activities of kinetin derivatives[20–22], and none of them explored effects of modifications of the purine ring system. Some purine isosters are revealed in patent literature, however.[23,24]

Here, we report the pharmacological activity of kinetin and 2-chlorokinetin purine isosteres, and show that some of them have activities not reported for the parent compounds. For example, compound 6 was originally identified as a compound that can protect FA fibroblasts against oxidative stress in our previously mentioned, unpublished high-throughput campaign. The same compound, together with several others, also protected neuron-like cells against oxidative stress damage after high dose glutamate treatment. It would be interesting to evaluate those compounds in other models of mitochondrial and neurodegenerative diseases.

To our disappointment, compound 6 did not correct aberrant splicing of ELP1 transcripts. It would be advantageous to have a compound with such combined activity for treating familial dysautonomia, where stress contributes to the neurodegeneration progression. Overall, activity in the splicing assay was most tolerant of isosteric replacement in the purine core. This tolerance was remarkable in the case of the 5-membered ring, suggesting that it faces toward the cytosolic part of the unknown target's binding site.

We anticipate that isosteric purine replacement could be beneficial not only for improving kinetin's activity toward some targets by increasing interaction with the binding sites but also for increasing the safety of the treatment by limiting affinity for off-targets. This may be particularly important for a compound such as kinetin that has adenine moiety that is present in many important regulatory and signaling molecules. A lower propensity to interact with the purinome generally is thus clearly a desirable property in most cases. Although molecular targets of kinetin remain mostly elusive, it seems highly unlikely that the wide range of reported activities is mediated by a single target or pathway. Kinetin isosteres could therefore also be used for studies of the independence of its various activities. Isosteric replacement also modulates pharmacokinetic properties. Although our data suggest that majority of kinetin isosteres can reach CNS after oral administration, they also show that replacement of the purine ring system of kinetin may result in reduced bioavailability, making development of derivatives with the better activity in the target tissues more difficult. We conclude

that isosteric replacement of kinetin's purine moiety is a fruitful strategy for not only improving its known activities but also for exploring therapeutic applications.

Declaration of Competing Interest

The authors declare that they have no known competing financial interests or personal relationships that could have appeared to influence the work reported in this paper.

Appendix A. Supplementary material

Supplementary data to this article can be found online at https://doi.org/10.1016/j.bmc.2021.115993.

References

1 Voller J, Maková B, Kadlecová A, Gonzalez G, Strnad M. Plant hormone cytokinins for modulating human aging and age-related diseases. In: Rattan S, Sharma R, eds. *Hormones in Ageing and Longevity*. *Healthy Ageing and Longevity*6.

2 Kadlecová A, Maková B, Artal-Sanz M, Strnad M, Voller J. The plant hormone kinetin in disease therapy and healthy aging. *Age Res Rev*. 2019;55:100958. https://doi.org/10.1016/j.arr.2019.100958.

3 Rattan SI, Clark BF. Kinetin delays the onset of ageing characteristics in human fibroblasts. *Biochem Biophys Res Commun*. 1994;201:665–672.

4 Barciszewski J, Siboska GE, Pedersen BO, Clark BFC, Rattan SIS. A mechanism for the in vivo formation of N6-furfuryladenine, kinetin, as a secondary oxidative damage product of DNA. *FEBS Lett*. 1997. https://doi.org/10.1016/S0014-5793(97)01037-5.

5 Slaugenhaupt SA, Mull J, Leyne M, et al. Rescue of a human mRNA splicing defect by the plant cytokinin kinetin. *Hum Mol Genet*. 2004;13:429–436. https://doi.org/10.1093/hmg/ddh046.

6 Pros E, Fernández-Rodríguez J, Benito L, et al. Modulation of aberrant NF1 pre-mRNA splicing by kinetin treatment. *Eur J Hum Genet*. 2010;18:614–617. https://doi.org/10.1038/ejhg.2009.212.

7 Axelrod FB, Liebes L, Gold-von Simson G, et al. Kinetin improves IKBKAP mRNA splicing in patients with familial dysautonomia. *Pediatr Res*. 2011;70:480–483.

8 Yannai S, Zonszain J, Donyo M, Ast G. Combinatorial treatment increases IKAP levels in human cells generated from Familial Dysautonomia patients. *PLoS One*. 2019;14. https://doi.org/10.1371/journal.pone.0211602.

9 Hertz NT, Berthet A, Sos ML, et al. A neo-substrate that amplifies catalytic activity of parkinson's-disease- related kinase PINK1. *Cell*. 2013;154:737–747. https://doi.org/10.1016/j.cell.2013.07.030.

10 Bowie LE, Maiuri T, Alpaugh M, et al. N6-Furfuryladenine is protective in Huntington's disease models by signaling huntingtin phosphorylation. *PNAS*. 2018;115:E7081–E7090.

11 Werner T, Schmülling T. Cytokinin action in plant development. *Curr Opin Plant Biol*. 2009;12:527–538.

12 Doležal K, Popa I, Hauserová E, et al. Preparation, biological activity and endogenous occurrence of N6-benzyladenosines. *Bioorg Med Chem*. 2007;15:3737–3747.

13 Colombo F, Falvella FS, De Cecco L, et al. Pharmacogenomics and analogues of the antitumour agent N 6 -isopentenyladenosine. *Int J Cancer*. 2009;124:2179–2185.

14 Ottria R, Casati S, Maier JAM, Mariotti M, Ciuffreda P. Novel isopentenyladenosine analogues: synthesis, characterization, and evaluation of antiproliferative activity on bladder carcinoma cells. *Nucleosides Nucleotides Nucleic Acids*. 2009;28:736–751. https://doi.org/10.1080/15257770903155550.

15 Ottria R, Casati S, Baldoli E, Maier JAM, Ciuffreda P. N6-Alkyladenosines: synthesis and evaluation of in vitro anticancer activity. *Bioorg Med Chem*. 2010;18:8396–8402. https://doi.org/10.1016/j.bmc.2010.09.030.

16 Amiable C, Pochet S, Padilla A, Labesse G, Kaminski PA. N6-substituted AMPs inhibit mammalian deoxynucleotide N-hydrolase DNPH1. Fraidenraich D, ed. *PLoS One*. 2013;8. https://doi.org/10.1371/journal.pone.0080755.

17 Castiglioni S, Ciuffreda P, Casati S, Ottria R, A.M. Maier J. N6-Isopentenyladenosine and its analogue n6-benzyladenosine induce cell cycle arrest and apoptosis in bladder carcinoma T24 cells. *Anticancer Agents Med Chem.* 2013;13:672–678. https://doi.org/10.2174/1871520611313040016.

18 Oslovsky VE, Drenichev MS, Alexeev CS, Solyev PN, Esipov RS, Mikhailov SN. Synthesis of Cytokinins via Enzymatic Arsenolysis of purine nucleosides. *Curr Protoc Nucleic Acid Chem.* 2018;75. https://doi.org/10.1002/cpnc.61.

19 Matušková V, Zatloukal M, Voller J, et al. New aromatic 6-substituted 2′-deoxy-9-(β)-d-ribofuranosylpurine derivatives as potential plant growth regulators. *Bioorg Med Chem.* 2020;28:115230. https://doi.org/10.1016/j.bmc.2019.115230.

20 Yoshida M, Kataoka N, Miyauchi K, et al. Rectifier of aberrant mRNA splicing recovers tRNA modification in familial dysautonomia. *PNAS.* 2015;112:2764–2769.

21 Salani M, Urbina F, Brenner A, et al. Development of a screening platform to identify small molecules that modify ELP1 Pre-mRNA splicing in familial dysautonomia. *SLAS Disc: Adv Sci Drug Disc.* 2019;24:57–67.

22 Hönig M, Plíhalová L, Spíchal L, et al. New cytokinin derivatives possess UVA and UVB photoprotective effect on human skin cells and prevent oxidative stress. *Eur J Med Chem.* 2018;150:946–957. https://doi.org/10.1016/j.ejmech.2018.03.043.

23 Slaugenhaupt SA, Johnson G, Paquette WD, Zhang W, Marugan J. *United States Patent: 10676475 – Compounds for improving mRNA splicing.* 2020.

24 de Roulet, DeVita. *United States Patent: 10167286 – Compositions and methods using the same for treatment of neurodegenerative and mitochondrial disease.* 2019.

25 Davoll J. 26. Pyrrolo[2,3-d]pyrimidines. *J Chem Soc.* 1960:131–138. https://doi.org/10.1039/JR9600000131.

26 Weiss R, Robins RK, Noell CW. Potential purine antagonists. XXIII. Synthesis of some 7-substituted amino-v-triazolo(d)pyrimidines1. *J Org Chem.* 1960:765–770. https://doi.org/10.1021/jo01075a023.

27 Rogozińska JH, Kroon C, Salemink CA. Influence of alterations in the purine ring on biological activity of cytokinins. *Phytochemistry.* 1973;12:2087–2092.

28 Savelieva EM, Oslovsky VE, Karlov DS, et al. Cytokinin activity of N6-benzyladenine derivatives assayed by interaction with the receptors in planta, in vitro, and in silico. *Phytochemistry.* 2018;149:161–177.

29 Kubiasová K, Mik V, Nisler J, et al. Design, synthesis and perception of fluorescently labeled isoprenoid cytokinins. *Phytochemistry.* 2018;150:1–11.

30 Robins RK, Furcht FW, Grauer AD, Jones JW. Potential purine antagonists. II. Synthesis of some 7- and 5,7-substituted pyrazolo [4,3-d]pyrimidines. *J Am Chem Soc.* 1956;78:2418–2422. https://doi.org/10.1021/ja01592a021.

31 Gervason S, Larkem D, Mansour AB, et al. Physiologically relevant reconstitution of iron-sulfur cluster biosynthesis uncovers persulfide-processing functions of ferredoxin-2 and frataxin. *Nat Commun.* 2019;10. https://doi.org/10.1038/s41467-019-11470-9.

32 Stone JS, Shang J-L, Tomarev S. Expression of Prox1 defines regions of the avian otocyst that give rise to sensory or neural cells. *J Comp Neurol.* 2003;460:487–502.

33 Carrasco RA, Stamm NB, Patel BKR. One-step cellular caspase-3/7 assay. *Biotechniques.* 2003;34:1064–1067.

34 Kim MS, Seo JY, Oh J. Neuroprotective effect of halophyte Salicornia herbacea L. is mediated by activation of heme oxygenase-1 in mouse hippocampal HT22 cells. *J Med Food.* 2017;20:140–151.

35 Anderson SL, Qiu J, Rubin BY. EGCG corrects aberrant splicing of IKAP mRNA in cells from patients with familial dysautonomia. *Biochem Biophys Res Commun.* 2003; 310:627–633.

36 Borková L, Frydrych I, Jakubcová N, et al. Synthesis and biological evaluation of triterpenoid thiazoles derived from betulonic acid, dihydrobetulonic acid, and ursonic acid. *Eur J Med Chem.* 2020;185:111806. https://doi.org/10.1016/j.ejmech.2019.111806.

37 Irvine JD, Takahashi L, Lockhart K, et al. MDCK (Madin-Darby Canine Kidney) cells: a tool for membrane permeability screening. *J Pharm Sci.* 1999;88:28–33.

38 Artursson P, Palm K, Luthman K. Caco-2 monolayers in experimental and theoretical predictions of drug transport. *Adv Drug Deliv Rev.* 2001;46:27–43. https://doi.org/10.1016/S0169-409X(00)00128-9.

39 Hammer O, Harper D, Ryan P. PAST: paleontological statistics software package for education and data analysis. *Palaeontol Electron.* 2001;4:1–9.

40 Wu J. Statistical inference for tumor growth inhibition T/C ratio. *J Biopharm Stat.* 2010;20:954–964.

41 Lemrová B, Smyslová P, Popa I, et al. Directed solid-phase synthesis of trisubstituted imidazo[4,5- c]pyridines and imidazo[4,5- b]pyridines. *ACS Comb. Sci.* 2014;16: 558–565.

42 Vanda D, Soural M, Canale V, et al. Novel non-sulfonamide 5-HT 6 receptor partial inverse agonist in a group of imidazo[4,5- b]pyridines with cognition enhancing properties. *Eur J Med Chem.* 2018;144:716–729.

43 Bürk K. Friedreich Ataxia: current status and future prospects. *Cerebellum Ataxias.* 2017;4:1–9. https://doi.org/10.1186/s40673-017-0062-x.

44 Richardson TE, Yang S-H, Wen Y, Simpkins JW. Estrogen protection in Friedreich's Ataxia skin fibroblasts. *Endocrinology.* 2011;152:2742–2749. https://doi.org/10.1210/en.2011-0184.

45 Richardson TE, Simpkins JW. R- and S-Equol have equivalent cytoprotective effects in Friedreich's Ataxia. *BMC Pharmacol Toxicol.* 2012;13:12. https://doi.org/10.1186/2050-6511-13-12.

46 Ferriero R, Manco G, Lamantea E, et al. Phenylbutyrate therapy for pyruvate dehydrogenase complex deficiency and lactic acidosis. *Sci Transl Med.* 2013;5. https://doi.org/10.1126/scitranslmed.3004986.

47 Bonnier F, Keating ME, Wróbel TP, et al. Cell viability assessment using the Alamar blue assay: a comparison of 2D and 3D cell culture models. *Toxicol In Vitro.* 2015;29: 124–131. https://doi.org/10.1016/j.tiv.2014.09.014.

48 Pastore A, Puccio H. Frataxin: a protein in search for a function. *J Neurochem.* 2013; 126:43–52.

49 Ali A, Zhang Q, Dai J, Huang X. Calcein as a fluorescent iron chemosensor for the determination of low molecular weight iron in biological fluids. *Biometals.* 2003;16: 285–293. https://doi.org/10.1023/A:1020642808437.

50 Xicoy H, Wieringa B, Martens GJM. The SH-SY5Y cell line in Parkinson's disease research: a systematic review. *Mol Neurodegener.* 2017;12:1–11. https://doi.org/10.1186/s13024-017-0149-0.

51 Kritis AA, Stamoula EG, Paniskaki KA, Vavilis TD. Researching glutamate – induced cytotoxicity in different cell lines: a comparative/collective analysis/study. *Front Cell Neurosci.* 2015;9:91. https://doi.org/10.3389/fncel.2015.00091.

52 Ito K, Eguchi Y, Imagawa Y, Akai S, Mochizuki H, Tsujimoto Y. MPP+ induces necrostatin-1-and ferrostatin-1-sensitive necrotic death of neuronal SH-SY5Y cells. *Cell Death Discov.* 2017;3:1–10. https://doi.org/10.1038/cddiscovery.2017.13.

53 Kulikov AV, Rzhaninova AA, Goldshtein DV, Boldyrev AA. Expression of NMDA receptors in multipotent stromal cells of human adipose tissue under conditions of retinoic acid-induced differentiation. *Bull Exp Biol Med.* 2007;144:626–629. https://doi.org/10.1007/s10517-007-0390-6.

54 Nishida Y, Adati N, Ozawa R, et al. Identification and classification of genes regulated by phosphatidylinositol 3-kinase- and TRKB-mediated signalling pathways during neuronal differentiation in two subtypes of the human neuroblastoma cell line SH-SY5Y. *BMC Res Notes.* 2008;1:95. https://doi.org/10.1186/1756-0500-1-95.

55 Slaugenhaupt SA, Blumenfeld A, Gill SP, et al. Tissue-specific expression of a splicing mutation in the IKBKAP gene causes familial dysautonomia. *Am J Hum Genet.* 2001; 68:598–605. https://doi.org/10.1086/318810.

56 Di L, Kerns EH. Profiling drug-like properties in discovery research. *Curr Opin Chem Biol.* 2003;7:402–408. https://doi.org/10.1016/S1367-5931(03)00055-3.

57 Zhang D, Luo G, Ding X, Lu C. Preclinical experimental models of drug metabolism and disposition in drug discovery and development. *Acta Pharmaceutica Sinica B.* 2012;2:549–561. https://doi.org/10.1016/j.apsb.2012.10.004.

58 Yu H, Wang Q, Sun Y, et al. A new PAMPA model proposed on the basis of a synthetic phospholipid membrane. Hofmann A, ed. *PLoS One.* 2015;10. https://doi.org/10.1371/journal.pone.0116502.

59 Wanitphakdeedecha R, Meeprathom W, Manuskiatti W. Efficacy and safety of 0.1% kinetin cream in the treatment of photoaging skin. *Indian J Dermatol Venereol Leprol.* 2015;81:547. https://doi.org/10.4103/0378-6323.157446.

Supplementary material IV.

Tammam, M. A.; Rárová, L.; Kvasnicová, M.; Gonzalez, G.; Emam, A. M.; Mahdy, A.; Strnad, M.; Ioannou, E.; Roussis, V., Bioactive Steroids from the Red Sea Soft Coral Sinularia polydactyla. *Marine Drugs* 2020, *18* (12), 632.

Article

Bioactive Steroids from the Red Sea Soft Coral *Sinularia polydactyla*

Mohamed A. Tammam [1,2] , **Lucie Rárová** [3,*] , **Marie Kvasnicová** [3], **Gabriel Gonzalez** [3] ,
Ahmed M. Emam [2], **Aldoushy Mahdy** [4] , **Miroslav Strnad** [3], **Efstathia Ioannou** [1] and
Vassilios Roussis [1,*]

1   Section of Pharmacognosy and Chemistry of Natural Products, Department of Pharmacy,
    National and Kapodistrian University of Athens, Panepistimiopolis Zografou, 15771 Athens, Greece;
    mtammam@pharm.uoa.gr (M.A.T.); eioannou@pharm.uoa.gr (E.I.)
2   Department of Biochemistry, Faculty of Agriculture, Fayoum University, Fayoum 63514, Egypt;
    ame01@fayoum.edu.eg
3   Laboratory of Growth Regulators, Institute of Experimental Botany, The Czech Academy of Sciences,
    Faculty of Science, Palacký University, Šlechtitelů 27, CZ-78371 Olomouc, Czech Republic;
    kvasnicova@ueb.cas.cz (M.K.); gonzalez.gabriel@seznam.cz (G.G.); miroslav.strnad@upol.cz (M.S.)
4   Department of Zoology, Faculty of Science, Al-Azhar University (Assiut Branch), Assiut 71524, Egypt;
    aldoushy@azhar.edu.eg
*   Correspondence: lucie.rarova@upol.cz (L.R.); roussis@pharm.uoa.gr (V.R.);
    Tel.: +420-5856-34698 (L.R.); +30-210-727-4592 (V.R.)

Abstract: Six new (**1**, **2**, **6**, **8**, **13**, and **20**) and twenty previously isolated (**3–5**, **7**, **9–12**, **14–19**, and **21–26**) steroids featuring thirteen different carbocycle motifs were isolated from the organic extract of the soft coral *Sinularia polydactyla* collected from the Hurghada reef in the Red Sea. The structures and the relative configurations of the isolated natural products have been determined based on extensive analysis of their NMR and MS data. The cytotoxic, anti-inflammatory, anti-angiogenic, and neuroprotective activity of compounds **3–7**, **9–12**, **14–20**, and **22–26**, as well as their effect on androgen receptor-regulated transcription was evaluated in vitro in human tumor and non-cancerous cells. Steroids **22** and **23** showed significant cytotoxicity in the low micromolar range against the HeLa and MCF7 cancer cell lines, while migration of endothelial cells was inhibited by compounds **11**, **12**, **22**, and **23** at 20 μM. The results of the androgen receptor (AR) reporter assay showed that compound **11** exhibited the strongest inhibition of AR at 10 μM, while it is noteworthy that steroids **10**, **16**, and **20** displayed increased inhibition of AR with decreasing concentrations. Additionally, compounds **11** and **23** showed neuroprotective activity on neuron-like SH-SY5Y cells.

Keywords: *Sinularia polydactyla*; soft coral; steroids; cytotoxic; anti-inflammatory; neuroprotective; androgen receptor

1. Introduction

The Red Sea, one of the warmest and most saline marine habitats, is an extension of the Indian Ocean, located between the Arabian Peninsula and Africa. The entire coastal reef complex extends along a 2000-km shoreline and is characterized by a high degree of chemodiversity, including more than 200 soft and 300 hard coral species [1]. Despite the diverse marine life hosted in the Red Sea, marine organisms from this ecosystem have not been thoroughly studied in comparison to other extended coral habitats, such as those encountered in the Great Barrier Reef or the Caribbean Sea [2].
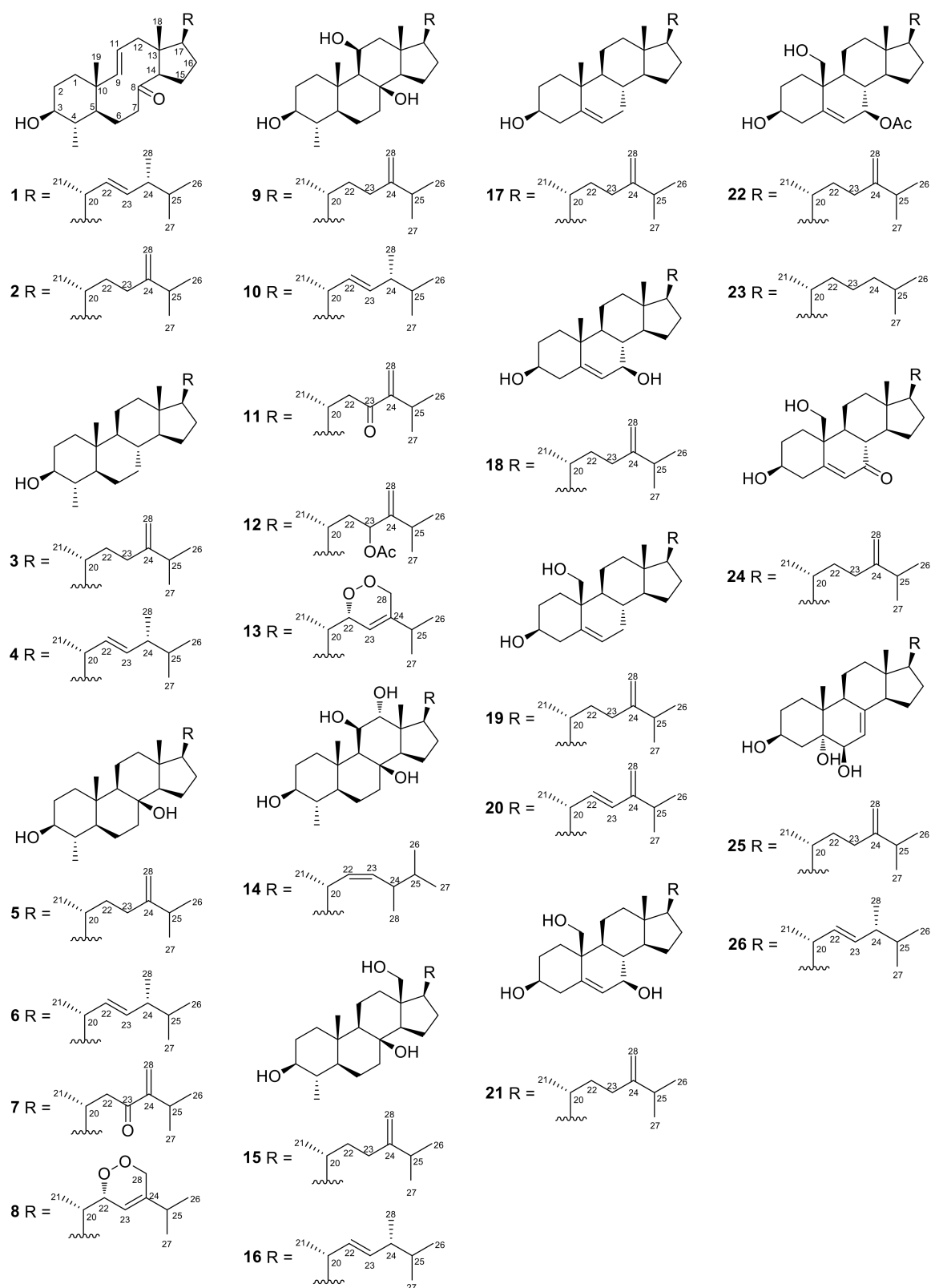
Figure 1. Chemical structures of compounds **1–26**.

Over the last 50 years, soft corals (Anthozoa, Gorgonacea) have been the subject of extensive chemical investigations which have resulted in the isolation of a large of number secondary metabolites, mainly sesquiterpenes, diterpenes, prostanoids, and highly functionalized steroids [3].

A significant number of these metabolites have exhibited potent biological properties, including cytotoxic, antibacterial, antifungal, anti-inflammatory, and antifouling activity [2]. Among soft corals, species of the genus *Sinularia* have been extensively studied as sources of new bioactive compounds, most often leading to the isolation of diterpenes and steroids with noteworthy levels of bioactivity [2,3].

In the context of our continuous interest for the isolation of bioactive metabolites from marine organisms, we recently had the opportunity to collect specimens of *Sinularia polydactyla* from the coastline of Hurghada in the Red Sea (Egypt) and investigate its chemical profile. Herein we report the isolation, structure elucidation, and evaluation of biological activity of six new (**1**, **2**, **6**, **8**, **13,** and **20**) and twenty previously isolated (**3–5**, **7**, **9–12**, **14–19,** and **21–26**) steroids (Figure 1).

2. Results and Discussion

2.1. Structure Elucidation of the Isolated Metabolites

A series of normal- and reversed-phase chromatographic separations of the organic extract of the soft coral *S. polydactyla* collected from the Egyptian Red Sea coastline at Hurghada allowed for the isolation of compounds **1–26**.

Compound **1**, isolated as a white amorphous solid, possessed the molecular formula $C_{29}H_{48}O_2$, as indicated by the HR-APCIMS and NMR data. The ^{13}C NMR and HSQC-DEPT spectra revealed the presence of 29 carbon atoms, corresponding to seven methyls, seven methylenes, twelve methines, and three non-protonated carbon atoms. Among them, evident were one carbonyl resonating at δ_C 213.1, four olefinic carbons resonating at δ_C 127.6, 132.6, 135.2, and 142.0 and an oxygenated carbon resonating at δ_C 76.6. In the ^1H NMR spectrum evident were two methyls on non-protonated carbons (δ_H 0.94 and 1.08), five methyls on tertiary carbons (δ_H 0.80, 0.81, 0.89, 0.99, and 1.04), one oxygenated methine (δ_H 3.09), and four olefinic methines (δ_H 5.15, 5.20, 5.28, and 5.41). Since the carbonyl moiety and the two carbon–carbon double bonds accounted for three of the six degrees of unsaturation, the molecular structure of **1** was determined as tricyclic. The spectroscopic features of metabolite **1** (Tables 1 and 2), in conjunction with the homonuclear and heteronuclear correlations observed in its HSQC, HMBC, and COSY spectra (Figure 2) suggested that compound **1** possessed a 8-oxo-3-hydroxy-4-methyl-8,9-seco steroidal nucleus with a $\Delta^{9,11}$ and a C_9H_{17} unsaturated side chain with a 1,2-disubstituted double bond between C-22 and C-23. Specifically, the correlations observed in the COSY spectrum identified three distinct spin systems, namely (a) a spin system starting from H-1 to H_2-7, incorporating H_3-29 which was coupled to H-4, (b) a short spin system from H-9 to H_2-12 through H-11, and (c) an extended branched spin system from H-14 to H_3-26, including H_3-21, H_3-27, and H_3-28 which were coupled to H-20, H-25, and H-24, respectively. The HMBC correlations of H_3-19 with C-1, C-5, C-9, and C-10 concluded the six-membered ring and positioned the first angular methyl on C-10, connecting at the same time spin systems (a) and (b). Additionally, the HMBC correlations of H_3-18 with C-12, C-13, C-14, and C-17 identified the five-membered ring and fixed the position of the second angular methyl on C-13, connecting spin systems (b) and (c). The HMBC correlations of H_2-6, H_2-7, and H-14 with the carbonyl carbon C-8 supported the cleavage of the C-8/C-9 bond, giving rise to the decalin ring and connecting spin systems (a) and (c). The geometry of the two double bonds was determined as *E* in both cases on the basis of the measured coupling constants ($J_{9,11}$ = 15.3 Hz and $J_{22,23}$ = 15.2 Hz). The enhancements of H-3/H-5, H-3/H_3-29, H-4/H_3-19, H-5/H-9, H-9/H-12α, H-9/H-14, H-11/H-12β, H-11/H_3-18, H-11/H_3-19, H-14/H-17, and H_3-18/H-20 observed in the NOESY spectrum (Figure 2) verified the *trans* fusion of the six-membered and the ten-membered rings, as well as the *trans* fusion of the latter with the five-membered ring and determined the relative configuration of the stereogenic centers. The *R* configuration at C-24 was proposed on the basis of the 0.3 ppm difference in the chemical shifts of C-26 and C-27 and the chemical shift of C-28 resonating at 17.6 ppm [4]. On the basis of the above, metabolite **1** was identified as (9*E*,22*E*,24*R*)-3β-hydroxy-4α,24-dimethyl-8,9-seco-5α-cholesta-9(11),22-dien-8-one.

Table 1. ^{1}H NMR data (δ in ppm, *J* in Hz) in CDCl$_3$ of compounds **1**, **2**, **4**, **6**, **8**, **13**, and **20**.

Position	1 [1]	2 [1]	4 [2]	6 [2]	8 [1]	13 [1]	20 [3]
1	1.33 m, 1.22 m	1.36 m, 1.24 m	1.71 m, 0.98 m	1.72 m, 0.93 m	1.72 m, 0.96 m	1.91 m, 1.00 m	1.91 m, 1.08 m
2	1.76 m, 1.48 m	1.76 m, 1.49 m	1.77 m, 1.46 m	1.77 m, 1.52 m	1.78 m, 1.52 m	1.79 m, 1.58 m	1.84 m, 1.40 m
3	3.09 td (10.1, 4.8)	3.10 m	3.06 td (10.5, 4.9)	3.04 td (10.2, 4.9)	3.06 td (10.5, 5.2)	3.05 td (10.8, 5.0)	3.56 m
4	1.27 m	1.28 m	1.27 m	1.31 m	1.33 m	1.41 m	2.37 m, 2.18 m
5	0.91 m	0.92 m	0.72 m	0.68 td (12.4, 2.9)	0.71 td (12.2, 2.2)	0.69 td (11.9, 2.2)	-
6	1.66 m, 1.60 m	1.66 m, 1.62 m	1.64 m, 1.47 m	1.50 m, 1.33 m	1.53 m, 1.33 m	1.56 m, 1.39 m	5.73 m
7	2.29 m, 1.75 m	2.48 m, 2.24 m	1.69 m, 1.50 m	1.63 m, 1.13 m	1.64 m, 1.19 m	1.71 m, 1.22 m	2.01 m, 1.51 m
8	-	-	1.28 m	-	-	-	1.82 m
9	5.28 d (15.3)	5.27 m	0.60 m	0.80 m	0.81 m	0.88 m	0.89 m
11	5.41 ddd (15.3, 11.1, 3.8)	5.41 m	1.47 m, 1.00 m	1.62 m, 1.49 m	1.62 m, 1.48 m	4.43 brd (1.9)	1.62 m, 1.53 m
12	2.47 m, 1.70 m	2.50 m, 1.72 m	1.92 m, 1.11 m	1.95 m, 1.16 m	1.93 m, 1.17 m	2.23 m, 1.37 m	2.01 m, 1.17 m
14	2.49 m	2.50 m	0.93 m	1.18 m	1.23 m	1.27 m	0.90 m
15	1.64 m, 1.48 m	1.64 m, 1.50 m	1.51 m, 1.02 m	1.45 m, 1.23 m	1.53 m, 1.33 m	1.60 m, 1.46 m	1.50 m, 1.05 m
16	1.70 m, 1.47 m	1.73 m, 1.49 m	1.63 m, 1.19 m	1.64 m, 1.23 m	1.99 m, 1.31 m	2.00 m, 1.35 m	1.64 m, 1.26 m
17	1.31 m	1.28 m	1.09 m	1.03 m	1.43 m	1.43 m	1.18 m
18	1.08 s	1.09 s	0.64 s	0.92 s	0.89 s	1.09 s	0.75 s
19	0.94 s	0.94 s	0.80 s	0.97 s	0.96 s	1.33 s	3.81 d (11.5), 3.59 d (11.5)
20	2.10 m	2.11 m	1.98 m	1.96 m	1.56 m	1.59 m	2.11 m
21	0.99 d (6.8)	0.93 d (6.1)	0.97 d (6.6)	0.94 d (6.4)	0.83 d (6.9)	0.85 d (7.0)	1.03 d (6.5)
22	5.15 dd (15.2, 8.1)	1.53 m, 1.14 m	5.12 dd (15.1, 7.6)	5.09 dd (15.2, 8.2)	4.72 brs	4.70 brs	5.56 dd (15.7, 8.7)
23	5.20 dd (15.2, 7.3)	2.08 m, 1.88 m	5.17 dd (15.1, 7.0)	5.16 dd (15.2, 7.4)	5.36 brs	5.36 brs	5.92 d (15.7)
24	1.83 m	-	1.83 m	1.80 m	-	-	-
25	1.44 m	2.21 m	1.44 m	1.42 m	2.24 septet (6.9)	2.24 septet (6.9)	2.53 septet (6.8)
26	0.81 d (6.8)	1.00 d (6.8)	0.81 d (6.8)	0.81 d (6.8)	1.05 d (6.9)	1.05 d (6.9)	1.06 d (6.8)
27	0.80 d (6.8)	1.01 d (6.9)	0.79 d (6.8)	0.79 d (6.8)	1.05 d (6.9)	1.06 d (6.9)	1.04 d (6.8)
28	0.89 d (6.8)	4.70 brs, 4.63 brs	0.88 d (6.8)	0.88 d (6.8)	4.62 d (15.7), 4.20 d (15.7)	4.59 d (15.7), 4.21 d (15.7)	4.83 brs, 4.79 brs
29	1.04 d (6.1)	1.04 d (6.1)	0.92 d (6.3)	0.95 d (6.8)	0.95 d (6.4)	0.96 d (6.4)	-

[1] Recorded at 600 MHz. [2] Recorded at 400 MHz. [3] Recorded at 950 MHz, - absence of value.

Table 2. ^{13}C NMR data (δ in ppm) in CDCl[3] of compounds **1**, **4**, **6**, **8**, **13**, and **20**.

Position	1 [1,2]	4 [3]	6 [1,4]	8 [1,2]	13 [2]	20 [1,5]
1	38.5	36.8	37.7	37.2	37.5	32.9
2	30.7	31.1	30.9	30.3	30.2	31.7
3	76.6	76.6	76.8	76.4	76.5	70.8
4	39.8	39.2	39.0	38.5	38.2	41.9
5	53.5	51.0	51.9	51.2	52.3	134.9
6	20.0	24.2	20.5	19.8	20.0	126.8
7	47.1	32.2	40.1	39.6	39.9	30.8
8	213.1	36.0	73.6	73.5	75.3	33.4
9	142.0	54.6	56.6	56.0	57.6	49.9
10	39.1	34.9	36.9	36.3	36.8	41.0
11	127.6	21.1	18.3	18.1	69.8	21.4
12	46.8	40.2	41.6	40.5	49.0	39.6
13	55.2	42.4	43.0	42.7	41.8	42.3
14	62.7	56.6	59.7	59.0	60.2	57.5
15	26.6	24.2	19.0	18.7	19.2	24.1
16	28.4	28.6	28.3	27.0	26.9	28.1
17	56.7	56.1	57.1	52.4	53.9	55.4
18	13.5	12.3	14.0	12.8	15.0	12.0
19	15.8	13.4	13.8	13.2	15.6	62.3
20	39.1	40.0	39.6	39.8	40.0	39.9
21	21.7	20.9	21.3	12.8	12.9	20.2
22	135.2	135.9	135.7	79.9	79.7	135.4
23	132.6	131.6	131.8	119.4	119.2	128.8
24	43.0	42.8	43.2	142.0	142.0	153.0
25	33.2	33.1	33.8	30.8	31.1	28.8
26	19.8	19.6	19.9	21.0	21.1	21.7
27	20.1	19.9	20.2	21.0	21.1	22.1
28	17.6	17.6	18.0	70.6	70.8	109.0
29	16.4	15.1	16.0	14.9	15.2	

[1] Chemical shifts were determined through HMBC correlations. [2] Recorded at 150 MHz. [3] Recorded at 50 MHz. [4] Recorded at 100 MHz. [5] Recorded at 237.5 MHz.

(**a**)　　　　　　　　　　　　　　　　　　　(**b**)
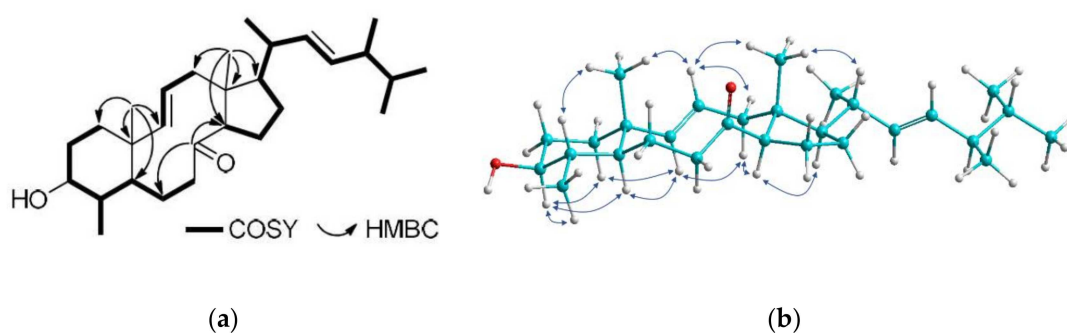
Figure 2. (**a**) COSY and key HMBC correlations and (**b**) key NOESY cross-peaks for compound **1**.

Compound **2**, isolated in minute amount as a white amorphous solid, displayed an ion peak at *m/z* 429.3725 (HR-APCIMS), corresponding to $C_{29}H_{49}O_2$ and consistent for $[M + H]^+$. Compound **2** shared quite similar spectroscopic features with **1**. In particular, all signals attributed to the steroidal nucleus, with the most prominent being the signals of the two angular methyls H[3]-18 and H[3]-19 (δ_H 1.09 and 0.94, respectively), the methyl at C-4 (δ_H 1.04), the oxymethine H-3 (δ_H 3.10), and the two olefinic protons H-9 and H-11 (δ_H 5.27 and 5.41, respectively), were also evident in the ^{1}H NMR spectrum of compound **2** (Table 1). The most significant difference observed was the replacement of the 1,2-disubstituted double bond in the side chain of **1** by a 1,1-disubstituted double bond (δ_H 4.63 and 4.70) in the side chain of **2**. The correlations observed in the COSY spectrum of **2** identified the relevant spin systems; however, metabolite **2** was proven unstable and degraded prior to the acquisition of heteronuclear NMR

spectra. Nevertheless, the high structural similarity of **2** with compound **1** renders safe the proposed identification of **2** as (9*E*)-3*β*-hydroxy-4*α*,24-dimethyl-8,9-seco-5*α*-cholesta-9(11),24(28)-dien-8-one.

　　Compound **6**, isolated as a white amorphous solid, possessed the molecular formula $C_{29}H_{50}O_2$, as suggested by its HR-APCIMS and NMR data. The spectroscopic data of **6** were quite similar to those of the previously reported metabolites **5** and **7** (Tables 1 and 2). The presence of the two angular methyls at δ_H 0.92 and 0.97, the doublet methyl at δ_H 0.95, the oxygenated methine at δ_H 3.04 and the quaternary oxygenated carbon at δ_C 73.6, in conjunction with the correlations observed in the HMBC and COSY spectra (Figure 3a), verified the 3,8-dihydroxy-4-methyl steroidal nucleus. The side chain of compound **6** included four doublet methyls ($\delta_{H/C}$ 0.79/20.2, 0.81/19.9, 0.88/18.0, and 0.95/16.0) and two olefinic methines ($\delta_{H/C}$ 5.09/135.7 and 5.16/131.8) that was assigned on the basis of the COSY and HMBC correlations. The *E* geometry of the Δ^{22} double bond was supported by the large coupling constant of H-22/H-23 (*J* = 15.3 Hz). The enhancements of H-3/H-5, H-3/H$_3$-29, H-4/H$_3$-19, H-5/H-9, H-5/H$_3$-29, H-9/H-12α, H-9/H-14, H-12β/H$_3$-18, and H$_3$-18/H-20 observed in the NOESY spectrum verified the *trans* fusion of rings A/B, B/C, and C/D and suggested the axial orientation of the hydroxy group at C-8. The configuration at C-24 was proposed as *R* due to the fact that the difference in the chemical shifts of C-26 and C-27 was 0.3 ppm and that C-28 resonated at 18.0 ppm [4]. Therefore, compound **6** was identified as (22*E*,24*R*)-4*α*,24-dimethyl-5*α*-cholest-22-en-3*β*,8*β*-diol.
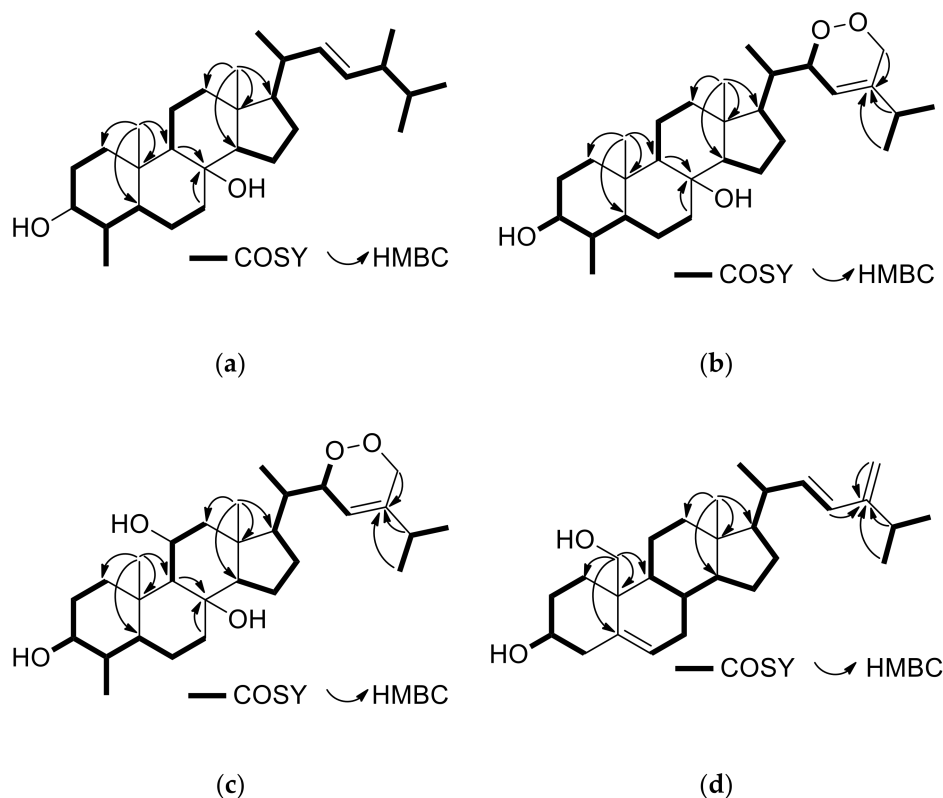
Figure 3. (**a**) COSY and important HMBC correlations for compound **6**. (**b**) COSY and important HMBC correlations for compound **8**. (**c**) COSY and important HMBC correlations for compound **13**. (**d**) COSY and important HMBC correlations for compound **20**.

　　Compound **8**, isolated as a white amorphous solid, exhibited an ion peak at *m/z* 459.3475 corresponding to $C_{29}H_{47}O_4$ and consistent with [M − H]$^-$. The high degree of similarity of the spectroscopic data of metabolite **8** (Tables 1 and 2) with those of **5**–**7** indicated the same 3,8-dihydroxy-4-methyl steroidal nucleus, further confirmed by the correlations observed in the HMBC and COSY spectra (Figure 3b). Taking into account that the steroidal nucleus of **8** accounts for four of the six degrees of unsaturation and the presence of one double bond on the side chain, the latter

should also contain an additional ring. The ^{1}H and ^{13}C NMR signals corresponding to the side chain of compound **8** included three doublet methyls ($\delta_{H/C}$ 0.95/14.9, 1.05/21.0, and 1.05/21.0), one oxygenated methine ($\delta_{H/C}$ 4.72/79.9), one oxygenated methylene ($\delta_{H/C}$ 4.20, 4.62/70.6), one olefinic methine ($\delta_{H/C}$ 5.36/119.4), and one non-protonated olefinic carbon (δ_C 142.0). The COSY cross-peaks of H-20/H$_3$-21, H-20/H-22, H-22/H-23, H-25/H$_3$-26, and H-25/H$_3$-27, in combination with the HMBC correlations of H$_3$-21 with C-17, C-20, and C-22, of H-23, H-25, H$_3$-26, and H$_3$-27 with C-24 and of H$_2$-28 with C-23, C-24, and C-25 verified the side chain. In accordance with the literature, H-22 was assigned to be on the opposite side of H$_3$-21, as also suggested by the chemical shift of C-23 which resonated at 119.4 ppm. Instead, when H-22 and H$_3$-21 are co-planar, C-23 is shielded, resonating at 115–116 ppm [5]. Thus, metabolite **8** was identified as (23*E*)-22α,28-epidioxy-4α,24-dimethyl-5α-cholest-23-en-3β,8β-diol.

Compound **13** was isolated as a white amorphous solid. The ion peak at *m/z* 475.3424 observed in its HR-APCIMS was consistent with [M − H]$^-$, dictating the molecular formula $C_{29}H_{48}O_5$. The spectroscopic data of metabolite **13** related to the steroidal nucleus (Tables 1 and 2) displayed high similarity with those of **9–12**, suggesting a 3,8,11-trihydroxy-4-methyl steroidal nucleus that was further verified by the correlations observed in the COSY, HMBC and NOESY spectra (Figure 3c). Additionally, the NMR data concerning the side chain of compound **13** were rather similar to those of **8**, thus allowing for the identification of **13** as (23*E*)-22α,28-epidioxy-4α,24-dimethyl-5α-cholest-23-en-3β,8β,11β-triol.

Compound **20**, isolated as a white amorphous solid, had the molecular formula $C_{28}H_{44}O_2$, as indicated by its HR-ESIMS and NMR data. In the ^{1}H NMR spectrum of metabolite **20** evident were only one methyl on a non-protonated carbon (δ_H 0.75), three methyls on tertiary carbons (δ_H 1.03, 1.04 and 1.06), one hydroxymethylene (δ_H 3.59 and 3.81), one oxygenated methine (δ_H 3.56), three olefinic methines (δ_H 5.56, 5.73 and 5.92) and an exomethylene group (δ_H 4.79 and 4.83). The spectroscopic data of **20** (Tables 1 and 2) closely resembled those of the co-occurring **19**, with the main difference being the presence of an additional 1,2-disubstituted double bond in the side chain of **20**. The homonuclear and heteronuclear correlations observed in the COSY, HMBC, and NOESY spectra (Figure 3d) verified the 3,19-dihydroxy steroidal nucleus with a Δ^5 double bond and the proposed side chain, as well as the relative configuration of the stereogenic centers. The *E* geometry of the Δ^{22} double bond was assigned on the basis of the measured coupling constant between H-22 and H-23 (*J* = 15.7 Hz). On the basis of the above, metabolite **20** was identified as (22*E*)-24-methyl-cholesta-5,22,24(28)-trien-3β,19-diol.

Compounds **3**, **5**, **7**, **9–12**, **14–19,** and **21–26** were identified by comparison of their spectroscopic and physical characteristics with those reported in the literature as 4α,24-dimethyl-5α-cholest-24(28)-en-3β-ol (**3**) [6], (22*E*,24*R*)-4α,24-dimethyl-5α-cholest-22-en-3β-ol (**4**) [7], 4α,24-dimethyl-5α-cholest-24(28)-en-3β,8β-diol (**5**) [8], 23-oxo-4α,24-dimethyl-5α-cholest-24(28)-en-3β,8β-diol (**7**) [9], nebrosteroid M (4α,24- dimethyl-5α-cholest-24(28)-en-3β,8β,11β-triol, (**9**) [10], (22*E*,24*R*)-4α,24-dimethyl-5α-cholest-22-en-3β,8β,11β-triol (**10**) [4], nebrosteroid A (23-oxo-4α,24-dimethyl-5α-cholest-24(28)-en-3β,8β,11β-triol, (**11**) [11], 23ξ-acetoxy-4α,24-dimethyl-5α-cholest-24(28)-en-3β,8β,11β-triol (**12**) [4], (22*Z*)-4α,24ξ-dimethyl-5α-cholest-22-en-3β,8β, 11β,12α-tetraol (**14**) [4], 4α,24-dimethyl-5α-cholest-24(28)-en-3β, 8β, 18-triol (**15**) [4], (22*E*,24*R*)-4α,24-dimethyl-5α-cholest-22-en-3β,8β,18-triol (**16**) [4], 24-methyl-cholesta-5,24(28)-dien-3β-ol (**17**) [12], 24-methyl-cholesta-5,24(28)-dien-3β,7β-diol (**18**) [13], 24-methyl-cholesta-5,24(28)-dien-3β,19-diol (**19**) [14], 24-methyl-cholesta-5,24(28)-dien-3β,7β,19-triol (**21**) [15], 7β-acetoxy-24-methyl-cholesta-5,24(28)-dien-3β,19-diol (**22**) [16], 7β-acetoxy-cholest-5-en-3β,19-diol (**23**) [15], 7-oxo-24-methyl-cholesta-5,24(28)-dien-3β,19-diol (**24**) [17], 24-methyl-cholesta-7,24(28)-dien-3β,5α,6β-triol (**25**) [18], and (22*E*,24*R*)-24-methyl-cholesta-7,22-dien-3β,5α,6β-triol (**26**) [18], previously isolated from various marine organisms, mainly soft corals of the genera *Litophyton* and *Nephthea*. Even though compound **4** has been isolated in the past, only a few characteristic ^{1}H NMR resonances have been reported. Analysis of its 1D and 2D spectra allowed for the full assignment of the ^{1}H and ^{13}C chemical shifts of compound **4** (Tables 1 and 2).

2.2. Evaluation of the Biological Activity of the Isolated Metabolites

Compounds **3–7**, **9–12**, **14–20,** and **22–26**, which were isolated in sufficient amounts, were evaluated in vitro in human tumor and non-cancerous cell lines for a number of biological activities, including cytotoxicity, anti-inflammatory, anti-angiogenic, and neuroprotective activity, as well as for their effect on androgen receptor (AR)-regulated transcription.

Initially, the cytotoxic activity of metabolites **3–7**, **9–12**, **14–20,** and **22–26** was evaluated in human cancer and normal cells after 72 h of treatment. Human cervical cancer (HeLa), human breast adenocarcinoma (MCF7) cell lines, and human normal fibroblasts (BJ) were used for the screening. Among the tested compounds, **22** and **23** strongly reduced the viability of cancer cells in the low micromolar range (Table 3), compounds **9–12**, **14–16**, **18,** and **24** showed moderate cytotoxic activity, while the remaining ten steroids were proven inactive. Most of the compounds with activity against cancer cells also showed cytotoxicity toward normal cells (BJ), except for compounds **11**, **12**, **14**, **15,** and **18**. Compared to cisplatin, these compounds exhibit a wide therapeutic window because of the absence of cytotoxicity on normal human fibroblasts. Moreover, metabolite **22** was proven more active against the HeLa cell line than the reference standard cisplatin.

Table 3. Cytotoxicity (IC_{50}; μM) of compounds **3–7**, **9–12**, **14–20,** and **22–26** against human cancer cell lines and fibroblasts after 72 h of treatment. Cisplatin was used as a positive control.

Compound	HeLa	MCF7	BJ
3	>50	>50	>50
4	>50	>50	>50
5	>50	>50	>50
6	>50	>50	>50
7	>50	>50	>50
9	25.9 ± 4.9	36.4 ± 5.7	18.3 ± 4.0
10	32.9 ± 6.8	32.7 ± 1.3	4.1 ± 1.9
11	18.8 ± 6.4	21.7 ± 1.4	>50
12	15.7 ± 2.0	25.3 ± 6.5	>50
14	>50	29.1 ± 5.0	>50
15	19.0 ± 4.3	18.9 ± 0.1	>50
16	32.9 ± 5.2	33.8 ± 1.0	23.2 ± 1.4
17	>50	>50	>50
18	22.6 ± 0.4	28.6 ± 5.3	>50
19	>50	>50	>50
20	>50	>50	>50
22	7.5 ± 0.1	8.9 ± 0.0	14.8 ± 5.8
23	12.0 ± 1.7	11.2 ± 0.5	14.5 ± 3.9
24	21.4 ± 2.0	31.7 ± 0.3	45.9 ± 2.8
25	>50	>50	>50
26	>50	>50	>50
cisplatin	11.4 ± 3.8	7.7 ± 1.7	6.9 ± 0.9

Subsequently, we examined whether the isolated steroids could influence angiogenesis or inflammation in vitro. Compounds **3–7**, **9–12**, **14–20,** and **22–26** and 2-methoxy-estradiol, which is known as an anti-angiogenic drug for the treatment of tumors and was used herein as positive control [19], were tested in the migration scratch and the tube formation assays using human umbilical vein endothelial cells (HUVEC). Only non-cytotoxic concentrations in HUVECs were used for the scratch assay. Metabolites **11**, **12**, **22,** and **23** partially inhibited HUVEC migration at 20 μM after 20 h of treatment (Figure 4), while in the tube formation assay, where HUVECs may form tube-like structures, no activity was observed for the tested compounds (data not shown). Thus, all tested steroids showed either little or no antiangiogenic activity.
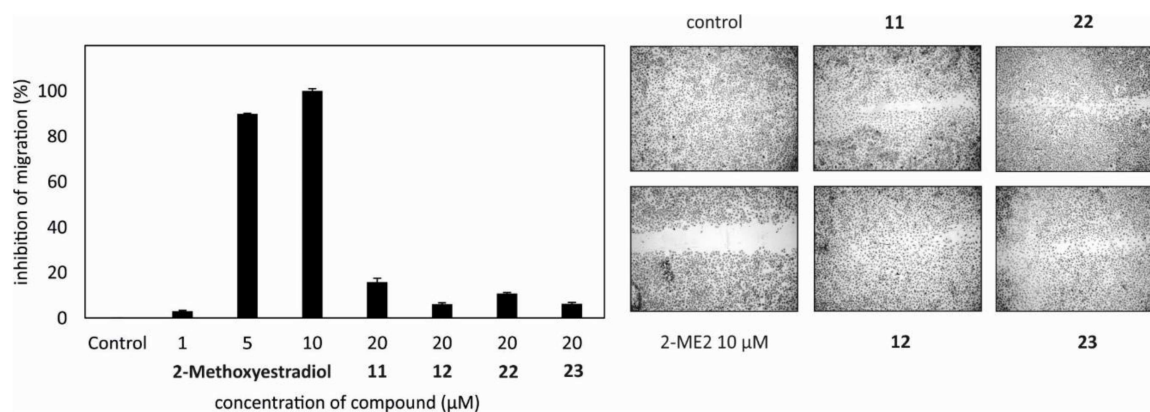
Figure 4. Compounds **11**, **12**, **22**, and **23** inhibited migration of HUVECs after 20 h of treatment at 20 µM. 2-Methoxy-estradiol was used as a positive control. The experiment was repeated three times in triplicates.
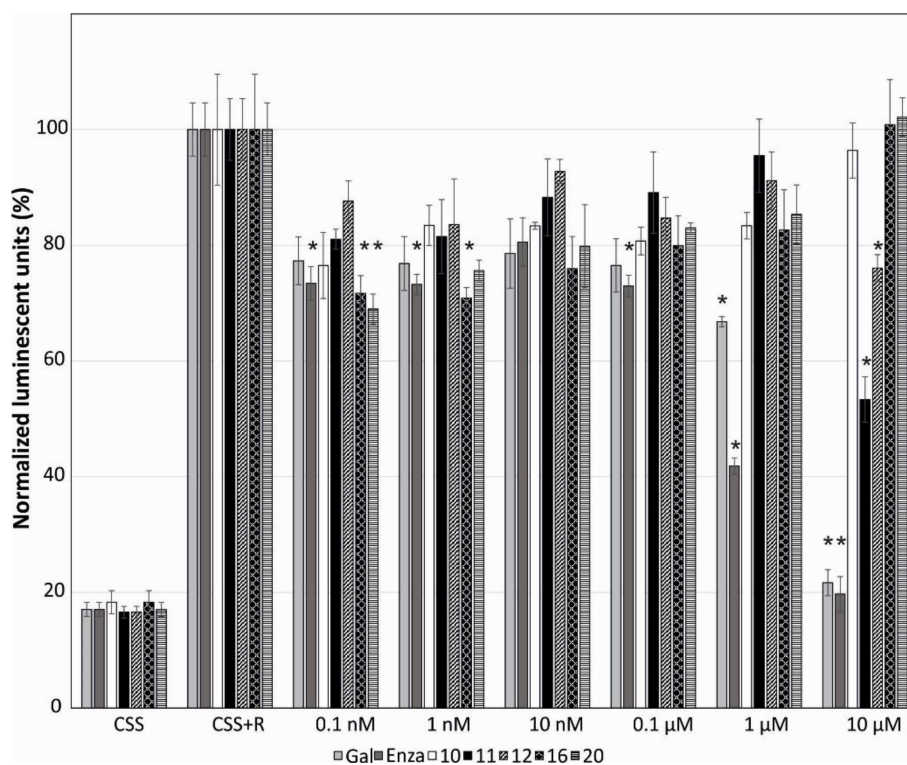

Figure 5. The influence of compounds **10**, **11**, **12**, **16**, and **20** on the androgen receptor-mediated transcription in the 22Rv1-ARE14 reporter cell line. Control cells were grown in charcoal-stripped serum medium (CSS). Cells were stimulated with either 1 nM methyltrienolone R1881 (R) or with the tested compounds in six different concentrations for 24 h in CSS. The luciferase activity was measured in the cell lysate. Enzalutamide (Enza) and galeterone (Gal) were used as positive controls. The experiment was repeated three times in triplicates. Bars with asterisk (*) are significantly different from the control (CSS+R) based on Tukey's multiple comparison test ($p \leq 0.05$).

The anti-inflammatory properties of metabolites **3**–**7**, **9**–**12**, **14**–**20**, and **22**–**26** were determined by measuring the levels of endothelial leukocyte adhesion molecule-1 (ELAM/E-selectin), which is a key molecular marker in the initiation of inflammation, expressed on the cell surface. Cell adhesion molecules (ICAM-1, VCAM-1, E-selectin) are significantly increased on the vascular endothelium activated by pro-inflammatory mediators (tumor necrosis factor α, TNFα) as a crucial step for the extravasation of leukocytes into inflamed tissue [20]. TNFα stimulates NFκB (nuclear factor

kappa-light-chain-enhancer of activated B cells) and thus E-selectin (CD62E, ELAM). Endothelial cells were pre-treated for 30 min with the tested compounds and then activated with TNFα for 4 h. Curcumin, which inhibits activation of NF-κB and thus inhibits expression and activity of the COX-2 gene induced by TNFα [21], was used as a positive control, decreasing ELAM production to 25% at 10 μM. None of the tested compounds decreased the levels of ELAM (Supplementary Materials Figure S1).

We have previously observed that several steroids with bulky or long side chains, such as galeterone derivatives or cholestanes, can also inhibit AR [22,23]. Therefore, we further analyzed the influence of the isolated steroids on AR-mediated transcription. Compounds **3–7**, **9–12**, **14–20**, and **22–26** in six different concentrations were evaluated on the reporter cell line 22Rv1-ARE14 for 24 h. Galeterone and enzalutamide, which were used as positive controls, showed a strong dose-dependent reduction of AR-regulated transcription (22% and 20% inhibition at 10 μM, respectively). Compounds **11**, **12**, **16**, and **20** showed clearly reduced luciferase activity in a dose-dependent manner, already at submicromolar concentrations (Figure 5). The strongest inhibition of AR was displayed by compound **11** at 10 μM. Surprisingly, steroids **10**, **16**, and **20** showed increased inhibition of AR (or decreased the luciferase activity) with decreasing concentrations (Figure 5). All other steroids tested inhibited AR by no more than 20% (data not shown).
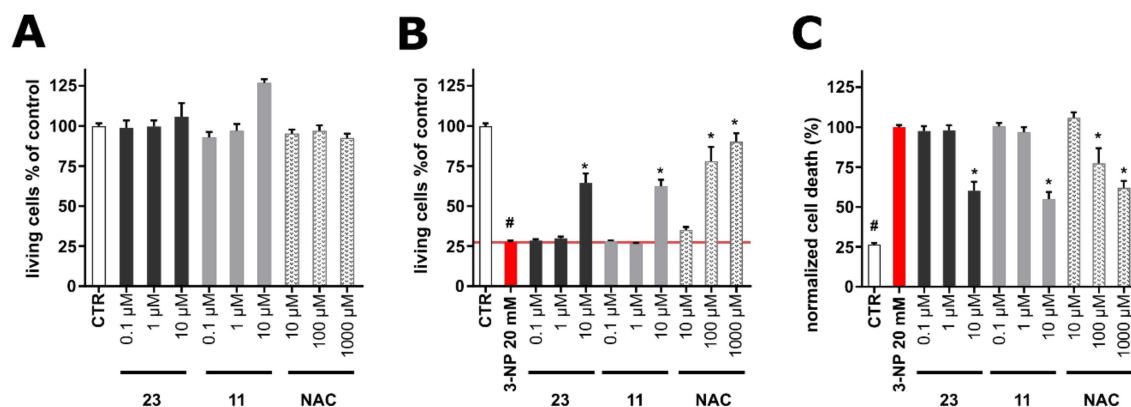
Figure 6. (**A**) Cytotoxicity of compounds **11** and **23** in human neuron-like SH-SY5Y cells after 48 h of treatment. All results are presented as mean ± standard error of the mean (SEM) from at least three independent experiments in triplicates. (**B**) Neuroprotective activity of compounds **11** and **23** in the 3-nitropropionic acid (3-NPA)-induced model of Huntington's disease on human neuron-like SH-SY5Y cells after 48 h of treatment. (**C**) Cell death of neuron-like SH-SY5Y induced by 3-NPA and the protective effect of compounds **11** and **23** after 48 h. The results are presented as mean ± standard error of the mean (SEM) from triplicates in four independent experiments ($n = 4$). *N*-acetylcysteine (NAC) was used as a positive control. * p compared with vehicle with 20 mM 3-NPA, # p compared with vehicle without 20 mM 3-NPA.

Since anti-androgens have shown neuroprotective effects in the in vivo model of Huntington's disease [24], selected compounds that showed cytotoxic activity and moderate activity in the migration scratch assay were tested for their cytotoxicity on differentiated human SH-SY5Y cells (neuron-like cells). Specifically, based on the combined results obtained for compounds **3–7**, **9–12**, **14–20**, and **22–26** in the cytotoxicity assay, the anti-inflammatory activity assay, the migration scratch assay, and the tube formation assay in HUVECs, as well as in the reporter assay with AR, compounds **11** and **23** were selected as the two most active compounds that were subsequently evaluated for their neuroprotective activity. As shown in Figure 6A, compounds **11** and **23**, as well as *N*-acetylcystein (NAC) that was used as a positive control, did not show cytotoxic, but rather stimulatory activity. In order to evaluate the potential neuroprotective effect of the compounds, neuroblastoma cell line SH-SY5Y was differentiated for 48 h and further exposed to 20 mM 3-nitropropionic acid (3-NPA)

as an agent mimicking Huntington's disease in vitro [25]. 3-NPA was used alone or in co-treatment with the tested compounds at concentrations of 0.1–10 μM. As shown in Figure 6B, 3-NPA caused dramatic (approx. 70%) decrease in cell viability determined by the Calcein AM assay. The positive control (NAC) showed partial (cell viability 77.9 ± 8.99% at 100 μM) or almost complete (cell viability 90.2 ± 5.28% at 1000 μM) protection of cells from the negative effect of 3-NPA. Compounds **11** and **23** showed significant protective effects at 10 μM (cell viability 64.4 ± 6.02% for **11** and 62.5 ± 3.95% for **23**), comparable to 100 μM of the positive control NAC. Being encouraged by the promising results, we further analyzed the protective effects of **11** and **23** using an orthogonal method (propidium iodide (PI) assay) to verify their activity. In general, PI as a positively charged dye is associated with an increase of cell damage or death, since it penetrates cells with cell-disrupted membranes [26]. Within the 3-NPA model, its toxic effect was considered as 100% of the PI signal and thus reduction of cell death was determined. As shown in Figure 6C, compounds **11** and **23** significantly reduced cell death (maximal effect at 10 μM) in a manner similar to NAC (100 μM, 77.2 ± 9.53%; 1000 μM, 62.1 ± 4.19%), thus confirming the protective effects of **11** and **23** observed in the viability assay.

3. Materials and Methods

3.1. General Experimental Procedures

Optical rotations were measured on a Krüss polarimeter (A. KRÜSS Optronic GmbH, Hamburg, Germany) equipped with a 0.5 dm cell. UV spectra were recorded on a Lambda 40 UV/Vis spectrophotometer (Perkin Elmer Ltd., Beaconsfield, UK). IR spectra were obtained on an Alpha II FTIR spectrometer (Bruker Optik GmbH, Ettlingen, Germany). Low-resolution EI mass spectra were measured on a Thermo Electron Corporation DSQ mass spectrometer (Thermo Fisher Scientific, Bremen, Germany). High-resolution APCI or ESI mass spectra were measured on a LTQ Orbitrap Velos mass spectrometer (Thermo Fisher Scientific, Bremen, Germany). NMR spectra were recorded on Bruker AC 200, DRX 400, and Avance NEO 950 (Bruker BioSpin GmbH, Rheinstetten, Germany) and Varian 600 (Varian, Inc., Palo Alto, CA, USA) spectrometers. Chemical shifts are given on the δ (ppm) scale with reference to the solvent signals. The 2D NMR experiments (HSQC, HMBC, COSY, NOESY) were performed using standard Bruker or Varian pulse sequences. Column chromatography separations were performed with Kieselgel 60 (Merck, Darmstadt, Germany). HPLC separations were conducted on a Waters 600 liquid chromatography pump equipped with a Waters 410 differential refractometer (Waters Corporation, Milford, MA, USA), using a Kromasil 100 C_{18} (25 cm × 8 mm i.d.) column (MZ-Analysentechnik GmbH, Mainz, Germany). TLC were performed with Kieselgel 60 F_{254} aluminum plates (Merck, Darmstadt, Germany) and spots were detected after spraying with 25% H_2SO_4 in MeOH reagent and heating at 100 °C for 1 min.

3.2. Biological Material

Specimens of *S. polydactyla* were hand-picked by SCUBA diving at a depth of 10 m from the reefs near the National Institute of Oceanography and Fisheries (NOIF), Hurghada, Egypt (GPS coordinates 27°17′06″N, 33°46′24″E) in June 2015 and transported to the laboratory in ice chests, where they were stored at −20 °C until analyzed. A voucher specimen has been deposited at the animal collection of NOIF in Hurghada and the animal collection of the Section of Pharmacognosy and Chemistry of Natural Products, Department of Pharmacy, National and Kapodistrian University of Athens (ATPH/MP0533).

3.3. Extraction and Isolation

Specimens of the freeze-dried gorgonian (119.9 g) were exhaustively extracted with mixtures of CH_2Cl_2/MeOH (2:1) at room temperature. Evaporation of the solvents under vacuum afforded a dark green residue (18.5 g) which was submitted to vacuum column chromatography on silica gel using cHex with increasing amounts of EtOAc followed by EtOAc with increasing amounts of MeOH as eluent to yield 9 fractions (A–I). Fraction B (2.5 g, 30–50% EtOAc in cHex) was fractionated by vacuum

column chromatography on silica gel using mixtures of cHex/EtOAc of increasing polarity as mobile phase to yield 6 fractions (B1–B6). Fraction B6 (0.5 g, 20–30% EtOAc in cHex) was further fractionated by gravity column chromatography on silica gel using mixtures of cHex/EtOAc of increasing polarity as mobile phase to afford 10 fractions (B6a–B6j). Fractions B6e, B6g, and B6h were subjected repeatedly to reversed-phase HPLC, using MeOH/H_2O (100:0 and 98:2) as eluent to yield compounds **3** (9.9 mg), **4** (8.8 mg), **5** (1.8 mg), **6** (5.9 mg), **8** (0.8 mg), and **17** (14.0 mg). Fraction C (2.5 g, 60–70% EtOAc in cHex) was submitted to vacuum column chromatography on silica gel using mixtures of cHex/EtOAc of increasing polarity as mobile phase to afford 9 fractions (C1–C9). Fractions C5, C6, C7, and C8 were subjected repeatedly to reversed-phase HPLC using MeOH/H_2O (100:0, 98:2, and 97:3) as eluent to afford compounds **1** (0.7 mg), **2** (0.3 mg), **7** (6.3 mg), **9** (5.7 mg), and **10** (5.7 mg). Fraction D (0.9 g, 80–90% EtOAc in cHex) was fractionated by gravity column chromatography on silica gel using cHex with increasing amounts of Me_2CO as mobile phase to afford 18 fractions (D1–D18). Fractions D8, D9, D11, and D12 were subjected repeatedly to reversed-phase HPLC using MeOH/H_2O (100:0 and 98:2) as eluent to yield compounds **11** (4.0 mg), **12** (2.2 mg), **13** (1.3 mg), **14** (1.1 mg), **15** (9.4 mg), and **16** (2.3 mg). Fraction E (0.23 g, 100% EtOAc) was fractionated by gravity column chromatography on silica gel using cHex with increasing amounts of Me_2CO as mobile phase to afford 10 fractions (E1–E10). Fractions E3, E5, and E6 were subjected repeatedly to reversed-phase HPLC using mixtures of MeOH/H_2O (100:0 and 97:3) as eluent to yield compounds **18** (1.7 mg), **19** (17.5 mg), **20** (2.0 mg), **22** (2.1 mg), and **23** (1.0 mg). Fraction G (1.7 g, 50% MeOH in EtOAc) was separated by vacuum column chromatography on silica gel using cHex with increasing amounts of EtOAc and EtOAc with increasing amounts of MeOH to yield 7 fractions (G1–G7). Fractions G5 and G7 were subjected repeatedly to reversed-phase HPLC using MeOH/H_2O (100:0 and 97:3) as eluent to yield compounds **24** (6.9 mg), **25** (2.0 mg), and **26** (3.1 mg). Fraction I (5.1 g, 100% MeOH) was subjected to vacuum column chromatography on silica gel using cHex with increasing amounts of EtOAc followed by EtOAc with increasing amounts of MeOH to afford 11 fractions (I1–I11). Fractions I6 and I7 were combined and subjected repeatedly to reversed-phase HPLC using MeOH (100%) as eluent to yield compound **21** (2.3 mg).

(9*E*,22*E*,24*R*)-3β-Hydroxy-4α,24-dimethyl-8,9-seco-5α-cholesta-9(11),22-dien-8-one (**1**): White amorphous solid; ^1H and ^{13}C NMR data, see Tables 1 and 2; HR-APCIMS *m/z* 429.3724 [M + H]$^+$ (calcd. for $C_{29}H_{49}O_2$, 429.3727).

(9*E*)-3β-Hydroxy-4α,24-dimethyl-8,9-seco-5α-cholesta-9(11),24(28)-dien-8-one (**2**): White amorphous solid; ^1H NMR data, see Table 1; HR-APCIMS *m/z* 429.3725 [M + H]$^+$ (calcd. for $C_{29}H_{49}O_2$, 429.3727).

(22*E*,24*R*)-4α,24-Dimethyl-5α-cholest-22-en-3β,8β-diol (**6**): White amorphous solid; $[\alpha]_D^{20}$ + 68 (*c* 0.25, CHCl$_3$); UV (CHCl$_3$) λ_{max} (log ε) 206 (2.85); IR (thin film) ν_{max} 3440, 2954, 2856, 1466, 1384, 964 cm^{-1}; ^1H and ^{13}C NMR data, see Tables 1 and 2; HR-APCIMS *m/z* 413.3773 [M − H_2O + H]$^+$ (calcd. for $C_{29}H_{49}O$, 413.3778).

(23*E*)-22α,28-Epidioxy-4α,24-dimethyl-5α-cholest-23-en-3β,8β-diol (**8**): White amorphous solid; $[\alpha]_D^{20}$ −50 (*c* 0.02, CHCl$_3$); UV (CHCl$_3$) λ_{max} (log ε) 206 (3.94), 225 (3.84); IR (thin film) ν_{max} 3458, 2927, 2861, 1723, 1462, 1378, 1243, 1013 cm^{-1}; ^1H and ^{13}C NMR data, see Tables 1 and 2; HR-APCIMS *m/z* 459.3475 [M − H]$^−$ (calcd. for $C_{29}H_{47}O_4$, 459.3480).

(23*E*)-22α,28-Epidioxy-4α,24-dimethyl-5α-cholest-23-en-3β,8β,11β-triol (**13**): White amorphous solid; $[\alpha]_D^{20}$ +30 (*c* 0.1, CHCl$_3$); UV (CHCl$_3$) λ_{max} (log ε) 206 (3.26), 230 (2.97); IR (thin film) ν_{max} 3403, 2923, 2873, 1725, 1450, 1377, 1261, 1045 cm^{-1}; ^1H and ^{13}C NMR data, see Tables 1 and 2; HR-APCIMS *m/z* 475.3424 [M − H]$^−$ (calcd. for $C_{29}H_{47}O_5$, 475.3429).

(22*E*)-24-Methyl-cholesta-5,22,24(28)-trien-3β,19-diol (**20**): White amorphous solid; $[\alpha]_D^{20}$ −133 (*c* 0.03, CHCl$_3$); UV (CHCl$_3$) λ_{max} (log ε) 206 (3.61), 232 (3.76); IR (thin film) ν_{max} 3433, 2919, 2857, 1462, 1377, 1261, 1037 cm^{-1}; ^1H and ^{13}C NMR data, see Tables 1 and 2; HR-ESIMS *m/z* 411.3271 [M − H]$^−$ (calcd. for $C_{28}H_{43}O_2$, 411.3269).

3.4. Cell Culture

The tested compounds were dissolved in DMSO to afford 10 mM stock solutions. Human cervical carcinoma (HeLa) and human breast adenocarcinoma (MCF7) cell lines were purchased from European Collection of Authenticated Cell Cultures (ECACC, Salisbury, UK) and cultivated in Dulbecco's Modified Eagle Medium (DMEM) (Merck, Darmstadt, Germany), as previously reported [27]. Human umbilical vein endothelial cells (HUVECs) were a kind gift of Prof. Jitka Ulrichová (Faculty of Medicine and Dentistry, Palacky University, Olomouc, Czech Republic). The cultivation and assay was performed in endothelial cell proliferation medium (ECPM, Provitro, Berlin, Germany) [23]. The 22Rv1-ARE14 reporter cell line [28] was a generous gift of Prof. Zdeněk Dvořák (Department of Cell Biology and Genetics, Palacky University). The 22Rv1-ARE14 cell line was grown in Roswell Park Memorial Institute 1640 Medium (RPMI 1640) [22]. All cells were maintained in a humidified CO_2 incubator at 37 °C using the standard trypsinization procedure twice or three times a week. The SH-SY5Y human neuroblastoma cell line (ECACC, Salisbury, UK) was cultivated in DMEM and Ham's F12 Nutrient Mixture (DMEM:F12, 1:1), as previously described [25]. Cells were used up to twenty passages. All trans-retinoic acid (10 μM) in 1% FBS DMEM/F12 medium was added to SH-SY5Y cells to achieve differentiation conditions [29,30], to reach longer neurites and reduced proliferation (48 h). All cells were maintained in a humidified CO_2 incubator at 37 °C using the standard trypsinization procedure twice or three times a week.

3.5. Evaluation of Cytotoxicity

In cytotoxicity assays, cancer cells were treated with six different concentrations of each tested compound for 72 h. Cells were stained with resazurin and IC_{50} values were calculated as previously reported [26]. Triplicates from at least three independent experiments were used. For the ELAM assay, the Calcein AM (Molecular Probes, Invitrogen, Karlsruhe, Germany) cytotoxicity assay, which assessed HUVEC viability after 4 h treatment, was used as previously described [31].

3.6. Cell-Surface ELISA CD62E (E-Selectin, ELAM)

An enzyme-linked immunosorbent assay (ELISA) was used to detect the levels of the cell adhesion molecule ELAM in HUVEC cells after 30 min of incubation with the tested compounds and 4 h of stimulation with TNFα, as previously described [31].

3.7. Migration Scratch Assay

The scratch test was performed with HUVEC cells and evaluated after 20 h of treatment, as previously reported [23].

3.8. AR-Transcriptional Reporter Assay

AR-transcriptional reporter assays were performed on 22Rv1-ARE14 cells after 24 h of incubation, as previously described [22].

3.9. SH-SY5Y Cell Treatments and Evaluation of Cell Viability/Cytotoxicity

Cell viability of neuron-like SH-SY5Y cells growing in 96-well plates (7000 cells/well) 24 h after treatment was evaluated using the Calcein AM assay [27], with minor modification of Calcein AM concentration (0.75 μM). Cell death of SH-SY5Y cells (20,000 cells/well) was determined using the propidium iodide (PI) assay according to Stone et al. with a slight modification [32]. Briefly, PI solution in PBS is added to cell medium to reach concentration 1 μg/mL, incubated for 15 min at room temperature and quantified at 535/617 nm (excitation/emission) by Infinite M200 Pro reader (Tecan, Austria). The resulting fluorescence of 3-NPA toxin was considered as 100% cell death. In the assays, neuron-like cells were treated with the tested compounds in 0.1–10 μM concentration range for 48 h. DMSO-treated cells (≤0.1% *v/v*) were used as healthy controls.

3.10. Statistical Analysis

All data are expressed as mean ± SD or SEM. Data were evaluated by non-parametric Kruskal–Wallis test followed by post-hoc Mann–Whitney test (Figure 6) with sequential Bonferroni correction of *p*-values or ANOVA followed by Tukey's multiple comparison test (Figure 5) using the PAST (version 1.97) software package [33]. *p*-values < 0.05 were considered statistically significant.

4. Conclusions

The chemical analysis of the organic extract of the soft coral *S. polydactyla* collected from the Hurghada reef in the Red Sea resulted in the isolation of 26 steroids, with six of them (**1**, **2**, **6**, **8**, **13,** and **20**) being new natural products. Among them, **1** and **2** display the rare 8,9-seco-cholestane steroidal nucleus. To the best of our knowledge, dictyoneolone, isolated from a sponge of the genus *Dictyonella*, is the only previously reported 4-methyl-8,9-seco-cholestane derivative [34]. Evaluation of cytotoxic, anti-inflammatory, anti-angiogenic, and neuroprotective activity of the majority of the isolated metabolites that were isolated in adequate quantities revealed significant cytotoxicity in the low micromolar range against the HeLa and MCF7 cancer cell lines for compounds **22** and **23**, while compounds **11**, **12**, **22,** and **23** inhibited the migration of endothelial cells at 20 μM. Most of the compounds with activity against cancer cells also showed cytotoxicity toward normal cells (BJ), except for compounds **11**, **12**, **14**, **15,** and **18**. Compared to cisplatin, these compounds have therefore a broad therapeutic window due to low or zero cytotoxicity on normal human fibroblasts. Moreover, metabolite **22** was more active against HeLa cells than cisplatin used as positive control. Furthermore, the effect of the isolated metabolites on AR-regulated transcription was evaluated in vitro in human tumor and non-cancerous cells, with compound **11** exhibiting the strongest inhibition of AR at 10 μM. It is worth-noting that metabolites **10**, **16,** and **20** displayed increased inhibition of AR with decreasing concentrations. In addition, compounds **11** and **23** showed neuroprotective activity on neuron-like SH-SY5Y cells.

References

1. Kotb, M.M.A.; Hanafy, M.H.; Rirache, H.; Matsumura, S.; Al-Sofyani, A.A.; Ahmed, A.G.; Bawazir, G.; Al-Horani, F.A. Status of coral reefs in the Red Sea and Gulf of Aden region. In *Status of Coral Reefs of the World: 2008*; Wilkinson, C., Ed.; Global Coral Reef Monitoring Network and Reef and Rainforest Research Centre: Townsville, Australia, 2008; pp. 67–78.

2. Carroll, A.R.; Copp, B.R.; Davis, R.A.; Keyzers, R.A.; Prinsep, M.R. Marine natural products. *Nat. Prod. Rep.* **2020**, *37*, 175–223. [CrossRef] [PubMed]

3. MarinLit. A Database of the Marine Natural Products Literature. Available online: http://pubs.rsc.org/marinlit/ (accessed on 30 September 2020).

4. Končić, M.; Ioannou, E.; Sawadogo, W.; Abdel-Razik, A.; Vagias, C.; Diederich, M.; Roussis, V. 4*a*-Methylated steroids with cytotoxic activity from the soft coral *Litophyton mollis*. *Steroids* **2016**, *115*, 130–135. [CrossRef] [PubMed]

5. Yu, S.; Deng, Z.; van Ofwegen, L.; Proksch, P.; Lin, W. 5,8-Epidioxysterols and related derivatives from a Chinese soft coral *Sinularia flexibilis*. *Steroids* **2006**, *71*, 955–959. [CrossRef] [PubMed]

6. Kokke, W.; Bohlin, L.; Fenical, W.; Djerassi, C. Novel dinoflagellate 4*α*-methylated sterols from four caribbean gorgonians. *Phytochemistry* **1982**, *21*, 881–887. [CrossRef]

7. Kobayashi, M.; Ishizaka, T.; Mitsuhashi, H. Marine sterols X. Minor constituents of the sterols of the soft coral *Sarcophyton glaucum*. *Steroids* **1982**, *40*, 209–221. [CrossRef]

8. Mehta, G.; Venkateswarlu, Y.; Rama, R.M.; Uma, R. A novel 4*α*-methyl sterol from the soft coral *Nephthea chabroli*. *J. Chem. Res.* **1999**, *23*, 628–629. [CrossRef]

9. Bortolotto, M.; Braekman, J.; Daloze, D.; Tursch, B. Chemical studies of marine invertebrates. XXIX. 4*α*-methyl-3*β*,8*β*-dihydroxy-5*α*-ergost-24(28)-en-23-one, a novel polyhydroxygenated sterol from the soft coral *litophyton viridis*. *Steroids* **1977**, *30*, 159–164. [CrossRef]

10. Cheng, S.; Huang, Y.; Wen, Z.; Hsu, C.; Wang, S.; Dai, C.; Duh, C. New 19-oxygenated and 4-methylated steroids from the formosan soft coral *Nephthea chabroli*. *Steroids* **2009**, *74*, 543–547. [CrossRef]

11. Huang, Y.; Wen, Z.; Wang, S.; Hsu, C.; Duh, C. New anti-inflammatory 4-methylated steroids from the formosan soft coral *Nephthea chabroli*. *Steroids* **2008**, *73*, 1181–1186. [CrossRef]

12. Viegelmann, C.; Parker, J.; Ooi, T.; Clements, C.; Abbott, G.; Young, L.; Kennedy, J.; Dobson, A.; Edrada-Ebel, R. Isolation and identification of antitrypanosomal and antimycobacterial active steroids from the sponge *Haliclona simulans*. *Mar. Drugs* **2014**, *12*, 2937–2952. [CrossRef]

13. Riccardis, F.; Minale, L. Marine sterols side-chain-oxygenated sterols, possibly of abiotic origin, from the new caledonian sponge *stelodoryx chlorophylla*. *J. Nat. Prod.* **1993**, *56*, 282–287. [CrossRef]

14. Iguchi, K.; Saitou, S.; Yamada, Y. Novel 19-oxygenated sterols from the okinawan soft coral *Litophyton viridis*. *Chem. Pharm. Bull.* **1989**, *37*, 2553–2554. [CrossRef]

15. Cheng, S.; Dai, C.; Duh, C. New 4-methylated and 19-oxygenated steroids from the formosan soft coral *Nephthea erecta*. *Steroids* **2007**, *72*, 653–659. [CrossRef] [PubMed]

16. Ellithey, M.; Lall, N.; Hussein, A.; Meyer, D. Cytotoxic, cytostatic and HIV-1 PR inhibitory activities of the soft coral *Litophyton arboretum*. *Mar. Drugs* **2013**, *11*, 4917–4936. [CrossRef]

17. Duh, C.; Wang, S.; Chu, M.; Sheu, J. Cytotoxic sterols from the soft coral *Nephthea erecta*. *J. Nat. Prod.* **1998**, *61*, 1022–1024. [CrossRef]

18. Iorizzi, M.; Minale, L.; Riccio, R. Polar steroids from the marine scallop *Patinopecten yessoensis*. *J. Nat. Prod.* **1988**, *51*, 1098–1103. [CrossRef]

19. Sattler, M.; Quinnan, L.R.; Pride, Y.B.; Gramlich, J.L.; Chu, S.C.; Even, G.C.; Kraeft, S.-K.; Chen, L.B.; Salgia, R. 2-Methoxyestradiol alters cell motility, migration, and adhesion. *Blood* **2003**, *102*, 289–296. [CrossRef]

20. Trepels, T.; Zeiher, A.M.; Fichtlscherer, S. The endothelium and inflammation. *Endothelium* **2006**, *13*, 423–429. [CrossRef]

21. Zhang, F.; Altorki, N.K.; Mestre, J.R.; Subbaramaiah, K.; Dannenberg, A.J. Curcumin inhibits cyclooxygenase-2 transcription in bile acid- and phorbol ester-treated human gastrointestinal epithelial cells. *Carcinogenesis* **1999**, *20*, 445–451. [CrossRef]

22. Jorda, R.; Řezníčková, E.; Kiełczewska, U.; Maj, J.; Morzycki, J.W.; Siergiejczyk, L.; Bazgier, V.; Berka, K.; Rárová, L.; Wojtkielewicz, A. Synthesis of novel galeterone derivatives and evaluation of their in vitro activity against prostate cancer cell lines. *Eur. J. Med. Chem.* **2019**, *179*, 483–492. [CrossRef]

23. Rárová, L.; Sedlák, D.; Oklestkova, J.; Steigerová, J.; Liebl, J.; Zahler, S.; Bartůněk, P.; Kolář, Z.; Kohout, L.; Kvasnica, M.; et al. The novel brassinosteroid analog BR4848 inhibits angiogenesis in human endothelial cells and induces apoptosis in human cancer cells in vitro. *J. Steroid Biochem. Mol. Biol.* **2018**, *178*, 263–271.

24. Calderon Guzman, D.; Bratoeff, E.; Chávez-Riveros, A.; Osnaya, N.; Barragan, G.; Hernandez Garcia, E.; Olguín, H.; Garcia, E. Effect of two antiandrogens as protectors of prostate and brain in a Huntington's animal model. *Anticancer Agents Med. Chem.* **2014**, *14*, 1293–1301. [CrossRef] [PubMed]

25. Colle, D.; Santos, D.; Hartwig, J.; Godoi, M.; Engel, D.; de Bem, A.; Braga, A.; Farina, M. Succinobucol, a lipid-lowering drug, protects against 3-nitropropionic acid-induced mitochondrial dysfunction and oxidative stress in SH-SY5Y cells via upregulation of glutathione levels and glutamate cysteine ligase activity. *Mol. Neurobiol.* **2016**, *53*, 1280–1295. [CrossRef] [PubMed]

26. Dengler, W.A.; Schulte, J.; Berger, D.P.; Mertelsmann, R.; Fiebig, H.H. Development of a propidium iodide fluorescence assay for proliferation and cytotoxicity assays. *Anticancer Drugs* **1995**, *6*, 522–532. [CrossRef]

27. Rárová, L.; Steigerová, J.; Kvasnica, M.; Bartůněk, P.; Křížová, K.; Chodounská, H.; Kolář, Z.; Sedlák, D.; Oklestkova, J.; Strnad, M. Structure activity relationship studies on cytotoxicity and the effects on steroid receptor of AB-functionalized cholestanes. *J. Steroid Biochem. Mol. Biol.* **2016**, *159*, 154–169. [CrossRef]

28. Bartonkova, I.; Novotna, A.; Dvorak, Z. Novel stably transfected human reporter cell line AIZ-AR as a tool for an assessment of human androgen receptor transcriptional activity. *PLoS ONE* **2015**, *10*, e0121316. [CrossRef]

29. Cheung, Y.-T.; Lau, W.K.-W.; Yu, M.-S.; Lai, C.S.-W.; Yeung, S.-C.; So, K.-F.; Chang, R.C.-C. Effects of all-trans-retinoic acid on human SH-SY5Y neuroblastoma as in vitro model in neurotoxicity research. *Neurotoxicology* **2009**, *30*, 127–135. [CrossRef]

30. Dwane, S.; Durack, E.; Kiely, P.A. Optimising parameters for the differentiation of SH-SY5Y cells to study cell adhesion and cell migration. *BMC Res. Notes* **2013**, *6*, 366. [CrossRef]

31. Morrogh-Bernard, H.C.; Foitová, I.; Yeen, Z.; Wilkin, P.; de Martin, R.; Rárová, L.; Doležal, K.; Nurcahyo, W.; Olšanský, M. Self-medication by orang-utans (*Pongo pygmaeus*) using bioactive properties of *Dracaena cantleyi*. *Sci. Rep.* **2017**, *7*, 16653. [CrossRef]

32. Stone, W.L.; Qui, M.; Smith, M. Lipopolysaccharide enhances the cytotoxicity of 2-chloroethyl ethyl sulfide. *BMC Cell Biol.* **2003**, *4*, 1. [CrossRef]

33. Hammer, O.; Harper, D.A.T.; Ryan, P.D. PAST: Paleontological statistics software package for education and data analysis. *Palaeontol. Electron.* **2001**, *4*, 9.

34. Woo, J.-K.; Yun, J.-H.; Ahn, S.; Sim, C.J.; Noh, M.; Oh, D.-C.; Oh, K.-B.; Shin, J. Dictyoneolone, a B/C ring juncture-defused steroid from a *Dictyonella* sp. sponge. *Tetrahedron Lett.* **2018**, *59*, 2021–2024. [CrossRef]

Supplementary material V.

Kiełczewska, U.; Jorda, R.; Gonzalez, G.; Morzycki, J. W.; Ajani, H.; Svrčková, K.; Štěpánková, Š.; Wojtkielewicz, A., The synthesis and cholinesterase inhibitory activities of solasodine analogues with seven-membered F ring. *The Journal of Steroid Biochemistry and Molecular Biology* **2021,** *205***, 105776.**

The synthesis and cholinesterase inhibitory activities of solasodine analogues with seven-membered F ring

Urszula Kiełczewska [a,1], Radek Jorda [b,c,1], Gabriel Gonzalez [b,d], Jacek W. Morzycki [a], Haresh Ajani [e], Katarína Svrčková [f], Šárka Štěpánková [f], Agnieszka Wojtkielewicz [a,*]

[a] *Faculty of Chemistry, University of Białystok, K. Ciołkowskiego 1K, 15-245, Białystok, Poland*
[b] *Laboratory of Growth Regulators, Palacký University & Institute of Experimental Botany of The Czech Academy of Sciences, Šlechtitelů 27, 78371, Olomouc, Czech Republic*
[c] *Institute of Molecular and Translational Medicine, Faculty of Medicine and Dentistry, Palacký University, Hněvotínská 5, 77900, Olomouc, Czech Republic*
[d] *Department of Neurology, University Hospital Olomouc and Faculty of Medicine and Dentistry, Palacky University Olomouc, Czech Republic*
[e] *Institute of Organic Chemistry and Biochemistry of the Czech Academy of Sciences, Flemingovo nam. 2, 166 10, Prague 6, Czech Republic*
[f] *Department of Biological and Biochemical Sciences, Faculty of Technology, University of Pardubice, Czech Republic*

ARTICLE INFO

ABSTRACT

Solasodine analogues containing a seven-membered F ring with a nitrogen atom placed at position 22a were prepared from diosgenin or tigogenin in a four-step synthesis comprising of the simultaneous opening of the F-ring and introduction of cyanide in position 22α, activation of the 26-hydroxyl group as mesylate, nitrile reduction, and N-cyclization. Solasodine, six obtained 22a(N)-homo analogues, as well as four 26a-homosolasodine derivatives and their open-chain precursors (13 in total) were tested as potential inhibitors of acetyl- and butyryl-cholinesterases and showed activity at micromolar concentrations. The structure-activity relationship study revealed that activities against studied esterases are affected by the structure of E/F rings and the substitution pattern of ring A. The most potent compound **8** acted as non-competitive inhibitors and exerted $IC_{50} = 8.51$ μM and 7.05 μM for eeAChE and eqBChE, respectively. Molecular docking studies revealed the hydrogen bond interaction of **8** with S293 of AChE; further rings are stabilized *via* hydrophobic interaction (ring A) or interaction with Y341 and W286 (rings B and C). Biological experiments showed no neurotoxicity of differentiated SH-SY5Y cells. More importantly, results from neuroprotective assay based on glutamate-induced cytotoxicity revealed that most derivatives had the ability to increase the viability of differentiated SH-SY5Y cells in comparison to galantamine and lipoic acid assayed as standards. The newly synthesized solasodine analogues are able to inhibit and to bind cholinesterases in noncompetitive mode of inhibition and exhibited neuroprotection potential of differentiated neuroblastoma cells after Glu-induced toxicity.

1. Introduction

Solanum alkaloids have been tested for a wide range of biological activities including anticholinesterase activity [1–4]. Cholinesterases (ChEs) represent a group of enzymes with hydrolytic properties. The most pronounced members, acetylcholinesterase (AChE) and butyrylcholinesterase (BChE), are responsible for the terminating the transmission of nerve signals by hydrolysing cholinergic neurotransmitter acetylcholine in the brain and periphery tissues.

Cholinesterases are mainly associated with the pathology of Alzheimer's disease (AD), Myasthenia gravis, and glaucoma, where the high activity of these enzymes (mainly AChE) is present. They also have notable non-catalytic functions contributing to amyloid aggregation. Nowadays, Alzheimer's disease is the most common cause of dementia. It is considered a progressive and irreversible degenerative disorder of the brain with memory loss and behavior change, followed by declining cognition, language, and ability to perform activities of daily living. It is associated with the loss of presynaptic markers of the cholinergic system. Important signs of the disease include the presence of neurofibrillary tangles and amyloid depositions in the brain [5,6]. Currently, inhibition of both cholinesterases (donepezil, galantamine, rivastigmine) along with antagonism of *N*-methyl-D-aspartate (NMDA)

---

receptors (memantine) were found to be the only effective therapeutic approach for treating Alzheimer's disease until now [7,8].

To date, three AChE inhibitors, donepezil, galantamine, and rivastigmine are approved for the treatment of different stages of AD together with *N*-methyl-D-aspartate antagonist memantine (Fig. 1) [8]. All inhibitors markedly differ in mechanistic and pharmacokinetic properties, but significant distinctions in efficacy have not been reported. They all exert favorable tolerability and a safe clinical profile with common adverse effects such as diarrhea, nausea, and vomiting [9]. Still, current research is focused on the development or natural isolation of new candidates based on several chemotypes, including steroids [4,10–13].

Previously, we described preparation of 26a-homosolasodine derivatives from readily available diosgenin (Fig. 2) [14]. Herein, we report the synthesis of homosolasodine analogues differing in nitrogen atom position (22a) (Fig. 2). The change of the nitrogen atom placement resulted in a different spiro bond character (alteration from 5/6 spirohemiaminal present in natural steroid alkaloids or 5/7 spirohemiaminal in 26a-homo analogues to 5/7 spiroether), that could significantly affect reactivity and biological activity of the designed compounds.

We studied the anticholinesterase activity of prepared derivatives, expressed the type of inhibition, and determined the effect on neuroblastoma cell line SH-SY5Y. The most potent derivative exhibited a single-digit micromolar inhibition value against eeAChE and eqBChE and acted as a noncompetitive inhibitor. Molecular binding studies were done to compare the binding of the derivative to human AChE and BChE to binding capabilities of solasodine.

2. Results and discussion

2.1. Chemistry

In previous studies, we proved that the diosgenin reaction with trimethylsilyl cyanide (TMSCN) under BF$_3$·OEt$_2$ catalysis took an unexpected course and led stereoselectively to (22*R*,25*R*)-3β-benzoyloxy-22-cyanofurost-5-en-26-ol (**2**) in 55 % yield in a single step (Scheme 1, Table 1, entry 1) . The absolute 22*R* configuration of the obtained product was unambiguously established by an X-ray analysis of compound **4** (Scheme 1) that is a 26-mesyl derivative of compound **2** [14].

We recognized this compound as a convenient intermediate for synthesis of unknown solasodine analogues containing a seven-membered F ring with a nitrogen atom placed at 22a position (Fig. 2). We began our study with a detailed investigation of the diosgenin benzoate reaction with TMSCN. The influence of various factors, such as type of Lewis or Bronsted acids (BF$_3$·OEt$_2$, TMSOTf, Tf$_2$NH, TfOH), amount of TMSCN, reaction time, and solvent used was examined to find the optimal reaction conditions. The results obtained are presented in Table 1. In all cases, the main product was nitrile **2**. The best yield (77 %) was obtained using 0.5 equiv. of BF$_3$·OEt$_2$ as catalyst in dichloromethane and a short reaction time (10 min; Table 1 entry 5). An extended time of reaction or use of a proton acid (Tf$_2$NH) resulted in the formation of a byproduct, 6β-cyano-3α,5-cyclosteroid-22-nitrile derivative **3**, *via* the involvement of a non-classical carbocation formed under

reaction conditions from the homoallylic system present in the steroid AB ring moiety (Table 1, entries 3, 9, and 10) [15].

Our strategy for the synthesis of desired solasodine analogues with an expanded F ring from 22-cyanofurostane derivative **2** involved nitrile reduction to corresponding amine, followed by cyclization under Mitsunobu conditions (Scheme 2, upper row).

Nitrile reduction with NaBH$_4$/CoCl$_2$ [16] employed in the previous synthesis [14] afforded the desired amine **5** in low yield. NaBH$_4$/NiCl$_2$ [17] proved to be a more effective reducing agent for the reaction, which gave amine **5** in 84 % yield (Scheme 2, upper row). The optimization of reduction conditions is shown in Table S1 (see Supplementary Information). Despite testing different reaction conditions, the direct cyclization of the obtained steroidal aminoalcohol **5** *via* the Mitsunobu reaction failed. Therefore, the 26–OH group in nitrile **2** was converted into mesylate **4**, followed by nitrile reduction under conditions previously described (NaBH$_4$/NiCl$_2$) to give amine **6** in 86 % yield (for two steps). The cyclic product **7** was obtained from **6** by treatment with K$_2$CO$_3$ in DMF at 80 °C in 62 % yield (Scheme 2, lower row). The cyclic structure of compound **7** was confirmed by ESI-MS: *m/z* 532 [M+H]$^+$ and other spectral data, as well as its considerably lower polarity in TLC compared with the aminoalcohol **5**. Using the elaborated procedure, the 5,6-dihydro derivative of **7** - 22a (*N*)-homosoladulcidine **7a** (Scheme 2, lower row) was obtained from tigogenin benzoate in total yield of 68 %. In addition, three *N*-acylated 22a (*N*)-homosolasodine derivatives **9-11** (*N*-*p*-nitrobenzyloxycarbonyl, *N*-*p*-nitrobenzoyl, and *N*-acetyl derivatives) were prepared for biological studies (Scheme 3). The ^{1}H NMR analysis of amides **9-11** at variable temperatures proved that they exist at room temperature as equilibrating rotamers around the amide bond (Fig. 3).

2.2. Inhibition of cholinesterases: the SAR study

The ability of obtained 22a(*N*)-homo analogues (**7**, **7a**, **8**, **9**, **10**, **11**), their open-chain intermediate **5**, previously described 26a-homosolasodine derivatives **14**–**17** (Table 2), and their acyclic precursors **12** and **13** (Table 2) [14] to inhibit AChE from electric eel (eeAChE) and BChE from equine serum (eqBChE) was screened *in vitro* using modified Ellman's method and compared with standard solasodine. The effectiveness of the inhibitors is expressed as IC$_{50}$, representing the concentration of an inhibitor required for 50 % inhibition of the enzyme. The obtained values of IC$_{50}$ are summarized in Table 2. Under given conditions, solasodine (used as standard) exhibits very good inhibitory activity for eeAChE (IC$_{50}$ = 28.46 ± 0.99 μM) and eqBChE (IC$_{50}$ = 6.30 ± 0.41 μM).

Our library includes F-homospirosolane-based derivatives differing mainly in the E/F-ring region (containing either 5/7 spiroether or 5/7 spirohemiaminal unit) and the *N*- or *O*- substitution pattern (free or *N*-acylated amine: *N*-(*p*-nitrobenzoyl), *N*-(*p*-nitrobenzyloxycarbonyl), *N*-acetyl; free 3β–OH, *O*-acetyl, or *O*-benzoyl moieties). Two synthesized 22a(*N*)-homo analogues **7a** and **8** displayed better efficacy on AChE than solasodine and its 26-homo derivatives obtained previously (compounds **14-17**). From the data presented in Table 2, it is evident that the disruption of ring F (compounds **5**, **12**, **13**) or *N*-acylation of amine in F-ring (compounds **9** and **16** bearing a bulky *p*-nitrobenzyloxycarbonyl group or acetamides **11**, **17**) yielded analogues with worse inhibitory activities on both esterases than those of solasodine (IC$_{50}$ > 42 μM). The

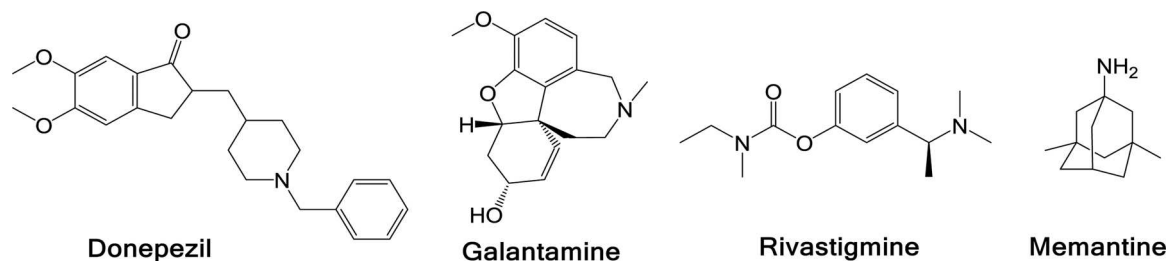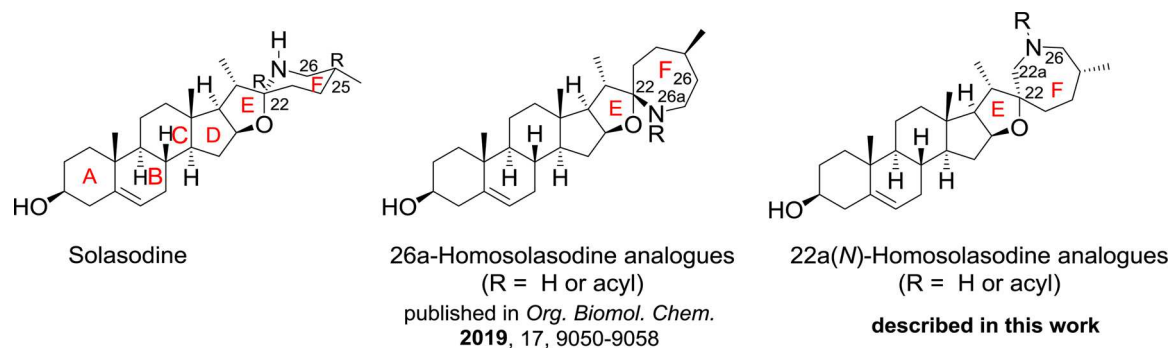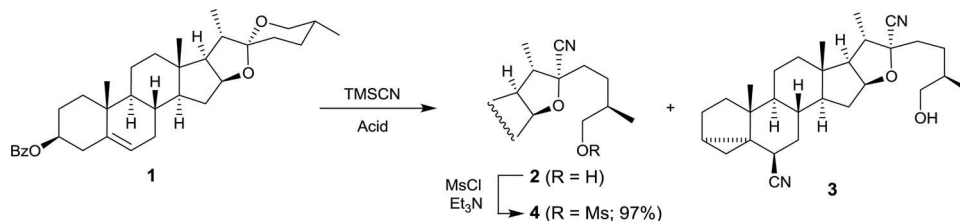**Fig. 1.** FDA approved anti-Alzheimer disease agents.

**Fig. 2.** Structure of solasodine and its homoanalogues.

Scheme 1. The F-ring opening reaction of diosgenin with TMSCN in presence of Lewis or Bronsted acid.

Table 1
The optimization of the nitrile **2** formation.

entry	Reagent (equiv)	Conditions	Yield of 2	Yield of 3
1[14]	BF$_3$·OEt$_2$ (2), TMSCN (6)	DCM:MeCN (4:1), rt, 10 min	55 %	<5%
2	BF$_3$·OEt$_2$ (6), TMSCN (6)	DCM:MeCN (4:1), rt, 1 h	54 %	–
3	BF$_3$·OEt$_2$ (6), TMSCN (6)	DCM:MeCN (4:1), rt, 16 h	30 %	30 %
4	BF$_3$·OEt$_2$ (4), TMSCN (4)	DCM:MeCN (4:1), rt, 16 h	50 %	<5%
5	BF$_3$·OEt$_2$ (0.5), TMSCN (6)	DCM:MeCN (4:1), rt, 10 min	77 %	–
6	TMSOTf (2), TMSCN (2)	DCM, rt, 16 h	30 %	–
7	TfOH (2), TMSCN (2)	DCM, rt, 0.5 h	<5%	–
8	TfOH (2), TMSCN (2)	DCM, rt, 16 h	<5%	–
9	Tf$_2$NH (2), TMSCN (2)	DCM, rt, 1 h	2%	40 %
10	Tf$_2$NH (2), TMSCN (2)	DCM, rt, 16 h	5%	55 %
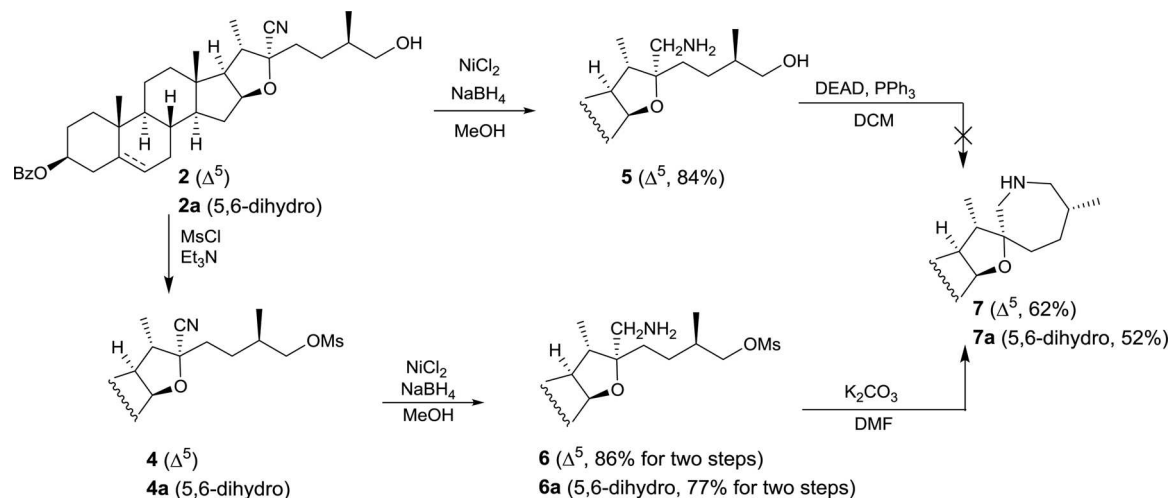
Scheme 2. The synthesis of 22a(*N*)-homosolasodine analogues **7** and **7a**.
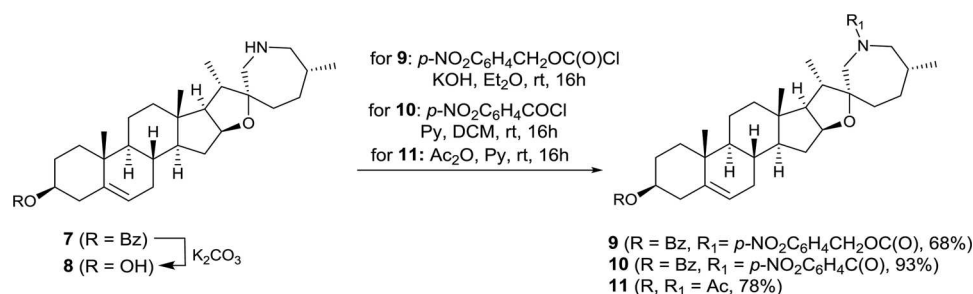
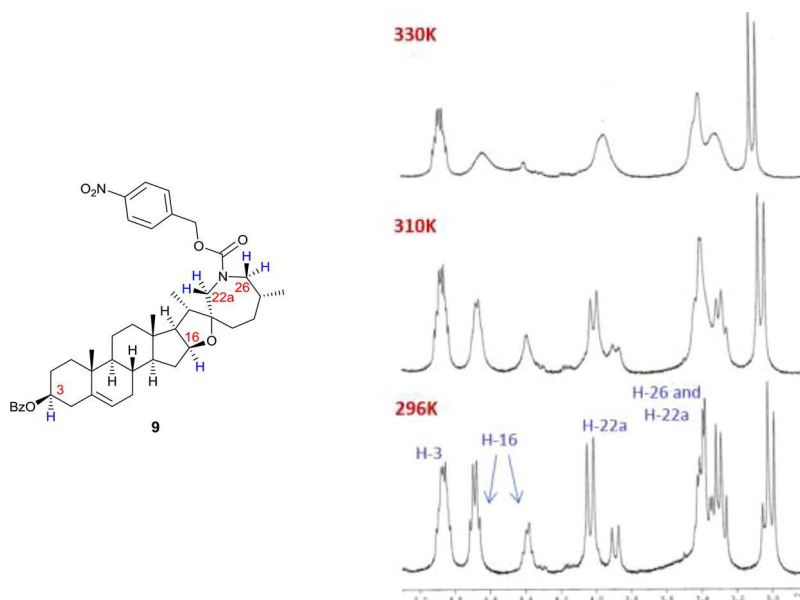**Scheme 3.** The synthesis of 22a(*N*)-homosolasodine *N*-acyl derivatives.

Fig. 3. Variable temperature ¹H NMR spectra of carbamate **9**.
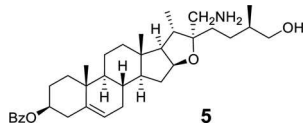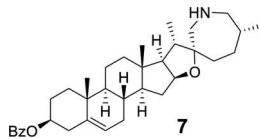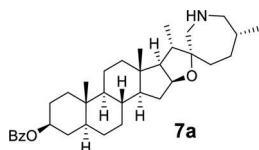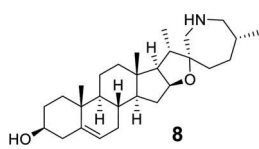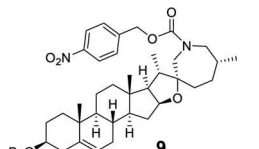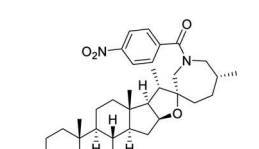
exception is 22a(*N*)-homosolasodine analogue **10**, which possesses a bulky *p*-nitrobenzoyl group and shows high AChE inhibition capacity (IC$_{50}$ = 9.57 μM). Notably, we found that not only E/F ring units can influence activity, but also the substitution pattern of A-ring has an effect on the affinity to cholinesterases. The a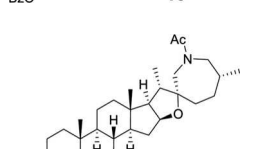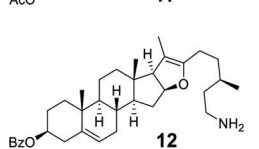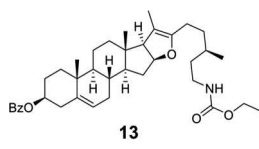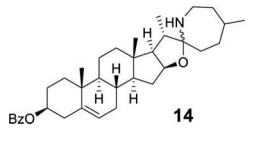nalogues with free hydroxyl groups in A ring had the most pronounced effect (compare activities of steroids **7** and **8** or **14** and **15**). Removing the benzoyl group caused the compounds to have single-digit micromolar IC$_{50}$ values on BChE (derivative **15**, IC$_{50}$ = 1.34 μM) or both enzymes (compound **8**). Apart from derivative **15**, all tested solasodine analogues exhibited selectivity to AChE (see Table 2) in low- or mid-micromolar ranges. Analogue **8** showed the highest activity with IC$_{50}$ values of 8.51 μM on AChE and 7.05 μM on BChE.

The type of inhibition was elucidated for analogues **7a**, **8**, and standard solasodine (all compounds for both ChEs) using a Lineweaver-Burk plot [18]. The plots proved that all three investigated compounds act as noncompetitive inhibitors. This means that increasing the concentration of inhibitor does not affect the value of Michaelis constant (K$_M$), but does affects the value of maximum velocity (V$_m$). The Lineweaver-Burk plot for the most effective inhibitor of both ChEs (*i.e.* analogue **8**) is shown in Fig. 4 as an example. The values of K$_M$ and V$_m$ calculated from Lineweaver-Burk plots are summarized in Tables S2-S8. The inhibition constant (*i.e.* dissociation constant of complex enzyme-inhibitor; K$_i$) was calculated using the regression equation of the dependence of slope (Lineweaver-Burk plot) *vs.* concentration of inhibitor (Fig. S1-S14).
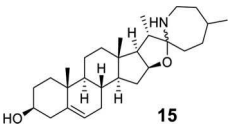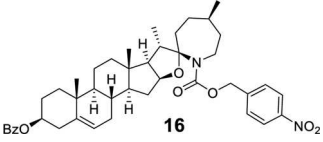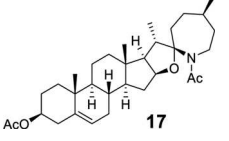
2.3. Molecular docking studies

The physicochemical properties of drug-like molecules follow Lipinki's rule of five, which states LogP ≤ 5, MW ≤ 500, HBA ≤ 10, and HBD ≤ 5. All compounds meet the Lipinski parameters, except LogP (Table 2). In addition, compounds with higher polar surface areas (tPSAs) have lower CNS permeability, and a tPSA less than 90 Å² indicates that a compound is able to penetrate the blood brain barrier (BBB). Based on their predicted tPSA values (between 35.46 and 83.94), the derivatives were assumed to penetrate the BBB. Molecular docking studies were performed for compound **8** (the most potent) and solasodine to investigate their binding modes in hAChE and hBChE using classical non-covalent docking using Glide software (Fig. 5). The docking results of both compounds showed that the cyclohexane ring (ring A) interacts mainly with the amino acids in the opening chamber of catalytic active site (CAS) gorge pocket *via* hydrophobic pi-pi stacking and hydrophobic pi-alkyl type interactions. Ring B and C are surrounded with Y341 and W286, respectively. Amine group of azepane ring in compound **8** creates hydrogen bond interaction with S293, which is located at the mid-gorge of CAS pocket. The compound **8** and solasodine showed promising predicated glide G-scores of -7.08 and -8.26, respectively for AChE, whereas BChE showed glide G-Scores of -5.97 and -6.27. Finally, we found that no of ligand fragments has participated in any of interactions with peripheral anionic site pocket of hAChE and hBChE receptor. The glide scores of known cholinesterase inhibitor such as donepezil in active site of AChE and BChE were calculated and scores are -12.68 and -6.75 respectively.

Table 2

Physicochemical properties and cholinesterases inhibitory activities of investigated solasodine derivatives.[a]

Compound	tPSA[b] (Å^2)	LogP[b]	H-Bond acc./don.	IC$_{50}$ ± SEM (μM)		SI*
				eeAChE	eqBChE	
5	67.2	7.0	6/3	44.09 ± 0.36	80.46 ± 2.70	1.82
7	39.6	7.5	5/1	42.38 ± 0.63	89.55 ± 3.84	2.11
7a	39.6	7.6	5/1	21.96 ± 0.53	24.89 ± 0.86	1.13
8	35.5	5.4	3/2	**8.51 ± 0.24**	**7.05 ± 0.18**	0.83
9	83.9	9.3	11/0	125.14 ± 8.55	> 500	—
10	77.5	8.9	10/0	9.57 ± 0.05	75.95 ± 1.21	7.93
11	45.2	6.1	6/0	69.11 ± 2.88	229.28 ± 7.10	3.32
12	49.7	7.7	5/2	42.12 ± 0.10	124.45 ± 1.62	2.95
13	61.2	10.2	7/1	123.97 ± 4.59	> 500	—
14	41.3	8.0	5/1	72.30 ± 0.40	211.20 ± 12.56	2.92

(continued on next page)

Table 2 (*continued*)

Compound	tPSA[b] (Å²)	LogP[b]	H-Bond acc./don.	IC$_{50}$ ± SEM (µM) eeAChE	IC$_{50}$ ± SEM (µM) eqBChE	SI*
15	37.1	5.9	3/2	44.49 ± 0.85	1.34 ± 0.01	0.03
16	83.3	10.1	11/0	81.60 ± 0.34	> 500	—
17	44.6	6.9	6/0	97.70 ± 5.96	259.64 ± 13.41	2.66
solasodine	36.7	5.5	3/2	28.46 ± 0.99	6.30 ± 0.41	0.22

[a] The synthesis of compounds **12–17** was described in our previous paper.[14] [b]tPSA and LogP calculated using Internal Coordinate Mechanics (ICM), Molsoft. IC$_{50}$ values are the mean ± standard error of mean (SEM) of two independent measurements at least. The best results of IC$_{50}$ are indicated in bold. *SI (index selectivity) = IC$_{50}$ (BChE)/IC$_{50}$ (AChE).

2.4. Cell viability assay

To evaluate the cytotoxic effect of new compounds, we treated undifferentiated neuroblastoma cell line SH-SY5Y with increasing concentrations of compounds for 24 h and determined GI$_{50}$ and then the viability at 10 µM with the MTT assay. Dinaciclib and solasodine were assayed as controls [19]. As shown in Table 3, most of compounds displayed low neurotoxicity; all compounds did not decrease the viability of cells below 90 % at 10 µM concentration.

2.5. Neuroprotective effect of novel compounds on glutamate-induced cytotoxicity

Further, we investigated the neuroprotective effect of solasodine analogues on retinoic acid-induced differentiated SH-SY5Y cells in the presence of 160 mM glutamate. Glutamate-induced neurotoxicity is characterized by ROS-generation, induction of cell death, and mimics the disruption of the central nervous system that is found in certain neurological diseases. We measured that 160 mM glutamate reduced viability of neuroblastoma cells to 28.4 % of the control, which was

Fig. 4. Lineweaver-Burk plot for analogue **8** inhibiting eeAChE. The measurements were done in duplicate and the points are expressed as average values.

consistent with previous reports [20]; galantamine and lipoic acid, both used as positive controls [21–23] protected the viability of SH-SY5Y cells to 34.9 % and 37.2 %, respectively (see normalized data in Table 3 and Fig. 6).

Our results showed that all derivatives are able to partially recover the viability of differentiated SH-SY5Y cells. Moreover, eleven compounds increase the percentage of viable cells (> 15 % than glutamate) more effectively than galantamine and lipoic acid. The most potent compounds, **11**, **13**, **14**, **16**, and **17,** showed the neuroprotection by more than 50 % against glutamate-induced cytotoxicity.

3. Conclusion

In summary, efficient synthesis of F-homosolasodine analogues containing 5/7 spiroether unit from diosgenin or tigogenin was described. The synthetic strategy benefited from the elaborated spirostane F ring opening with TMSCN and BF$_3$·Et$_2$O. The resulting product, (22R)-3β-benzoyloxy-22-cyanofurost-5-en-26-ol, was subjected consecutively to mesylation, reduction, and N-cyclization, and afforded the corresponding F-homo analogue in an excellent yield. Newly synthesized solasodine analogues were investigated for their ability to inhibit cholinesterases. Additional testing proved that almost all of the tested compounds inhibit eeAChE better than eqBChE and act as noncompetitive inhibitors of cholinesterases. Furthermore, all derivatives exhibited neuroprotection potential; they recovered the viability of differentiated neuroblastoma cells after Glu-induced toxicity.

4. Material and methods

4.1. General information

Melting points presented here were determined on a Kofler bench of the Boetius type. NMR spectra were recorded with Bruker Avance II 400 spectrometers operating at 400 MHz, respectively, using CDCl$_3$ solutions with TMS as the internal standard (only selected signals in the ¹H NMR spectra are reported. The ATR-IR spectra were recorded with Nicolet 6700 FT-IR Spectrometer in the 600−4000 cm⁻¹ range. Mass spectra were recorded with AMD-604 and Accurate-Mass Q-TOF LC/MS 6530
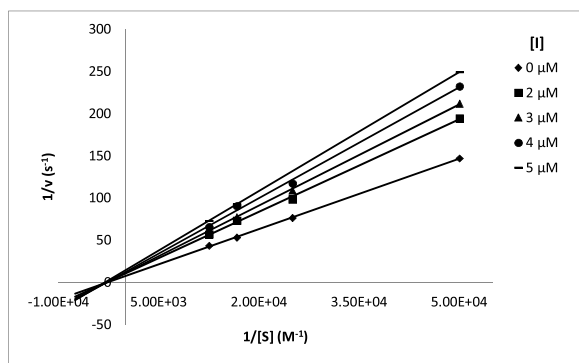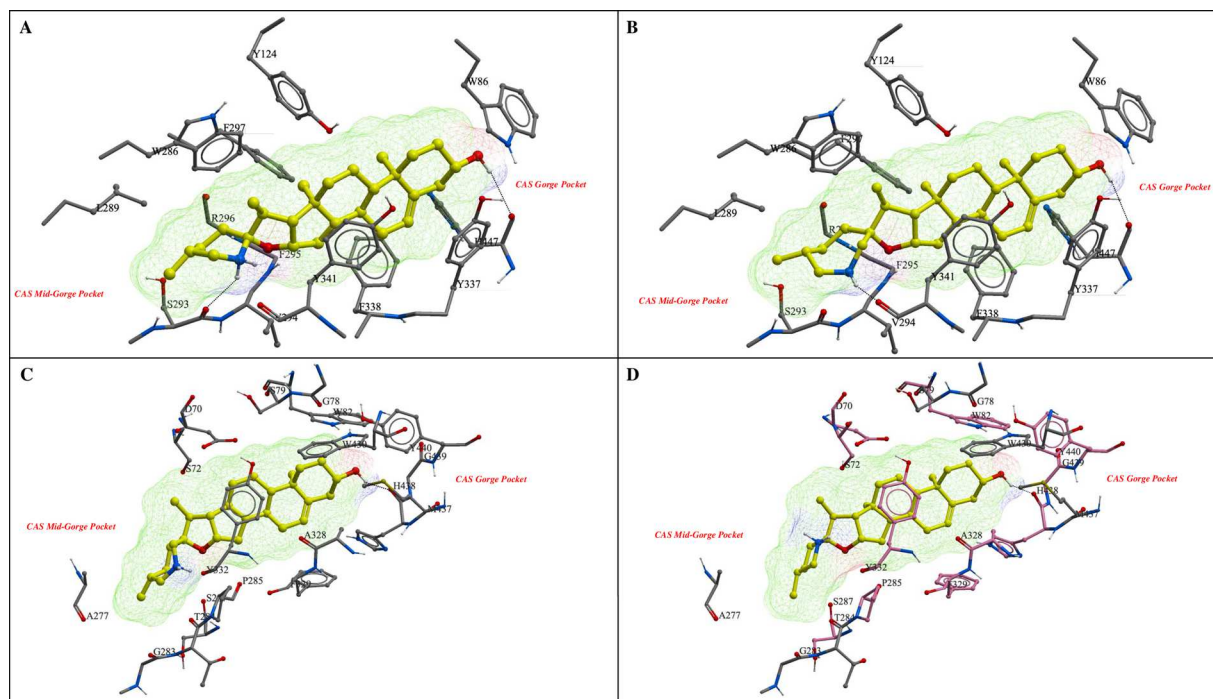
Fig. 5. Docked binding pose of A) solasodine and B) compound **8** (yellow sticks & wire) in human AChE and C) compound **8** and D) solasodine in human BChE. hAChE and hBChE interacting residues are shown as color coded sticks: grey for carbon, blue for nitrogen, and red for oxygen. Figure was prepared with Maestro, Schrodinger, LLC.

spectrometers with electrospray ionization (ESI).

All reactions sensitive to air or moisture were performed in dried round bottom flasks. Air and moisture-sensitive liquids and solutions were transferred *via* syringe and stainless steel cannula. Tetrahydrofuran (THF) and diethyl ether (Et$_2$O) were distilled from sodium/benzophenone, methylene chloride (DCM) from calcium hydride. Methanol was distilled over Mg, triethylamine over KOH. DMF was dried by vacuum distillation and keeping over molecular sieves 4 Å. Merck Silica Gel 60, F 256 TLC aluminum sheets were applied for thin-layer chromatographic analysis. For a visualization of the products, a 5% solution of phosphomolybdic acid was used. The reaction products were isolated by column chromatography, performed using 70–230 mesh silica gel (J. T.

Baker).

4.2. (22R,25R)-3β-benzoyloxy-22-cyanofurost-5-en-26-ol (2)

To a solution diosgenin benzoate (**1**, 155 mg, 0.3 mmol) and TMSCN (0.02 mL, 0.149 mmol) in dry DCM (8 mL) and MeCN (2 mL) boron trifluoride etherate (0.02 mL, 1.793 mmol) was added dropwise under an argon atmosphere. The reaction mixture was monitored by TLC. After 10 min the substrate was completely converted. The reaction was quenched by addition of aqueous solution of NaHCO$_3$, extracted with DCM (3 × 50 mL). The combined organic layers were washed with brine,

Table 3
Antiproliferative and neuroprotective properties of studied compounds on SH-SY5Y neuroblastoma cell line.

Compound	GI$_{50}$ (µM)	Viability[a] (%, 10 µM)	Neuroprotection assay[b] (10 µM, 24 h)
5	>20	99.8 ± 0.2	1.01 ± 0.04
7	>20	99.7 ± 0.4	1.42 ± 0.31
7a	>20	100	1.14 ± 0.12
8	>20	100	1.22 ± 0.21
9	>20	99.2 ± 0.9	1.44 ± 0.17
10	>20	92.5 ± 0.2	1.43 ± 0.13
11	>20	86.5 ± 3.5	1.51 ± 0.13
12	>20	100	1.24 ± 0.28
13	>20	94.3 ± 2.3	1.59 ± 0.22
14	>20	100	1.84 ± 0.20
15	>20	100	1.31 ± 0.31
16	>20	93.8 ± 2.5	1.51 ± 0.18
17	>20	100	1.67 ± 0.10
solasodine	>20	100	0.24 ± 0.03
dinaciclib	0.048	–	–
glutamate (160 mM)	–	–	1.0
galantamine (50 µM)	–	–	1.23 ± 0.13
lipoic acid (50 µM)	–	–	1.33 ± 0.16

[a]tested in duplicates; [b]data normalized to glutamate-induced toxicity (5 replicates included).
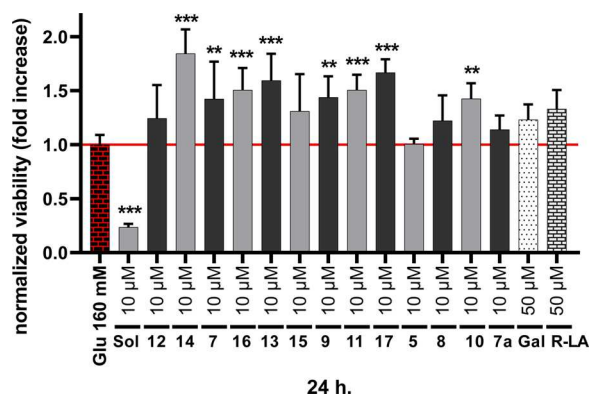
Fig. 6. Evaluation of novel solasodine analogues in glutamate-induced model of cell death on human differentiated SH-SY5Y cells after 24 h of treatment. Differentiated SH-SY5Y were exposed to 160 mM Glutamate (Glu) alone or in co-treatment with compounds and *R*-Lipoic acid (R-LA) and Galantamine (Gal) for 24 h. After 24 h cell viability was measured by MTT assay. Data were normalized to glutamate 160 mM alone as fold increase of viability. The results are presented as mean ± standard deviation (SD) from at least duplicate (n = 2 - 3) in two independent experiments. ANOVA, Tukey post hoc test; * P < 0.05; **P < 0.01; *** P < 0.001; *P compared with vehicle with 160 mM Glu. Values of P < 0.05 – 0.001 is considered statistically significant.

water, dried over Na_2SO_4, and concentrated under reduced pressure. Flash column chromatography (elution with hexane/ethyl acetate 7:3) gave **2** (113 mg, 0.207 mmol, 77 %); as a white solid mp 183−185 °C (hexane/ethyl acetate); ^{1}H NMR (400 MHz, CDCl$_3$) δ 8.04 (m, 2 H), 7.54 (m, 1 H), 7.43 (m, 2 H), 5.42 (m, 1 H), 4.85 (m, 1 H), 463 (m, 1 H), 3.50 (m, 2 H), 2.47 (m, 2 H), 1.22 (d, J = 6.8 Hz, 3 H), 1.08 (s, 3 H), 0.95 (d, J = 6.5 Hz, 3 H), 0.82 (s, 3 H); ^{13}C NMR (100 MHz, CDCl$_3$) δ 165.9 (C), 139.6 (C), 132.7 (CH), 130.7 (C), 129.5 (2xCH), 128.2 (2xCH), 122.2 (CH), 118.6 (C), 89.0 (C), 84.1 (CH), 74.3 (CH), 67.7 (CH$_2$), 62.9 (CH), 56.7 (CH), 49.7 (CH), 41.9 (CH), 40.7 (C), 39.2 (CH$_2$), 38.1 (CH$_2$), 36.9 (CH$_2$), 36.7 (C), 35.5 (CH$_2$), 34.7 (CH$_2$), 31.8 (CH$_2$), 31.5 (CH$_2$), 31.4 (CH), 28.2 (CH$_2$), 27.8 (CH$_2$), 20.6 (CH$_2$), 19.3 (CH$_3$), 17.1 (CH$_3$) 16.5 (CH$_3$), 16.4 (CH$_3$); ESI-MS 546 [M+H]$^+$. HRMS calcd for C$_{35}$H$_{48}$NO$_4$ [M+H]$^+$, 546.3578; found 546.3540; IR ATR, ν_{max} (cm^{-1}) 3442, 2922, 2857, 2021, 1701, 1452, 1275, 1110, 1021, 805, 715.

4.3. (22R,25R)-3β-benzoyloxy-22-cyanofurost-5-en-26-yl mesylate (4)

To the cooled to 0 °C solution of nitrile **2** (95 mg, 0.17 mmol) and Et$_3$N (0.04 mL, 0.26 mmol) in dry DCM (10 mL) solution of MsCl (0.02 mL, 0.209 mmol) in DCM (5 mL) was added dropwise. After 30 min the reaction mixture was removed from the ice bath and stirred at ambient temperature for 16 h. Next the reaction mixture was poured into aq. NaHCO$_3$ and extracted with DCM (3 × 50 mL). The combined organic layers were washed with brine, dried over Na$_2$SO$_4$, and concentrated under reduced pressure. DFC chromatography on silica gel (elution with hexane/ethyl acetate 7:3) gave **4** (83 mg, 0.133 mmol, 97 %) as a white solid, mp 197−199 °C (hexane/ethyl acetate); ^{1}H NMR (400 MHz, CDCl$_3$) δ 8.05 (m, 2 H), 7.55 (m, 1 H), 7.44 (m, 2 H), 5.42 (m, 1 H), 4.86 (m, 1 H), 4.63 (m, 1 H), 4.10 (m, 2 H), 3.03 (s, 3 H), 2.48 (m, 2 H), 1.22 (d, J = 6.8 Hz, 3 H), 1.09 (s, 3 H), 1.04 (d, J = 6.8 Hz, 3 H), 0.82 (s, 3 H); ^{13}C NMR (100 MHz, CDCl$_3$) 165.8 (C), 139.6 (C), 132.7 (CH), 130.6 (C), 129.4 (2xCH), 128.2 (2xCH), 122.1 (CH), 118.3 (C), 88.7 (C), 84.1 (CH), 74.2 (CH), 73.5 (CH$_2$), 62.8 (CH), 56.6 (CH), 49.6 (CH), 41.9 (CH), 40.6 (C), 39.1 (CH$_2$), 38.0 (CH$_2$), 37.2 (CH$_3$), 36.8 (CH$_2$), 36.6 (C), 34.3 (CH$_2$), 32.7 (CH), 31.8 (CH$_2$), 31.4 (CH$_2$), 31.3 (CH), 27.8 (CH$_2$), 27.7 (CH$_2$), 20.5 (CH$_2$), 19.3 (CH$_3$), 17.0 (CH$_3$), 16.4 (CH$_3$) 16.3 (CH$_3$); ESI-MS: 597 [M-CN]$^+$, 683 [M + AcOH]$^+$, 1269 [2M + Na]$^+$; IR ATR, ν_{max} (cm^{-1}) 2921, 2854, 1705, 1454, 1344, 1273, 1172, 1109, 969, 822, 711.

4.4. (22R,25R)-3β-benzoyloxy-22-aminomethylfurost-5-en-26-ol (5)

A solution of nitrile **2** (89 mg, 0.16 mmol) in MeOH (5 mL) was cooled in an ice bath. NiCl$_2$·6H$_2$O (0.1 g, 0.4 mmol) was added and the mixture was stirred until all solids dissolved. After that, NaBH$_4$ (0.08 mg, 1.95 mmol) was carefully added in three portions over a period of 10 min. The black reaction mixture was removed from the ice bath and stirred at ambient temperature for 16 h. Then portion of silica gel (1 g) was added to the flask and the solvent was evaporated *in vacuo*. Chromatographic purification (chloroform/methanol 4:1) gave **5** in 84 % yield (75 mg, 0.14 mmol) as a beige powder; mp 203−205 °C (chloroform/methanol); ^{1}H NMR (400 MHz, CDCl$_3$) δ 8.04 (m, 2 H), 7.55 (m, 1 H), 7.43 (m, 2 H), 5.42 (m, 1 H), 4.86 (m, 1 H), 4.38 (m, 1 H), 3.49 (m, 2 H), 3.02 (m, 4 H), 2.66 (m, 1 H), 2.48 (m, 2 H), 2.19 (m, 1 H), 1.10 (s, 3 H), 0.97 (d, J = 6.6 Hz, 3 H), 0.90 (d, J = 7.1 Hz, 3 H), 0.88 (s, 3 H); ^{13}C NMR (100 MHz, CDCl$_3$) δ 166.0 (C), 139.7 (C), 132.7 (CH), 130.8 (C), 129.5 (2xCH), 128.2 (2xCH), 122.4 (CH), 80.5 (CH), 74.4 (CH), 66.4 (CH$_2$), 64.5 (CH), 56.4 (CH$_2$), 49.9 (CH), 41.0 (C), 39.7 (CH$_2$), 39.0 (C), 38.2 (CH$_2$), 37.0 (CH$_2$), 36.8 (C), 35.19 (CH), 35.16 (CH), 32.3 (CH$_2$), 32.0 (CH$_2$), 31.4 (CH), 30.4 (CH$_2$), 29.7 (CH$_2$), 27.8 (CH$_2$), 25.7 (CH$_2$), 20.8 (CH$_2$), 19.4 (CH$_3$), 16.7 (CH$_3$), 16.4 (CH$_3$), 15.7 (CH$_3$); ESI-MS 550 [M+H]$^+$, 1099 [2M+H]$^+$. HRMS calcd for C$_{35}$H$_{55}$NO$_4$ [M+H]$^+$, 550.3891; found 550.3865; IR ATR, ν_{max} (cm^{-1}) 3515, 2936, 1708, 1426, 1359, 1276, 1221, 1099, 903.

4.5. (22R,25R)-3β-benzoyloxy-22-aminomethylfurost-5-en-26-yl mesylate (6)

A solution of nitrile **4** (29 mg, 0.047 mmol) in MeOH (25 mL) and DCM (4 mL) mixture was cooled in an ice bath. NiCl$_2$x6H$_2$O (0.06 mg, 25 mmol) was added and the mixture was stirred until all solids dissolved. Then NaBH$_4$ (0.023 mg, 0.65 mmol) was carefully added in three portions over a period of 10 min. The black reaction mixture was removed from the ice bath and stirred at ambient temperature for 16 h. Then portion of silica gel (1 g) was added to the flask and the solvent was evaporated in vacuo. Flash column chromatography on silica gel (elution with chloroform/methanol 85:15) gave **6** in 89 % yield (25 mg, 0.04 mmol) as a beige powder, mp 209−211 °C (chloroform/methanol); ^{1}H NMR (400 MHz, CDCl$_3$) δ 8.03 (m, 2 H), 7.54 (m, 1 H), 7.42 (m, 2 H), 5.41 (m, 1 H), 4.86 (m, 1 H), 4.39 (m, 3 H), 4.11 (m, 2 H), 3.03 (s, 3 H), 2.77 (m, 1 H), 2.48 (m, 2 H), 2.21 (m, 1 H), 1.09 (s, 3 H), 1.02 (d, J = 6.7 Hz, 3 H), 0.95 (d, J = 7.0 Hz, 3 H), 0.87 (s, 3 H); ^{13}C NMR (100 MHz, CDCl$_3$) δ 165.9 (C), 139.7 (C), 132.7 (CH), 130.7 (C), 129.5 (2xCH), 128.3 (C), 128.2 (2xCH), 122.3 (CH), 80.8 (CH), 74.4 (CH), 74.3 (CH$_2$), 63.7 (CH), 56.4 (CH), 53.4 (C), 49.8 (CH), 41.1 (CH$_2$), 40.7 (CH$_2$), 39.6 (CH$_2$), 38.1 (CH$_2$), 37.2 (CH), 36.9 (CH$_2$), 36.7 (C), 33.3 (CH), 32.2 (CH$_2$), 32.0 (CH$_2$), 31.3 (CH), 27.8 (CH$_2$), 26.1 (CH$_2$), 20.7 (CH$_2$), 19.3 (CH$_3$), 16.6 (CH$_3$), 16.55 (2xCH$_3$), 15.1 (CH$_3$); ESI-MS 628 [M+H]$^+$, HRMS calcd for C$_{36}$H$_{54}$NO$_6$S [M+H]$^+$, 628.3666; found 628.3681; IR ATR, ν_{max} (cm^{-1}) 3414, 2924, 2856, 1712, 1664, 1454, 1357, 1272, 1169, 1108, 1035, 953, 715.

4.6. (22R,25R)-22a(N)-homospirosol-5-en-3β-yl benzoate (7)

A solution of amine **6** (25 mg, 0.046 mmol) in 1 mL of dry DMF was placed in the flask and 0.01 g of powdered K$_2$CO$_3$ (0.01 g, 0.07 mmol) was added. The reaction mixture was heated in 80 °C for 16 h. After cooling, the solvent was evaporated *in vacuo* and the crude product was purified by silica gel column chromatography (elution with chloroform/methanol 85:15). The product **7** was obtained in 62 % yield (13 mg, 0.03 mmol) as a white solid; mp 215−217 °C (chloroform/methanol); ^{1}H NMR (400 MHz, CDCl$_3$) δ 8.05 (m, 2 H), 7.56 (m, 1 H), 7.44 (m, 2 H), 5.43 (m, 1 H), 4.86 (m, 1 H), 4.44 (m, 1 H), 3.34 (m, 2 H), 2.80 (m, 2 H), 2.48 (m, 2 H), 1.09 (s, 3 H), 1.00 (d, J = 7.0 Hz, 3 H), 0.99 (d, J = 8.8 Hz, 3 H), 0.85 (s, 3 H); ^{13}C NMR (100 MHz, CDCl$_3$) δ 166.0 (C), 139.7 (C) 132.7 (CH), 130.8 (C), 129.5 (2xCH), 128.2 (2xCH), 122.3 (CH), 87.5 (C), 81.6 (CH), 74.4 (CH), 62.7 (CH), 56.4 (CH), 51.6 (CH$_2$), 49.8 (CH), 44.7 (CH$_2$), 42.0 (CH), 40.8 (C), 39.6 (CH$_2$), 38.9 (CH$_2$), 38.1 (CH$_2$), 37.0 (CH$_2$), 36.7 (C), 32.1 (CH$_2$), 32.0 (CH$_2$), 31.4 (CH), 31.0 (CH), 30.2 (CH$_2$), 27.8 (CH$_2$), 20.8 (CH$_2$), 20.3 (CH$_3$), 19.4 (CH$_3$), 16.6 (CH$_3$), 14.3 (CH$_3$); ESI-MS 532 [M+H]$^+$. HRMS calcd for C$_{35}$H$_{50}$NO$_2$ [M+H]$^+$, 532.3785; found 532.4083; IR ATR, ν_{max} (cm^{-1}) 3410, 2922, 2855, 1712, 1454, 1368, 1270, 1109, 714.

(22R,25R)-22a(N)-homospirosolan-3β-yl benzoate (**7a**) was obtained from tigogenin benzoate according to the synthetic protocol used for synthesis of compound **7** (see supporting information).

4.7. (22R,25R)-22a(N)-homospirosol-5-en-3β-ol (8)

To a solution of amine **7** (0.03 g, 0.056 mmol) in MeOH (10 mL) K$_2$CO$_3$ (0.04 g, 0.29 mmol) was added. Reaction mixture was stirred at rt for 16 h. The solvent was removed under reduced pressure and product was purified by column chromatography on silica gel with chloroform/methanol (85/15) elution to give **8** in 82 % (0.023 g, 0.05 mmol) as a white solid. mp 207−210 °C (chloroform/methanol); ^{1}H NMR (400 MHz, CDCl$_3$) δ 5.35 (m, 1 H), 4.38 (m,1 H), 3.54 (m, 2 H), 3.24 (m, 2 H), 2.70 (d, J = 14.0 Hz, 1 H), 2.58 (dd, J = 11.3 Hz, 13.0 Hz, 1 H), 2.28 (m, 2 H), 1.03 (s, 3 H), 0.955 (d, J = 6.2 Hz, 3 H), 0.953 (d, J = 7.4 Hz, 3 H), 0.83 (s, 3 H); ^{13}C NMR (100 MHz, CDCl$_3$) δ 140.7 (C), 121.3 (CH), 88.6 (C), 81.3 (CH), 71.7 (CH), 62.8 (CH), 56.5 (CH), 53.1 (CH$_2$), 49.9 (CH), 45.6 (CH$_2$), 42.2 (CH$_2$), 41.7 (CH), 40.7 (C), 39.7 (CH$_2$), 39.0 (CH$_2$),

37.2 (CH$_2$), 36.6 (C), 32.3 (CH), 32.1 (CH$_2$), 31.9 (CH$_2$), 31.6 (CH$_2$), 31.4 (CH), 30.2 (CH$_2$), 20.8 (CH$_2$), 20.3 (CH$_3$), 19.4 (CH$_3$), 16.6 (CH$_3$), 14.2 (CH$_3$); ESI-MS 428 [M+H]$^+$. HRMS calcd for C$_{28}$H$_{46}$NO$_2^+$ [M+H]$^+$, 428.3523; found 428.3528; IR ATR, ν_{max} (cm^{-1}) 3389, 2927, 2843, 1625, 1456, 1375, 1056.

4.8. (22R,25R)-N-(p-nitrobenzyloxycarbonyl)-22a(N)-homospirosol-5-en-3β-yl benzoate (9)

The compound **9** was prepared according the procedure described previously by us[14]. Elution with hexane/ethyl acetate 93:7 gave **9** (0.02 g, 0.028 mmol, 68 %) as a white solid. mp 215−217 °C (hexane/ethyl acetate); ^{1}H NMR (400 MHz, CDCl$_3$) δ 8.23 (m, 2 H), 8.04 (m, 2 H), 7.53 (m, 3 H), 7.43 (m, 2 H), 5.42 (m, 1 H), 5.30 (m, 2 H), 4.87 (m, 1 H), 4.68 (m, 1 H), 4.03 (d, J = 14.5 Hz, 1 H), 3.41 (m, 1 H), 3.32 (m, 1 H), 3.06 (m, 1 H), 2.48 (m, 2 H), 1.09 (s, 3 H), 1.00 (d, J = 5.9 Hz, 3 H), 0.97 (d, J = 6.0 Hz, 3 H), 0.84 (s, 3 H); ^{13}C NMR (100 MHz, CDCl$_3$) δ 166.0 (C), 156.4 (C), 147.5 (C), 144.7 (C), 139.6 (C), 132.7 (CH), 130.8 (C), 129.5 (2xCH), 128.2 (2xCH), 127.8 (CH), 123.7 (CH), 122.6 (CH), 89.2 (C), 81.2 (CH), 74.5 (CH), 65.6 (CH$_2$), 62.7 (CH), 56.3 (CH), 54.7 (CH$_2$), 49.9 (CH), 47.4 (CH$_2$), 43.3 (CH), 40.5 (CH$_2$), 39.9 (CH$_2$), 39.3 (CH$_2$), 38.2 (CH$_2$), 37.0 (CH$_2$), 36.8 (CH$_2$), 33.4 (CH2), 32.4 (CH$_2$), 32.0 (CH$_2$), 31.8 (CH), 31.3 (CH2), 27.8 (CH$_2$), 21.2 (CH$_2$), 20.9 (CH$_2$), 19.4 (CH$_3$), 16.7 (CH$_3$), 16.6 (CH$_3$), 15.0 (CH$_3$); ESI-MS 711 [M+H]$^+$. HRMS calcd for C$_{43}$H$_{55}$N$_2$O$_7$ [M+H]$^+$, 711.4004; found 711.4011; IR ATR, ν_{max} (cm^{-1}) 3475, 2923, 2856, 1741, 1605, 1524, 1456, 1347, 1231, 1170, 1108, 1041, 853, 723.

4.9. (22R,25R)-N-(p-nitrobenzoyl)-22a(N)-homospirosol-5-en-3β-yl benzoate (10)

To a solution of **7** (10 mg, 18.8 mmol) in mixture DCM (5 mL) and pyridine (2 mL) 4-nitrobenzoyl chloride (7 mg, 0.038 mol) was added. The reaction mixture was stirred at room temperature for 16 h. After this time 5 mL of 10 % HCl was added to the reaction mixture. The crude product was extracted with DCM (3 × 10 mL). The organic layer was washed by NaHCO$_3$, water and dried by sodium sulfate and concentrated *in vacuo*. The crude product was purified by silica gel chromatography (elution with hexane/ethyl acetate 88/12). The product **10** was obtained in 93 % yield as a yellow solid, mp 231−233 °C (hexane/ethyl acetate); ^{1}H NMR (400 MHz, CDCl$_3$) δ 8.28 (m, 2 H), 8.05 (m, 2 H), 7.56 (m, 3 H), 7.44 (m, 2 H), 5.42 (m, 2 H), 4.86 (m, 1 H), 4.69 (m,1 H), 4.22 (d, J = 13.7 Hz, 1 H), 3.35 (d, J = 14.5 Hz, 1 H), 3.28 (dd, J$_1$ = 13.6 Hz, J$_2$ = 4.3 Hz, 1 H), 2.96 (dd, J$_1$ = 20.7 Hz, J$_2$ = 11.9 Hz, 1 H), 2.48 (m, 2 H), 1.10 (s, 3 H), 1.06 (d, J = 6.4 Hz, 3 H), 0.86 (s, 3 H), 0.80 (d, J = 6.1 Hz, 3 H); ^{13}C NMR (100 MHz, CDCl$_3$) δ 166.0 (C), 148.0 (C), 146.3 (C), 143.9 (C), 142.1 (C), 139.7 (C), 132.7 (CH), 130.8 (C), 129.6 (2xCH), 129.5 (2xCH), 128.3 (2xCH), 127.6 (CH), 123.9 (CH), 123.5 (CH), 122.5 (CH), 89.5 (C), 81.6 (CH), 74.5 (CH), 62.6 (CH), 58.0 (CH$_2$), 56.3 (CH), 49.9 (CH), 46.2 (CH$_2$), 43.6 (CH), 40.6 (C), 39.9 (CH$_2$), 39.5 (CH$_2$), 38.2 (CH$_2$), 37.0 (CH$_2$), 32.4 (CH$_2$), 32.0 (CH$_2$), 31.6 (CH$_2$), 31.3 (CH), 27.8 (CH$_2$), 20.9 (CH$_2$), 20.7 (CH$_3$), 19.4 (CH$_3$), 16.7 (CH$_3$), 14.9 (CH$_3$); ESI-MS 681 [M+H]$^+$. HRMS calcd for C$_{42}$H$_{53}$N$_2$O$_6$ [M+H]$^+$, 681.3898; found 681.3908; IR ATR, ν_{max} (cm^{-1}) 3366, 2920, 2854, 1711, 1634, 1520, 1450, 1345, 1270, 1107, 1017, 852, 706.

4.10. (22R,25R)-N-acetyl-22a(N)-homospirosol-5-en-3β-yl acetate (11)

The compound **8** (23 mg, 0.049 mol) was dissolved in pyridine (2 mL) and acetic anhydride (0.02 mL, 0.029 mmol) was added. The reaction mixture was stirred at room temperature for 16 h. After this time 5 mL 10 % HCl was added to the reaction mixture. The crude product was extracted with DCM (3 × 10 mL). The organic layer was washed by NaHCO$_3$, water and dried by sodium sulfate and concentrated *in vacuo*. Elution with hexane/ethyl acetate (7:3) gave **11** with 78 % yield as a white solid, mp 162−165 °C (hexane/ethyl acetate); ^{1}H NMR (400 MHz,

CDCl$_3$) δ 5.36 (m, 1 H), 4.62 (m, 2 H), 4.23 (d, J = 6.1 Hz, 2 H), 3.41 (dd, J$_1$ = 12.8 Hz, J$_2$ = 4.2 Hz, 1 H), 3.11 (dd, J$_1$ = 12.6 Hz, J$_2$ = 11.0 Hz, 1 H), 3.0 (d, J = 14.6 Hz, 1 H), 2.13 (s, 3 H), 2.03 (s, 3 H), 1.03 (s, 3 H), 0.99 (d, J = 5.8 Hz, 3 H), 0.98 (d, J = 6.3 Hz, 3 H), 0.81 (s, 3 H); ^{13}C NMR (100 MHz, CDCl$_3$) δ 171.3 (C), 170.5 (C), 139.6 (C), 122.5 (C), 89.2 (C), 81.2 (CH), 73.9 (CH), 62.5 (CH), 56.9 (CH$_2$), 56.2 (CH), 49.9 (CH), 44.9 (CH$_2$), 43.7 (CH), 40.4 (C), 39.9 (CH$_2$), 39.1 (CH$_2$), 38.1 (CH$_2$), 36.9 (CH$_2$), 36.7 (CH), 33.8 (CH), 32.4 (CH$_2$), 32.01 (CH$_2$), 31.97 (CH$_2$), 31.3 (CH), 27.7 (CH$_2$), 22.5 (CH$_3$), 21.4 (CH$_3$), 21.2 (CH$_3$), 20.8 (CH$_2$), 19.3 (CH$_3$), 16.6 (CH$_3$), 15.0 (CH$_3$); ESI-MS 512 [M+H]$^+$. HRMS calcd for C$_{32}$H$_{50}$NO$_4$ [M+H]$^+$, 512.3734; found 512.3740; IR ATR, ν_{max} (cm^{-1}) 2930, 2854, 1725, 1648, 1423, 1368, 1239, 1167, 1023, 906, 737.

4.11. AChE and BChE inhibition studies

The eeAChE and eqBCHE inhibitory activity of the tested compounds was determined using a modified spectrophotometric Ellman's method. This is a simple, rapid and direct method to determine the -SH and -S-S- groups contained in proteins [24]. Activity of ChEs is measured indirectly by quantifying the concentration of 5-thio-2-nitrobenzoic acid (TNB$^-$) ion formed in the reaction between the thiol reagent 5,5-dithio-bis-2-nitrobenzoic acid (DTNB) and thiocholine (TCh), a product of substrate (*i.e.* acetylthiocholine, ATCh, or butyrylthiocholine, BTCh) hydrolysis catalysed by cholinesterase [25]. All the assays were carried out in 0.1 M phosphate buffered saline (PBS, pH 7.4) in glass cuvette with 1 cm optical path at 25 °C. The activity of eeAChE (or eqBChE) in total reaction mixture (2000 μL) was 0.2 U/mL, concentration of ATCh (or BTCh) 40 μM and concentration of DTNB 0.1 mM for all reactions. The uninhibited reaction was started by adding the enzyme. The absorbance of product of given enzymatic reaction, TNB$^-$, was recorded by spectrophotometer with diode array Hewlett-Packard 8453 at the wavelength of 412 nm against comparative solution for 2 min and the reaction rate was calculated ($\nu_0 = \frac{\Delta A}{\Delta t}$). The reaction rate of inhibited reaction was determined for assay medium consisting of PBS, DTNB, ATCh (or BTCh), eeAChE (or eqBChE) and inhibitor (concentrations of DTNB, substrate and enzyme were the same as for the reaction in absence of the inhibitor). For all tested compounds four or five different concentrations of inhibitor were used. All tested solasodine analogues were dissolved in DMSO to concentration 0.01 M and then diluted using demineralized water as necessary. Enzymatic reaction as well as absorbance (412 nm) recording were started by adding of the enzyme. From obtained dependence A *vs.* t reaction rate of inhibited reaction (v_i) was calculated. All measurements were carried out in duplicate at least. Finally, the dependence v_0/v_i *vs.* concentration of inhibitor was constructed and IC$_{50}$ was calculated from obtained equation of regression curve (based on the definition of IC$_{50}$).

4.12. Kinetic studies

The kinetic studies of eeAChE and eqBChE inhibition were performed using modified Ellman's method as well. For the measurement, the following concentrations of the substrate were used: 20, 40, 60 and 80 μM. For each of substrate concentration, four or five different concentrations of inhibitor were chosen (according to the IC$_{50}$ values). Each measurement was performed in duplicate at least. From obtained dependences A (412 nm) *vs.* t, reaction rates of uninhibited and inhibited reactions were calculated. Then, a Lineweaver-Burk plot was constructed, and the values of K$_M$ and V$_m$ were calculated. The purpose was to observe the effect of inhibitor on kinetic parameters.

4.13. Cell viability assay

SH-SY5Y cells (ECACC) were cultivated according to manufacture protocol in DMEM/F12 medium (Merck) supplemented with 10 % FBS, 100 IU/mL penicillin and 100 mg/mL streptomycin and the culture was

maintained in a humidified CO_2 incubator at 37 °C. Cell viability was determined using the 3-(4,5-dimethylthiazol-2-yl)-2,5-diphenyltetrazolium bromide (MTT) assay. Briefly, cells were seeded in triplicates at a density of 8×10^3 cells per well. After 24 h, cells were incubated with drug-containing medium for 24 h. Cells were incubated with MTT solution (5 mg/mL; Merck) and medium was replaced with DMSO after five hours. The absorbance was measured at 620 nm using a Tecan M200Pro microplate reader (Biotek). The GI_{50} value, the drug concentration lethal to 50 % of the cells, was calculated from the dose response curves that resulted from the assays.

4.14. Neuroprotection assay

The SH-SY5Y cells were seeded at the appropriate density (20 000 cells/well) in DMEM/F12 medium (Merck) supplemented with 1% FBS. After 24 h, the cells were treated with 10 μM all-trans retinoic acid (Merck) to induce differentiation. After six days, the culture medium was replaced with fresh medium supplemented with 160 mM monosodium L-glutamate hydrate (Merck) alone or in the combination with tested compound (assayed in triplicates). The cells were further incubated at 37 °C with 5% CO_2 conditions for 24 h and then the viability was determined by MTT assay described above. Positive controls, galantamine and (R)-(+)-α-lipoic acid, were purchased from Merck.

4.15. Molecular docking

Ligand preparation, protein preparation, and initial docking calculations were performed using the Schrödinger Suite molecular modeling package (version 2018–4), using default parameters unless otherwise noted. The Human AChE protein structure (PDB ID: 4EY7) and human BChE protein structure (PDB ID: 4XII) were prepared using the Protein Preparation Wizard. In this step, force field atom types and bond orders were assigned, missing atoms were added, tautomer/ionization states were assigned, water orientations were sampled, and ionizable residues (Asn, Gln, and His residues) have their tautomers adjusted to optimize the hydrogen bond network. A constrained energy minimization was then performed. Three crystallographically resolved water molecules were retained. Receptor grids were generated using a receptor site that was defined by the centroid of the cognate ligand. Docking using the Glide (version 81,012) in standard precision (SP) and Extra precision (XP) mode with flexible ligand docking utilizes precomputed grids [26, 27]. The docking hierarchy starts with the systematic conformational expansion of the ligand, followed by placement in the receptor site. Minimization of the ligand in the field of the receptor is then carried out using the OPLSe force field with a distance- dependent dielectric (default) 2.0. The best pose for a given ligand is determined by the composite Glide G-score. Default van der Waals scaling was used (1.0 for the receptor and 0.8 for the ligand). The Glide G-score using this receptor conformations were better (down to −5.0) compared with the initial protein conformation in the crystal structure.

4.16. Statistical analysis

All data are expressed as mean ± SD. The data analysis was performed by GraphPad Prism 8.4.3 software (La Jolla, USA). A Student *t*-test was used for analysis of data from differentiation experiment. A one-way analysis of variance (ANOVA) with Tukey's multiple comparisons post hoc test was used in remaining experiments in *in vitro* models of neurodegeneration. A value of $P < 0.05$ was considered significant.

CRediT authorship contribution statement

Urszula Kiełczewska: Methodology, Investigation, Visualization, Writing - original draft. **Radek Jorda:** Methodology, Investigation, Conceptualization, Writing - review & editing. **Gabriel Gonzalez:** Methodology, Visualization. **Jacek W. Morzycki:** Writing - review &

editing, Funding acquisition. **Haresh Ajani:** Software, Methodology. **Katarína Svrčková:** Methodology, Investigation. **Šárka Štěpánková:** Methodology, Investigation. **Agnieszka Wojtkielewicz:** Conceptualization, Methodology, Investigation, Writing - review & editing.

Declaration of Competing Interest

The authors report no declarations of interest.

Appendix A. Supplementary data

Supplementary material related to this article can be found, in the online version, at doi:https://doi.org/10.1016/j.jsbmb.2020.105776.

References

[1] M. Taveira, C. Sousa, F. Ferreres, J.P. Teixeira, P.B. Andrade, J. Steroid Biochem. Mol. Biol. 140 (2014) 106–115, https://doi.org/10.1016/j.jsbmb.2013.12.013.
[2] E.V. Rozengart, N.E. Basova, A.A. Suvorov, J. Evol. Biochem. Physiol. 42 (1) (2006) 11–20, https://doi.org/10.1134/S0022093006010029.
[3] M. Weissenberg, A.L. Leonard, Phytochemistry 56 (6) (2001) 603–610, https://doi.org/10.1016/s0031-9422(00)00420-9.
[4] M.E. García, J.L. Borioni, V. Cavallaro, M. Puiatti, A.B. Pierini, A.P. Murray, A.B. Peñéñory, Steroids 104 (2015) 95–110, https://doi.org/10.1016/j.steroids.2015.09.001.
[5] N. Choubdar, M. Golshani, L. Jalili-Baleh, H. Nadri, T.T. Küçükkilinç, B. Ayazgök, A. Moradi, F.H. Moghadam, Z. Abdolahi, A. Ameri, F. Salehian, A. Foroumadi, M. Khoobi 91 (2019), 103164, https://doi.org/10.1016/j.bioorg.2019.103164.
[6] D. G. van Greunen, C. Johan van der Westhuizen, W. Cordier, M. Nell, A. Stander, V. Steenkamp, J. L. Panayides, D. L. Riley, (2019) 179, 680-693, DOI: 10.1016/j.ejmech.2019.06.088.
[7] G. Ahmad, N. Rasool, K. Rizwan, I. Imran, A. Zahoor, M. Zubair, A. Sadiq, U. Rashid, Bioorg. Chem. 92 (2019), 103216, https://doi.org/10.1016/j.bioorg.2019.103216.
[8] K.G. Yiannopoulou, S.G. Papageorgiou, J. Cent. Nerv. Syst. Dis. 12 (2020) 1–12, https://doi.org/10.1177/1179573520907397.
[9] A. Atri, Semin. Neurol. 39 (02) (2019) 227–240, https://doi.org/10.1055/s-0039-1678581.
[10] V. Richmond, A.P. Murray, M.S. Maier, Steroids 78 (2013) 1141–1147, https://doi.org/10.1016/j.steroids.2013.08.003.
[11] S. Cheenpracha, J. Jitonnom, M. Komek, T. Ritthiwigrom, S. Laphookhieo, Steroids 108 (2016) 92–98, https://doi.org/10.1016/j.steroids.2016.01.018.
[12] Y.M. Liu, Y.D. Feng, X. Lu, J.B. Nie, W. Li, L.N. Wang, L.J. Tian, Q.H. Liu, Eur. J. Med. Chem. 137 (2017) 280–291, https://doi.org/10.1016/j.ejmech.2017.06.007.
[13] G. Mohebbia, I. Nabipoura, A. Vazirizadeh, H. Vatanpour, M. Farrokhnia, A. Maryamabadi, A. Bargahi, Rev. Bras. Farmacogn. 28 (2018) 568–574, https://doi.org/10.1016/j.bjp.2018.06.002.
[14] U. Kiełczewska, J.W. Morzycki, L. Rárová, A. Wojtkielewicz, Org. Biomol. Chem. 17 (2019) 9050–9058, https://doi.org/10.1039/c9ob01888c.
[15] Q. Sun, S. Cai, B.R. Peterson, Org. Lett. 11 (2009) 567–570, https://doi.org/10.1021/ol802343z.
[16] J.O. Osby, S.W. Heinzman, B. Ganem, J. Am. Chem. Soc. 108 (1986) 67–72, https://doi.org/10.1021/ja00261a011.
[17] S.M. Weinreb (Ed.), Science of Synthesis: Houben-Weyl Methods of Molecular Transformations, Three Carbon-Heteroatom Bonds: Amides and Derivatives; Peptides; Lactams, 21, Georg Thieme Verlag, Stuttgart, Germany, 2005, p. 235.
[18] H. Lineweaver, D. Burk, J. Am. Chem. Soc. 56 (1934) 658–666. DOI:0.1021/ja01318a036.
[19] Z. Chen, Z. Wang, J.C. Pang, Y. Yu, S. Bieerkehazhi, J. Lu, T. Hu, Y. Zhao, X. Xu, H. Zhang, J.S. Yi, S. Liu, J. Yang, Sci. Rep. 6 (2016) 29090, https://doi.org/10.1038/srep29090.
[20] C. Li, S. Chai, Y. Ju, L. Hou, H. Zhao, W. Ma, T. Li, J. Sheng, W. Shi, Mol. Neurobiol. 54 (2017) 5286–5299, https://doi.org/10.1007/s12035-016-0064-3.

[21] J.P. Lopes, G. Tarozzo, A. Reggiani, D. Piomelli, A. Cavalli, Brain Behav. 3 (2013) 67–74, https://doi.org/10.1002/brb3.118.

[22] Y. Takada-Takatori, T. Kume, M. Sugimoto, H. Katsuki, T. Niidome, H. Sugimoto, T. Fujii, S. Okabe, A. Akaike, Eur. J. Pharmacol. 7 (549) (2006) 19–26, https://doi.org/10.1016/j.ejphar.2006.08.017.

[23] O. Tirosh, C.K. Sen, S. Roy, M.S. Kobayashi, L. Packer, Free Radic. Biol. Med. 26 (1999) 1418–1426, https://doi.org/10.1016/s0891-5849(99)00014-3.

[24] S. Ou, K.C. Kwok, Y. Wang, H. Bao, Food Chem. 88 (2004) 317–320, https://doi.org/10.1016/j.foodchem.2004.05.001.

[25] G. Šinko, M. Calić, A. Bosak, Z. Kovarik, Anal. Biochem. 370 (2007) 223–227, https://doi.org/10.1016/j.ab.2007.07.023.

[26] R.A. Friesner, J.L. Banks, R.B. Murphy, T.A. Halgren, J.J. Klicic, D.T. Mainz, M. P. Repasky, E.H. Knoll, M. Shelley, J.K. Perry, D.E. Shaw, P. Francis, P.S. Shenkin, J. Med. Chem. 47 (2004) 1739–1749, https://doi.org/10.1021/jm0306430.

[27] T.A. Halgren, R.B. Murphy, R.A. Friesner, H.S. Beard, L.L. Frye, W.T. Pollard, J. L. Banks, J. J. Med. Chem 47 (2004) 1750–1759, https://doi.org/10.1021/jm030644s.

Palacký University Olomouc

Faculty of Science

Laboratory of Growth Regulators

Mgr. Gabriel Gonzalez

Summary of the Doctoral Thesis

Heterocyclic compounds targeting the neurodegenerative diseases

P1527 Biology

1501V019 Experimental biology

Supervisor

Prof. Ing. Miroslav Strnad, CSc. DSc

Olomouc

2021

The presented PhD. thesis was realized in the Laboratory of Growth Regulators within the framework of internal Ph.D. The Ph.D. program of Experimental Biology, guaranteed by the Laboratory of Growth Regulators, Faculty of Science, Palacký University in Olomouc, between the years 2016-2021.

Ph.D. candidate: **Mgr. Gabriel Gonzalez**

Supervisor: **Prof. Ing. Miroslav Strnad, CSc. DSc.,**
Laboratory of Growth Regulators, Faculty of Science, Palacký University in Olomouc & Institute of Experimental Botany AS CR, Šlechtitelů 27, CZ-78371 Olomouc, Czech Republic

Opponents: **RNDr. Hana Chodounská, CSc.**
Institute of Organic Chemistry and Biochemistry of the Czech Academy of Sciences, Flemingovo náměstí 2, CZ-166 10, Prague 6, Czech Republic

doc. MVDr. Aleš Hampl, CSc.
Department of Histology and Embryology, Faculty of Medicine, Masaryk University, Kamenice 5, CZ-625 00, Brno, Czech Republic

Doc. MUDr. Kateřina Menšíková, Ph.D.
Clinic of neurology, Faculty of medicine, Palacký University, The University Hospital Olomouc, I. P. Pavlova 6, CZ-77900 Olomouc, Czech Republic

The evaluation of this Ph.D. thesis was written by **Prof. Ing. Miroslav Strnad, CSc. DSc.**, Laboratory of Growth Regulators, Faculty of Science, Palacký University in Olomouc.

The oral defence will take place on 22th June 2021 before the Commission for the Ph.D. thesis of the Study Program Experimental Biology, room…………., Šlechtitelů 27, Olomouc – Holice.

The PhD. thesis and expert reviews will be available 14 days before the defence in the Study Department of Faculty of Science (Mgr. M. Karásková), Palacký University, 17. listopadu 12, Olomouc.

After the defence, the Ph.D. thesis will be stored in the Library of the Biological Departments, Faculty of Science, Palacký University, Šlechtitelů 27, Olomouc – Holice.

Prof. Ing. Miroslav Strnad, CSc. DSc.
Chairman of the Commission for the Ph.D. thesis
Study Program Experimental Biology
Faculty of Science,
Palacký University in Olomouc

Content

Aims and scope

Various natural and synthetic compounds display promising activities in Parkinson's disease-modifying therapy based on neuroprotection. Human *in vitro* models of PD, especially those induced by natural metabolites of dopamine known to possess some neurotoxicity, serve as a suitable tool for identification of new neuroprotective agents. Up to now natural plant hormones cytokinins have demonstrated promising protective activities in several stress-induced models and some Parkinson's disease-related models. However, no systematic study of cytokinins on idiopathic PD model has been published. Similarly, in the case of triterpenes, especially betulines, only few publications demonstrated neuroprotective effect in *in vitro* PD models. The new natural compounds and their synthetic analogues bring a new possibility to find suitable neuroprotective drug candidates as disease-modifying medications for PD.

The main aims of this doctoral thesis are:

- Testing and searching new neuroprotective agents in *in vitro* salsolinol-, glutamate- and 3-nitropropionic acid-induced models of PD, oxidative damage and Huntington's disease/mitochondrial damage on human dopaminergic neuron-like SH-SY5Y cells.

- The systematic evaluation of potential neuroprotective effects of natural cytokinins and their metabolites.

- Screening of neuroprotective effects of novel synthetic pentacyclic triterpenes with a deeper study of processes involved in the neuroprotection.

- Testing of novel kinetin bioisosteres in a glutamate-induced model of oxidative damage focusing on oxidative stress and the caspase-3/7 activity.

- Identification of new protective agents in a series of steroids isolated from soft coral *Sinularia polydactyla* using 3-nitropropionic acid-induced model of Huntington's disease/mitochondrial damage.

Introduction

Nowadays, the neurodegenerative diseases have experienced a dramatic rise in the number of newly diagnosed patients. Additionally, the well-known motor-related neurodegeneration such as Parkinson's disease is limited to symptomatic treatment, and thus the call for disease-modifying agents is even more urgent now. Currently the field of drug discovery of new disease-modifying drug candidates expanded from FDA-drug repurposing over natural compounds towards novel designed synthetic compounds. Within the doctoral thesis, the main focus was dedicated towards the establishing and usage of *in vitro* models associated with the disorder related to dopaminergic neurons such as Parkinson's disease by the cell death inducers such as salsolinol, glutamate and 3-nitropropionic acid on human SH-SY5Y cells differentiated by *all-trans* retinoic acid into neuronal dopaminergic and cholinergic phenotype.

In vitro models served as a tool for measurement of neuroprotective activity of several drug candidates. During the evaluation of neuroprotection *in vitro,* the main part of my work was to screen the drug candidates of natural origin: the plant hormones cytokinins and their metabolites and steroids isolated from the Red Sea Soft Coral; and to those synthetically prepared such as novel synthetic pentacyclic triterpenes and kinetin bioisosteric derivatives.

The neuroprotective effect of the most active derivatives was subsequently validated by orthogonal cytotoxicity tests (lactate dehydrogenase (LDH) release assay and propidium iodide (PI) test), followed by measurement of superoxide radical formation as a marker of oxidative stress (dihydroethidium (DHE) assay), and finalised by a caspase-3,7 activation assay. In the case of active triterpenes, their neuroprotective effect was evaluated using mitochondria by either mitochondrial membrane potential (MMP) measurement (JC10 assay) or by mitochondrial permeability transition pore (mPTP) opening assay (Calcein AM/CoCl$_2$ assay).

Materials and methods

SH-SY5Y cell culture

The SH-SY5Y human neuroblastoma cell line obtained from ATCC (American Type Culture Collection, Manassas, VA, USA) and ECACC (European Collection of Authenticated Cell Culture, Salisbury, UK) was cultivated in Dulbecco's modified Eagle's Medium and Ham's F12 Nutrient Mixture (DMEM:F-12, 1:1), supplemented with 10% fetal bovine serum (FBS) and 1 % penicillin and streptomycin at 37 °C in a humidified atmosphere of 5 % CO_2. The cell culture was used for all experiments until it reached passage 20. For each experiment, SH-SY5Y cells were seeded at a density according to the type of assay (5000, 7000, 10000 and 20000 cells/well) in 96-multiwell plates in 100 µl total volume of medium. The next day*, all-trans* retinoic acid in 1 % FBS DMEM/F12 medium was added to the SH-SY5Y cells at a final concentration of 10 µM. The cells were kept under differentiated conditions for 48 h to achieve longer neurites and reduced proliferation.

Microscopy

Neuron-like SH-SY5Y cells were observed under a Leica DM IL LED (Leica Microsystems, Germany) fluorescence microscope with different excitation filters according to the type of assay or a brightfield setup. Images were captured using an Olympus DP73 high-performance digital camera (Olympus, Tokyo, Japan) and processed by ImageJ software (Fiji). Since the signal-to-noise ratio for staining was moderate the contrast was slightly adjusted in ImageJ software (Fiji) without affecting the resulting observation.

Cell membrane staining (neurite outgrowth kit, Invitrogen™)

SH-SY5Y cells (5000 cells/well) after 48 h of the differentiation procedure were stained by a neurite outgrowth kit (Invitrogen™) according to the manufacturer's protocol with small modifications. Briefly, cells were washed by PBS and stained with a solution of membrane staining dye (protocol for 96 multiwell plates) in PBS for 20 min at 37 °C. After 20 min, the dye in PBS was aspirated and replaced by fresh PBS. Microphotographs of the cells were recorded under the fluorescence microscope.

Cell treatment

Before treatment 3-nitropropropionic acid (3-NPA) was properly dissolved in distilled water and neutralized by fresh NaOH solution to obtain 1M solution, which was subsequently filtered using 0.2 µm syringe filter. Glutamate (Glu) monosodium salt was dissolved in media to reach 160 mM solution. After 48 h differentiation, the old differentiation medium was replaced by fresh 1 % DMEM/F12 medium containing the tested compounds at 0.1, 1 and 10 µM concentration (7 000 cells/well – cytotoxicity) as a co-treatment with 500 µm salsolinol (SAL) and 3-NPA (7000 – 10000 and 20000 cells/well) or 160 mM Glu (20 000 cells/well) for a duration according to the assay type. Control cells were treated by medium containing ≤ 0.1 % of DMSO.

Cell viability and cell death

After 24 h of treatment, the cell viability of neuron-like SH-SY5Y cells growing in 96-well plates (7000 cells/well) was evaluated by the calcein AM assay [1]. Calcein AM solution (Invitrogen™) was added to a final concentration of 0.75 µM, and cells were incubated for 50 min. The fluorescence of free intracellular calcein was measured at 495/517 nm (excitation/emission) using an Infinite M200 Pro (Tecan, Austria) microplate reader. The cell viability was calculated as a percentage of control (DMSO control cells). Cell death of the neuron-like cells (salsolinol (SAL) model: 10 000 cells/well; glutamate (Glu) and 3-nitropropionic acid (3-NP) model: 20 000 cells/well) was determined by the PI assay according to Stone et al. 2003[2]. Briefly, PI was diluted to a 1 mg/mL solution in DMSO. Basic solution was diluted in PBS and then added to cell medium to reach concentration 1 µg/mL (Glu- or 3-NP model). In the SAL model, the old medium was replaced with a PBS solution of PI (1 µg/ml). The cells were incubated for 15 - 25 min. at r.t. PI stained cells were quantified at 535/617 nm (excitation/emission) using an Infinite M200 Pro reader (Tecan, Austria). The fluorescence after treatment with the toxins was considered to correspond to 100 % cell death.

Measurement of oxidative stress by dihydroethidium (DHE) assay

The superoxide radical formation as marker of oxidative stress was evaluated using DHE assay as used in [3]. Cells were left to differentiate and subjected to treatment protocols according to the model of study for 24 h (SAL, 10 000 cells/well) or 4 h (Glu, 20 000 cells/well) in a 96-well plate, as described above. Then, cells were centrifuged at 500 g for 5 min and 30 s,

followed by replacement of the old medium with PBS solution containing 10 μM dihydroethidium (DHE). Afterwards, the plate with cells was kept in the dark at r.t. for 30 min, and then superoxide radical formation (DHE signal) was quantified at 500/580 nm (excitation/emission) using an Infinite M200 Pro (Tecan, Austria) microplate reader. The resulting fluorescence intensity of DHE after toxin treatment was considered to be 100 % superoxide radical formation, relative to which the individual percentages for the co-treatments were calculated. For visualization, cell images were observed using fluorescence microscopy.

Measurement of caspase 3/7 activity

A one-step caspase 3/7 assay was performed according to Carrasco et al. 2003[4] with small modifications. Neuron-like SH-SY5Y cells were co-treated by toxins and the tested compounds and then incubated for 24 h (SAL model) or 1 h (Glu model). Afterwards, a solution of 3x caspase-3,7 assay buffer (containing 150 mM HEPES pH 7.4, 450 mM NaCl, 150 mM KCl, 30 mM $MgCl_2$, 1.2 mM EGTA, 1.5 % Nonidet P40, 0.3 % CHAPS, 30 % sucrose) with DTT (30 mM), PMSF (3 mM) and 75 μM Ac-DEVD-AMC (Enzo Life Sciences) was added to each well of a 96-well plate, and the plate was incubated at 37 °C. Caspase-3,7 activity was measured using an Infinite M200 Pro (Tecan, Austria) microplate reader at 346 nm/438 nm (excitation/emission) after 2 h (SAL model) and 3 h (Glu model). The fluorescence after treatment with the toxins was considered to correspond to 100 % caspase 3/7 activity.

Measurement of mitochondrial membrane potential by JC10 assay

SH-SY5Y cells (20 000 cells/well) were subjected to the co-treatment procedure for 24 h (SAL model) and 1 h (Glu model). After incubation, neuron-like cells were evaluated by the JC10 assay according to the manufacturer's procedure (mitochondrial membrane potential kit MAK-159, Sigma Aldrich, Merck).

Measurement of mitochondrial permeability transition pore opening
by Calcein AM/CoCl₂ assay

Mitochondrial permeability transition pore opening was estimated by the Calcein AM/$CoCl_2$ assay with modifications as described in another study [5]. Briefly, neuron-like SH-SY5Y cells (20 000 cells/well) intoxicated by SAL or its combination with the tested compounds for 24 h

were centrifuged at 500 g for 5 min 30 s. Then, the medium was aspirated and a solution of 1 µM Calcein AM and 2 mM $CoCl_2$ in Hank's balanced salt solution (HBSS) was added and incubated at 37 °C for 20 min in a 5 % CO_2 atmosphere. After incubation, the fluorescence intensity was measured by an Infinite M200 Pro (Tecan, Austria) microplate reader at 488 nm/517 nm (excitation/emission). The resulting signals were calculated as percentages of the DMSO control. Images of the cells were observed using a fluorescence microscope with subsequent processing in ImageJ software. For detailed observation the region of interests was taken.

In vitro models of cell death – acridine orange (AO) / propidium iodide (PI) double staining

Neuron-like SH-SY5Y cells (10 000 cells/well) were treated according to the SAL model, and the cells were kept with toxin for 24 h. The next day, the cells were centrifuged at 500 g for 5.5 min and the medium was replaced by AO (0.5 µM)/PI (1 µg/mL) PBS solution. The cells were kept at room temperature for 25 min, and then representative fluorescence microphotographs were obtained.

Statistical analysis

All data are expressed as mean ± SEM calculated and visualized by GraphPad Prism 8.4.3 software (La Jolla, USA). For statistical analysis of publications I-IV [6-9], the PAST (ver. 1.97) software package [10] and in case of publication V [11] GraphPad Prism 8.4.3 software (La Jolla, USA) were used. The statistical significance was determined by Student t test (used for differentiation experiment see publication I. [6]), ANOVA or non-parametric Kruskal-Wallis followed by Tukey *post hoc* or Mann-Whitney *post hoc* test with sequential Bonferroni correction of p-values. A $P<0.05$ value was considered as significant.

Survey of published results

Cytokinins are adenine-based phytohormones that regulate key processes in plants, such as cell division and differentiation, root and shoot growth, apical dominance, branching and seed germination. In preliminary, studies they have also shown protective activities against human neurodegenerative diseases. To extend knowledge of the protection (protective activity) they offer, we investigated activities of natural cytokinins against salsolinol (SAL)-induced toxicity (a Parkinson's disease model) and glutamate (Glu)-induced death of neuron-like dopaminergic SH-SY5Y cells. Therefore, this study was undertaken to examine neuroprotective (anti-parkinsonian) activities of almost all known naturally occurring CKs in the selected SAL- and Glu-induced models of neurodegeneration. First, we evaluated each of the CKs' oxygen radical absorbance capacity (ORAC) and (in safety tests) cytotoxicity towards neuron-like SH-SY5Y cells. Then we evaluated the compounds' neuroprotective effects and influence on oxidative stress levels by measuring superoxide ($O_2^{\cdot-}$) production (dihydroethidium, DHE assay) and apoptotic caspase-3,7 activities. The results provide the first reported systematic indications of the relationships between natural CKs' structures and neuroprotective activities. We found that kinetin-3-glucoside, *cis*-zeatin riboside and N^6-isopentenyladenosine were active in the SAL-induced PD model. In addition, *trans-*, *cis*-zeatin and kinetin along with the iron chelator deferoxamine (DFO) and the necroptosis inhibitor necrostatin 1 (NEC-1) significantly reduced cell death rates in the Glu-induced model. Lactate dehydrogenase assays revealed that the cytokinins provided lower neuroprotective activity than DFO and NEC-1. Moreover, they reduced apoptotic caspase-3/7 activities less strongly than DFO. However, the cytokinins had very similar effects to DFO and NEC-1 on superoxide radical production. Overall, they showed protective activity in the SAL-induced model of parkinsonian neuronal cell death and Glu-induced model of oxidative damage mainly by reduction of oxidative stress [6].

Next class of compounds which was selected to the evaluation of neuroprotective activity in two models of neurodegeneration on human neuron-like SH-SY5Y cells were pentacyclic triterpenes synthetized by Dr. Milan Urban and his group from the Department of Organic Chemistry and Instituted of Molecular and Translational Medicine, Palacký University Olomouc. In the present work, a series of pentacyclic triterpenes was prepared and evaluated in *in vitro* models of neurodegeneration in neuron-like SH-SY5Y cells [12-14]. The primary aim was to investigate the protective effect of new triterpenes in salsolinol- and glutamate-induced models of cell death mimicking aspects of PD. Novel triterpene derivatives were prepared and evaluated on neuron-like SH-SY5Y cells. Among the tested compounds, betulin triazole 4 bearing a tetraacetyl-β-D-glucose substituent showed a highly potent neuroprotective effect. Further studies revealed that removal of tetraacetyl-β-D-glucose part (free triazole derivative 10) resulted in strong neuroprotection in the SAL model at 1 μM, but this derivative suffered from cytotoxicity at higher concentrations. Both compounds modulated oxidative stress and caspase-3,7 activity, but 10 showed a superior effect comparable to the Ac-DEVD-CHO caspase-3,7 inhibitor. Interestingly, while both 4 and 10 outperformed the positive controls in blocking mitochondrial permeability transition pore opening, only 4 demonstrated potent restoration of the mitochondrial membrane potential (MMP) in the model. Derivatives 4 and 10 also showed neuroprotection in the Glu model, with 10 exhibiting the strongest oxidative stress reducing effect among the tested compounds, while the neuroprotective activity of 4 was probably due recovery of the MMP [7] .

Publication III

Maková, B.; Mik, V.; Lišková, B.; Gonzalez, G.; Vítek, D.; Medvedíková, M.; Monfort, B.; Ručilová, V.; Kadlecová, A.; Khirsariya, P.; Gándara Barreiro, Z.; Havlíček, L.; Zatloukal, M.; Soural, M.; Paruch, K.; D'Autréaux, B.; Hajdúch, M.; Strnad, M.; Voller, J., Cytoprotective activities of kinetin purine isosteres. *Biorganic Medicinal Chemistry* 2021, *33*, 115993.

A panel of kinetin bioisosteres was purchased or synthetized and accurately characterised by analytical methods such as ^{1}H NMR, ^{13}C NMR, purity was determined by HPLC, by high resolution mass (HRMS) and C, H, N analysis. Their biological activity was evaluated on the *in vitro* model of GSH depletion induced by buthionine sulphoximine (BSO) on the Friedrieich's ataxia (FA) patient-derived fibroblasts and glutamate-induced (Glu-) model of oxidative damage on human neuron-like SH-SY5Y cells. From the panel of compounds, selected derivative 6 was identified as highly active against BSO-induced toxicity to FA fibroblasts. In addition, kinetin bioisosteres have been proved to be effective in correcting aberrant splicing of the *ELP1* gene in FA patient fibroblasts. In the Glu-model, the most promising scaffolds 6, 10 and 22 were identified as active, decreasing Glu toxicity to neuron-like SH-SY5Y from both cellular banks (ATCC and ECACC). These derivatives also showed the protective effect against oxidative stress, and the selected derivative 6 reduced caspase-3/7 activity in the Glu-model. Finally, kinetin bioisosteres also displayed suitable parameters of absorption, distribution, metabolism and excretion (ADME) [8].

Publication IV

Tammam, M. A.; Rárová, L.; Kvasnicová, M.; Gonzalez, G.; Emam, A. M.; Mahdy, A.; Strnad, M.; Ioannou, E.; Roussis, V., Bioactive Steroids from the Red Sea Soft Coral Sinularia polydactyla. *Marine Drugs* 2020, *18* (12), 632.

Six new and twenty already isolated steroids from soft coral *Sinularia polydactyla* collected from the Hurghada reef in the Red Sea were characterized by NMR and HPLC-MS. Furthermore, biological activities such as cytotoxicity, anti-inflammatory, anti-angiogenic, androgen receptor-regulated transcription and neuroprotective activity on 3-nitriopropionic acid-induced (3-NPA) model of Huntington's disease or mitochondrial damage of compounds 3-7, 9-12, 14-20 and 22-26 were studied. The steroids demonstrated the cytotoxic effect on HeLa and MCF7 cancer cell lines (22 and 23), inhibition of migration of endothelial cells (11,

12, 22 and 23), and inhibition of androgen receptor (11, 10, 16, 20). Steroids 11 and 23 at 10 µM did not show cytotoxic activity for neuron-like SH-SY5Y cells, while likely to increase viability and reduce cell death comparable to 100 µM *N*-acetylcysteine in the 3-NPA model on neuron-like SH-SY5Y cells [9].

<u>Publication V</u>

Kiełczewska, U.; Jorda, R.; Gonzalez, G.; Morzycki, J. W.; Ajani, H.; Svrčková, K.; Štěpánková, Š.; Wojtkielewicz, A., The synthesis and cholinesterase inhibitory activities of solasodine analogues with seven-membered F ring. *The Journal of Steroid Biochemistry and Molecular Biology* 2021, *205*, 105776.

Thirteen derivatives with solasodine scaffold bearing seven-membered F ring with nitrogen placed at position 22a were synthetized. These compounds were evaluated for their ability to inhibit acetylcholinesterase (AChE) and butyrylcholinesterase (BChE). The inhibitory activity was found in micromolar concentrations, especially derivative 8 showed non-competitive inhibition with $IC50_{eeAChE}$ = 8.51 µM and $IC50_{eqBChE}$ = 7.05 µM. Further molecular docking study of derivative 8 with AChE revealed following interactions: hydrogen bonds with S293, stabilization of rings by hydrophobic interaction of the ring A (compound 8) or the side chain amino acids Y341 and W286 in case of the ring B and C. Finally, the biological tests demonstrated no toxic effects of compounds on differentiated SH-SY5Y cells. Moreover, the derivatives 13, 14 and 17 showed a strong neuroprotective effect against glutamate-induced oxidative damage outperforming positive controls galantamine and lipoic acid [11].

Conclusions and Perspectives

All three *in vitro* models were successfully used as tools for identification of several lead structures within all candidate groups. In addition, the protective activities of the positive controls observed in the models used are consistent with previously published results. In several cases, such as cytokinins and betuline derivatives, not much known in the literature in the field of PD research, the newly identified neuroprotective activity of these compounds opened the way to study their mechanism of actions but also design and develop new more potent analogues.

- All neuroprotective cell models have been successfully used according to published literature data.

- A large panel of cytokinins was evaluated in the salsolinol-induced (SAL-) model of PD and the glutamate-induced (Glu-) model of oxidative damage on neuron-like SH-SY5Y cells. The identified compounds with neuroprotective activities were kinetin-3-glucoside, *cis*-zeatin riboside and N^6-isopentenyladenosine (SAL-model), and *cis-/trans*-zeatin and kinetin (Glu-model).

- The new pentacyclic triterpenes were evaluated in the salsolinol and glutamate model, from which the two most promising compounds were selected for a further study. This research revealed that the effects caused by compound 4 was due to the protection of mitochondria, while derivative 10 showed a strong effect on caspase-3/7 activity and on the reduction of oxidative stress. Both compounds have undergone the structure-activity relationship study (SAR) and can serve as a tool for the development of the next generation of compounds.

- Among the prepared bioisosteres of kinetin, three derivatives (6, 10 and 22) showed a promising neuroprotective activity in Glu-model by reducing oxidative stress. In addition, substance 6 contributed to its significant neuroprotection by reducing the caspase-3/7 activity in the Glu-model.

- Interestingly, two steroids isolated from Red Sea soft coral *Sinularia polydactyla* increased viability and reduced cell death of neuron-like SH-SY5Y cells after 3-nitropropionic acid intoxication.

Together, the primary goal of this thesis, the identification of several neuroprotective agents within our PD models, was achieved. In addition, the selection of active compounds gave us the opportunity to study their mechanism of action in subsequent molecular biological studies. In the case of active cytokinins in particular, mechanistic studies have focused on their effects on oxidative stress in both models. As astrocytes are the primary defence against oxidative stress for neurons, our goal in the future is to study the effects of cytokinins on astrocytes and to evaluate their mechanism of action. In the case of triterpenes, the published study gave us two leading structures, which will be studied in detail in the following works. More specifically, the following can be selected as future aims: i) reduction of undesired cytotoxicity at higher concentration (more suitable heterocycles and removal of Michael acceptor moiety), ii) modification of betulines by various sugar substitutions to make compounds more soluble and iii) the study of their mechanism of action in oxidative stress (Glu-model) and on mitochondria (Sal- and Glu-model to identify the molecular target). Finally, our *in vitro* models and several new toxin-induced models are in development: for example, the 3-nitropropinoic-induced model of death of glial A172 cells or the scopolamine-induced cognitive impairment model on U87MG-derived cholinergic neurons and on neuron-like SH-SY5Y cells, and oligomers-induced models (synuclein/amyloid-beta fragment 25-35) of PD (or Alzheimer disease) on neuron-like SH-SY5Y or U87MG-derived cholinergic neurons, respectively. We also hope that the newly discovered active substances will also be tested on more complex 3D *in vitro* models, for example on cerebral organoids also known as "minibrains".

List of publications and other contributions

I.   **Gonzalez, G.**; Grúz, J.; D'Acunto, C.W.; Kaňovský, P.; Strnad, M. Cytokinin Plant Hormones Have Neuroprotective Activity in In Vitro Models of Parkinson's Disease. *Molecules* 2021, *26*, 361.

II.   **Gonzalez, G.**; Hodoň, J.; Kazakova, A.; D'Acunto, C. W.; Kaňovský, P.; Urban, M.; Strnad, M., Novel pentacyclic triterpenes exhibiting strong neuroprotective activity in SH-SY5Y cells in salsolinol- and glutamate-induced neurodegeneration models. *European Journal of Medicinal Chemistry* 2021, *213*, 113168

III.   Maková, B.; Mik, V.; Lišková, B.; **Gonzalez, G.**; Vítek, D.; Medvedíková, M.; Monfort, B.; Ručilová, V.; Kadlecová, A.; Khirsariya, P.; Gándara Barreiro, Z.; Havlíček, L.; Zatloukal, M.; Soural, M.; Paruch, K.; D'Autréaux, B.; Hajdúch, M.; Strnad, M.; Voller, J., Cytoprotective activities of kinetin purine isosteres. *Biorganic Medicinal Chemistry* 2021, *33*, 115993.

IV.   Tammam, M. A.; Rárová, L.; Kvasnicová, M.; **Gonzalez, G.**; Emam, A. M.; Mahdy, A.; Strnad, M.; Ioannou, E.; Roussis, V., Bioactive Steroids from the Red Sea Soft Coral *Sinularia polydactyla*. *Marine Drugs* 2020, *18* (12), 632.

V.   Kiełczewska, U.; Jorda, R.; **Gonzalez, G.**; Morzycki, J. W.; Ajani, H.; Svrčková, K.; Štěpánková, Š.; Wojtkielewicz, A., The synthesis and cholinesterase inhibitory activities of solasodine analogues with seven-membered F ring. *The Journal of Steroid Biochemistry and Molecular Biology* 2021, *205*, 105776.

Book chapter

I.   Voller, J.; Maková, B.; Kadlecová, A.; **Gonzalez, G.**; Strnad, M., Plant Hormone Cytokinins for Modulating Human Aging and Age-Related Diseases. In *Hormones in Ageing and Longevity*, Rattan, S.; Sharma, R., Eds. Springer International Publishing: Cham, 2017; pp 311-335.

Conference contributions

1. Gonzalez G.; Acunto C.W.; Zatloukal M.; Grúz J.; Aarts, J. M. M. J. G.; Górová V.; Strnad M. NEURODEGENERATION IN LGR: RECENT ADVANCES IN PD PROJECT.
CBPRS 2017 Kouty nad Desnou, Czech Republic (oral presentation).

2. Gonzalez G. - NEURODEGENERATION IN LGR: RECENT ADVANCES IN PD PROJECT

   CBPRS 2018 Luhačovice, Czech Republic. Oral presentation.

3. Gonzalez G.- NEURODEGENERATION IN LGR: THE REALM OF NEUROPROTECTION

   CBPRS 2019 Luhačovice, Czech Republic. Oral presentation.

4. Hényková E.; Gonzalez G.; Grúz J.; Rárová L.; Kaňovský P.; Strnad M. Possible Neuroprotective Activity of Embryonic Plant Tissue Extracts from *Fraxinus excelsior* (*Oleaceae*), *Rubus plicatus* (Rosaceae), *Rubus idaeus* (Rosaceae) And *Tilia cordata* (*Malvaceae*). The 13th world congress on Polyphenols, Malta 2019 (Poster).

Contribution report

I.   The first author – performing *in vitro* culture and neuroprotection experiments, methodology, interpretation of results, creation of graphics (graphs, figures and tables), statistical analysis and manuscript writing.

II. The first author – performing *in vitro* culture and neuroprotection experiments, deeper cellular biology study, methodology, interpretation of results, creation of graphics (graphs, figures and tables), statistical analysis and manuscript writing.

III. Co-author – cooperation in writing results, materials and methods (glutamate model), performing *in vitro* culture and neuroprotection experiments, methodology (glutamate model for neuron-like SH-SY5Y) and statistical analysis.

IV. Co-author – writing results, materials and methods (3-nitropropionic acid-model), creation of figure 6A, B, C, performing *in vitro* culture and neuroprotection experiments, methodology (3-nitropropionic acid-induced model for neuron-like SH-SY5Y cell culture) and statistical analysis.

V.   Co-author – co-operation in writing results and materials, providing cell line SH-SY5Y (ECACC) with culture and treatment protocols for glutamate model, statistical analysis and creation of graphics (Figure 6).

Book chapter

I.   Co-author – co-operation in writing section "14.5. Neuroprotective Activity of Cytokinins".

Souhrn (in Czech)

Název disertační práce: Heterocyklické sloučeniny cílené proti neurodegenerativním onemocněním

Předložená dizertační práce je zaměřena na zavedení *in vitro* modelů Parkinsonovy choroby a souvisejících patologií, jako nástrojů pro identifikaci a studium účinků neuroprotektivních sloučenin. V rámci této práce se podařilo zavést tři klíčové *in vitro* modely neurodenegerace na lidských neuronálních SH-SY5Y buňkách pro účely screeningu a hlubší molekulárně-biologické studie aktivit kandidátních sloučenin. Těmito *in vitro* modely jsou salsolinolem-(Sal-)indukovaný model Parkinsonovy choroby (PD), glutamátový-(Glu-)model oxidativního poškození a model poškození mitochondrií indukovaný kyselinou 3-nitropropinovou.

Mezi kandidátní skupiny těchto látek patřily i) přírodní cytokininy a jejich metabolity, ii) nové pentacyklické triterpeny nasyntetizované skupinou doc. Milana Urbana (Katedra organické chemie a Ústav translační medicíny, přírodovědecké a lékařské fakulty Univerzity Palackého v Olomouci), iii) bioisosterické deriváty kinetinu (cytokinin) a iv) izolované steroidy z korálu *Sinularia polydactyla*.

V prvním případě se podařilo identifikovat cytokininy kinetin-3-glukosid, *cis*-zeatin ribosid a N^6-isopentenyladenosin jako látky chránící před toxicitou salsolinolu. Účinek těchto látek byl způsoben snížením oxidativního stresu, který vedl i ke snížení aktivity kaspáz-3/7, jakožto markerů apoptózy. Zvláště aktivita *cis*-zeatin ribosidu byla pozorována v nízkých submikromolárních koncentracích. Na druhé straně cytokininové báze *cis*- a *trans*-zeatin a kinetin jako jediné vykazovaly protektivní účinky proti Glu-indukovanému oxidativnímu poškození neuronálních SH-SY5Y buněk. I přes nižší protektivní účinek cytokininových bází oproti pozitivním kontrolám deferoxaminu a nekrostatinu-1, byly prokázané účinné koncentrace na submikromolární úrovni, speciálně u *cis*-zeatinu. Dále byly cytokininy schopny snížit oxidativní stres ve stejné míře jako tyto kontrolní sloučeniny, ale rovněž v nižších koncentracích.

V rámci studia aktivit pentacyklických triterpenů byly objeveny dva velmi aktivní deriváty, sloučeniny 4 a 10, a to i v Sal- a Glu-modelu. Tyto sloučeniny i přes strukturní podobnost vykazovaly odlišné účinky. Zatímco derivát 4 indukoval neuroprotektivní účinek především udržením či obnovou membránového potenciálu mitochondrií, aktivita sloučeniny 10 byla zprostředkována velmi silnou inhibicí kaspázy-3/7 a účinnou redukcí oxidativního stresu. Mechanismus účinku těchto derivátů bude předmětem budoucí práce, spolu s přípravou

sloučenin nové generace a jejich evaluací v těchto *in vitro* modelech PD, ale i na jiných typech neurodegenerací.

V neposlední řadě byly v rámci dizertační práce studovány vybrané bioisosterické deriváty kinetinu, které vykazovaly neuroprotektivní aktivitu cestou snížení buněčné smrti, oxidativního stresu a v případě derivátu 6 i snížením kaspázové aktivity v Glu-indukovaném modelu degenerace. Na závěr byly otestovány a identifikovány nové steroidní látky izolované z korálu *Sinularia polydactyla* v modelu degenerace indukované kyselinou 3-nitropropionovou. Do budoucna budou studované toxiny využity i pro jiné astrocytální linie či cholinergní neurony odvozené z linie U87MG. Budoucí výzkum bude zahrnovat i testování aktivních sloučenin v 3D *in vitro* modelu cerebrálních organoidů známých též jako „minimozky“.

References

[1] Rárová, L.; Steigerová, J.; Kvasnica, M.; Bartůněk, P.; Křížová, K.; Chodounská, H.; Kolář, Z.; Sedlák, D.; Oklestkova, J.; Strnad, M., Structure activity relationship studies on cytotoxicity and the effects on steroid receptors of AB-functionalized cholestanes. *J. Steroid Biochem. Mol. Biol.* **2016,** 159, 154-169.

[2] Stone, W. L.; Qui, M.; Smith, M., Lipopolysaccharide enhances the cytotoxicity of 2-chloroethyl ethyl sulfide. *BMC Cell Biol.* **2003,** 4, 1-1.

[3] Kim, M. S.; Seo, J. Y.; Oh, J.; Jang, Y. K.; Lee, C. H.; Kim, J. S., Neuroprotective Effect of Halophyte Salicornia herbacea L. Is Mediated by Activation of Heme Oxygenase-1 in Mouse Hippocampal HT22 Cells. *J. Med. Food* **2017,** 20, (2), 140-151.

[4] Carrasco, R. A.; Stamm, N. B.; Patel, B. K. R., One-step cellular caspase-3/7 assay. *BioTechniques* **2003,** 34, (5), 1064-1067.

[5] Riley, J. S.; Quarato, G.; Lopez, J.; O'Prey, J.; Pearson, M.; Chapman, J.; Sesaki, H.; Carlin, L. M.; Passos, J. F.; Wheeler, A. P.; Oberst, A.; Ryan, K. M.; Tait, S. W. G., Activated BAX/BAK enable mitochondrial inner membrane permeabilisation and mtDNA release during cell death. *EMBO J.* **2018**, 272104.

[6] Gonzalez, G.; Grúz, J.; D'Acunto, C. W.; Kaňovský, P.; Strnad, M., Cytokinin Plant Hormones Have Neuroprotective Activity in In Vitro Models of Parkinson's Disease. *Molecules* **2021,** 26, (2).

[7] Gonzalez, G.; Hodoň, J.; Kazakova, A.; D'Acunto, C. W.; Kaňovský, P.; Urban, M.; Strnad, M., Novel pentacyclic triterpenes exhibiting strong neuroprotective activity in SH-SY5Y cells in salsolinol- and glutamate-induced neurodegeneration models. *Eur. J. Med. Chem.* **2021,** 213, 113168.

[8] Maková, B.; Mik, V.; Lišková, B.; Gonzalez, G.; Vítek, D.; Medvedíková, M.; Monfort, B.; Ručilová, V.; Kadlecová, A.; Khirsariya, P.; Gándara Barreiro, Z.; Havlíček, L.; Zatloukal, M.; Soural, M.; Paruch, K.; D'Autréaux, B.; Hajdúch, M.; Strnad, M.; Voller, J., Cytoprotective activities of kinetin purine isosteres. *Biorg. Med. Chem.* **2021,** 33, 115993.

[9] Tammam, M. A.; Rárová, L.; Kvasnicová, M.; Gonzalez, G.; Emam, A. M.; Mahdy, A.; Strnad, M.; Ioannou, E.; Roussis, V., Bioactive Steroids from the Red Sea Soft Coral Sinularia polydactyla. *Mar. Drugs* **2020,** 18, (12), 632.

[10] Hammer, O.; Harper, D.; Ryan, P., PAST: Paleontological Statistics Software Package for Education and Data Analysis. *Palaeontol. Electron.* **2001,** 4, 1-9.

[11] Kiełczewska, U.; Jorda, R.; Gonzalez, G.; Morzycki, J. W.; Ajani, H.; Svrčková, K.; Štěpánková, Š.; Wojtkielewicz, A., The synthesis and cholinesterase inhibitory activities of solasodine analogues with seven-membered F ring. *J. Steroid Biochem. Mol. Biol.* **2021,** 205, 105776.

[12] Kurnik-Łucka, M.; Panula, P.; Bugajski, A.; Gil, K., Salsolinol: an Unintelligible and Double-Faced Molecule-Lessons Learned from In Vivo and In Vitro Experiments. *Neurotox. Res.* **2018,** 33, (2), 485-514.

[13] Wanpen, S.; Govitrapong, P.; Shavali, S.; Sangchot, P.; Ebadi, M., Salsolinol, a dopamine-derived tetrahydroisoquinoline, induces cell death by causing oxidative stress in dopaminergic SH-SY5Y cells, and the said effect is attenuated by metallothionein. *Brain Res.* **2004,** 1005, (1), 67-76.

[14] Kritis, A. A.; Stamoula, E. G.; Paniskaki, K. A.; Vavilis, T. D., Researching glutamate - induced cytotoxicity in different cell lines: a comparative/collective analysis/study. *Front. Cell. Neurosci.* **2015,** 9, 91-91.